ACTA DE EVALUACIÓN DE LA TESIS DOCTORAL
(FOR EVALUATION OF THE ACT DOCTORAL THESIS)

Año académico *(academic year)*: 2016/17

DOCTORANDO *(candidate PHD)*: **BÁRCENA HUMANES, JOSÉ LUIS**
D.N.I./PASAPORTE *(Id.Passport)*: ******7101X**
PROGRAMA DE DOCTORADO *(Academic Committee of the Programme)*: **D347 DOCTORADO EN TECNOLOGÍAS DE LA INFORMACIÓN Y LAS COMUNICACIONES**
DEPARTAMENTO DE *(Department)*: **TEORÍA DE LA SEÑAL Y COMUNICACIONES**
TITULACIÓN DE DOCTOR EN *(Phd title)*: **DOCTOR/A POR LA UNIVERSIDAD DE ALCALÁ**

En el día de hoy 19/12/16, reunido el tribunal de evaluación, constituido por los miembros que suscriben el presente Acta, el aspirante defendió su Tesis Doctoral **con Mención Internacional** *(In today assessment met the court, consisting of the members who signed this Act, the candidate defended his doctoral thesis with mention as International Doctorate)*, elaborada bajo la dirección de *(prepared under the direction of)* Mª. PILAR JARABO AMORES.
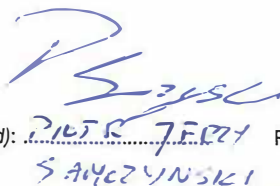
Sobre el siguiente tema *(Title of the doctoral thesis)*: *IMPROVED SIGNAL PROCESSING TECHNIQUES FOR PASSIVE RADAR APLLICATIONS. DESIGN OF A TECHNOLOGICAL DEMONSTRATOR (TÉCNICAS DE PROCESADO DE SEÑAL MEJORADAS PARA RADARES PASIVOS. DISEÑO DE UN DEMOSTRADOR TECNOLÓGICO)*

Finalizada la defensa y discusión de la tesis, el tribunal acordó otorgar la CALIFICACIÓN GLOBAL[2] de **(no apto, aprobado, notable y sobresaliente)** *(After the defense and defense of the thesis, the court agreed to grant the GLOBAL RATING (fail, pass, good and excellent):* _Sobresaliente_____

Alcalá de Henares, a ...19... de ...diciembre... de 2016

Fdo. *(Signed)*: _Manuel Rosa Zurera_

FIRMA DEL ALUMNO (candidate's signature),

Fdo. *(Signed)*: _PIOTR SAMCZYNSKI_

Fdo. *(Signed)*: _David Escot Bocanegra_

Con fecha **25** de **enero** de **2017** la Comisión Delegada de la Comisión de Estudios Oficiales de Posgrado, a la vista de los votos emitidos de manera anónima por el tribunal que ha juzgado la tesis, resuelve:

☒ Conceder la Mención de ''Cum Laude''
☐ No conceder la Mención de ''Cum Laude''

La Secretaria de la Comisión Delegada

Fdo. *(Signed)*: _José Luis Bárcena Humanes_

[2] La calificación podrá ser "no apto" "aprobado" "notable" y "sobresaliente". El tribunal podrá otorgar la mención de "cum laude" si la calificación global es de sobresaliente y se emite en tal sentido el voto secreto positivo por unanimidad. *(The grade may be "fail" "pass" "good" or "excellent". The panel may confer the distinction of "cum laude" if the overall grade is "Excellent" and has been awarded unanimously as such after secret voting.).*

INCIDENCIAS / OBSERVACIONES:
(Incidents / Comments)

Universidad de Alcalá

**COMISIÓN DE ESTUDIOS OFICIALES
DE POSGRADO Y DOCTORADO**

En aplicación del art. 14.7 del RD. 99/2011 y el art. 14 del Reglamento de Elaboración, Autorización y Defensa de la Tesis Doctoral, la Comisión Delegada de la Comisión de Estudios Oficiales de Posgrado y Doctorado, en sesión pública de fecha 25 de enero, procedió al escrutinio de los votos emitidos por los miembros del tribunal de la tesis defendida por *BÁRCENA HUMANES, JOSÉ LUIS*, el día 19 de diciembre de 2016, titulada *IMPROVED SIGNAL PROCESSING TECHNIQUES FOR PASSIVE RADAR APLLICATIONS. DESIGN OF A TECHNOLOGICAL DEMONSTRATOR (TÉCNICAS DE PROCESADO DE SEÑAL MEJORADAS PARA RADARES PASIVOS. DISEÑO DE UN DEMOSTRADOR TECNOLÓGICO)*, para determinar, si a la misma, se le concede la mención "cum laude", arrojando como resultado el voto favorable de todos los miembros del tribunal.

Por lo tanto, la Comisión de Estudios Oficiales de Posgrado **resuelve otorgar** a dicha tesis la

MENCIÓN "CUM LAUDE"

Alcalá de Henares, 25 de enero de 2017
EL PRESIDENTE DE LA COMISIÓN DE ESTUDIOS
OFICIALES DE POSGRADO Y DOCTORADO

Juan Ramón Velasco Pérez

Copia por e-mail a:
Doctorando: BÁRCENA HUMANES, JOSÉ LUIS
Secretario del Tribunal: DAVID ESCOT BOCANEGRA.
Directora de Tesis: M. PILAR JARABO AMORES

Universidad de Alcalá

PROGRAMA DE DOCTORADO EN TECNOLOGÍAS DE LA INFORMACIÓN Y LAS COMUNICACIONES

Tesis Doctoral

IMPROVED SIGNAL PROCESSING TECHNIQUES FOR PASSIVE RADAR APPLICATIONS. DESIGN OF A TECHNOLOGICAL DEMONSTRATOR

JOSÉ LUIS BÁRCENA HUMANES

Directora: Dra. María del Pilar Jarabo Amores

Alcalá de Henares, 2016

Dña. Mª PILAR JARABO AMORES, Titular de Universidad del Departamento de Teoría de la Señal y Comunicaciones de la Universidad de Alcalá,

CERTIFICA:

Que la tesis "*Improved Signal Processing Techniques for Passive Radar Applications. Design of a Technological Demonstrator*", presentada por *D. Jose Luis Bárcena Humanes*, realizada en el Departamento de Teoría de la Señal y Comunicaciones y bajo mi dirección, reúne méritos suficientes para optar al grado de Doctor, por lo que puede procederse a su depósito y defensa.

Alcalá de Henares, 3 de noviembre de 2016

Fdo: Dra. Dña. Mª Pilar Jarabo Amores
Departamento de Teoría de la Señal y Comunicaciones
Universidad de Alcalá

Universidad de Alcalá

DEPARTAMENTO DE TEORÍA DE
LA SEÑAL Y COMUNICACIONES
Escuela Politécnica Superior
Campus Universitario s/n
28805 Alcalá de Henares (Madrid)
Teléfono: 91 885 66 90
Fax: 91 885 66 99
dpto.teoriadelasenal@uah.es

UNIVERSIDAD DE ALCALÁ. PATRIMONIO DE LA HUMANIDAD

D. FRANCISCO JAVIER ACEVEDO RODRÍGUEZ, Director del Departamento de Teoría de la Señal y Comunicaciones de la Universidad de Alcalá,

CERTIFICA:

Que *D. Jose Luis Bárcena Humanes* ha realizado en el Departamento de Teoría de la Señal y Comunicaciones y bajo la dirección de la Doctora *Dña. Mª del Pilar Jarabo Amores*, la tesis doctoral titulada "***Improved Signal Processing Techniques for Passive Radar Applications. Design of a Technological Demonstrator***", cumpliéndose todos los requisitos para la tramitación que conduce a su posterior defensa.

Alcalá de Henares, 3 de noviembre de 2016

Fdo: Dr. D. Fco. Javier Acevedo Rodríguez
DIRECTOR DEL DEPARTAMENTO DE TEORÍA DE LA
SEÑAL Y COMUNICACIONES
UNIVERSIDAD DE ALCALÁ

Contents

i

List of Figures

List of Tables

Chapter 1

Motivation and objectives

1.1 Motivation

Modern societies must face a great number of critical situations: terrorism, migratory pressure, coastal surveillance, a fast and efficient natural or man-made disaster response, etc. The actual security context is defined in a ever-increasing globalization society that generates a growing asymmetrical threat environment. Threats can be related to small menaces more likely than large-scale aggressions. Furthermore, there are collateral aspects that must be considered: environmental impact, economic and social consequences, etc.

Because of that, non collaborative targets detection and tracking is a challenging problem of great interest. It basically involves the detection and estimation of target characteristics, such as position, velocity and trajectory. This information will be a useful tool in different security areas:

- Border management: national defences, migratory control, smuggling fight, etc.

- Surveillance for management or protection of restricted areas or critical infrastructures, as reservoir, power plants, communications hubs.

- Aerial, maritime and ground traffic monitoring for security and management purposes.

A great researching effort was developed in a wide spectrum of sensor technologies. Some of them have been widely used, and have been the subject of intense research and industrial development for decades. Optical technology and digital image processing solutions have the disadvantage of requiring a light source and depend critically on weather conditions. In contrast, conventional active radar systems provide their own illumination, and, with a correct working-frequency choice, can be insensitive to weather, but they must afford collateral on-use restrictions: radio-spectrum congestion, public health regulations for band allocation and transmitted power control, and location regulations in order to avoid public opinion rejection.

Among the new emerging sensor technologies, passive systems are under an intense research effort that focus on overcoming the aforementioned drawbacks of using RF dedicated transmitters, maintaining the operating capabilities of active radars. In order to achieve this goal, they make an opportunistic use of the transmissions of other systems present in their surrounding area, mainly related to civil radio-communication services (Illuminators of Opportunity, IoOs).

A Passive Bistatic Radar (PBR) can be defined as a set of techniques using non-cooperative signals, such as broadcast, communications, radar, or radio-navigation signals as illumination sources, rather than using a dedicated radar transmitter [IEE, 2008]. The non-cooperative sources are known as Illuminators of Opportunity (IoO), and are a critical element in the design of a passive radar due to the fact that they were not designed taking into consideration radar applications requirements.

Through the coherent processing of the IoO direct signal and the radar echoes generated by objects when they are illuminated by the IoO, targets detection and the estimation of its positions and speeds are possible. In Figure1.1 a simplified PBR working scheme is depicted. PBR systems exploiting frequency multiplicity (the system uses several frequency channels), and space multiplicity (the system uses several issuers) can be considered when using one or multiple IoO's.
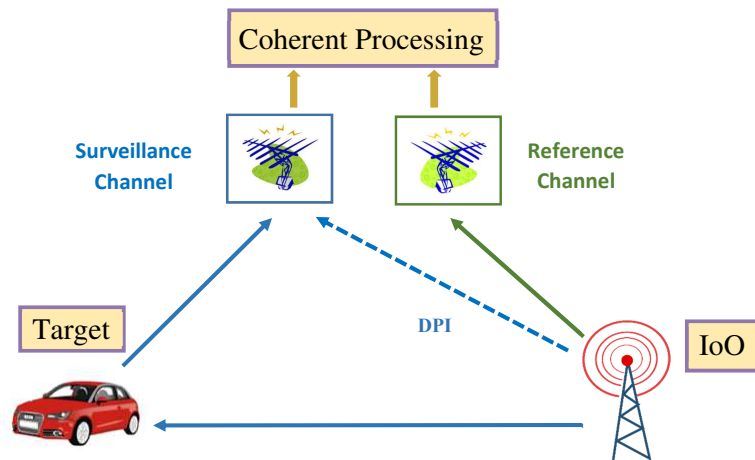
Figure 1.1: Passive radar system geometry and main elements.

Passive radars main advantages with respect to active ones are mainly related to the absence of a dedicated transmitter:

1. In active radars, transmitters are usually a large fraction of radar system cost and design effort, and typically require a major share of system prime power and maintenance. PBRs exploit IoOs available in the area of interest, so only receiving chains are required.

2. Possibility of using Commercial Off-The-Shelf, COTS, components developed for the radiocommunication systems the selected IoO belongs to. This implies a further re-

duction in development, maintenance and updating associated costs. This reduction is especially relevant in the design and development of research oriented technological demonstrators, for which the additional flexibility and versatility achievable using this kind of components are truly appreciated.

3. Passive radars do not require frequency band allocation and are not affected by the communications systems progressive erosion of traditional radar frequencies. In addition they are not subject to public health or electromagnetic compatibility regulations.

4. Possible solution to communications systems progressive erosion of traditional radar frequencies.

5. System deployment does not require expensive works projects (solar panels can be used as energy suppliers).

6. Low interception probability can be assumed if the visual impact of the receiver antenna is neglected. In addition, the use of a bistatic geometry, or the possibility of use working frequencies not associated with conventional radar technologies provide them with some innate defences against electromagnetic countermeasures.

However the use of non-controlled transmitters and signal waveforms not designed for detection purposes, leads to research on design and implementation of complex signal processing techniques:

- Commercial communication signals were not designed for detection purposes. An exhaustive study is required in order to make an optimal selection of the IoO taking into consideration waveform, transmission parameters, IoO emplacement, selected area of interest, and possible PBR receiver emplacements.

  Analog signals usually have high transmission power levels, so good system coverages are expected. But their effective bandwidth is usually low and signal content dependent, making system resolution poor and variable. On the other hand, higher and content independent bandwidths are usually associated with digital communication signals, and lower coverages are expected due to their lower transmitted power. Then, early detection objectives are often assigned to FM based systems, while smaller coverages with higher resolutions are usually fulfilled by passive radars exploiting digital signals [Griffiths and Baker, 2005b, Baker et al., 2005].

- Commercial signals waveforms usually include synchronization pilots, cyclic prefixes, reserved data slots and other structures that make possible signal reception fulfilling the defined service quality. These elements can turn into undesirable effects from the passive radar point of view, degrading its detection capabilities. The use of signal waveforms not designed for detection purposes, gives rise to the necessity

of complex signal processing techniques oriented to overcome those difficulties for fulfilling the desired detection performance.

Thanks to platforms for easier Field-Programmable Gate Array (FPGA) programming, or Graphics Processing Units (GPUs), the fulfilment of real time operation requirements is feasible [SELEX Sistemi Integrati Passive Radar, 2015, Bernaschi et al., 2012, Szumski et al., 2009].

Many published studies focussed on the analysis of IoOs waveforms and the design of system demonstrators. Digital signals reached great relevance against analogue ones due to their bigger and information content independent bandwidths [Baker et al., 2005], [Griffiths and Baker, 2005a]. Among them, Digital Video Broadcasting-Terrestrial (DVB-T) is of special interest due to its growing availability, transmitted power and waveform [Saini and M.Cherniakov, 2005], [Ruck et al., 2009], [Barcena-Humanes et al., 2014], [O Hagan et al., 2014], [Bolvardi et al., 2015]. Most of the demonstrators were validated in aerial scenarios (i.e. detection of commercial aircrafts and performance analysis using secondary radar outputs). In [Edrich et al., 2014] a multi-band, multi-illuminator system at near-production stage is presented. In [Baker, 2014], Professor Chris Baker presented a detailed study about surveillance applications trends and the role of passive radars as emerging technologies. He stated the necessity of facing the study of terrestrial and maritime applications and of developing clutter models for detection parameters prediction. These were the objectives of the IDEPAR project (Improved Detection techniques for Passive Radars), funded by the Spanish Ministry of Economy and Competitiveness (TEC2012-38701). The present PhD Thesis was developed under the scope of this project, with the main objective of designing and developing a DVB-T multichannel passive radar demonstrator for terrestrial and maritime scenarios [Jarabo-Amores et al., 2016, del Hoyo et al., 2015, del Rey-Maestre et al., 2015]. This technological demonstrator is a valuable design, development and validation platform, the base of the passive radar research line developed by the Remote Sensing and Surveillance Systems Laboratory of the University of Alcalá High Frequency Technologies research group, coordinated by Dr. María Pilar Jarabo Amores.

1.2   European research groups

The exploitation of commercial transmitters has opened the door to the use of Commercial Off-The-Shelf (COTS) devices for signal reception (antenna, RF front-end and acquisition systems), and the development of an intense research activity by companies, universities, and other institutions. European research groups with a relevant trajectory in passive radar research are the following:

1. **Institute of Electronic Systems, Warsaw University of Technology**. An intense research in radar signal processing was developed: radar detection, classification, data fusion, Synyhetic Aperture Radar (SAR) and passive radar. They are

involved in research on passive radars since 1999. The first passive radar demonstrator, PaRaDe, used FM radio signals, and was built in 2006. The family of Passive Radar Demonstrators (PARADE I, II and C) constitute a basic reference in passive radar design and development [Malanowski et al., 2008, Malanowski and Kulpa, 2008]. In 2009 the first DBV-T transmission started in Poland, and in 2011 a DVB-T demonstrator was presented [Malanowski et al., 2011].

2. **Radar and Surveillance Systems (RaSS) center of the Italian National Interuniversity Consortium for the Telecommunications (CNIT)**, originated from a joint effort of the universities of Florence, Pisa and Siena in putting together a team of researchers working on the field of radar, remote sensing and applied electromagnetics. The main expertise of the CNIT-RaSS centre is radar system design and analysis, radar data and signal processing, electromagnetic surface and man-made target scattering modelling, as well as other issues relevant for remote sensing. Specific research activities have been focused on ISAR image formation, Bistatic/multistatic ISAR, CFAR and STAP target detection, DVB-T and UMTS Passive radar. Under the direction of Professor Fabrizio Berizzi, the research team at the University of Pisa has developed systems based on DVB-T, and UMTS signals [Petri et al., 2011, Capria et al., 2015, Moscardini et al., 2015, Olivadese et al., 2013]

3. **FGAN FHR Research Institute for High Frequency Physics and Radar Techniques**. Concepts, methods and electromagnetic sensor systems are developed, particularly in the field of radar, in close conjunction with novel signal processing methods and innovative technologies. An intensive research was developed in passive radar technology. CORA (COVERT RADAR) is a system capable of exploiting alternatively DAB or DVB-T signals, using a circular antenna array with elements for the VHF and the UHF-range [Glende et al., 2007, Kuschel et al., 2008]. The department of Antenna Technology and Electromagnetic Modelling (AEM) has developed various antenna element types for the different frequencies of interest for improving CORA antenna array [Knott, 2011]. LORA11 array antenna is composed of 11 UHF discone antennas with an operation bandwidth ranging from 470MHz to 870MHz [Knott et al., 2011, Basavarajappa, 2012]. SABBIA (Sattelite Based Bistatic Imaging Accessory) is the last passive system developed at FHR. This system exploits DVB-Satellite signals using parabolic antennas with an operative bandwidth ranging from 10,700MHz to 12,750MHz.

4. **University of Rome, La Sapienza** The Department of Information Engineering, Electronics and Telecommunications (DIET, former INFOCOM) is part of the Faculty of Information Engineering, Statistics and Informatics, of the University of Rome "La Sapienza". The Radar Remote Sensing & Navigation (RRSN) group is a young research-active one whose focus areas range from remote-sensing and

navigation theory to technology and practice, radar and radio positioning system analysis and data processing. An intense activity was carried out on passive radar technology, with projects funded by radar industries and the European Union.

A summary of some relevant publications includes FM transmitters [Colone et al., 2013a, Colone et al., 2013b, Colone et al., 2009a, Villano et al., 2013], satellite Illuminators [Cristallini et al., 2010], DVB-T [Colone et al., 2014], WiFi [Falcone et al., 2012, Colone et al., 2012a, Falcone et al., 2014], although the most of the proposed solutions can be applied to passive radars exploiting different types of illuminators.

5. **SELEX** AULOS is the passive radar system designed by Selex ES to provide detection and tracking capability for defence and homeland security applications [Lallo et al., 2012, Cantini et al., 2009, Fulcoli et al., 2015]. SELEX has been carrying an intense research and development activity in passive radar technology [Mancinelli, 2010]:

   - 2D AULOS (2006-2007). Design, development and test on real data of a passive radar exploiting a single FM transmitter, and implementing co-channel interference removal by adaptive filtering, range-Doppler processing, azimuth estimation, bi-static and Cartesian tracking.
   - 3D adaptive AULOS (2008-2009). Spatial nulling, STAP (Space Time Adaptive Processing) and ADBF (Adaptive Digital Beam Forming) are applied to further remove co-channel interference and to reject multi-path. Estimation of target elevation angle.
   - 3D multi-static multi-band AULOS (2008-nowadays). Multiple FM transmitters exploitation, analysis of multi-band configuration (DTV-B, GSM, etc.), link and data fusion.

   Selex ES was awarded an industrial prize for its AULOS radar system in 2013 (http://www.uk.leonardocompany.com/-/aulos-radar), and a great effort was carried out for real time operation requirements fulfilment [SELEX Sistemi Integrati Passive Radar, 2015], [Bernaschi et al., 2012].

6. **Cassidian Electronics**: PCL activities at Cassidian started few years ago with the development of a experimental system, which was evaluated in various measurement campaigns followed by intensive theoretical analysis of the results. CAssidian passive radar system is capable of processing DVB-T SFN, DAB-SFN and 8 FM channels simultaneously with cross-band data fusion capability [Schroder, 2011, Schroeder et al., 2012a, Edrich and Schroeder, 2013]. Multistatic configurations were presented in [Schroeder et al., 2012b, Schroeder and Edrich, 2014]. In 2012 Cassidian decided to set up a second stationary FM Passive Radar system on top of a building on the Cassidian premises in Ulm for permanent 24/7 operation and first sensor cluster measurements [Schroeder et al., 2013].

1.3   Related research projects

This is the first PhD Thesis related to passive radar technology carried out in the research group coordinated by Dr. María Pilar Jarabo Amores.

The origin of the passive radar technology research line was the participation in the **APIS project "On Array Passive ISAR Adaptive Processing" (Contract A-1086-RT-GC, European Defense Agency (EDA); A-0900-RT-GC - ICET Call 2 Data Capture and Exploitation)**. The objective of this project was the development of a passive radar demonstrator for the prove of concept of the capability of this technology for the detection of commercial airlines flying at low altitudes, and the generation of Inverse Synthetic Aperture Radar (ISAR) images. The APIS demonstrator was a multichannel DVB-T system, using an antenna array for the surveillance system, with the capability of ISAR image generation. The system exploited the highest three consecutive channels (24 MHz centered on 850 MHz), that nowadays are assigned to LTE services. It was validated for the detection and tracking of commercial airplanes in the Barajas Adolfo Suarez Airport (Madrid), during landing and tacking off manoeuvres.

Thanks to the knowledge and expertise acquired in the APIS project, the research group participated in the Spanish Ministry of Economy and Competitiveness call in 2012, and obtained funding for the project **IDEPAR (Research on Improved Detection techniques for Passive Radars, TEC2012-38701)**. The main objective of this project was to carry out an intensive research in order to improve the detection capabilities of passive radars. A technological demonstrator was designed and developed, directly related to the objectives and results of the present PhD Thesis. For the acquisition of real data in terrestrial and maritime scenarios, and to propose solutions for reducing the effect of different interference sources: the Direct Path Interference or DPI (the signal transmitted by the Illuminator of Opportunity sneaking in through the surveillance channels), the multipath, and the effect of ambiguity peaks in the Ambiguity Function (AF) of the signal IoO.

The upgrade of the IDEPAR demonstrator for improving system robustness with respect to the new and variable DVB-T channels allocations, increasing acquisition bandwidth and making possible the exploitation of satellite illuminators is now possible thanks to the **MASTERSAT project (MultichAnnel paSsive radar receiver exploiting TERrestrial and SATellite Illuminators, TEC2015-71148-R)**.

In parallel with IDEPAR, the follow-on project of APIS, **MAPIS (Multichannel passive ISAR imaging for military applications, CONTRACT Nº: B-1359 IAP2 GP)** was approved. MAPIS project arose with the objective of studying, defining, and analysing a new system concept for implementing and demonstrating

ISAR imaging capability in a plug-in multistatic array passive radar finalized to target recognition. University of Alcalá research activity is focused on scenario definition, target characterization from the point of view of detection and imaging, target detection and classification.

Passive radar technologies were also proposed in the **SCOUT project, Multitech SeCurity system of intercOnnected space control groUnd staTions, Collaborative project, FP7 THEME [SEC-2013.2.2-5]**. The goal of the project was to study, design and analyze on a risk-based approach a security system relying on multiple technologies for the protection of space control ground stations against physical and cyber attacks, and for intelligent reconfiguration of the ground station network in the case that one or more nodes should fail. The scalable distributed multisensor network for protection against physical attacks includes passive sensors. Dr. María Pilar Jarabo Amores is the executive leader of WP 4 (SCOUT system design and analysis).

Other projects closely related to passive radar technology were funded by the University of Alcalá.

- **RIDPAR (Robust Intelligent Detectors for PAssive Radars applications, CCG2013/EXP-92)**. The main objective of this project was the design of robust solutions for the detection of terrestrial targets using DVB-T based passive radars operating in scenarios characterized by spatial-time variable clutter.

- **RSS-BIRASAT (Remote Sensing and Surveillance BIstatic RAdar systems using SATellite illuminators, CCG2014/EXP-060)**. In this project, the study of passive radars exploiting satellite illuminators for remote sensing and surveillance applications was considered. Geostationary, medium and low orbit satellites were analized; a complex labour taking into consideration the different geometries involved and the long distances (high propagation losses).

- **ARTEPAS (ARray signal processing TEcniques for PASsive radar applications, CCG2015/EXP-070)**. The objectives of this project were the following: study of design and system requirements for the antenna array and the space adaptive processing techniques for passive radars operating in the DVB-T frequency band, analysis of frequency sparse signals, and updating of IDEPAR RF and acquisition chains to be compatible with the new DVB-T channels allocation.

1.4   Objectives

The main objective of this PhD Thesis is the deep study of passive radars, taking into consideration different but highly intertwined issues:

- Applications and associated scenarios of interest.

- Analysis of potential IoOs radiation parameters and waveforms.

- Feasibility of COTS devices designed for commercial radiocommunication services reception: antennas, RF front-ends.

- Use of general purpose acquisition chains.

- Array antennas based on commercial single radiating elements.

- DPI and clutter rejection.

- Optimization of proposed processing techniques considering system performance and computational cost.

Specific objectives are described in the following subsections.

1.4.1   Reference and surveillance channels pre-processing

.

A study of signal processing techniques for reducing the effects of the DPI, the multi-pah, the clutter and the IoO waveform components for receiver synchronization is carried out:

- Surveillance channels signals must be pre-processed to reduce DPI and multipath: The DPI component present in the surveillance channels correlates perfectly with the reference signal, masking many of the targets that are sought, and generating false alarms. DPI multipaths and clutter also increase the Probability of False Alarm (P_{FA}).

- The reference channel must be processed to obtain a reference signal free of multi-path interferences and to reduce the effects of the components for receiver synchronization.

The main contributions of this PhD Thesis focus on the proposal of solutions for improving state of the art ones described in radar literature, and for new scenarios generated as a result of the continuous changes in frequencies and bandwidth allocations that the strong spread of communication services are producing, and the growing interest in the exploitation of higher bandwidths for improving system resolution.

1.4.2   Analysis of potential scenarios of interest

Due to the passive radar particular characteristics, the analysis of the potential radar scenarios is one of key point in the systems design and development in order to achieve the required detection capabilities. Among other elements, the resulting possible system geometries, available IoOs in the surrounding area, elevation maps and targets characterization must be taken into consideration.

In this PhD work, different scenarios were analysed to be used as suitable ones for IDEPAR demonstrator system: expected detection capabilities and systems coverage estimation were obtained through reception chain performance and the studies of the surrounding area. Target characterization was considered of great relevance due to the shortage of studies of radar cross section of targets in bistatic geometries and at frequencies lower than typical radar ones.

1.4.3   Proposal of antenna solutions based on commercial single radiating elements

Different commercial antennas were studied (simulated and/or measured in anechoic chamber) to analyse their feasibility for the reference and the surveillance channels. The possibility of building antenna arrays was explored to increase angular coverage and angular resolution through the application of beamforming techniques.

1.4.4   Robustness improvement with respect to available IoOs channel allocation

The DVB-T is one of the most promising IoOs due to the channel bandwidth (approximately 8 MHz), and the possibility, at least at the beginning of its deployment, of acquiring consecutive channels. But as one of the main drawbacks of the lack of dedicated illuminators, passive radar systems are responsive to transmitted DVB-T channels allocation, that is not under the control of the system developer or user.

As an example of this undesired effect, along the PhD developing process, a channel frequency reallocation has been carried out in Spain in order to facilitate the digital dividend, and, additional future changes are expected.

On the other side, different countries and different regions of the same country can have completely different sets of available frequencies, reducing dramatically the probability of acquiring consecutive channels and increasing the complexity of the receiver chain. In this PhD Thesis this problem was studied and solutions based on commercial devices were proposed as a compromise between cost and final performance.

1.4.5   Passive radar demonstrator design and development

As a result, a passive radar demonstrator was built. It was used for data acquisition that was a key element for algorithms design and evaluation. This demonstrator was the base for most of the projects described in section 1.3, not only for proving research group capabilities, but also for proving hardware availability and justify proposed improvements. This research strategy has allowed a continuous upgrade of the system.

1.5   Structure of the document

The rest of this document is organized as follow:

- First part of the document is composed of a series of chapters that focused on the study of the theory fundamentals on witch this work is based. A theoretical analysis of the Passive Radars basic principles is included in Chapter 2. In addition, the main design parameters that must be considered in the system development stage are described.

- In Chapter 3, a brief summary of the digital signals characteristics when are used as passive illuminators are enumerated, including also a description of the Ambiguity Function as signal analysis tool. The DVB-T broadcasting signal is presented as one of the most promising commercial signals to be used as IoO, and as the selected one in this work. In addition a brief study of two space-borne illuminators is also included: DVB-S broadcasting signals and radar signals designed for Synthetic Aperture Radar applications.

- Chapter 4 is the last of the chapters of this theoretical review, and focused on the adaptive filtering fundamentals, presenting the algorithms that will be used in the PhD thesis, also including, for each of them, a brief state of the art of their use in passive radar applications.

- A description of the IDEPAR demonstrator acquisition system can be found in Chapter 5. The most relevant among the hardware and software components are presented: antenna subsystem, acquisition chain, processing tools, etc.

- In Chapter 6, a radar scenario analysis methodology is presented due to its relevance as a key tool for system development and validation stages. The study mainly focuses on the characterization of the target through the bistatic radar cross-section, and on the estimation of the excess propagation losses.

- Chapter 7 is based on the adaptive filtering analysis results, focusing on the variations on the RDS the different filtering strategies gives rise.

- An analysis of the results obtained with IDEPAR demonstrator for data acquired in the main IDEPAR scenario and considering cooperative vehicles is carried out in Chapter 8, for system validation purposes. In addition, a comparison between the results obtained applying the selected ZDI cancellation techniques is also presented, considering system detection and tracking capabilities.

- Chapter 9 consists of the description of a set of robustness and versatility system improvements: a low cost approach for the DVB-T channel dispersion and an analysis for an additional commercial antenna to improve angular resolution.

- In Chapter 10, the main conclusions obtained in this works, and some future research lines this thesis gives rise are enumerated.

Chapter 2

Passive Radar Fundamentals

The main objective of a Passive Bistaic Radar (PBR) is to detect targets and to estimate parameters such as position and speed, using commercial broadcasting, communications, radar or radio-navigation systems as IoOs, rather than a dedicated transmitter. In this chapter, a brief summary of the operating principle of passive radars and their basic architecture are presented.

2.1 Passive Radar operation principle

In Figure 2.1 the system geometry and the basic components of a PBR system are shown.
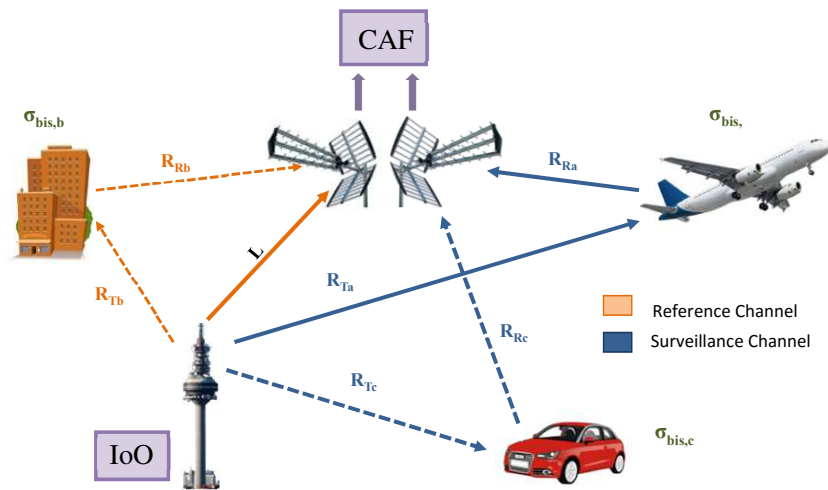
Figure 2.1: Passive radar system geometry and main elements.

Where

- L is the IoO-to-receiver distance, which is called base-line.

- $\sigma_{bis,i}$, $i \in \{a, b, c\}$ are the Bistatic Radar Cross Sections (BRCS) of the aeroplane, the building and the car, respectively. This parameter models the power that is

13
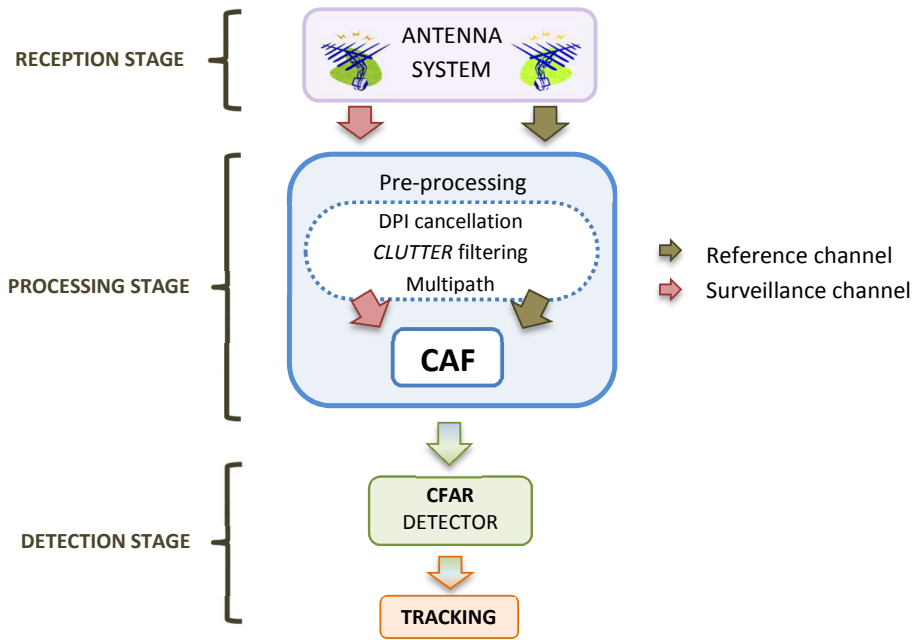
Figure 2.2: PBR architecture main stages.

scattered from the target towards the receiver, when it is illuminated by the IoO.

- R_{Ri} and R_{Ti}, $i \in \{a, b, c\}$ are the radar-to-target and target-to-IoO distances, for the aeroplane, the building and the car, respectively.

- β_i, is the bistatic angle defined by R_{Ri} and R_{Ti}, where, again, $i \in \{a, b, c\}$ stands for the aeroplane, the building and the car, respectively.

In Figure 2.2, the basic scheme of the PBR signal processing architecture is depicted:

1. Reception Stage: Due to the bistatic geometry and the lack of control over the IoO, the use of a dual-channel reception system is mandatory:

   - A Surveillance channel focused on the acquisition of target echoes. In order to reduce the DPI, IoOs direct signals must be rejected.

   - A Reference channel focused on the acquisition of the IoO transmitted signal. Only the selected IoO must be acquired, while rejecting the signals from other IoOs belonging to the same communication system, especially in Single Frequency Networks, SFN. These signals will be considered as interfering IoOs.

2. Processing Stage:

   The system principle of operation, the coherent processing of the two channels, is based on the correlation of time delayed and Doppler-shifted copies of the selected IoO signal, the reference channel, with target echoes acquired by the surveillance

one. As a result, the Cross Ambiguity Function (CAF) is generated (2.1), obtaining the Range-Doppler Surface(RDS).

$$s_{CAF}[m,p] = \sum_{n=0}^{N-1} s_{REF}^*[n-m] \cdot s_{SURV}[n] \cdot \exp(-j2\pi\frac{p}{N}n) \qquad (2.1)$$

- T_{int} and f_s are the coherent processing time and the sampling frequency, respectively.

- $N = T_{int} \cdot f_s$ is the number of samples.

- m represents the time bin associated with a delay $\tau_m = \frac{m}{f_s}$.

- p is the Doppler bin corresponding to Doppler shift $f_{D_p} = f_s \cdot (\frac{p}{N})$

- $s_{REF}[n]$ and $s_{SURV}[n]$ are the reference and surveillance signals, respectively.

In Figure 2.3, a generation scheme of a RDS for an integration time (signal duration) T_{int}, is presented. An object, T_1, present in the area of interest will generate a CAF local maximum at the pair (m_1, p_1) associated with the target bistatic delay, τ_{m_1}, and Doppler shift, $f_{D_{p_1}}$.
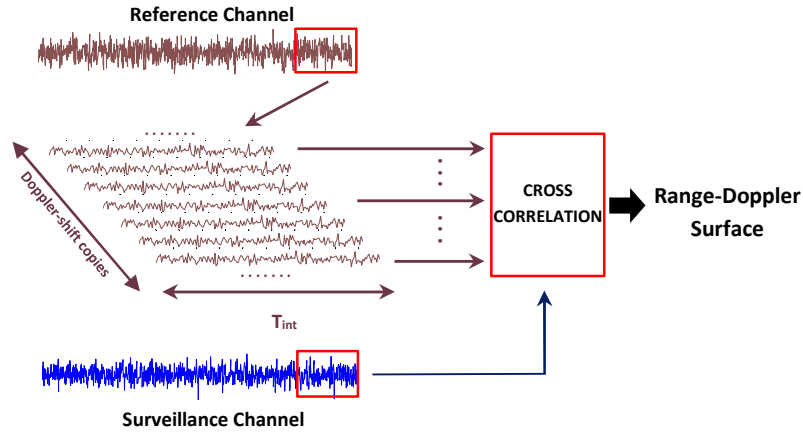
Figure 2.3: CAF generation basic scheme.

For each target of the coverage area, the result of the CAF is the Ambiguity Function (AF) of the transmitted signal, scaled and shifted to be centered on the time delay and Doppler shift corresponding to the bistatic range and bistatic Doppler shift of the target. Figure 2.4 presents an example of CAF generated in a scenario with the following elements:

- Two stationary targets are at bistatic ranges $Rb1$ and $Rb2$. These bistatic ranges are calculated as $Rb = \tau_{bistatic} \cdot c$, where $\tau_{bistatic}$ is the bistatic delay calculated in (2.2) as a function of the target-IoO, the target-PR, and the IoO-PR or baseline distances, denoted as R_T, R_R and L, respectively and c is the
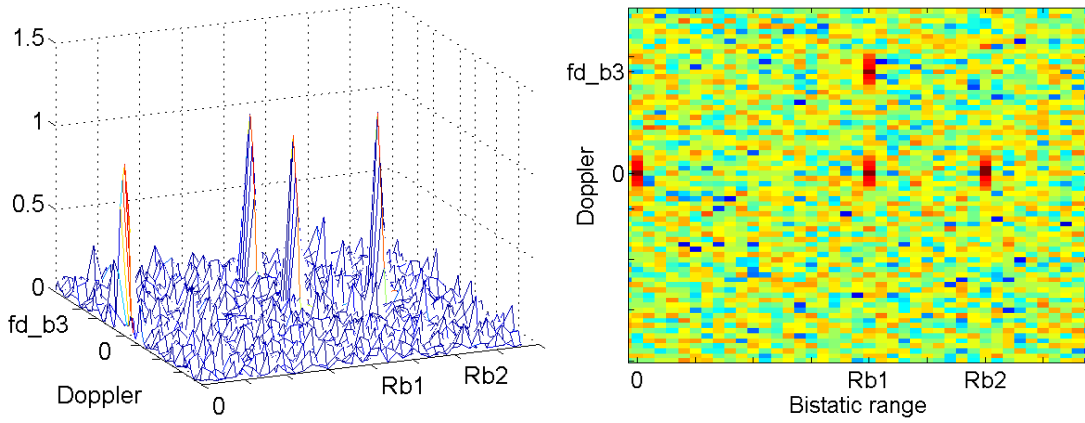
Figure 2.4: Example of CAF generated in an scenario with 3 targets. The effect of the DPI signal is also shown: 3D (left) and 2D (right)

velocity of light. Stationary targets appear in the zero Doppler line of the range-Doppler map.

$$\tau_{bistatic} = \frac{R_T + R_R}{c} - \frac{L}{c} \tag{2.2}$$

- One moving target is detected at a bistatic range $Rb1$. Its echo appears in the range-Doppler map at $(Rb1, fd_{b3})$, where fd_{b3} is the bistatic Doppler generated by target movement relative to the IoO and the PBR.

- The direct signal transmitted by the IoO is captured by the reference and surveillance channels. The surveillance antenna is designed for rejecting this direct signal, but as it can be $100 - 80$dB higher than the target radar echoes, the level captured by the surveillance antenna can be significant compared to target echoes ones. This signal, known as the Direct Path Interference (DPI) signal, correlates perfectly with the reference antenna signal and, as a result, a peak appears in the range-Doppler map of the CAF, located at zero bistatic range and zero Doppler.

Besides the radar echo generated by the targets to be sought, there is a set of undesired effects generated by other signals contributions that can reduce dramatically system detection performance. The most important are:

- Clutter and multipath.

- The Direct Path Interference (DPI) is the result of the direct IoO signal acquired by the surveillance channel. Although the surveillance chain introduces a high attenuation, $s_{DPI}[n] = A_{tt} \cdot s_{REF}[n]$, its level can be $80 - 100$ dB higher than the received target echoes. $s_{DPI}[n]$ correlates perfectly with the reference

(a) Only DPI (b) DPI plus stationary target (c) DPI plus 4 stationary target
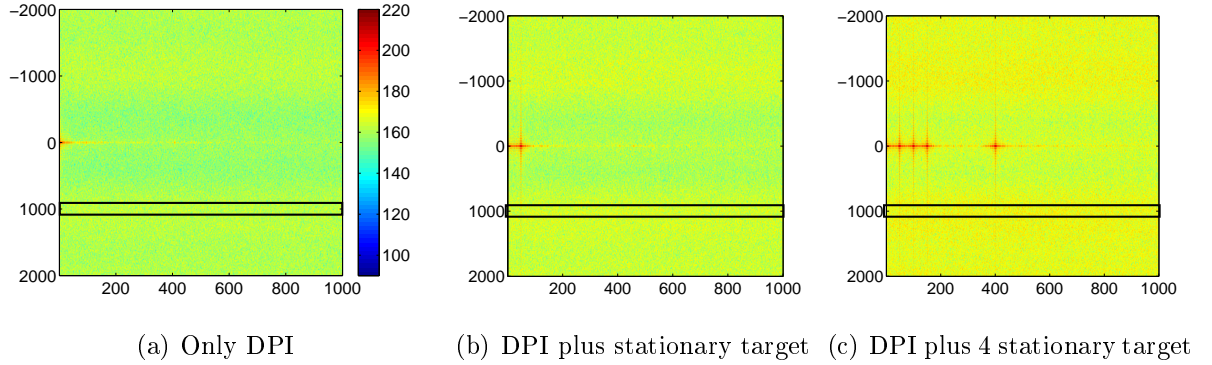
Figure 2.5: Examples of different CAF output (RDS) considering several scenario conditions

signal. When it is included in (2.1), a new component is added to the CAF output, that spreads throughout all the range-Doppler map.

$$
\begin{aligned}
s_{CAF}[m,p] &= \sum_{n=0}^{N-1} s_{REF}^*[n-m] \cdot (s_{target}[n] + A_{tt} \cdot s_{REF}[n]) \cdot \exp(-j2\pi \frac{p}{N} n) \\
s_{CAF}[m,p] &= s_{CAF,target}[m,p] + s_{CAF,DPI}
\end{aligned}
$$

(2.3)

- Other transmitting IoOs belonging to the same SFN will generate new terms at the output of the CAF, so they must be rejected.

- As the IoO signal waveforms have not been designed for detection purposes, the CAF can present different types of artefacts or ambiguity peaks, that can decrease the detection capabilities of the system.

In a ground-based PBR, the main contributions of interfering IoOs and clutter generated by non-moving non-desired objects mainly are located along the zero-Doppler line, but actually, their effect spreads along all the RDS. As examples, in Figure 2.5 the CAFs generated by the DPI, a stationary point target and the DPI, and a set of 4 stationary point targets and the DPI, are compared. Main peaks spillover along the Doppler dimension is clearly observed; signal powers in a Doppler line far from the zero Doppler line were estimated to demonstrate how objects (targets or clutter) affect all the range-Doppler map of the CAF.

The detection of moving targets with low Doppler shifts is dramatically affected by this phenomenon. Due to the bistatic geometry and its relation with the Doppler shift in the bistatic passive scenarios, section 2.2.1, this problem is more important that it may appear at first glance.

Pre-processing techniques can be considered in order to face these problems, as for example the inclusion of a stage designed for disturbance cancellation purposes.

Due to the variability of the IoO signals, and its unknown statistical characteristics, adaptive filtering strategies are usually chosen for this task. For those radar systems that selected antennae systems are based on array and digital beamforming, spatial filtering techniques can be implemented as an additional improvement. Other pre-processing tools, focused on the reduction of the artefacts and spurious that the IoO nature gives rise on the CAF, are the equalization and the reconstruction of the transmitted signal.

3. Detection Stage: The output of the CAF will be applied to the detection stage which implements a detection rule to decide between target absence or target presence, guaranteeing the specified Probability of Probability of Detection, P_D and False Alarm, P_{FA} values.

   The most common detectors used in PBRs are based on incoherent Constant False Alarm Rate (CFAR) [Gandhi and Kassam, 1988, Cao et al., 2010]. The magnitude of each element of the CAF is compared with an adaptive threshold estimated from surrounding cells. This approach assumes that main interference components due to DPI, clutter, and IoO signal artefacts were rejected by the pre-procesing stages, and the detection rule can be designed under thermal noise dominated interference conditions. So complex CAF samples are incorrelated and Gaussian distributted.

4. Tracking Stage:The detector outputs must be processed to estimate the trajectories of the detected targets, improving the detection performance by the fusion of the outputs generated in different coherent processing intervals. Then, the estimated tracks could be analysed in order to extract targets information for classification or management purposes.

   The most commons tracker designs on radar systems are those based on Kalman filters methodologies. These techniques work on the bistatic range - bistatic Doppler domain, where the target trajectories obtained by the PBR can be defined. For low-angular resolution systems, an additional problem the bistatic nature of the PBR gives rise, is the definition of the estimated tracks on a geo-referenced coordinated system in order to provide real target location within the area of interest. On systems with high angular (azimuth) discrimination, improved 3D tracking algorithms can be implemented [Howland et al., 2005]. Solutions based on particle filters or multiple IoOs can be found in [Jishy et al., 2010, Malanowski and Kulpa, 2012].

2.2   System Design Parameters

2.2.1   PBR resolutions

In a monostatic configuration, time delay and Doppler resolutions are defined by the transmitted waveform, and are proportional to range and velocity resolutions, respectively.

In a bistatic configuration, delay-range and Doppler-speed relations depend, in addition, on the relative position of target (T_i), transmitter and receiver (system geometry). In Figure 2.6, time delay and Doppler shift are studied in a bistatic scenario, where β is the bistatic angle, and ψ is the aspect angle with respect to the bistatic bisector.
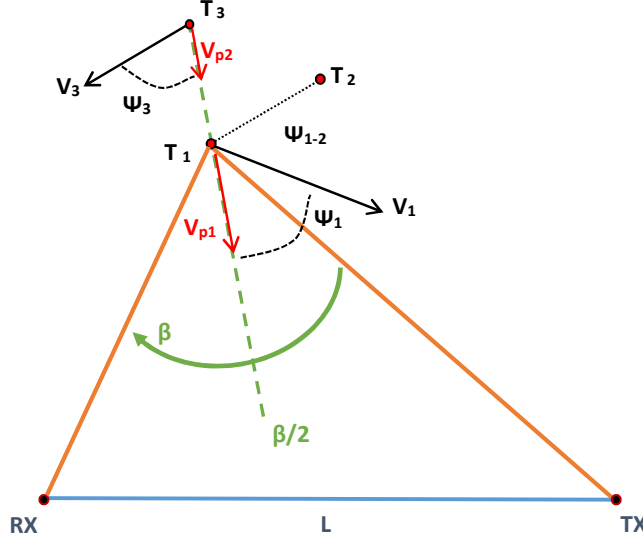
Figure 2.6: Geometry for range resolution and Doppler resolution calculations.

- **Bistatic Range resolution** (ΔR) is defined as the minimum distance between two targets that guarantees a time delay between their respective radar echoes equal to the radar compressed pulsewidth [Willis, 2005]. ΔR can be calculated using expression (2.4):

$$\Delta R_{T_1 T_2} = \frac{c}{2B\cos(\beta/_2)\cos(\psi_{T_1 - T_2})} \tag{2.4}$$

where B is the signal bandwidth, τ_1 is considered the bistatic delay calculated in (2.2) as a function of T_1-IoO distance, R_T, T_1-PBR distance, R_R, and L the baseline length.

$$\tau_1 = \frac{R_T + R_R}{c} - \frac{L}{c} \tag{2.5}$$

- **Doppler resolution**. For monostatic and bistatic Doppler resolution, $1/_{T_D}$ is considered as an adequate degree of Doppler separation between two target echoes, where T_D is the coherent integration time:

$$|f_{D_{T_1}} - f_{D_{T_2}}| = \frac{1}{T_D} \tag{2.6}$$

For a target, T_1, with speed vector $\mathbf{v}_1 = V_1 \tilde{v}_1$, expression (2.7) allows the calculation of the observed Doppler shift when the PBR and the IoO are stationary using the

velocity vector and system geometry.

$$f_{D1}(Hz) = \frac{2 \cdot V_1}{\lambda} \cdot \cos(\psi) \cdot \cos(\beta/2) \tag{2.7}$$

- **Angular resolution**. A conservative estimation of the distance between two targets lying on the same isorange contour is given by the expresion (2.8) [Willis, 2005], where $\phi_{3dB,T}$ and $\phi_{3dB,R}$, are the -3dB (one way) antenna beamwidths of the transmitting and receiving antennas respectively, and the cross range dimension of the 3dB transmitting beam is assumed larger than the receiver's null-to-null beam cross-range dimension.

$$\Delta R_\phi = \frac{2R_R \phi_{3dB,R}}{cos(\beta/_2)} \tag{2.8}$$

2.2.2   System performance

The radar detection problem can be formulated as a binary hypothesis test, where the system has to decide if target is present (alternative hypothesis, H_1) or absent (null hypothesis, H_0). The Neyman-Pearson detector is widely used in radar applications. It maximizes the P_D, maintaining the P_{FA}, lower than or equal to a given value [Neyman and Pearson, 1933].

System coverage must be defined for specific target and interference models, as the maximum range where a target is detected fulfilling P_D and P_{FA} requirements. In a thermal noise dominated radar scenario, the relation between the detection threshold to be applied to the square-law detector output and the P_{FA} is given by expression (2.9), where $N_0 = kT_0 f_{SYS}$, being k the Boltzman constant ($k = 1.38 \cdot 10^{-23}$), $T_0 = 290K$ the system input noise temperature, and f_{SYS} the noise figure of the whole receiving chain.

$$P_{FA} = e^{\frac{-\gamma}{N_0}} \tag{2.9}$$

The required signal-to-noise ratio at the input of the detector for a specified pair (P_{FA}, P_D), can be determined. Detection curves for $P_{FA} \in \{10^{-8}, 10^{-6}, 10^{-4}\}$ are presented in Figure 2.7 for non-fluctuating targets (snr_{DET} is constant) and Swerling I targets (snr_{DET} is an exponential random variable of mean $\overline{snr}_{DET}$).

2.2.3   System coverage

Given design values of P_D and P_{FA}, the snr at the antenna terminals, snr_{IN}, for the required snr at the detector input, snr_{DET}, must be calculated, being snr the signal-to-noise ratio in natural units, and $SNR(dB) = 10 \cdot log_{10}(snr)$ (Figure 2.7).

snr_{IN} can be calculated using (2.10) for a target with a bistatic radar cross section σ_{bis}, located at R_T and R_R distances, taking into consideration the following parameters:

(a)   (b)
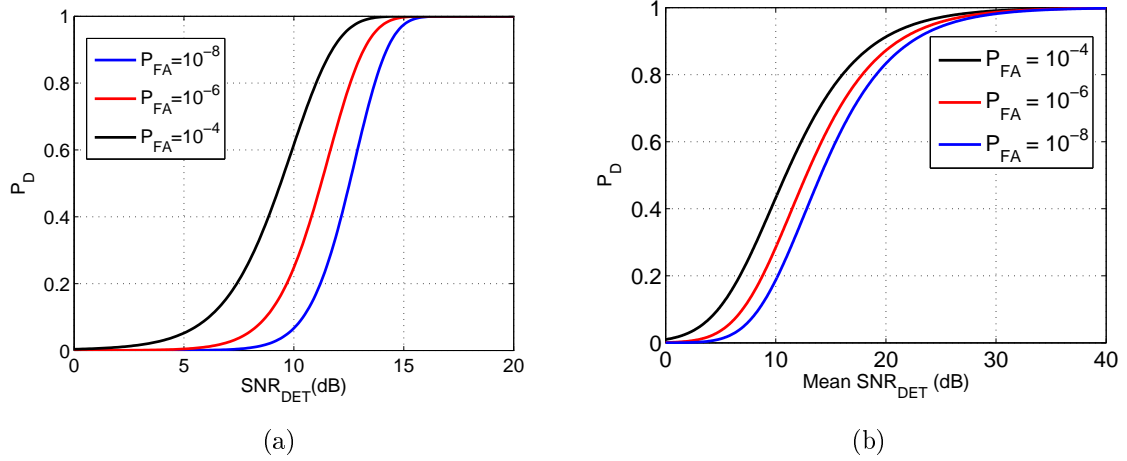
Figure 2.7: Detection curves for the square-law detector in thermal noise interference: non-fluctuating target (a), Swerling I target (b)

- Receiver input noise power characterized by $n_{IN} = k(Ta + T_{ant-con})B$, being T_a the antenna noise temperature, $T_{ant-con}$ the interconnection elements equivalent noise temperature, k the Boltzman constant, and B the receiver effective bandwidth.

- p_T is the IoO transmitted power.

- g_T and g_R are the transmitter and receiver antenna gains respectively.

- λ is the wavelength.

- Free space propagation losses are usually assumed to obtain preliminary results.

$$snr_{IN} = \frac{p_T g_T g_R \lambda^2 \sigma_{bis}}{(4\pi)^3 (R_R R_T)^2} \cdot \frac{1}{k \cdot (Ta + T_{ant-con}) \cdot B} \tag{2.10}$$

Rewriting the above exoression, an estimation of the system coverage can be obtained through the main system paramters and required detection capabilities:

$$(R_R R_T)^2 = \frac{p_T g_T g_R \lambda^2 \sigma_{bis}}{(4\pi)^3 snr_{IN}} \cdot \frac{1}{k \cdot (Ta + T_{ant-con}) \cdot B} \tag{2.11}$$

The loci corresponding to $R_T \cdot R_R =$ constant is known as Cassini's oval. In Figure 2.8, for a baseline length $L = 10km$, coverage limits for $\sqrt{R_R \cdot R_T}$ varying from 4 to 8 km are shown, simulating a variation in the receiver signal intensity. If $L > 2 \cdot \sqrt{R_R \cdot R_T}$ the oval of Cassini breaks into two parts, reducing the coverage area and making mandatory the area of interest of the surveillance channel lies in the coverage region centred on the receiver.
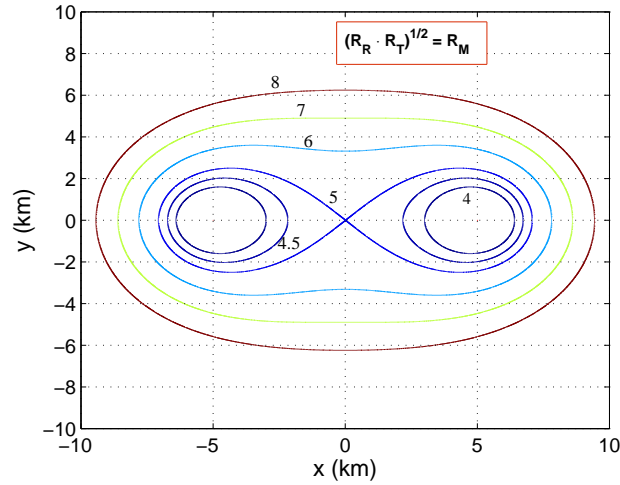
Figure 2.8: Coverage limits for $L = 10km$ and $\sqrt{R_R \cdot R_T}$ varying from 4 to 8 km.

2.2.4   Targets bistatic radar cross section

The Radar Cross Section (RCS) is the parameter used for modelling the power scattered from the target towards the radar receiver, when it is illuminated by the radar transmitter (active radar) or the selected IoO (passive radar). The RCS is defined as a (fictional) area that intercepts a part of the power incident at the target which, if scattered uniformly in all directions, produces an echo power at the radar equal to that produced by the real target [Skolnik, 2008]. This parameter is measured in square meters, and depends on signal frequency and polarization, incidence and scattering angles, and physical and electrical properties of the target.

In monostatic configurations, incidence and scattering directions are the same, but in bistatic configurations the bistatic RCS, BRCS, of a target is a function of the aspect and the bistatic angles. Because of that, its characterization is more complex than in the monostatic case. In the optical region, three bistatic regions are considered: the pseudo-monostatic, the bistatic and the forward scatter.

- **The pseudo-monostatic RCS region** [Skolnik, 2008]. Complex targets defined as an assembly of discrete scattering centers (simple centers such as flat plates, reflex centers such as corner reflectors, skewed reflex centers such as a dihedral with corner $\neq 90°$ and stationary phase regions for creeping waves).

  For small bistatic angles (typically less than 5°), the BRCS of a complex target is equal to the monostatic RCS measured on the bisector of the bistatic angle at a frequency lower by a factor of $\cos(\beta/2)$.

  When the wavelength is small compared with the target dimensions, these complex target models approximate many aircraft, ships, ground vehicles, and some missiles. The targets can be composed of conducting and dielectric materials.

- **The bistatic RCS region** [Skolnik, 2008]: In this region, the bistatic RCS diverges from the monostatic one. Three sources of this divergence for complex targets and for a target aspect angle fixed with respect to the bistatic bisector were identified: changes in relative phase between discrete scattering centers, changes in radiation from discrete scattering centers, and appearance of new centers or disappearance of centers.

  In general, this divergence results in a bistatic RCS lower than the monostatic RCS for complex targets. Exceptions include:

  1. Some target aspect angles that generate a low monostatic RCS and a high bistatic specular RCS at specific bistatic angles.

  2. Targets that are designed for low monostatic RCS over a range of aspect angles.

  3. Shadowing that sometimes occurs in a monostatic geometry, and not in a bistatic one.

  The second exception is somewhat surprising and should be discussed. Stealth technology can be based on target shaping, as well as on the application of radar absorbing materials or structures, or on a combination of both. Such techniques, generally, focus on the reduction of RCS of a target within a so called threat cone around nose-on aspect. Radar wavelengths in the metric dimensions (VHF/UHF) pose a considerable challenge to stealth target engineering, as well as bistatic or multi-static radar system concepts, where the position of the receiver is unknown [Kuschel et al., 2008].

  Another effect than can occur in the bistatic region is the glint reduction: when the returns from dominant scatterers are reduced in the bistatic region, the source and hence the magnitude of glint excursions are reduced.

- **The forward-scatter RCS region** [Skolnik, 2008]. In this region, the bistatic angle approaches 180°. This technology has been specially designed for detecting very low RCS targets. For targets with linear sizes much bigger than wavelength, the forward scattering RCS rises sharply (in $10^3 - 10^4$ times) in comparison with the monostatic RCS [Cherniakov et al., 2010, Sizov et al., 2007].

2.2.5 Bistatic clutter characterization

Clutter refers to all radar echoes generated by objects present in the coverage area that are not considered as desired targets. As targets, point clutter sources are modelled using the (RCS).

Due to the distributed nature of ground clutter, for modelling the energy backscattered by the ground surface when it is illuminated by a transmitter, the scattering coefficient σ^0 is used. It is defined as the clutter radar cross section, $\sigma_{RCS,C}$ per unit area, $\sigma^0 =$

$\sigma_{RCS,C}/A_C$, being A_C the radar clutter resolution cell [Skolnik, 2008]. A_C is a function of the geometry and the signal waveform.

The mainlobe bistatic clutter cell area, $A_{C,bistaic}$ is defined as the intersection of the range cell, the Doppler cell, and the main beam footprint in the area of the ground common to the one-way transmitting and receiving beams [Willis, 2005]. The calculus of $A_{C,bistaic}$ is really complex [Willis and Griffiths, 2007]. In (2.12), an approximation of the range-limited $A_{C,bistaic}$ for small grazing angles and $R_T + R_R >> L$ is presented [Willis, 2005]: $\Delta\phi_R$ is the receiver antenna azimuth beamwidth, B is the signal bandwidth, and β is the bisatic angle.

$$A_{C,bistaic} = \frac{c \cdot R_R \cdot \Delta\phi_R}{2 \cdot B \cdot \cos(\beta/2)^2} \tag{2.12}$$

Bistatic clutter studies are significantly less numerous than monostatic ones. In [Willis and Griffiths, 2007] a detailed review of the bistatic σ^0 database for terrain and sea at microwave and optical frequencies published by Weiner in 1980 is presented. Most of the data were acquired at X band, and no results were presented for VHF nor UHF frequencies. In [Al-Ashwal et al., 2011], monostatic and bistatic sea clutter were measured simultaneously at 2.4 GHz. The K+noise distribution was used for modeling amplitude statistics. In [Malanowski and Kulpa, 2012] two techniques were proposed for modeling the land and sea clutter profiles at FM frequencies. In [Maio et al., 2008] and [Maio et al., 2010], bistatic land clutter was measured at $1,853.6$ and $2,162.6$ MHz. A statistical study of the in phase and in-quadrature components proved their deviation from the Gaussian model. In [Al-Ashwal et al., 2014b] and [Al-Ashwal et al., 2014a] a detailed study of real data at S band was presented: mean σ^0 values and statistical models for clutter amplitude.

2.2.6   Time processing parameters

Reference and surveillance channels collected data are divided into data segments of T_{int} s (Coherent Processing Intervals, CPIs), using a periodic pulse train with a selected Pulse Repetition Interval (PRI) (Figure 2.9).
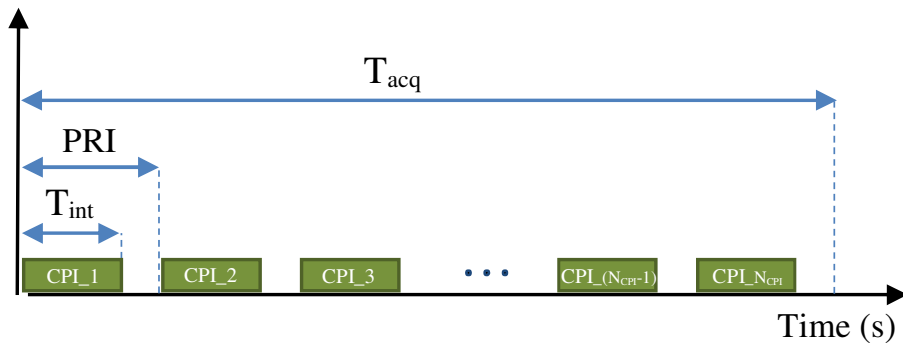
Figure 2.9: Time processing parameters definition

Taking into consideration desired targets dynamics, Doppler resolution and processing techniques to be applied, T_{int} and PRI are selected. In many cases, $T_{int} = PRI$. A Range-Doppler Surface (RDS) is generated for each CPI. The associated integration gain is defined by T_{int}. Preprocessing and detection techniques are also applied to each CPI, while the traking techniques operate on the generated plots at a data updating rate equal to PRI.

Time parameters must be carefully selected considering their impact on the different processing stages and system parameters:

- The higher T_{int}, the higher the CAF processing gain, but also the associated computational cost.

- To exploit all the possible integration gain, during T_{int} the target must be illuminated, and a targets dynamic study is required to minimize the target lack of focus due to its movement.

- System Doppler resolution is defined as $1/T_{int}$, so the higher T_{int}, the higher the Doppler resolution.

- PRI determines potential time integrations applied in the detection stage. This time integration capability is critically limited by desired targets size and dynamics, system resolution, and the application of range-Doppler migration compensation techniques.

- PRI defined the tracker data updating rate, and affects tracker manoeuvre detection performance.

Chapter 3

Digital signals as IoOs

3.1 Introduction

Numerous works can be found in radar literature that focus on the study of the IoO waveform, using the Ambiguity Function (AF) as the main analysis tool. The analysis of the AF of a waveform allows a fairly accurate estimation of the radar system resolutions, and the prediction of potential ambiguities.

In this chapter, the definition and main properties of the AF are summarized and different digital communications waveforms are studied. A comparative study of several mobile communications and broadcasting commercial digital signals is presented, from a radar engineer point of view, in order to determine their impact on the final passive radar system performance. The study is completed with the study of a radar signal consisting in a set of coherent Linear Frequency Modulated, LFM, pulses, designed for Synthetic Aperture Radar applications.

3.2 The ambiguity function

The Ambiguity Function (AF) is a key tool for analysing the main properties of a waveform for radar detection purposes. It describes how a signal is correlated with itself delayed in time by an amount τ, and shifted in frequency an amount f. It is also known as the time-frequency autocorrelation function. The Doppler-sensitive autocorrelation function performs two important tasks:

- It provides the necessary signal processing gain to allow detection of the target echo, acting as a matched filter for the radar system.

- It allows the estimation of the bistatic range and Doppler shift of the target.

The AF is a two dimensional function (3.1):

$$s_{AF}(\tau, f) = \frac{1}{T_{int}} \int_0^{T_{int}} x(\nu) x^*(\nu - \tau) \exp{-j2\pi f \nu} d\nu \qquad (3.1)$$

A discrete-time implementation of the AF is shown in expression 3.2:

$$s_{AF}[m, p] = \sum_{n=0}^{N-1} s[n] \cdot s^*[n - m] \cdot \exp(-j2\pi \frac{p}{N} n) \qquad (3.2)$$

- T_{int} and f_s are the coherent processing time and the sampling frequency, respectively.

- $N = T_{int} \cdot f_s$ is the number of samples.

- m represents the time bin associated with a delay $\tau_m = \frac{m}{f_s}$.

- p is the Doppler bin corresponding to Doppler shift $f_{D_p} = f_s \cdot \left(\frac{p}{N}\right)$.

- $s[n] = x(n/f_s)$.

The AF has the following properties that must be taken into account in the IoO selection:

1. The maximum of the absolute value of the AF always appears at the origin.

2. The magnitude of the AF is symmetric with respect to the origin: $|s_{AF}[m, p]| = |s_{AF}[-m, -p]|$.

3. The value of the AF at the origin is related to the energy of the signal: $|s_{AF}[0, 0]| = |\sum_{n=0}^{N-1} |s[n]|^2|$

4. In a PBR system, when the AF is applied to the reference and surveillance signals, it has a maximum at the pair (τ_0, f_d), that is the Maximum Likelihood estimation of the relative delay, τ, and Doppler, f_D, shift values between both signals and directly related to the target echoes parameters.

5. The cut of the AF along the frequency axis allows the study of frequency resolution. This cut is expressed as the Fourier transform of the squared amplitude of the signal.

6. The cut along the delay axis is the autocorrelation of the signal, that is related to the Energy Spectral Density of the signal through the Fourier transform. The delay resolution will depend on the signal bandwidth.

3.2.1 Range and Doppler Resolutions

The resolution in delay estimation is inversely proportional to the signal bandwidth. In monostatic radars, the relation between delay and target-to-radar distance is calculated as: $\Delta R = c/(2 \cdot B)$, being c the light speed and B the signal bandwidth. The AF cut for zero Doppler is the autocorrelation of the signal, but it can be also interpreted as the output of the matched filter for different signal delays, allowing the study of the system range resolution.

The AF cut for zero delay provides information about the response of the matched filter to targets with a zero delay, but with a Doppler shift different from zero. The Doppler resolution is inversely proportional to signal length. It is determined by the amplitude modulation of the signal, and not by the phase.

3.2.2 Types of AFs

The AFs (or the waveforms which produce them) can be classified in three different classes [Rihaczek, 1971]:

- **Class A**: The AF consists of a ridge along $\tau = 0$ or $f = 0$, and is typical of waveforms for which the product of length and bandwidth is approximately unity. The waveforms with this class of AF can provide good resolution in time or Doppler, but not both at the same time. An example is shown in Figure 3.1.
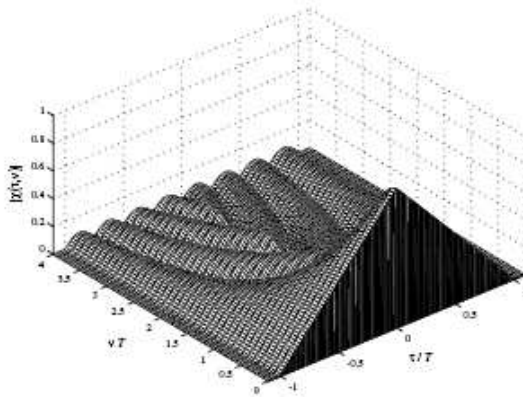
Figure 3.1: Class A ambiguity function example [Levanon and Monzeson, 2004].

- **Class B1**: These waveforms are noise-like, and are almost uncorrelated with themselves. The AF consists of a spike at the origin with the largest part of the volume distributed in a low level pedestal. There exists an inverse relationship between the length, the bandwidth, and the volume of the spike at the origin (Figure 3.2).

  This class of waveforms can resolve targets very well in both time delay and Doppler shift, if long durations and high bandwidths are used, but the targets with low RCS

can be masked by the pedestal. Long pseudo-random sequences are good examples
of Class B1 waveforms.
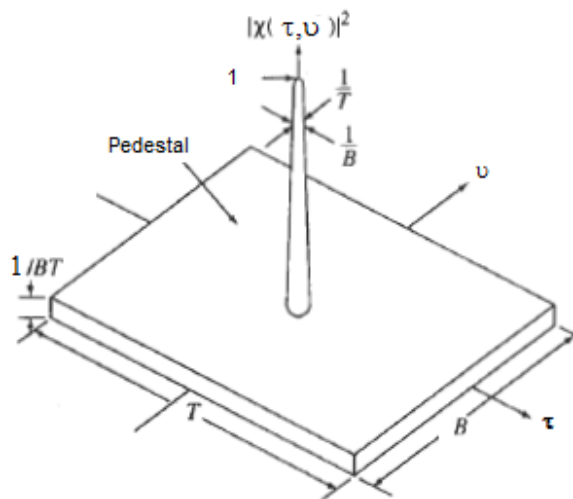
Figure 3.2: Class B1 ambiguity function example [Levanon and Monzeson, 2004].

- **Class B2**: The AF consists of a ridge oriented at an angle to the axis. The
  waveforms are non-periodic deterministic signals, with a length-bandwidth product
  much bigger than unity. They are obtained by modulating a class A signal (Figure
  3.3).

3.2.3   Periodic Ambiguity Function. Type C signals

Signaling and synchronization components of digital communication systems waveforms
are periodic, and produce ambiguity peaks in the AF. They can be explained by studying
the Periodic Ambiguity Function (PAF), which was introduced for the purpose of analyz-
ing the response of a filter matched to a finite interval T_f of a Continuous Waveform (CW)
signal, modulated by a periodic waveform $u(t)$ with period T_0 [Levanon and Monzeson,
2004,Freedman and Levanon, 1994].

A CW signal is an infinite duration signal with constant amplitude and frequency, and
the PAF can be defined with the following expression:

$$s_{PAF}(\tau, f) = \frac{1}{T_f} \int_0^{T_f} u(t)x^*(t - \tau) \exp{-j2\pi ft} dt \qquad (3.3)$$

The multiperiod PAF (T_f is a multiple of T_0, the period of the periodic signal) can be
related to the ambiguity function of the finite duration signal of one period. The single
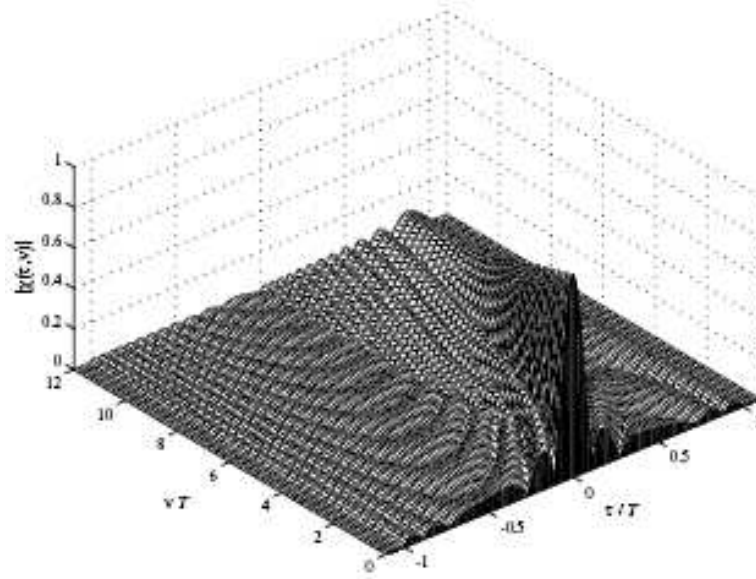
Figure 3.3: Class B2 ambiguity function example [Levanon and Monzeson, 2004].

pediod PAF is multiplied by a function to obtain the multiperiod PAF. This function presents peaks at frequencies that are multiples of T_0^{-1}, and nulls at frequencies that are integer multiples of $(T_0 \cdot N)^{-1}$, except $f = kT_0^{-1}$. These nulls correspond to Doppler frequencies that cannot be detected. In (3.4), the PAF of a set of N periods, $s_{PAF,NT}(\tau, f)$ is expressed as the product of the one period AF $s_{AF,T}(\tau, f)$ and the defined function (Figure 3.4):

$$s_{PAF,NT}(\tau, f) = s_{AF,T}(\tau, f) \cdot \frac{\sin(\pi \cdot f \cdot N \cdot T)}{N \cdot \sin(\pi \cdot T)} \cdot \exp\left(j\pi \cdot f \cdot (N-1) \cdot T\right) \tag{3.4}$$

In this case, the cut along the delay axis ($f = 0$) is the periodic autocorrelation of u(t), and the cut along the Doppler axis ($\tau = 0$) is the Fourier transform of $|u(t)|^2$. As the periodic autocorrelation of u(t) is also periodic with the same period, the cut of the PAF along the frequency axis is periodic with the same period T.

All these properties should be taken into consideration in the analysis of different IoOs, because they can impose some constraints to the Doppler frequencies or delays of the target in order to be detected without ambiguity

Type C signals include all deterministic periodic waveforms. In Figure 3.5 the PAF of N periods of a signal composed by rectangular pulses of length T with a pulse repetition interval T_r is depicted.
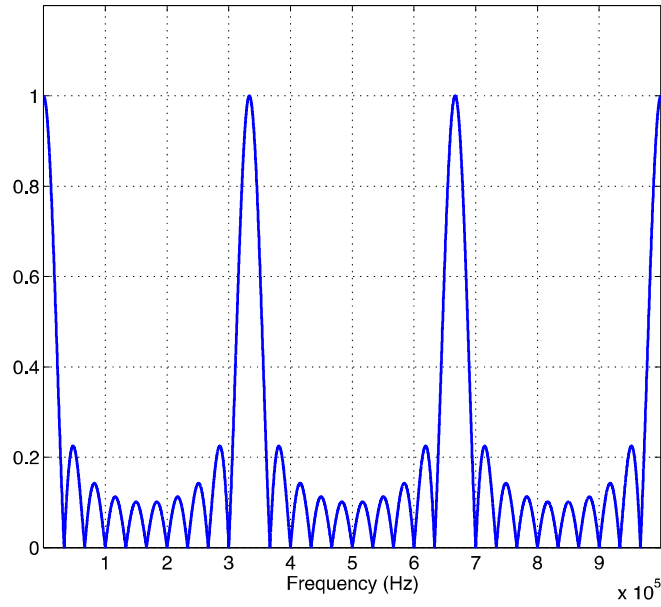
Figure 3.4: $|\frac{\sin(\pi \cdot f \cdot N \cdot T)}{N \cdot \sin(\pi \cdot T)}|$ for $N = 10$, $T = 3 \cdot 10^{-6}$ s, and $f \in (0,1)MHz$.
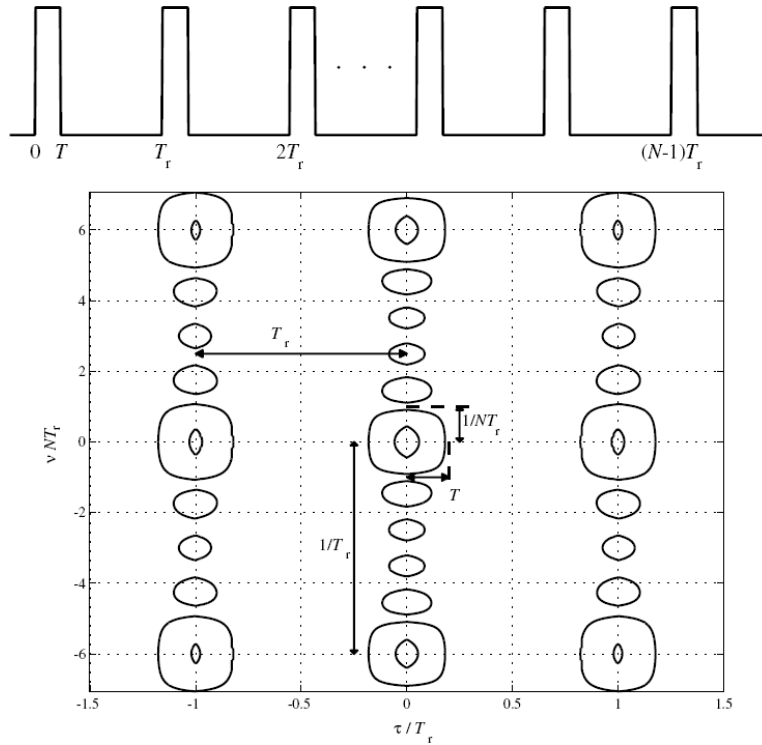
Figure 3.5: Class C ambiguity function example [Levanon and Monzeson, 2004].

3.3   IoO selection

Many published studies focus on the analysis of IoOs waveforms using the AF. But there are other characteristics that must be also considered:

- **Reliability of IoO**: the IoO must be available in the geographical Area of Interest (AoI), or at least, it should be possible to predict when and where it fulfils this condition.

- **Known position**: the IoO should have a known position or, at least, it should be possible to locate it easily in order to estimate the target position from the radar system measurements [Willis, 2005].

- **Known waveform**: the IoO should have a known waveform in order to allow optimum reception and detection with appropriate signal processing.

- **Signal bandwidth**: It should be large enough to ensure the required range resolution.

- **Signal source power levels**: They should be high enough to accomplish with the performance requirements of the radar application. Technological limitations can impose input signal sensitivity and SNR performance limitations, which ultimately bound the radar performance.

- **Area illuminated by the IoO**: The IoO should illuminate the passive radar and the target simultaneously, allowing the acquisition of the target echo and the reference signal for matched filtering.

- **Target Illumination time for passive radar applications**: The signal should have enough length to allow coherent time processing required for target detection.

3.4   DVB-T Broadcasting as IoO

Digital signals reached great relevance against analogue ones due to their bigger and information content independent bandwidths [Baker et al., 2005, Griffiths and Baker, 2005a]. Among them, Digital Video Broadcasting-Terrestrial (DVB-T) is of special interest due to its availability, transmitted power and waveform [Saini and M.Cherniakov, 2005, Ruck et al., 2009, Barcena-Humanes et al., 2014, O Hagan et al., 2014, Bolvardi et al., 2015].

DVB-T is the Digital Television Broadcast transmission standard most used in the European Union. It feasibility as PBR waveform has been studied in radar literature [Saini and M.Cherniakov, 2005]. In this section, a brief summary is presented, focussing on the exploitation of consecutive DVB-T channels for increasing signal bandwidth and, consequently, PBR range resolution.

Table 3.1: Configuration modes of the DVB-T signal

Mode	2k	8K
Number of carriers, K_c	1705	6817
Symbol length, T_u	224 μs	896 μs
Guard Interval length, $\Delta(1/4)$	56 μs	224 μs
Carrier modulation	64-QAM	64-QAM
Total bandwidth	7.61 MHz	7.61 MHz

In Table 3.1 the transmission modes enumerated in the ETSI standard, [300-744, 1999], are summarized. The single channel bandwidth is assumed as $7.61MHz$. with a monostatic range resolution approximately equal to $20m$, but this resolution can be improved using multichannel signals.

The Ambiguity Function is the basic tool for analyzing detection capabilities of waveforms. Its expression can be obtained substituying $s_{SURV}[n]$ by s_{REF} in (2.1). The general DVB-T signal generation scheme is presented in Figure 3.6 [300-744, 1999, Saini and M.Cherniakov, 2005].
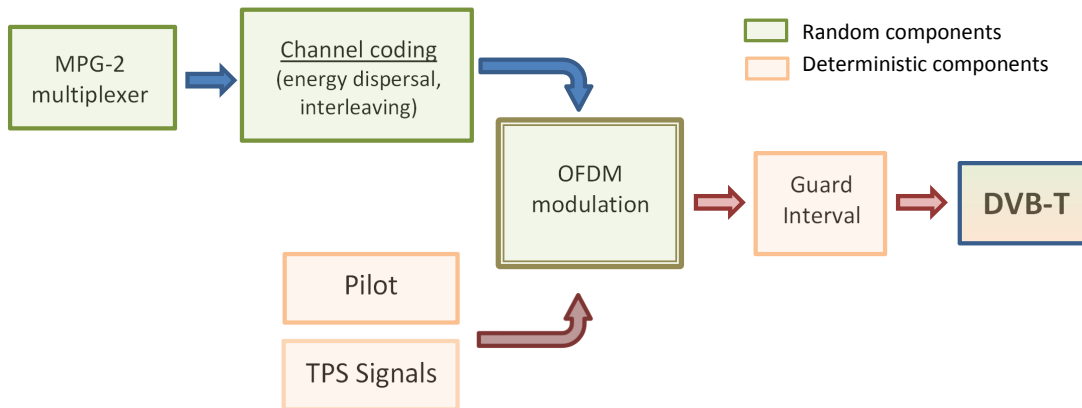
Figure 3.6: Basic scheme of DVB-T transmission system

- The random signal component is a B1 class waveform, whose AF consists of a spike at the origin with the largest part of the volume distributed in a low level pedestal ("thumbtack" function). This class of waveforms can resolve targets in both time delay and Doppler shift, if long integration times and high bandwidths are used, but the targets with low RCS can be masked by the pedestal [Rihaczek, 1971].

- The deterministic component is generated by Pilot Carriers (PC), Transport Parameters Signalling (TPS) and the Guard Interval (GI). They have well known positions into the transmission frame, and generate high correlation peaks in the range-Doppler map, their positions are summarized in Table 3.2.

Table 3.2: Ambiguity peaks location in the range domain

Mode	GI peaks (km)	Scattered PC (km)	Continual PC (km)	TPS (km)
2k, $T_U = 224\mu s$	Every 33.6	Every 2.8 & 138.6	Every 11.2 & 34.65	34.65
8k, $T_U = 896\mu s$	Every 134.4	Every 11.2 & 554.4	Every 44.8 & 138.6	138.6

The 3D AF of a signal composed by a real DVB-T channel is depicted in Figure 3.4. The aforementioned ambiguity peaks distribution it is shown in Figure 3.4where the first peak pattern is clearly presented. Deep studies about the effect of these deterministic components, can be found in [Saini and Cherniakov, 2002, Saini and M.Cherniakov, 2005, Conti et al., 2011, Conti et al., 2012, Barcena-Humanes et al., 2014].

(a) 3D   (b) AF zero Doppler cut
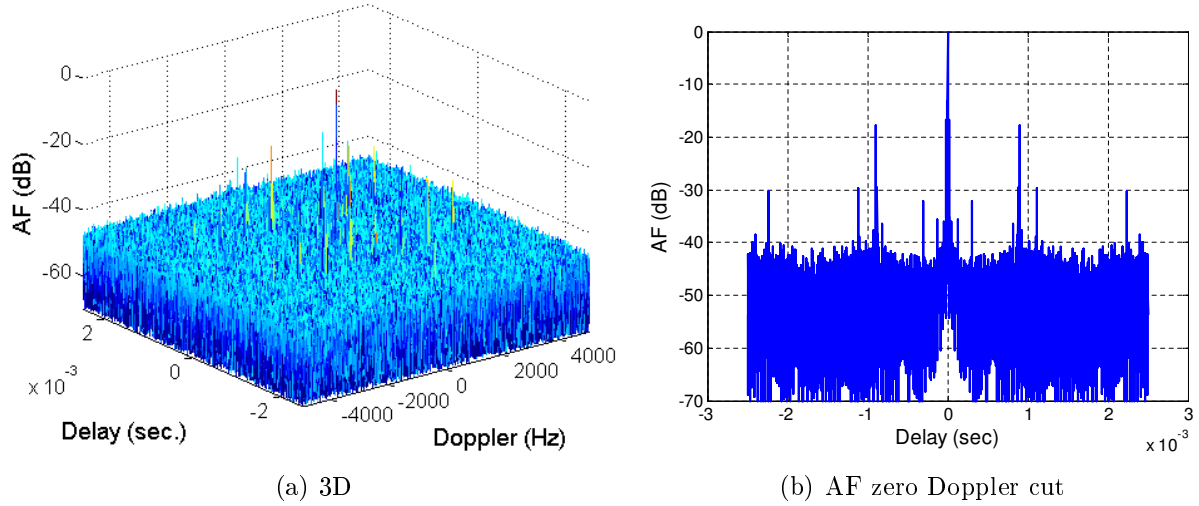
Figure 3.7: AF of an acquired DVB-T channel

The DVB-T broadcasting configuration can allow, if consecutive channels are available, the use of more than only one. As the signal bandwidth its increased, an improvement in the expected system range resolution can be achieved. An additional consequence of using consecutive channels is the reduction on the AF pedestal level due to the B1 noise-like signals AF characteristics: the pedestal levels is controlled by the $\frac{1}{BT}$ value. This level determines the ratio between the main lobe level and the noise one. Then, through the use of multiple consecutive channel, the SNR of the AF is slightly improved. In Figure 3.8, the AF of a real 8K mode signal composed by three consecutive channels is presented. The "thumbtack" function centered on $(0,0)$ is observed, together with ambiguity peaks generated by the deterministic components. In Figure 3.9 a comparison between the zero-Doppler cut of the AF using one, two and three consecutive channels is depicted showing the commented pedestal level improvement.

In Table 3.3, the conclusions about the suitability of the DVB-T signal as IoO in passive radar applications are summarized.

Table 3.3: Main features of DVB-T signals as IoO in passive radars.

Characteristics	DVB-T as IoO in passive radar
Reliability of the IoO	- Emitter locations are fixed. - The bandwidth is not data dependent.
Known position	- Emitters location are public and accessible to everyone.
Known waveform	- The characteristics of the transmitter waveform and its bandwidth are known. - There is no uncertainty in range resolution. - There are ambiguity peaks in the range domain, due the deterministic components, but can be avoided using signal processing. - There exits ambiguity peaks in the Doppler domain, that generate ambiguity velocity peaks, but the values of ambiguity velocities are high enough for most of the applications.
Signal bandwidth	- The DVB-T signal bandwidth is constant, and high enough to obtain range resolutions of about 20m.
Signal source power levels	- High enough to ensure a big coverage area.
Area iluminated by the IoO	- Both the target and the radar can be easily illuminated at the same time.
Target illumination time for passive radar applications	- Due to signal continuous transmission, the target illumination time is only limited by the coverage of the selected IoO and the target dynamics.

(a)
(b)

Figure 3.8: Real multichannel signal (a). Ambiguity function (b)
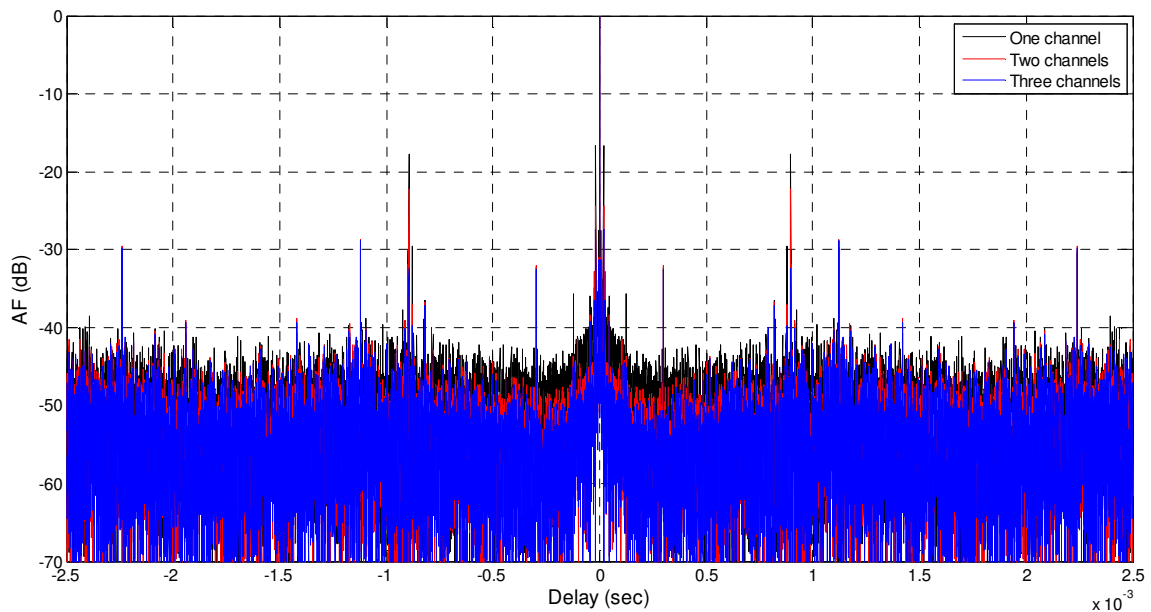
Figure 3.9: AF comparison between using one and three consecutive channels.

3.5 Space-Borne illuminators

Space-born emitters, such as communication, global positioning and Digital Video Broadcasting satellites, have some characteristics that make them suitable to be used as IoOs. They are mainly related to the use of higher frequencies, which reduces de physical sizes of the antennas, big bandwidths and the possibility of almost global availability. On the other hand, some drawbacks must be taken into consideration:

- The big distance between target and transmitter gives rise to very low scattered power from the target. Increasing the transmitter power is very difficult, due to power supply limitations in space platforms.

- Target-to-transmitter range is much longer than the target-to-receiver range. Because of that, Cassini ovals are split into two coverage areas, one centered on the transmitter and the other is centered on the receiver.

- An important reduction of the passive radar coverage is expected compared to that achievable using DVB-T transmitters.

- The bistatic angle can be too high, giving rise to a poor range resolution.

In [Cherniakov et al., 2008], an analysis about the power issue in the space-born IoO is presented. Considering only the power level, the most promising space-born IoO are the new digital video broadcasting satellites W2A and I-4 EMEA. These new satellites have more directive antennas, but the transmitted power is almost the same. The main disadvantage of these satellites is that they are geostationary. This means that they are above the Equator and there are target positions with a bistatic angle close to 180°, giving rise to unacceptable range resolutions. The "spot beam" GPS is expected to be able to provide an increase in received power on the Earth surface of 20dB. In these systems, new problems related to the low orbit of the emitters and their non-constant coverage area, must be addressed.

3.5.1   Digital Video Broadcasting - Satellite

In this section, DVB-S commercial broadcasting signals are considered, so all the study focusses on geostationary satellites. The DVB-S standard dates from 1994 and only specifies the characteristics of the physical link and framing, and describes the modulation and channel coding system for satellite television (multi-programme and High Definition Television). It uses the MPEG-2 video codec, and is suitable to be used on different satellite transponder bandwidths. DVB-S2 defines a "second generation" of satellite broadcasting, with improved modulation and channel coding stages. The new standard dates from 2005, and improves the previous one in the coding and modulation blocks but it does not specify any constraints about carrier frequency or transmission bandwidth that are characteristics of the satellite transponder. In fact, the standard is defined as the functional block diagram of equipment performing the adaptation of the baseband digital signals from the output of a single or multiple data sources (MPEG transport for example) to the satellite channel characteristics.

The DVB-S2 standard, [302-307, 2009], specifies the following application areas: Broadcast services, Interactive services, Digital Satellite News Gathering (DSNG) and Professional services. Different configurations for each application area are possible, but not all of them are suitable for being used as IoO: there is a configuration mode that changes the modulation characteristics and the code ratios frame to frame, to achieve the best performance. In a passive bistatic radar system, the variability of the IoO characteristics with time must be avoided.

In Figure 3.10 the main blocks of the global architecture of the DVB-S2 signal is presented. Those stages grouped in red are those that can generate ambiguity peaks, considering the data stream at the input of that group as a pseudo-random sequence. There are two stages that could generate repetitive patterns that must be taken into account to obtain the possible range ambiguity peaks:

- In the Physical layer framing block, the data stream provided by the bit-mapper (XFECFRAME) is divided in slots of 90 symbols, then a header symbols, the Physical Layer Header (PLHEADER), are added to a set of slots in order to form the Physical Layer frame (PLFRAME). If the characteristics of modulation are constant during transmission, the whole PLHEADER will be repeated every frame. In other cases, only the Star of Frame code (SOF), a small portion at the start of the PLHEADER, will be repeated.

- In the transmission mode with pilot blocks, they are included every 16 slots (i.e. every 16x90 symbols). This pattern generates a range ambiguity peak in the ambiguity function that must be taken into consideration.
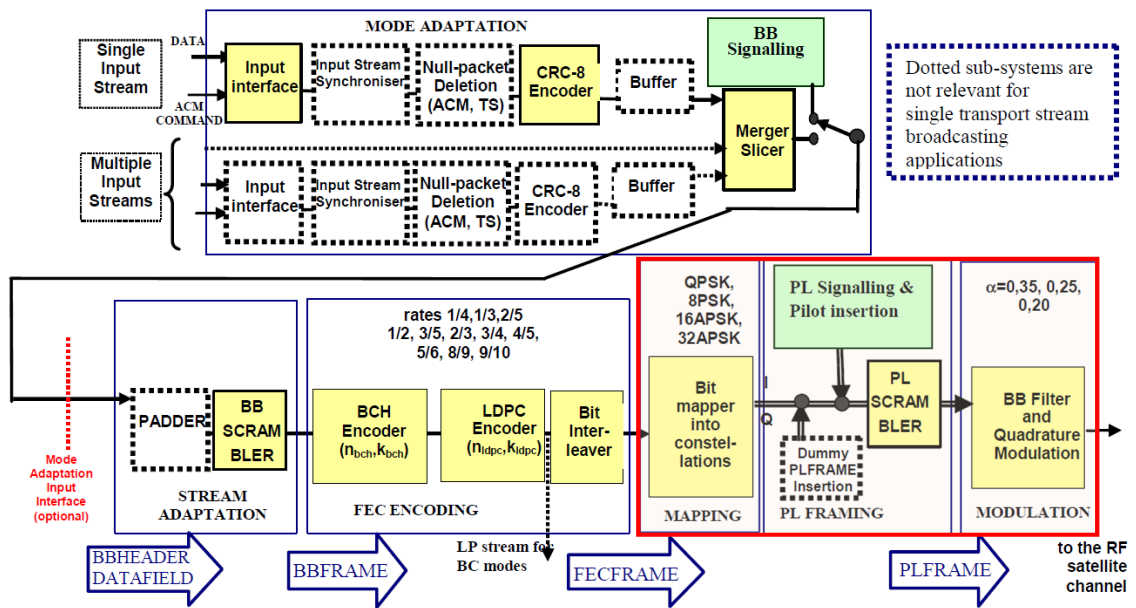
Figure 3.10: DVB-S signal generation block diagram, [302-307, 2009]

The PLFRAME, excluding the PLHEADER, will be randomised for energy dispersal by multiplying the complex value by a random sequence. The influence of the scrambling process in the repetitive patterns that have been found in the PLFRAME must be also studied:

- As Scrambling is not applied to the PLHEADER, the sequence is still periodic after the process, and the ambiguity peaks generated are still relevant.

- The ambiguities associated with the pilot blocks are not completely removed. The scrambling code will be reset at the end of each PLHEADER. Therefore, the scrambling code will be the same from the pilot block from one frame to the equivalent block in the next frame. The same repetitive pattern from one frame to the next remains (which has the same time interval than the header), but the inter-pilot block pattern disappears.

For obtaining the range ambiguity value, the satellite transponder bandwidth must be known, and the length of the PLFRAME, that depends on the length of the FECFRAME, frame form the stages before modulation, on the characteristics of the bit mapping and on the number of pilot symbols in the transmitted signals, shall be calculated using equation (3.5), for a DVB-S signal with $\mu mod = 2$, corresponding to a QPSK modulation, and with pilots incorporated, (the length of the PLFRAME changes if the pilots symbols are added or not).

$$l_{PLFRAME} = (360 + 1) \cdot 90 + \frac{360 + 1}{16} \cdot 32 = 361 \cdot 90 + 22 \cdot 32 \, [Symb] \qquad (3.5)$$

As transmitted bandwidth and carrier frequency are determined by the satellite characteristics, the locations of the aforementioned ambiguity peaks are transponder dependent. Simulated signal was generated assuming HISPASAT satellite transponder: a roll factor of the modulation raise cosine of $\alpha = 0.35$, QPSK modulation (parallelism level = 2), and a transponder with a bandwidth of 36MHz were considered. The range ambiguity derived from the PLFRAME frame repetitions can be obtained, before obtaining the frame duration T_{FRAME} equation (3.6):

$$T_{Frame} = \Delta\tau = \frac{33.194}{R_S} = 1.245ms \qquad (3.6)$$

where R_S is the transmitted signal symbol rate that depends on the signal bandwidth and on α, equation (3.7):

$$Rs = \frac{B}{1 - \alpha} \qquad (3.7)$$

For the selected modulation and satellite transponder $l_{PLFRAME} = 33.194$, $R_S = 26.67MB$, giving rise to a frame duration of $T_{FRAME} = 1.245$ms. This value is associated with a monostatic equivalente range of 186.75 km, being great enough to have no relevance in most of the situations. Furthermore, the randomized nature of the signal gives rise to a very good AF. In Figure 3.11(a), the 3D ambiguity function of the simulated transmitted signal, assuming an integration time of 25 ms is presented. The range resolution and ambiguities can be seen in Figure 3.11(b). Their position in the delay axis is located at 1.245 ms (186.75km in the range axis).

In order to check the influence of the satellite transponder bandwidth, the same process has been implemented using a 33 MHz satellite transponder. The new ambiguity peaks are located at 1.354 ms, corresponding to 203.8km in the range axis (Figure 3.12).

(a) 3D
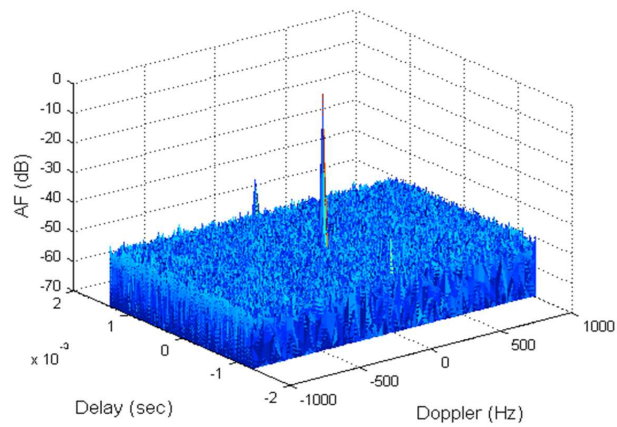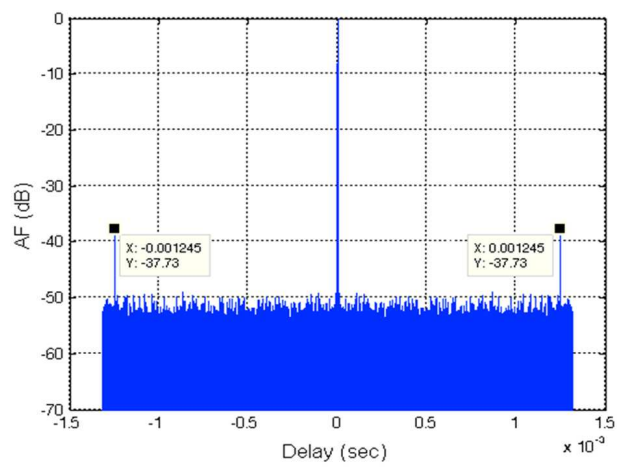
(b) AF zero Doppler cut

Figure 3.11: AF obtained for a 36 MHz satellite transponder
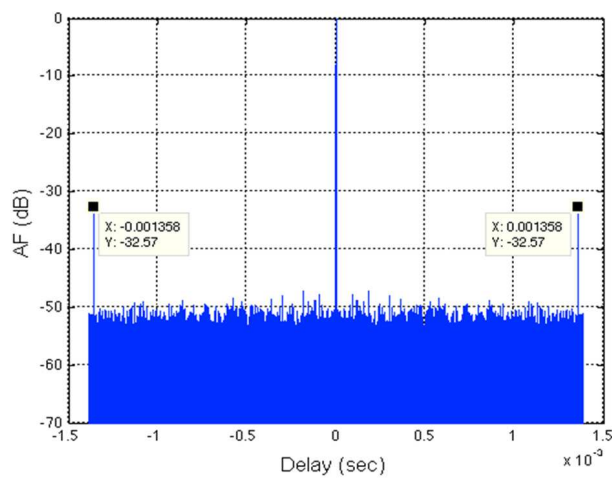
Figure 3.12: Range ambiguities peaks for a 33 MHz satellite transponder

Table 3.4: Main features of DVB-S signals as IoO in passive radars.

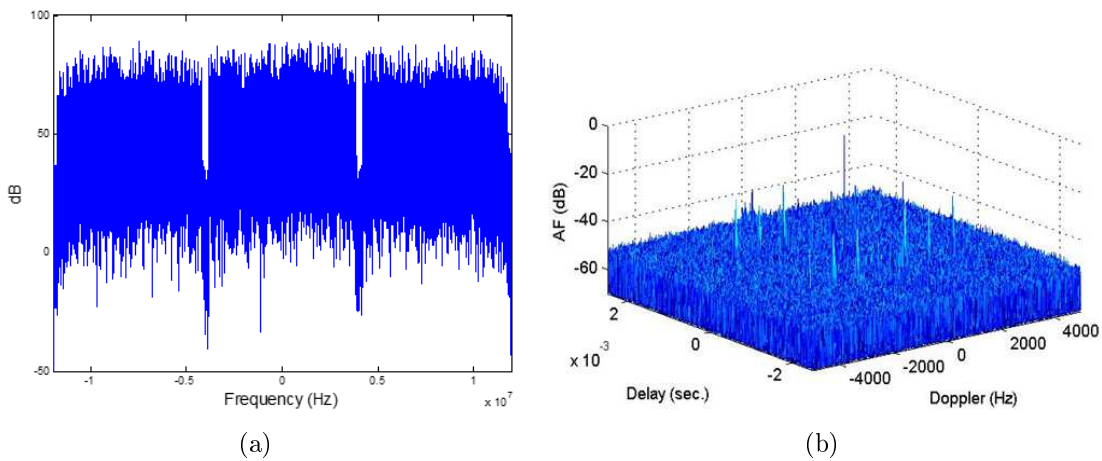| Characteristics	DVB-S2 as IoO in passive radar
Reliability of the IoO	- The bandwidth is not data dependent. - Continouos transmission with a fixed power.
Known position	- Emitters location are public and accessible to everyone.
Known waveform	- The characteristics of the transmitter waveform and its bandwidth are known. - There is no uncertainty in range resolution. - There are ambiguity peaks in the range domain that depend on the satellite transponder characteristcs.
Signal bandwidth	- The B is constant, and high enough to obtain range resolutions of about 4 m (it depends on the satellite transponder).
Signal source power levels	- Power levels are very high but the attenuation due to the large distances makes the receiver echo power very low.
Area illuminated by the IoO	- Both the target and the radar can be illuminated at the same time, but additional considerations about the system geometry must be taken into account.
Target illumination time for passive radar applications	- Due to signal continuous transmission, the target illumination time is only limited by the coverage of the selected IoO and the target dynamics.

In Table 3.4 the main conclusions about the suitability of the DVB-S signal as IoO in passive radar have been summarized.

3.5.2   Coherent LFM pulse train

In this PhD Thesis, passive radar systems exploiting satellite IoOs were also considered. A feasibility study of Earth Observation Synthetic Aperture Radar, EO-SAR, as IoOs was performed. In this section, the analysis of a basic radar signal used in EO-SAR sensors is presented. The use of radar signals was expected to provide significant advantages with respect to commercial broadcasting ones. In this section, the study of the coherent train of LFM pulses is presented, because in the considered passive radar application, the coherent processing time will be longer than the pulse duration, so the matching filtering stage is different from that used for SAR images generation, [Bárcena-Humanes et al.,

2015].

The AF of a synthetic signal is depicted in Figures 3.13 and 3.14. The synthetic signal was generated with the following parameters:

- Pulse Repetition Frequency, PRF = 3.03886 kHz

- Duty cycle, $\tau = 19\%$.

- Modulation factor, $k_r = 2.0383 \cdot 10^{12}$ Hz/s

- Bandwidth, $\Delta B = 127.44$ MHz

- Pulse duration, $T = 62.523\mu$ s.

- Number of LFM (Linear Frequency Modulation) pulses, 50.
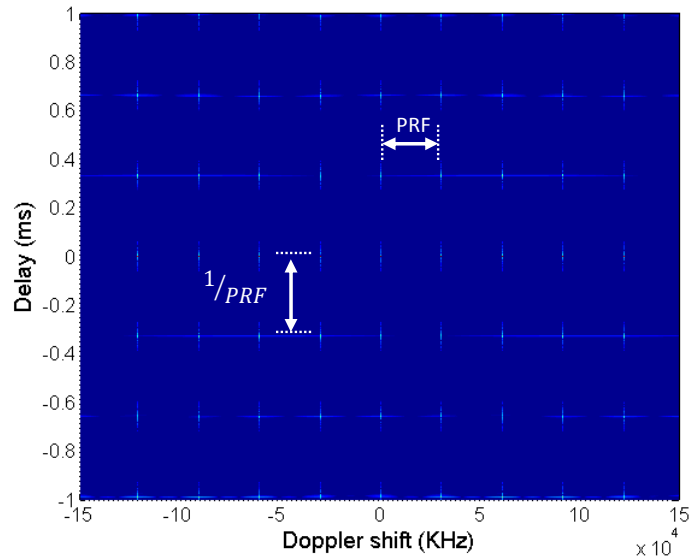
Figure 3.13: Ambiguity function (AF) estimation for a synthetic signal composed of a set of LFM pulses.

The ambiguity peak pattern predicted in [Levanon and Monzeson, 2004] can be clearly identified along the time delay dimension, with a period equal to $\frac{1}{PRF}$, and also along Doppler shift dimension with a period equal to PRF.
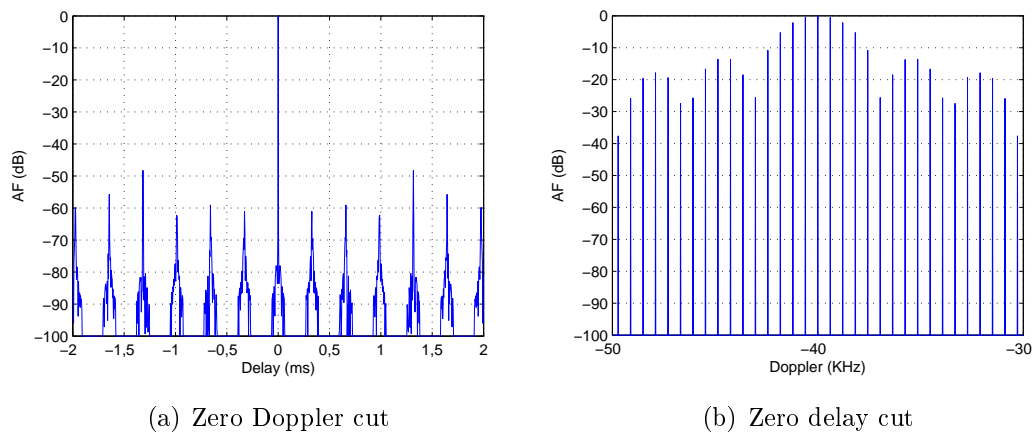
(a) Zero Doppler cut

(b) Zero delay cut

Figure 3.14: AF main cuts.

Chapter 4

Adaptive Filtering Fundamentals

In previous chapters the problems that must be faced in the design of a passive radar were enumerated. Among them, the degradation in the detection capabilities that DPI and other interferences give rise, is one of the most relevant. Nowadays there are numerous analyses and studies aimed at the suppression of DPI as set forth in [Colone et al., 2006], [Saini et al., 2003] and [Wu et al., 2012a], which are based on the adaptive algorithms ability to follow the variations of the signal. The main problem these algorithms currently present are the evaluation of their impact in the system performance and their high computational cost.

4.1 Adaptive Filtering basic principles

In the statistical approach to the linear filtering problem, prior knowledge of certain statistical parameters of the signal and of the undesired additive noise is assumed. When the prior signal information is not available, adaptive filters can be used due its recursive operation: they are able to follow slow time varying signals. Only FIR filters are taken into consideration in order to avoid feedbacks in the filter structures.

Taking the Wiener-Kolmogorov scheme as the starting point for most of adaptive filters, a basic filter scheme is presented in Figure 4.1, [Diniz, 2008] and [Haykin, 2008]. The transversal filter is composed of only three basic elements: time delay units, multipliers and adders. Assuming a filter order of K-1, the structure consist on K-1 delays and adders and K multipliers or weighs.

For a given time instant *(n)*, the filter output *y(n)* is an estimation of the desired signal *d(n)*. The main aim of this structure is minimizing e(n), defined as the difference between the desired signal and the output of the filter $e[n] = d(n) - y(n)$, according to a previously defined cost function, through the calculus of a weight vector $\mathbf{W}_{n,K} = [w_{n,0}, w_{n,1}, w_{n,2}, \cdots w_{n,K-1}]$ for each time instant n. The definition of the target function that depends on $e(n)$, and the selected approach for minimizing it will determine the implemented solution and will be key points in the adaptive filtering selection:
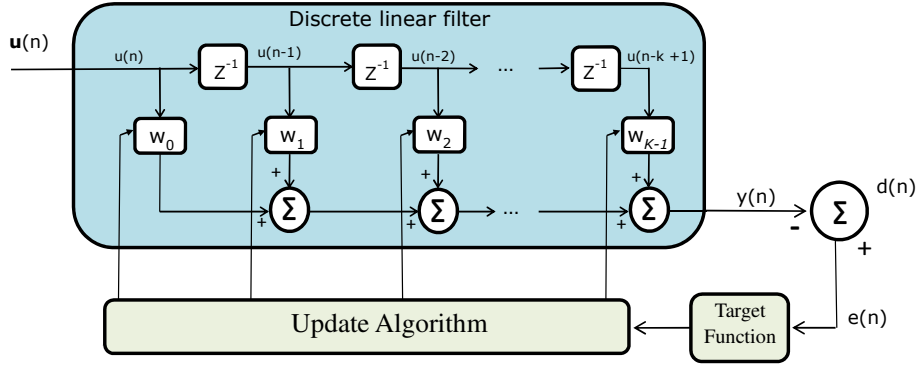
Figure 4.1: Transversal filter scheme.

- **Performance function definition:** The selection of the function to be minimized by the algorithm strongly affects its complexity, convergence and stability. One of the most common target functions is the Mean Squared Error, MSE: $F[e(k)] = E[|e(k)|^2]$, where E denotes the expectation operation. Different mean squared error estimators were proposed:

  1. Sum of Squares Error (SSE): $F_{SSE}(k) = \sum_{i=0}^{L-1} |e(k-i)|^2$. The value of L is a compromise solution between the estimation error accuracy, and the changes on the input signal properties.

  2. Weight Least Squares (WLS): $F_{WLS}(k) = \sum_{i=0}^{L-1} \lambda^i |e(k-i)|^2]$, with $\lambda < 1$.

  3. Instantaneous Squared Value (ISV): $F_{ISV}(k) = |e(k)|^2$.

- **Performance function minimization algorithm definition:** Taking into consideration that the main objective is the minimization of the selected performance function, the way in witch this task is afforded depends on the optimization approach selected. A adaptive process based on minimization descent methods is presented in (4.1), where Δ is the algorithm update term based on performance function gradient and α_K is a non-negative scalar that minimizes $F[e(k)]$ and generally is a function of the weight vector:

$$(n+1) = d(n) + \alpha_K \Delta F[e(k)] \tag{4.1}$$

Newtown's, Quasi-Newton's and Steepest Descent methods are widely applied. The convergence time (time that the system takes to obtain a stable output response) and the computational complexity of the selected adaptive filtering strategy mainly depend on this algorithm selection.

In order to clarify how the transversal filter scheme can be used in the Zero-Doppler interference suppression context, signal models of the reference, $S_{REF}(n)$, and surveillance, $S_{SURV}(n)$, channels are presented in (4.2).
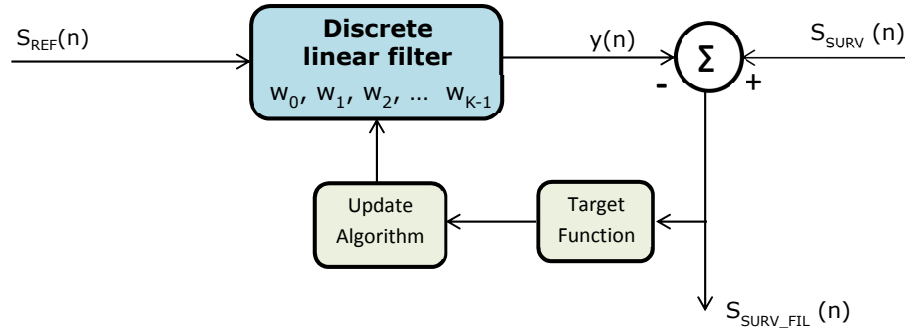
Figure 4.2: DPI and Clutter cancellation scheme.

$$
\begin{aligned}
S_{REF}(n) &= s_{IoO}(n) + n_{R_{ref}}(n) \\
S_{SURV}(n) &= S_T(n) + \nu_o(n) = S_T(n) + S_{CLUTTER}(n) + S_{DPI}(n) + n_{R_{surv}}(n)
\end{aligned}
\tag{4.2}
$$

where $s_{IoO}(n)$ is the direct signal from the IoO, $n_{R_{ref}}$ is the thermal noise contribution at the reference channel receiver antenna. The term $S_T(n)$ refers to the desired signal in the surveillance channel, the targets echoes. The term $\nu_0(n)$ represents the interferences in the surveillance channel: clutter components, $S_{CLUTTER}(n)$, the DPI, $S_{DPI}(n)$, and the thermal noise in the surveillance channel, $n_{R_{surv}}(n)$.

Taking into consideration this signal model, the proposed structure to solve the Zero Doppler Interference (ZDI) problem is a transversal adaptive canceller, Figure 4.2 [Diniz, 2008, Haykin, 2008]. The filtered signal, $S_{SURF_{FIL}}(n)$ is expressed in (4.3), where $\omega_{k,n}$ denotes the k-*th* filter weight at iteration n (in this example, filter weights are updated sample by sample).

$$
S_{SURV_{FIL}}(n) = S_{SURV}(n) - y(n) = S_{SURV}(n) - \sum_{k=0}^{K-1} w_{k,n} S_{REF}(n-k)
\tag{4.3}
$$

The objective of the process is to minimize the performance function in order to reject, for the range locations associated with the first K range bins, the contributions of clutter and DPI interferences. Actually, $S_{SURV_{FIL}}(n)$ is the error measured between the desired signal (S_{SURV}) and the filter output ($y(n)$): $e[n] = S_{SURV_{FIL}}(n)$.

4.2 Adaptive Filtering Algorithms for ZDS in passive radar

In this section, theoretical fundamentals of the considered algorithms are presented. The Least Mean Square algorithm, LMS, belongs to the family of the *stochastisc gradient algorithms*. Recurxive Leasr Square, RLS, and the Extensive CAncellation, ECA, algorithm, are based on the Least Squares approach So a brief introduction to the Least Squares fundamentals is also included.

4.2.1   Least Squares fundamentals

The goal of the Least Squares Method is the minimization of the sum of squared differences between the constructed curve $y(n)$), Figure 4.2 and the vector $\mathbf{S}_{REF,n} = [S_{REF}(n), S_{REF}(n-1), ...S_{REF}(n-(K-1))]$. The transversal filter structure proposed in the signal model section is also applied here, as the algorithm chooses the tap weights of the filter, $\mathbf{w}_k$, to minimize a performance function that consists of the sum of error squares:

$$F(w_0, ..., w_{K-1}) = \sum_{n=1}^{N} |e(n)|^2 \tag{4.4}$$

To describe the least squares condition of the linear transversal filter, the system of normal equations will be presented [Haykin, 2008]. The minimum estimation error $e_{min}(n)$ is defined as the estimation error that the filter gives rise using the weight vector obtained when the system is optimized to operate in the least-squared condition, equation (4.5).

$$e_{min}(n) = d(n) - \hat{\mathbf{w}}^H \mathbf{S}_{REF,n} \tag{4.5}$$

$$\sum_{n=K}^{N} \mathbf{S}_{REF}(n-K) e_{min}^*(n) = 0 \tag{4.6}$$

Substituting equation (4.5) in equation (4.6), principle of orthogonality, and rearranging terms, a system of K equations can be declared:

$$\sum_{n=K}^{N} \mathbf{S}_{REF}(n-k)d^*(n) = \sum_{t=0}^{k-1} \hat{w}_t \sum_{n=k}^{N} \mathbf{S}_{REF}(n-k)\mathbf{S}_{REF}^*(n-t) \qquad k = 0, \ldots, K-1 \tag{4.7}$$

This system of ecuations can be rewritten in matrix from (4.8):

1. The K x K time-averaged correlation matrix of the filter input vector $S_{REF,n}$:

$$\mathbf{\Phi} = \begin{bmatrix} \phi(0,0) & \phi(1,0) & \ldots & \phi(K-1,0) \\ \phi(0,1) & \phi(1,1) & \ldots & \phi(K-1,1) \\ \vdots & \vdots & \ldots & \vdots \\ \phi(0,K-1) & \phi(1,K-1) & \ldots & \phi(K-1,K-1) \end{bmatrix} \tag{4.8}$$

where each element of the matrix, the time averaged autocorrelation function of the tap-input vector (4.9):

$$\phi(t,k) = \sum_{i=K}^{i-t} \mathbf{S}_{REF,n}(i-k)\mathbf{S}_{REF,n}^*(i-t) \qquad 0 \le (t,k) \le K-1 \tag{4.9}$$

2. The K x 1 time-averaged cross correlation vector between the tap inputs and the desired response:

$$\mathbf{z}_{S_{REF},d} = [z_{S_{REF},d}(0), z_{S_{REF},d}(-1), \cdots, z_{S_{REF},d}(-K+1)]^T \qquad (4.10)$$

where each element of the matrix can be expressed as:

$$z_{S_{REF},d}(-m) = \sum_{i=K}^{N} \mathbf{S}_{REF,n}(i-m)d^*(i) \qquad 0 \le m \le K-1 \qquad (4.11)$$

3. The K-by-1 tap-weight vector of the least-squares filter:

$$\mathbf{w}_K = [\mathbf{w}_0, \mathbf{w}_1, \cdots, \mathbf{w}_{K-1}]^T \qquad (4.12)$$

Therefore, we may rewrite the system of K equations as:

$$\Phi \hat{\mathbf{w}}_K = \mathbf{z}_{S_{REF},d} \qquad (4.13)$$

Thanks to the uniqueness theorem, the problem of minimizing the sum of error squares, $F(n)$, always has a solution, [Stwart, 1973].

4.3   Least Mean Square, LMS, algorithm

The LMS (Least Mean Square) algorithm belongs to the family of *stochastisc gradient algorithms* as has already commented, the updating process of the filter weight vector uses an estimation of the error function gradient. One of its main features is its simplicity. It is usually used as a reference solution [Widrow and Hoff, 1960, Guillemin and Kalman, 1971].

The selected error function is the ISV, $F_{ISV}(k) = |e(k)|^2$. Attending section 4.2, two main stages can be distinguishes within the algorithm.

- A linear filtering process, expression (4.14), where the filtering stage output is the error e(n), defined as the difference between the filtered signal and the surveillance channel, expression (4.15).

$$y(n) = \mathbf{w}^H(n)\mathbf{S}_{REF,n} \qquad (4.14)$$

$$e(n) = \mathbf{S}_{SURV,n}(n) - y(n) \qquad (4.15)$$

- An adaptive mechanism that iteratively adjust the weighs of the transversal filter. At each iteration, a correction of the weight vector is carried out using an estimation of the gradient of the system error surface, $\mathbf{w}(n+1) = \mathbf{w}(n) - \mu\widehat{\nabla}(n)$ [Widrow and

Stearns, 1985]. A scaled factor μ is used as the algorithm learning constant or step-size parameter. This update mechanism is shown in Figure 4.3. If complex samples are available for the input and reference signals, the LMS algorithm uses expression (4.16) for weight update, [Haykin, 2008]:

$$
\begin{aligned}
\mathbf{w}(n+1) &= \mathbf{w}(n) + \mu \cdot \mathbf{S}_{REF,n}(n)e^*(n) \\
\mathbf{w}(n+1) &= \mathbf{w}(n) + \mu \cdot \mathbf{S}_{REF,n}(n)[\mathbf{S}_{SURV,n}(n)^* - \mathbf{S}_{REF,n}^H(n)\mathbf{w}(n)]
\end{aligned}
\tag{4.16}
$$
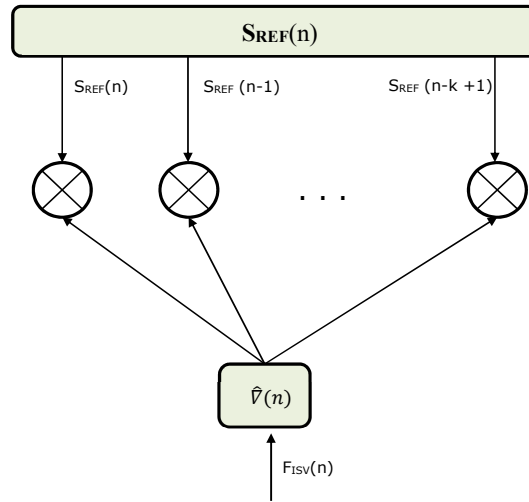
Figure 4.3: Weights control mechanism for LMS algorithm.

The LMS algorithm is convergent in the mean square sense [Haykin, 2008], if satisfies:

$$
E[|\epsilon(n)|^2] \longrightarrow constant \qquad\qquad as \quad n \longrightarrow \infty
\tag{4.17}
$$

where $\epsilon(n)$ is the weight error vector defined as the difference between the estimated and the optimum weight vectors. If $F_{min}[|e(n)|^2]$ is defined as the performance function value obtained using the optimal filter (assuming the optimal weight vector), and using the trace operator properties, an expression that relates the mean-squared error terms and the autocorrelation matrices of the tap-input vector and weight error vector, $\mathbf{R}(n) = \mathbf{S}_{REF,n}\mathbf{S}_{REF,n}^H$ and $\mathbf{K}(n) = \epsilon(n)\epsilon^H(n)$ respectively, can be enunciated:

$$
F[|e(n)|^2] = F_{min}[|e(n)|^2] + tr[\mathbf{R}\mathbf{K}(n)]
\tag{4.18}
$$

Through the study of expression (4.18) the convergence of the LMS algorithm could be assured if and only if the step-size parameter μ satisfies the condition, (4.19), where λ_{max} is associated with the largest eigenvalue of the correlation matrix. The knowledge of λ_{max} is not always available, but it is possible to redefine convergence condition using

the sum of the mean squared values of the signal input vector samples [Haykin, 2008]:

$$o < \mu < \frac{2}{\lambda_{max}}$$
$$o < \mu < \frac{2}{\sum_{m=0}^{K-1} E|\mathbf{S}_{REF,n}(n-m)|^2} \tag{4.19}$$

The convergence time required by the algorithm is related to the step-size parameter: as smaller is the parameter, the convergence time get higher. Therefore, through the selection of the μ parameter, a trade-off between performance and convergence time could be achievable taking into consideration each scenario characteristics.

Otherwise, in terms of computational cost, for a filter of order $(K-1)$, the LMS algorithm requires $(2K)$ complex multiplications and $(2K)$ complex additions per iteration, so the computational complexity of the LMS algorithm is $O(K)$. Both main parameters, μ and the filter order, are closely related to the algorithm performance for ZDS problem through the convergence time.

4.3.1 Normalized LMS algorithm

One drawback of the LMS algorithm is the gradient noise increase as the filter order increases, due to each correction to the tap-weight vector is proportional to the input vector $\mathbf{S}_{REF,n}$. In addition, filter order determines two more filtering parameters: the maximum range bin till the ZDS takes place, and the step-size parameter upper limit due to the convergence rule. The filter orders required for a fixed distance, could be associated with high convergence times through too small μ values.

Normalized LMS algorithm is a variation of the standard LMS, which applies a normalization to the tap-weight vector $\mathbf{w}$(n+1) with respect to the squared Euclidean norm of the input vector, in order to adapt the algorithm to *the principle of minimum disturbance* [Haykin, 2008] . The new update expression can be written as:

$$\mathbf{w}(n+1) = \mathbf{w}(n) + \frac{\tilde{\mu}}{\|\mathbf{S}_{REF,n}(n)^2\|} \mathbf{S}_{REF,n}(n)e^*(n) \tag{4.20}$$

NLMS algorithm convergence is assured if the step size parameter satisfies the following condition [Weiss and Mitra, 1979] [Hsia, 1983]. Then the NLMS algorithm allows the detachment of the relationship between the parameter μ and the filter order K.

$$0 < \tilde{\mu} < 2 \tag{4.21}$$

4.3.2 Batches error estimation

In order to improve the gradient estimation for the target function, and make the filter response less dependent with respect to the fast input signal variations, a batches esti-

mation process can be used instead of the instant one. For this purpose, the estimation of the gradient is obtained through the last L_{batch} samples of the signal. In (4.22) an example of this is presented, assuming a LMS as starting point.

$$\mathbf{w}(n+1) = \mathbf{w}(n) + \mu \cdot \mathbf{S}_{REF,n}(n) \cdot \frac{1}{L_{batch}} \sum_{i=0}^{L_{batch}-1} e^*(n-i) \qquad (4.22)$$

4.3.3   LMS Application in passive radar systems

Nowadays, the research effort on LMS disturbance removal on passive radar systems is mainly focused on the reduction of the convergence time.

One of the most promising strategies for achieving a reduction in the convergence time is the use of variable step-size parameter instead of a fixed one: in [Wu et al., 2012b] the time evolution of the elements of the weight vector shows that their convergence rate is not constant in time and for discrete clutter distributions, different weights do not have to share the same convergence velocity. The Variable Step-size LMS algorithm, VSLMS algorithms, take advantage of these weights properties.

- In [Wu et al., 2012b] the weight adaptation algorithm is based on the selection of big μ for those coefficients that changes more quickly in each iteration. The individual weight evolution is managed using the cross correlation function $R(n)$ between $S_{REF}(n)$ and the output of the filtering process. An estudy of the proposed algorithms performance is carried out using simulated DVB-T signals as IoO.

- Other VSLMS algorithms exploit time variability: selecting higher step-size parameters at the beginning of the filtering and reducing them as the algorithm approaches convergence. Defining Steady State Misadjustment, SSM, as the fluctuating error the weight vector suffers when the algorithms has converged, generally smaller step-size gives rise low SSM but generally increases convergence time. The step-size time varying strategy could improve the trade off between both parameters. In [Jie et al., 2013] this approach is proposed, though a comparison of different LMS based disturbance cancellation algorithms in terms of convergence rate and SSM. For the top of the art, the time evolution of the weight coefficients is managed by a dual parameter based sigmoid function presenting the best performance among the considered LMS-based algorithms.

- In [Masjedi et al., 2011] a previous filter bank stage is added in order to minimize the effect of the dependency of the convergence rate with respect of the spectral density of the input signal. The reference and surveillance signals are processed by the filter bank and each subband is then decimated and filtered using a VSLMS algorithm. A synthesis filterbank is then used to reconstruct the output signal. Using FM simulated signals, the subband VSLMS shows an improved behaviour in terms of convergence time when compared to other LMS algorithms.

Using a variable step-size parameter, an improved convergence rate is achievable, but the computational cost of the filtering process increases considerably.

One way of improving the computational efficiency of an algorithm is the paralellization of the code, but in general, LMS algorithms are not well suited for this technique. In [Zhao et al., 2013] a block based LMS algorithm is proposed, BNLMS, in order to reduce the execution time for passive radar disturbance reduction purposes. The proposed algorithm uses a frequency-domain implementation instead of the time-domain conventional one. It takes advantage of the optimized fast algorithm for the Discrete Fourier transform (DFT) computation. In addition, the weight vector is updated following a occurrence law based on a block gradient estimation. Both techniques allow the paralellization of several parts of the algorithm. Taking into consideration a real-time strategy, in [Zhao et al., 2013], the filtering is implemented in C using Computed Unified Device Architecture, CUDA, libraries in order to run the algorithm in Graphics Processing Unit, GPU, devices.

In passive radar scenarios, the presence of strong targets (undesired or desired) could sometimes mask weaker ones, lowering system detection capabilities and giving rise to dynamic ranges problems. LMS-based solutions were also proposed for this goal.

- In order to face the dynamic range problem, in [Meller, 2012] a clutter and strong targets echoes removal strategy based on an extended LMS algorithm was proposed. LMS output could be pass through a set of linear filters designed to minimize the mean-square clutter tracking error in its respective range cells to improve the performance in case of moving echoes. Adaptive and non-adaptive notch filters were applied to simulated data. If additional delays were permissible, non-causal filters could be implemented.

- In [Xiaode et al., 2014] a different approach to strong echoes cancellation is shown. A Range-Doppler NLMS algorithm is tested using Chinese digital television signals. After a first conventional NLMS filtering, range and Doppler shift of the strongest echoes were estimated from the CAF. Then reference and surveillance signals were shifted to each estimated position, and then, filtered using the RDMLS for removing strongest echoes and improving weak ines detection capability..

Most of the these research works focused on the comparison of the convergence time and the SSM and the reduction of the disturbance to main peak ratio on the CAF, but there is a lack in the analysis of the LMS algorithms behaviour from the point of view of the detection and tracking stages and considering the evolution of the whole system performance.

4.4   Recursive Least Square, RLS, algorithm

The Recursive Least Square, RLS, objective is the minimization of the WLS error function: $F_{WLS}(n) = \sum_{i=1}^{n} \lambda^{n-i} |e(i)|^2$. Where $0 < \lambda \leq 1$ is the forgetting factor, and gives more relevance to recent inputs with respect to older ones. This algorithm uses all the available input signal samples, from the filter process starting time. The elements of the general expression for LS algorithms can be rewritten assuming a recursive approach. In equation (4.23) the recursive form for the time-averaged correlation function, ϕ is presented, [Haykin, 2008]:

$$\phi(n) = \lambda \cdot \phi(n-1) + \mathbf{S_{REF,n}}\mathbf{S_{REF,n}}^H \tag{4.23}$$

This expression could be reformulated in order to obtain ϕ^{-1}, that is required to obtain the weight vector estimation, $\mathbf{w}(n) = \phi^{-1} \cdot \mathbf{S}_{SURV}$, taking advantage of the matrix inversion lemma:

$$\phi^{-1}(n) = \lambda^{-1}\phi^{-1}(n-1) - \lambda^{-1}\mathbf{k_G}(n)\mathbf{S_{REF,n}}^H \phi^{-1}(n-1) \tag{4.24}$$

The associated adaptation rule is defined in (4.25), where $\mathbf{k_G}(n)$ is the gain vector defined in (4.26) [Haykin, 2008].

$$\mathbf{w}(n) = \mathbf{w}(n-1) + \mathbf{k_G}(n)F_{WLS}^*(n) \tag{4.25}$$

$$\mathbf{k_G}(n) = \frac{\lambda^{-1}\Phi^{-1}(n)\mathbf{S}_{REF,n}}{1 + \lambda^{-1}\mathbf{S_{REF,n}}^H \phi^{-1}(n-1)\mathbf{S}_{REF,n}} \tag{4.26}$$

$$\Phi(n) = \sum_{i=1}^{n} \lambda^{n-1}\mathbf{S}_{REF,i}\mathbf{S}_{REF,i}^H \tag{4.27}$$

For $\lambda = 1$, the RLS matches the LMS method. The forgetting factor affords the possibility of following the statistical variations of the observable data when the filter operates in a nonstationary environment, which leads to a fast convergence of the algorithm. This theoretical improvement in performance, however, is achieved at the expense of a large increase in computational complexity compared to the simple LMS.

4.4.1   RLS application in passive radar systems

In passive radar bibliography, RLS algorithms are usually used in the studies of other solutions, that are the real objective of the work. The proposed filtering technique performance is usually compared with a list of well known algorithms in terms of computational cost, convergence time, stability or SSM. RLS can be frequently found among these algorithms for different values of the forgetting factor.

Examples of the use of RLS strategies as a comparison tools can be found in [Cardinali et al., 2007] where a comparison between LMS, ECA and RLS based algorithms is performed in terms of estimated clutter attenuation. In [Zhai and Wu, 2015] a new

approach for disturbance cancellation is proposed based on MUSIC algorithm, and RLS is use, among others, to carry out the algorithm performance evaluation.

4.5   Extensive CAncellation Algorithm, ECA

The Extensive CAncellation, ECA, algorithm is based on a Least Square, LS, approach, [Colone et al., 2006, Cardinali et al., 2007]. It exploits all the data available in a CPI, so a unique filter weights vector is calculated for each CPI. Data structure must be redefined for the implementation of this solution. For a K -1 filter order:

- **Input vector**, $\mathbf{S}_{REF}$, composed of the $N = T_{int} \cdot f_s$ samples of $S_{REF}(n)$ acquired in a CPI, plus a number of additional samples defined by R (4.28), so the total number of samples used in the filtering process rise to N+R-1.

$$\mathbf{S}_{REF} = [S_{REF}(-R+1), ..., S_{REF}(0), S_{REF}(1), ...S_{REF}(N)]^T \qquad (4.28)$$

- **Reference signal matrix**, $\mathbf{X}_{REF}$, whose columns are delayed versions of $\mathbf{S}_{REF}$ (4.29). Operator $\mathbf{D}^i(.)$ applies a delay of i samples to the vector it is applied to, and ^{T} denotes the transpose operation. The resulting $\mathbf{X}_{REF}$ is a (N+R-1)xK matrix.

$$\mathbf{X}_{REF} = [\mathbf{S}_{REF} \quad \mathbf{D}(\mathbf{S}_{REF}) \quad \mathbf{D}^2(\mathbf{S}_{REF}) \quad ... \quad \mathbf{D}^{K-1}(\mathbf{S}_{REF})] \qquad (4.29)$$

- **Desired signal vector** composed of the $N = T_{int} \cdot f_s$ samples of $S_{SURV}(n)$ acquired in a CPI (4.30)

$$\mathbf{S}_{SURV} = [S_{SURV}(0), S_{SURV}(1), ...S_{SURV}(N-1)] \qquad (4.30)$$

- **Clutter subspace matrix**, $\mathbf{X}$, whose columns define a $M - dimensions$ clutter subspace, where $M = (2P + 1)K$, being P the number of Doppler bins located at each side of the zero Doppler line in the RDS, from which clutter interference is intended to be rejected. The process for generating $\mathbf{X}$ is the following:

  1. Matrix $\mathbf{X}_T$ is obtained, using the matrix operator $\mathbf{\Lambda}_i$, that applies the phase delay related to the $i - th$ Doppler resolution cell, to the matrix it is applied to (4.31). The resulting $\mathbf{X}_T$ is a $(N + R - 1)\text{x}(M \cdot K)$ matrix.

$$\mathbf{X}_T = [\mathbf{\Lambda}_{-P}(\mathbf{X}_{REF}) \quad ... \quad \mathbf{\Lambda}_{-1}(\mathbf{X}_{REF}) \quad \mathbf{\Lambda}_1(\mathbf{S}_{REF}) \quad ... \quad \mathbf{\Lambda}_P(\mathbf{X}_{REF})] \qquad (4.31)$$

  2. Using the vector operator $\mathbf{B_N}$, a selection of the last N rows of $\mathbf{X}_T$, (4.32) is carried out, obtaining a resulting $N\text{x}(M \cdot K)$ matrix.

$$\mathbf{X} = \mathbf{B}(\mathbf{X}_T) \qquad (4.32)$$

- **Filtered surveillance signal vector** (4.33).

$$\mathbf{S}_{SURV_{FIL}} = [S_{SURV_{FIL}}(0), S_{SURV_{FIL}}(1), ...S_{SURV_{FIL}}(N-1)] \qquad (4.33)$$

With the underlying objective of minimizing the sum of squared errors, the tap-weight vector can be expressed as the solution of expression (4.34):

$$\min_{\mathbf{w}} ||\mathbf{S}_{SURV} - \mathbf{X} \cdot \mathbf{w}||^2 \qquad (4.34)$$

The filtered signal vector is calculated as the projection of the desired input vector $\mathbf{S}_{SURV}$ on the subspace orthogonal to the zero Doppler interference subspace (4.35) [Colone et al., 2006]. The filter weight vector is estimated using 4.36:

$$\mathbf{S}_{SURV_{FIL}} = [\mathbf{I}_N - \mathbf{X}(\mathbf{X}^H\mathbf{X})^{-1}\mathbf{X}^H]\mathbf{S}_{SURV} \qquad (4.35)$$

$$\hat{\mathbf{w}} = (\mathbf{X}^H\mathbf{X})^{-1}\mathbf{X}^H\mathbf{S}_{SURV} \qquad (4.36)$$

The computational cost is one of the most important problems associated with the ECA solution. Due to it is mainly defined by the dimensions of the clutter subspace matrix, $\mathbf{X}$, and then directly related to the filter order K-1 and signal length N. In [Zhao et al., 2012], assuming $M = (2P + 1)K$ and N is the signal length, the overall computational cost was estimated as $O(NM^2 + M^2 logM) + 2NM + M^2$. In addition, the required dinamic memory also increases with this parameters.

4.5.1   ECA application in passive radar systems

For passive radar systems, large signal segments are used to increase integration gain and Doppler resolution, high signal bandwidth are desired for increasing resolution range(high signal sampling) and high filter orders are required because of the clutter spread along range. As a result, ECA computational cost becomes a critical parameter, especially for the evaluation and inversion of the clutter subspace matrixes.

In [Colone et al., 2009b] a multistage processing version of the algorithm is proposed and tested on FM based signals with a nomianl bandwidth of 200 KHz an integration time of 1.1 seconds and K = 140. The associated computational cost estimated using the expression proposed in [Zhao et al., 2012] is equal to $4.37 \cdot 10^9$ complex operations. First, in order to reduce the computational cost with a similar cancellation performance, an algorithm based on a batched processing was presented, ECA-Batches, ECA-B: each CPI, of a duration of T_{int}, is divided into segments of length T_B, and each segment is filtered with an ECA filter. The data length reduction ratio reduces the computational cost associated to the calculation and inversion of the $(\mathbf{X}^H\mathbf{X})$ matrix, and also to the system dynamic memory requirements, but the Doppler resolution is also reduced. This is shown as a widening effect in the filtered region around the zero-Doppler line in the RDS, directly

related to the ratio $\frac{T_{int}}{T_B}$. This algorithm version is used as the base for a multiestage approach used to improve the ZDS, defining an extended cancellation mask based on clutter and detected targets information estimated from the ECA-Batches algorithm. This process allows the removal of the strongest targets with the goal to improve the detectability of the weakest one. The use of a customizable mask, makes possible a reduction of the computational cost, if a limited set of range or Doppler points are selected.

This disturbance cancellation technique was also used in the validation of the WI-FI signals for passive radar purposes in outdoor and indoor scenarios [Colone et al., 2012b, Pastina et al., 2015]. Batches of 0.1 s of a signal of 22MHz are processed, with a filter with K=50. The associated computational cost estimated using the expression proposed in [Colone et al., 2016] is equal to $2.28 \cdot 10^{11}$ per batch.

But the use of ECA-B algorithm also affects to radar performance through the T_B selection, if system adaptation capability is considered. The reduction of T_B could improve the system robustness against slowly variant IoO signal characteristics, and improve the system performance when a highly time-varying disturbance is the predominant one in the selected scenario. But, the Doppler resolution degradation effect could imply a reduction in low Doppler shift targets detection capabilities. In [Cardinali et al., 2007, Palmarini et al., 2015] these effect was commented using FM and WiFi signals.

In [Palmarini et al., 2015, Colone et al., 2016] a modified version of ECA-B was proposed and tested on FM and WI-FI signals, in order to decouple T_B and the minimun detectable target velocity. To achieve this goal, a sliding window technique is applied to the input data , renaming the algorithm as ECA-Sliding. This window of length T_S is the data segment that is filtered in a given time instant, but the weight vector used during this filtering process is obtained considering a segment T_B symmetrically taken around T_S. Then the minimum velocity is determined by $\frac{1}{T_s}$ but the algorithm performance against highly variable disturbances is till controlled by T_B parameter selection, making possible to improve the trading off between both behaviours.

Other approach to reduce computational cost is presented in [Zhao et al., 2012], where the ECA-by-Carrier, ECA-C, algorithm is proposed and proved using DRM signals with a bandwidth of 12 KHz and an integration time of 13.6 seconds. The algorithm, first down-convertes the received signals into baseband and then separate them into their carriers. Then, for each carrier, an ECA algorithm is applied, with a low computational cost. The dimension of the new matrix, **X**, under study was reduced from MxM to $1xL$ where L is the number of OFDM symbols in the filtered signal segment. This is possible taking advantage of the OFDM properties that stablish that along a symbol and for each carrier, the contributions of multipaths and clutter to the disturbance sub-space matrix are almost completely correlated. But ECA-C removes only disturbance components distributed along the zero Doppler line of the RDS. In [Schwark and Cristallini, 2016] an additional improvement was proposed. The ECA-by-Carrier Doppler was applied to a signal composed by a DVB-T channel, expanding each carrier clutter subspace by two replicas shifted by a given Doppler frequency achieving low-Doppler disturbance removal.

Chapter 5

IDEPAR acquisition system

5.1 Introduction

IDEPAR is a technological demonstrator developed in the University of Alcalá, under the Spanish Ministry of Economy and Competitiveness project TEC2012-38701. The main objective was the design and development of the DVB-T PBR demonstrator, to be used as a development and test platform to face the study of terrestrial and maritime applications, the generation of databases of real data acquired under controlled conditions to test and optimize the pre-processing techniques that this kind of radar requires, and to develop clutter models for detection parameters prediction. Because of that, the general design requirements were the following:

- Use of COTS components in order to reduce costs and allow an easy update as the research on the different system stages progresses.

- Modular system: easier maintenance and growth capability.

- Use of standard development tools, data formats and interfaces.

- Off-line digital signal processing for providing a high level of configurability, with the drawback of significant signal processing latencies.

   In the following sections, a brief description of the different sub-systems that conforms IDEPAR demonstrator were presented.

5.2 IDEPAR system description

The IDEPAR demonstrator developed was designed to operate in the higher frequency band of the Spanish DVB-T. In order to be able to exploit the three higher consecutive channels, the acquisition system operates with a bandwidth up to 25 MHz, obtaining an improved range resolution.
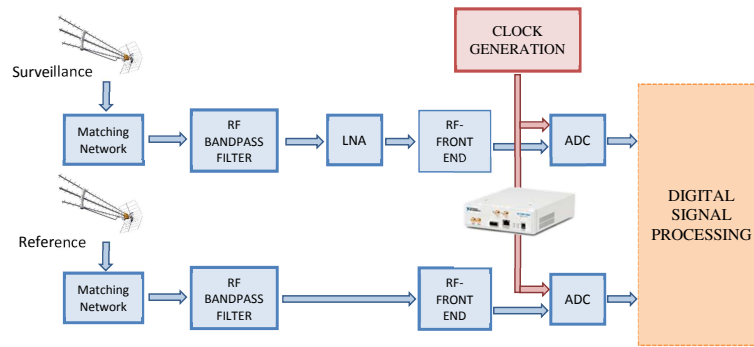
Figure 5.1: Basic IDEPAR architecture

According the basic PBR architecture depicted in Figure 2.2, the main elements implemented in the IDEPAR demonstrator are shown in Figure 5.1.

5.2.1 Antenna subsystem

The acquisition subsystem was implemented using commercial DVB-T antennas: one for the reference channel and other for the surveillance one. Antenas DAT HDBOSS 75 [TELEVES DAT HD BOSS 75, 2015], were selected due to their good gain, high return losses and high front-to-back ratios for the demonstrator frequency band. In Figure 5.2 the antenna 3D model, and the radiation patterns for azimuth and elevation planes obtained through electromagnetic simulation using the Ansoft HFSS tool (High Frequency Structure Simulator), are depicted.

(a) 3D model   (b) Azimuth   (c) Elevation
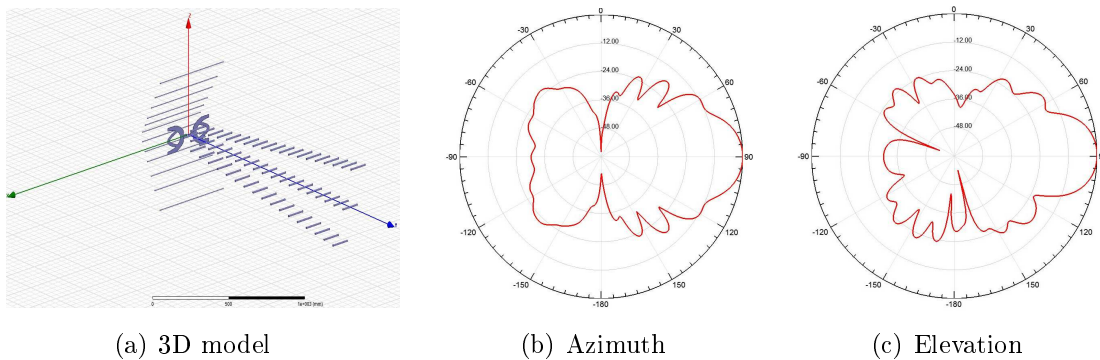
Figure 5.2: Antenna DATHD 75 BOSS: 3D Model and radiation patterns.

5.2.2 Adquisition chain

The receiving chain is composed of:

- Input RF cavity bandpass filters in both channels and Low Noise Amplifiers, LNA, in the surveillance one, are used in order to improve system detection capabilities.

- Software Defined Radio acquisition boards were selected due to their versatility, research-oriented design and customizable software for storing the acquired digitized samples in RAM (Random-Access Memory). The system is composed of RF-Daughter boards and ADC system.

- An external clock of 10 MHz and a shared squared-start signals were provided to the acquisition boards for synchronization purposes.

Acquisition and processing IDEPAR components were mounted in a protective structure which facilitates the system deployment and transport, Figure 5.3. Main parameters of the IDEPAR acquisition chain components are summarized in Table 5.1
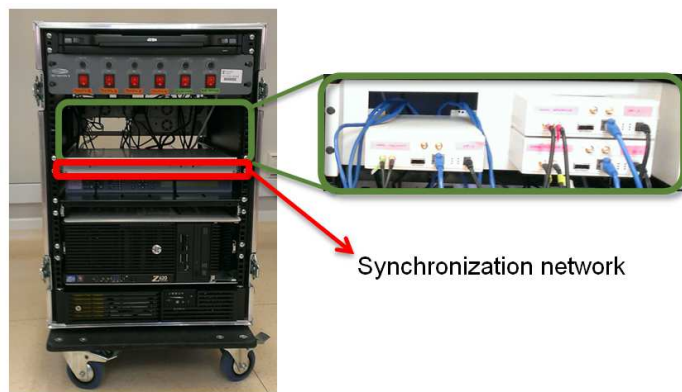
Figure 5.3: Rack front-side view (synchronization network and acquisition boards are marked in red and green, respectively).

5.2.3 Signal Processing Stages

The digitized samples provided by the USRP devices were saved to disk in a high performance processing unit. Different processing algorithms were implemented in Matlab for testing the receiving chains. The main processing stages were implemented: the CAF, the zero Doppler interference algorithms described in Chapter 4, and different detectors based on CFAR techniques.

Maximum acquisition lengths around several tens of seconds are assumed, following time processing structure presented in 2.2.6. T_{int} around 250 ms was generally selected for proccesing purposes in this work. At the output of the CAF stage, a RDS, is generated for each CPI and filtering, processing, detection and tracking stages were implemented off-line.

5.2.3.1 Zero Doppler Interference (ZDI) suppression

The relevance of the stationary clutter, interfering IoOs and DPI, all of them known as *zero Doppler interferences*, was highlighted in section 2. ZDI phenomenon specially affects

Table 5.1: IDEPAR receiver chain parameters: antenna system, RF-front-end ans ADC T_a' is the apparent temperature of the sky as viewed at the radar frequency, and L_a is the dissipative loss within the antenna.

Receiver Chain Elements	Parameters
Antenna System	$T_a' = 90$ °
	$L_a = 10 \cdot log_{10}(la) = 1$ dB
	$T_a = \frac{0.88 \cdot T_a' - 254}{l_a} + 290$
	$F_{ant-con} = 4$ dB $\rightarrow T_{ant-con} = 438.45K$
Matching Network	$L_{MN} = 1.2$ dB
Band-Pass Filter	$L_{BPF} = 1$ dB
LNA	$G_{LNA} = 32$ dB;,$F_{LNA} = 0.8$ dB
Conectors	$L_{Con} = 8.5$ dB
Daughter board	$F_{FE} = 4.34$ dB; $G_{FE} = 19.3$ dB
ADC	$F_{ADC} = 34.5$ dB; $G_{ADC} = 0$ dB

the detection of moving targets with low Doppler shifts, but due to the bistatic geometry, low speed vehicles are not the unique targets whose echo could be located in this RDS region (section 2.2.1). In Figure 5.4 an example of a RDS generated using reference and surveillance signals without applying any ZDI suppression technique is presented showing details of a target and interference contributions.
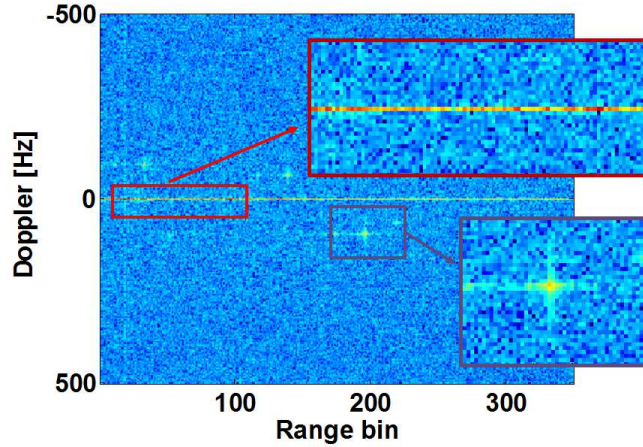
Figure 5.4: Range-Doppler surface for $T_{int} = 200ms$, with details related to a target (purple) and zero-Doppler interferences (red) contributions.

Pre-processing stage focused on the adaptive filtering of the surveillance channel was implemented. LMS and ECA cancellers were selected, both of them explained in sections 4.3 and 4.5 respectively. In Figure 5.5, examples of RDSs generated after the combination of the zero-Doppler processing are shown, for the basic LMS (Figure 5.5.a) and the ECA

(a) LMS algorithm
(b) ECA algorithm
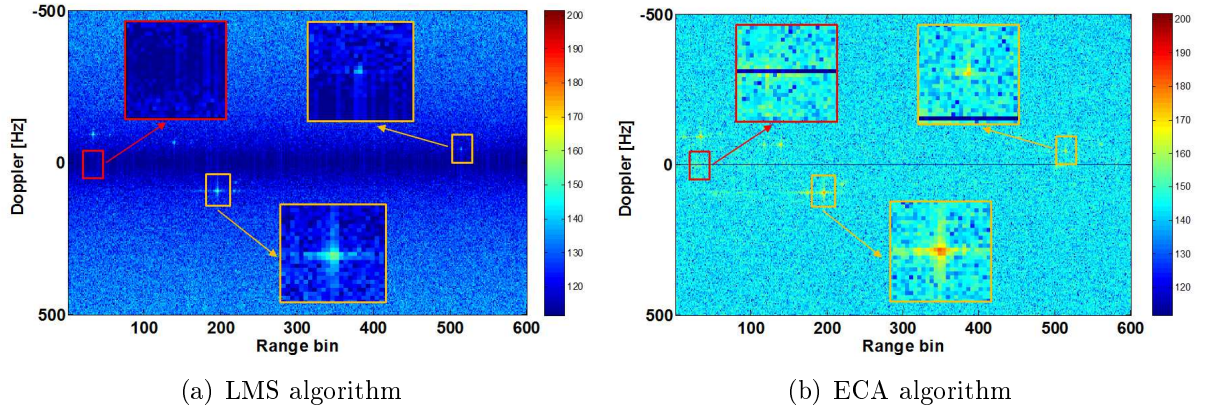
Figure 5.5: RDSs generated using the filtered signal $S_{SRUV_{FIL}}$ provided by the zero-Doppler interference cancellers.

(Figure 5.5.b) algorithms.

Three regions have been detailed, in order to show how both algorithms affect to the zero-Doppler line area (red) and targets location (orange), selecting the targets with echoes of different power levels and with located at different distances from the zero Doppler line. A deeper analysis of the considered different filtering strategies is presented in section 7.

5.2.3.2 Detection Stage

Detector stage transforms each RDS in a logical matrix composed of zeros (target absent) and ones (target present). The most common detectors used in PBRs are based on incoherent Constant False Alarm Rate (CFAR) techniques [Gandhi and Kassam, 1988, Cao et al., 2010]. These solutions adjust the detection threshold to be applied to each cell of the squared magnitude of the RDS, according to the estimated statistics of the surrounding cells. In Figure 5.6, the general detection scheme is presented, where q_0 is the Cell Under Test or CUT, $[q_1 \ldots q_R]$ are the R reference cells that will be used for estimating clutter statistics, T is the multiplicative factor that depends on the desired P_{FA}, and T_q is the threshold estimated by the CFAR technique. The Cell-Averaging CFAR, CA-CFAR, detection rule and T constant calculation are presented in Figure (5.1). This detector is optimum under the assumption of independent and identically distributed interference samples with exponential probability density function [Gandhi and Kassam, 1988].

$$q_0 \underset{H_0}{\overset{H_1}{\gtrless}} T \cdot \sum_{i=1}^{R} q_i \qquad T = \ (P_{FA})^{-1/R} - 1 \qquad (5.1)$$

Guard cells around the CUT guarantee that the spillover contributions of a target on the CUT, are not considered in the clutter statistics estimation. The considered strategies for the reference cells selection, using 1D or 2D windowing techniques, are depicted in 5.7.
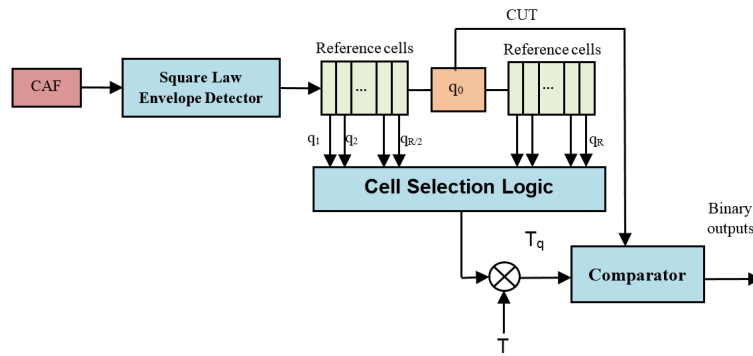
Figure 5.6: CFAR detector scheme

(a) Range window   (b) Doppler window   (c) Rectangular window
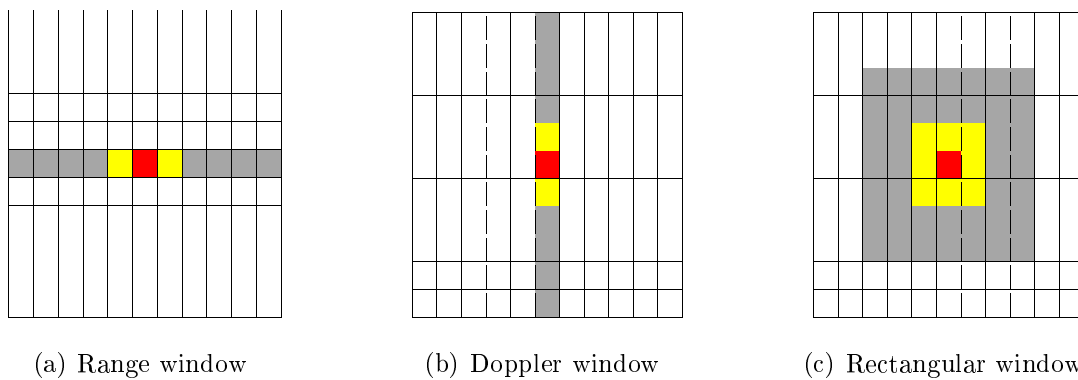
Figure 5.7: Reference windows for the CFAR detector: CUT (red), reference cells (gray), guard cells (yellow).

- *1D windowing techniques.* For each CUT, the reference window can extend along range (RANGE detector) or Doppler (DOPPLER detector) as depicted in Figure 5.7(a) and 5.7(b).

- *Combination of two detectors.* Through the use of the AND operator, the output of two detector with the reference cells extended along range and Doppler dimensions respectively are combined in order to declare a target if and only if both detectors have declared it simultaneously. This mechanism makes its P_{FA} always better that the best of the two detectors, but its P_D worse that the worst of them.

- *2D windowing technique.* As additional 2D CA-CFAR technique use rectangular window (2D-Window detector) as depicted in Figure 5.7.

5.2.3.3   Tracking stage

A tracking system based on a Kalman filter operating in the range-Doppler plane was implemented. The desired targets were ground vehicles moving in an adverse environment, characterized by the presence of obstacles. The tracking stage is compose of three steps:

1. Bidimensional Kalman filter: From the individual RDS detection plots along whole considered acquisition time T_{adq}, the Kalman filter stage isolates (in space between different targets) and attaches (in time for a same target) this set of detections in order to obtain tracks that contain as much target dynamic information as possible. A brief mathematical description of the kalman filter applied to a bistatic scenario was carried out. In (5.2), the dynamic model used to describe the target manoeuvres, [Li and Jilkov, 2003], is expressed:

$$R_b(k) = R_b(k-1) + V_{Rb}(k-1)T + 1/2a_{Rb}(k-1)T^2 + w(k) \qquad (5.2)$$

where $R_b(k)$ is the bistatic range position of the target in the *k-th* CPI , V_{R_b} and a_{R_b} are its velocity and acceleration components in the bistatic range dimension, and $w(k)$ is the small acceleration variation modelled as noise. T is defined as the time between consecutive iterations. The actualization stage equation is declared in (5.3):

$$\mathbf{x}(k+1) = \mathbf{F}\mathbf{x}(k) + \mathbf{u}(k)$$
$$\mathbf{x}(k) = [R_b(k), V_{Rb}(k), f_d(k), V_{fd}(k)]^T \qquad (5.3)$$

where $\mathbf{x}(k)$ is the state vector composed of the bistatic range, R_b , Doppler shift, f_d, and the velocity in both dimensions, V_{Rb}, V_{fd} , $\mathbf{u}(k)$ models the errors sources of the process. The relations between the bistatic range and Doppler components of target speed, and the bistatic Doppler shift allow the definition of the state transition matrix $\mathbf{F}$ (5.4), being λ the wavelength measured at the central frequency.

$$
\begin{aligned}
V_{Rb}(k) &= -f_d(k)\lambda \\
f_d(k) &= f_d(k-1) + V_{fd}(k-1)
\end{aligned}
\;;\;
\mathbf{F} = \begin{pmatrix} 1 & 0 & -\lambda T & -\lambda T^2 \\ 0 & 0 & -1 & -\lambda T \\ 0 & 0 & 1 & T \\ 0 & 0 & 0 & 1 \end{pmatrix}
\qquad (5.4)
$$

2. Track confirmation: In order to reduce the false-track declaration, specially in the zero-Doppler zone, where a high concentration of false tracks is expected, a two-rules system was implemented to restrict as much as possible the track confirmation to real targets:

   – Temporal rule: recursive detections in an identified track must be associated with the same target in order to confirm the trajectory. Markov logic was selected due to its low false alarm rate and time confirmation [Bar-Shalom et al., 1989].

   – Spatial rule: the relationship between Doppler shift and the range rate should be obeyed, imposing several dynamic constrains to the considered trajectories.

3. Geodesic coordinate converter: Due to the absence of angular discrimination, the target manoeuvres could not be unambiguously defined. A preliminary study of the

radar scenario was carried out, where the GIS, Geographic Information Systems In-
formation, was analysed focussing on existing roads and their characteristics. Then,
using this reference velocity profile, the target tracks were associated with a road,
through a recursive process, assuming that the target follows predictable movements
on the existing road. However, the converter is not able to determinate the real tar-
get manoeuvre for targets describing unexpected trajectories. But the presence of
these unexpected tracks could be used as alarm system on the surveillance area.

Chapter 6

Scenarios of interest analysis

6.1 Introduction

The bistatic nature of the passive radar and the lack of control of IoO location and parameters, make the study of the scenario a key issue: system coverage, range and cross-range resolutions and targets detectability mainly depend on the selected scenario through the system geometry.

The main tool in radar scenario analysis is the system coverage, defined as the maximum range where a target is detected fulfilling P_D and P_{FA} requirements, taking into consideration specific target and interference models. In the present chapter, the main elements that allow a system coverage estimation are presented:

- A first estimation of the system coverage can be obtained using expression (2.10), that is repeated in (6.1) for convenience.

$$snr_{IN} = \frac{p_T g_T g_R \lambda^2 \sigma_{bis}}{(4\pi)^3 (R_R R_T)^2} \cdot \frac{1}{k \cdot (Ta + T_{ant-con}) \cdot B} \tag{6.1}$$

  This expression requires the knowledge of IoO parameters such as emplacement, frequency, bandwidth, and radiated power, and a complete characterization of the passive radar receiving chain.

- An estimation of the excess propagation looses taking into consideration topographical information of the area of interest and the IoO and radar receiver areas.

- The estimation of the Bistatic-RCS, BRCS, of the target of interest, for the frequency band and the scenario geometry.

APIS project focused on the problem of primary radar coverage gaps filling to detect low altitude flying targets. The developed demonstrator was validated in the Aldolfo Suarez - Madrid Barajas airport in Madrid. On the other hand, this PhD Thesis was

developed under the frame of the IDEPAR project, which objective was the detection and tracking of terrestrial vehicles in semi-urban scenarios. The University of Alcalá campus was selected as main trial site due to the possibility of maintaining the system deployed on the Polytechnic School roof during the design and pre-validation phases. As an alternative, a more challenging scenario was also presented, located in Guadalajara, and characterized by a complex relief and very bad DVB-T illumination conditions.

6.2 Analysis of the acquisition chain for coverage estimation purposes

Using equation (6.2) an estimation of the system coverage is obtained:

$$(R_R R_T)^2 = \frac{p_T g_T g_R \lambda^2 \sigma_{bis}}{(4\pi)^3 snr_{IN}} \cdot \frac{1}{KT_{in}B} \tag{6.2}$$

where $T_{in} = Ta + T_{ant-con}$ with Ta and $T_{ant-con}$ the antenna and interconnection elements equivalent temperatures respectively, and snr_{in} is the signal to noise ration at the antenna terminals.

The relation between snr_{IN} and the detection parameters, the signal to noise ratio at the detector input, snr_{DET} is the key element for the estimation of the system coverage for specified PFA and P_D values, section 2.2.2.

A detailed study of the impact of the different elements of the receiving chain, using Figure 6.1 as reference, gives rise to a general expression that can be a useful tool for the design of the PBR System.
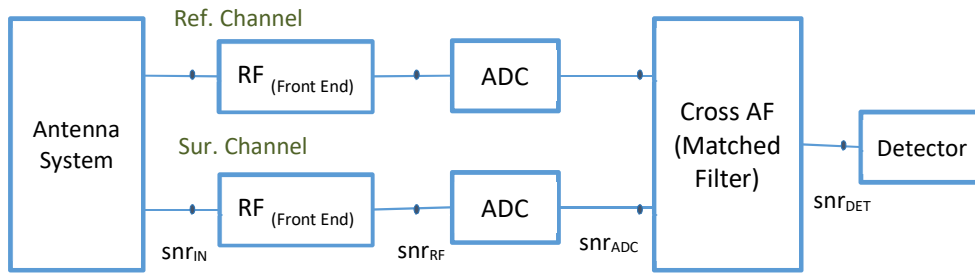
Figure 6.1: General scheme of a PBR receiver chain.

- In this study, the dominant interference is the receiving chain thermal noise, so pre-processing stages can be ignored, and only the processing gain associated with the matched filter operation performed by the CAF is considered, giving rise to a Signal to Noise Ratio at the output of the Analog to Digital Converter (ADC) equal to $snr_{ADC} = snr_{DET}/g_P$, being $g_P = T_{int}B$ the CAF processing gain.

- snr_{ADC} can be also expressed using the values of the signal and noise power at the input of the element, and then, it could be related with snr_{RF}:

$$snr_{ADC} = \frac{S_{RF} \cdot g_{ADC}}{n_{RF} \cdot g_{ADC} + n_{CADC}} = snr_{RF} \cdot \frac{1}{1 + \dfrac{n_{CADC}}{n_{RF} \cdot g_{ADC}}} \qquad (6.3)$$

  where g_{ADC} and n_{CADC} are the power gain and the noise contribution at the output of the ADC, and S_{RF} and n_{RF} are the signal and noise power at the input of the ADC, respectively.

- Applying a similar procedure to the RF block, an expression that relates this block parameters and snr_{IN} is obtained:

$$snr_{IN} = snr_{RF} \cdot \left(1 + \frac{n_{CRF}}{n_{IN} \cdot g_{RF}}\right) \qquad (6.4)$$

  where g_{RF} and n_{CRF} are the power gain and the noise contribution at the output of the RF front-end, and S_{IN} and n_{IN} are the signal and noise power at the input of the receiver chain, respectively.

- The final equation that relatse the minimum snr_{IN} and snr_{DET}, is obtained:

$$snr_{IN} = snr_{DET} \cdot \frac{1 + \dfrac{n_{CADC}}{n_{RF} \cdot g_{ADC}}}{B \cdot T_{int}} \cdot \left(1 + \frac{n_{CRF}}{n_{IN} \cdot g_{RF}}\right) \qquad (6.5)$$

Using (6.5) for the snr_{DET} value required by the implemented detection rule for the specified P_{FA} and P_D, the limit of the coverage can be calculated from (6.2).

An estimation of the required received power level at the input of demonstrator acquisition system to fulfil detection constrains can be obtained, taking into consideration the selected system components and scenario characteristics: $snr_{in} = -145.4458 dBm$.

6.2.1   Excess propagation losses estimation

Using equation (6.2), the Cassini ovals are obtained, but this estimated coverage only assumes free space propagation losses. There are scenarios, specially those oriented to ground targets, where excess propagation losses will not be negligible, making this estimation very inaccurate. In expression (6.6) an estimation of the radar coverage taking into consideration this effect is presented.

$$(R_R R_T)^2 = \frac{p_T g_T g_R \lambda^2 \sigma_{bis}}{(4\pi)^3 \, snr_{IN}} \cdot \frac{1}{KT_{in}B} \cdot l_{IoO-target} \cdot l_{IoO-PBR} \qquad (6.6)$$

where $l_{IoO-target}$ is the excess propagation losses associated with the path between the IoO and the sought target, while $l_{target-PBR}$ is the path the target echo follows until reaching

the passive receiver. Topographical information of the radar scenario is required in order to estimate those additional losses.

The modelling of excess propagation losses is usually carried out using electromagnetic simulators. In this work, WinProp (AWE Communications GmbH) was used. This software allows the selection of different propagation models and the integration of GIS data in order to model the relief of the area of interest.

The Dominant Path Prediction Model, DPM, was selected as the electromagnetic method for simulations in this work due to selecting a full 3D approach for the path searching, obtaining more realistic results that for example Hata-Okumura model, where the topography is not considered, or Knife-Edge Diffraction Model, KEDM, where the direct ray is always considered generating a too dominant effect. DMP accuracy also exceeds the obtained using empirical models, with short associated computation times. The selected strategy for coverage estimation is described as follows:

- The incident power at each point within the AoI, is obtained assuming the scenario characteristics and an additional height added to the topographical information: a target with that altitude is assumed to be located at each point of the AoI.

- The $l_{target-PBR}$ is calculated for all the points considered in the previous step.

- Using both results in combination with the desired target BRCS and IoO and radar receiver parameters, the received power and the snr_{in} can be calculated for each target location in the area of interest. Then the system coverage mask is estimated through the comparison with a threshold, if the value is greater or equal than the required power derived from snr_{in}, the detection of the selected target at this point, is achievable.

In Figure 6.3 an example of the scenario analysis carried out with this method is depicted in order to shown the influence of considering the excess propagation losses. The topographical information of the selected scenario is depicted in Figure 6.2.
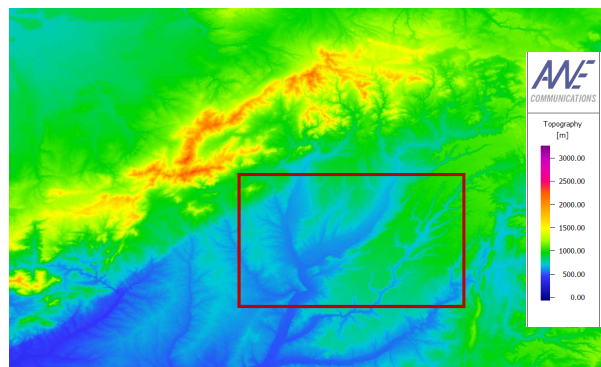
Figure 6.2: Topographical map of the example scenario.

At this point the IDEPAR receiver chain was specified, so a sensitivity equal to -145.4458 dBm was used for generating the coverage maps, in addition, a BRCS of 10 dBsm was assumed. The IoO and the receiver were located in Madrid and Alcalá de Henares respectively, assuming a baseline of 28 km. In 6.3(a) the Cassini's Ovals obtained considering only free space propagation losses are depicted, expression (6.2). Assuming the same IoO and radar receiver characteristics, but including excess propagation losses estimated using WinProp, system coverages were calculated for targets located at different heights: 100m and 25m, Figures 6.3(b) and6.3(c) respectively.

(a) Coverage stimation based on Cassini's oval
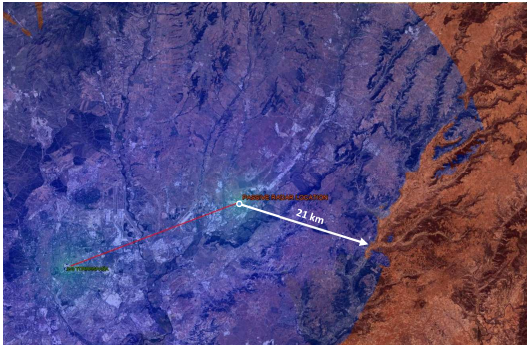
(b) Considering exceed propagation losses: $h_t = 100m$
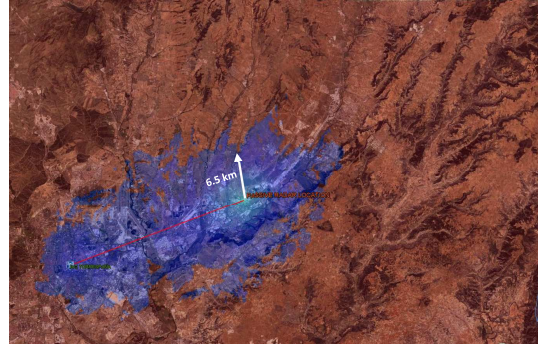
(c) Considering exceed propagation losses: $h_t = 25m$

Figure 6.3: Estimated system coverage comparison between different target heights. Representative coverages are marked with white arrows.

6.2.2 BRCS estimation

In section 2.2.4 BRCS definition was presented. An estimation of its value must be considered in order to carry out the passive radar coverage analysis. In this work, the POFACETS software (Naval Postgraduate School, California) [Jenn, 2016],was used for modelling target BRCS using the Physical Optics, PO, approximation. This method yields good results for targets with large size ($\frac{L_{Target}}{\lambda} \geq 10$), but multiple reflections, diffraction and surface waves effects are not considered.

Two different methodologies were applied in order to estimate the BRCS: a global approach and a bistatic angle dependant one.

- Global approach: the elevation angles for the incidence and the scattering directions were fixed and obtained through the scenario geometry analysis. Azimuth incidence angles varied from 0 to 180° taking advantage of the symmetrical geometry of the targets. For each azimuth incidence angle, the observation one was varied from 0° to 360°. A matrix that models the BRCS of a target for all angular combinations was obtained.

- Bistatic angle dependant approach: in this case, and still assuming fixed elevation angles, the relation between incidence and observation azimuth angles is considered constant and equal to the target bistatic angle. Then the 3D model is rotated 360 in the horizontal plane. The results show an estimation of the BRCS particularized for the target location within the scenario.

For methodology comparison purposes, two targets of interest were analysed using both approaches: a car located at ground level, and a small CESSNA-like aeroplane, Figure 6.4. In Table 6.1 the main parameters assumed for BRCS estimation are presented, and in Table 6.2 results are summarized; for the second methodology, values of $\beta = \{60°, 90°, 120°\}$ were selected.

Length: 8.3m

Width: 11m

Height: 2.7m

Length: 7.735m

Width: 1.795m

Height: 1.440m.

(a) Commercial car: Mazda 6 SPORT   (b) Small aeroplane: CESSNA 172
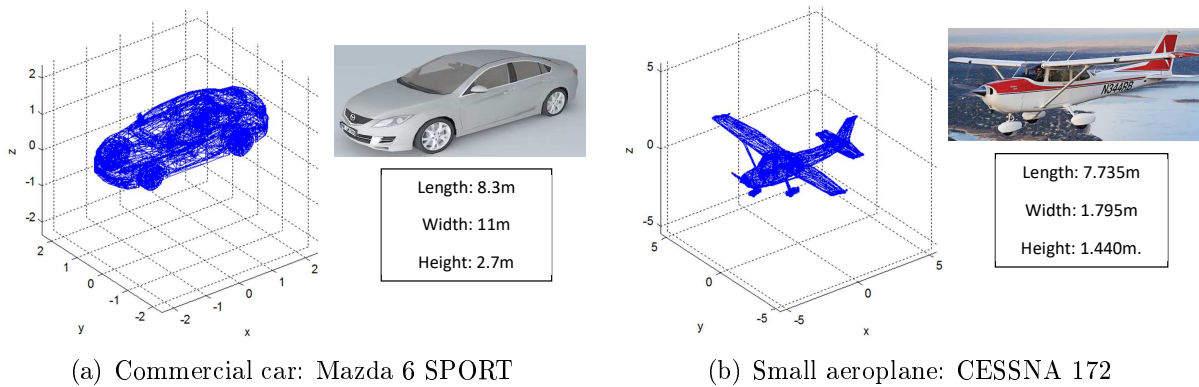
Figure 6.4: 3D models and main characteristics of the selected targets of interest.

Results show great differences between the mean values obtained with both approaches. In Figure 6.5 the estimated BRCS values for all incidence and scattering azimuth angles considered in the global methodology are presented. Higher values concentrate in the forward scatter region, proving that these are the responsible of the higher values obtained using this methodology. This peaks do not affect to the second methodology if the considered β is not close to 180°

Table 6.1: Main parameters for BRCS estimation

Parameter	Mazda 6 SPORT	Cessna 172
Elevation angles	$\theta_{inc} = 89.03°$	$\theta_{inc} = 91.23°$
	$\theta_{obs} = 89.69°$	$\theta_{obs} = 94.04°$
R_T	13 Km	
R_R	6.5 Km	
h_{IoO}	650 m	
h_{Target}	430 + 0 = 430m	430 + 500 = 930 m
h_{PBR}	465 m	

Table 6.2: Estimated BRCS for the selected targets assuming the selected scenario.

BRCS (dBsm)	Mazda 6 SPORT			CESSNA 172		
	Max.	Min.	Average	Max.	Min.	Average
Global	29.9215	9.9191	22.4518	26.9163	8.2673	18.1746
$\beta = 60°$	26.835	-18.769	12.4281	25.8053	-19.6858	13.0442
$\beta = 90°$	25.855	-18.3710	12.7078	24.797	-26.2283	11.4141
$\beta = 120°$	22.748	-21.2287	12.1045	22.812	-21.783	10.45
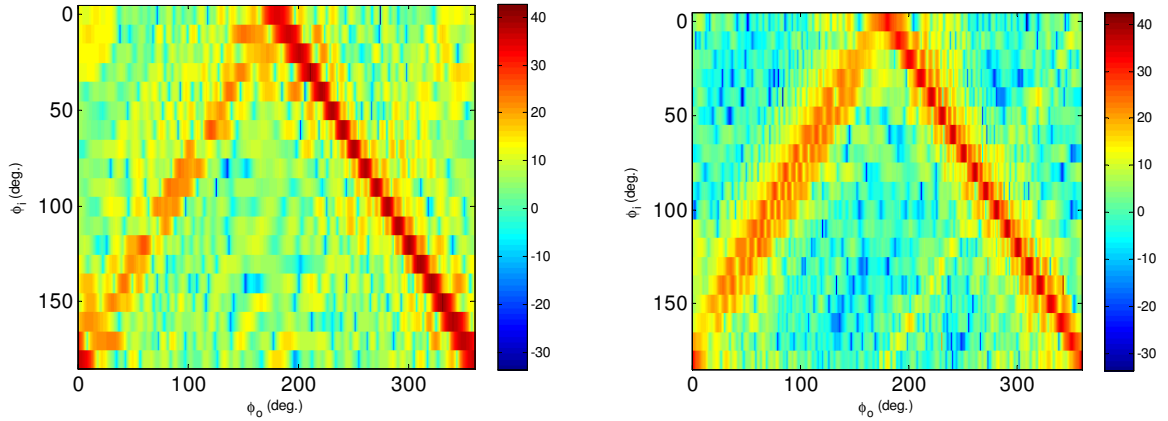
(a) Commercial car: Mazda 6 SPORT   (b) Small aeroplane: CESSNA 172

Figure 6.5: 2D BRCS maps for two representative target models. ϕ_i and ϕ_0 stand for the incidence and scattering azimuth angles, respectively.

6.3   Main trial scenario: University of Alcalá Campus

In this section, the main IDEPAR demonstrator scenario is presented. The passive receiver was located at the roof of the Superior Polytechnic School of the University of Alcalá in order to facilitate the test and validation measurements along the system developing time. This scenario is characterized as semi-urban environment: low-height buildings belonging

(a) Passive receiver point of view   (b) Scenario top view
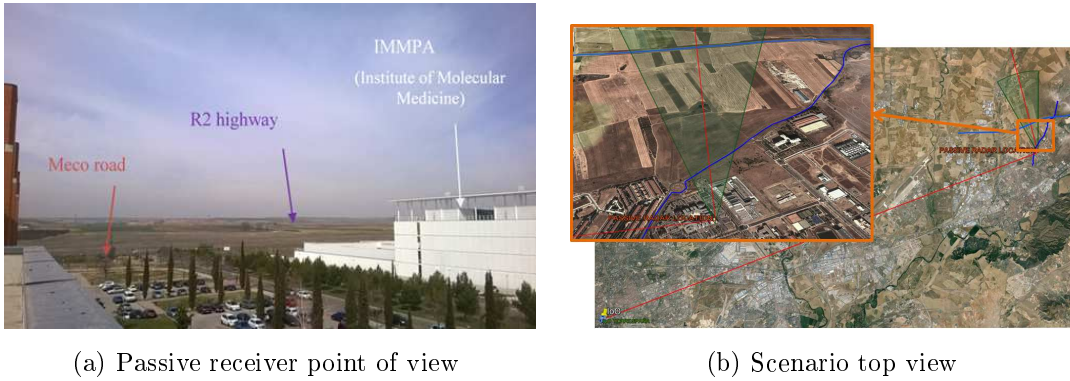
Figure 6.6: Main IDEPAR scenario.

to the university campus, surrounded by countryside and several roads: Alcalá-Meco road, R2 highway and inner-campus secondary roads. In Figure 6.3 the view from the passive receiver location is shown.

In Table 6.3 coordinates of the main elements of the geometry are presented. Torrespaña transmitter was selected as IoO among those available in the surrounding area, taking into consideration its higher radiated power and its omnidirectional radiation pattern. In Figure 6.6(b), the scenario is shown with a detail of the receiver antenna angular coverage: the antennas were placed to ensure that the maximum of the radiation pattern was pointed to the area of interest in order to enclose roads under study.

Table 6.3: Transmitter and passive receiver location coordinates

Transmitter	Latitude	Longitude	Altitude
Torrespaña illuminator	$40°25'16.64''N$	$3°39'51.39''W$	658 m
Passive receiver	$40°30'47.19''N$	$3°20'55.02''W$	628 m

In order to obtain the system coverage, the BRCSs of the targets of interest were estimated: a Mazda 6 SPORT vehicle was considered as a representative of car vehicles; in addition, a drone flying at low altitude was selected (AAI RQ-2, whose 3D model is shown in Figure 6.7). In Table 6.4 main scenario parameters are summarized.

In Table 6.5 BRCSs estimation results are summarized for the two targets, using the two proposed methodologies. For the second one, the following bistatic angles were selected: $\beta = 55°, 70°, 90°, 105°$. In order to make a conservative coverage estimation, the lowest average BRCS was selected for each target: 10.61 dBsm and 3.10 dBsm for car and drone 3D models, respectively. Again, a sensitivity equal to -145.4458 dBm was considered for coverage estimation.

In Figure 6.8 the estimated coverage for a commercial car is depicted for these scenario parameters and assuming a target at ground level. The resulting area is a irregular circular-like region of about 4 km of radius that encloses segments of the roads under study. This estimated area is coherent with the target detection and tracking results
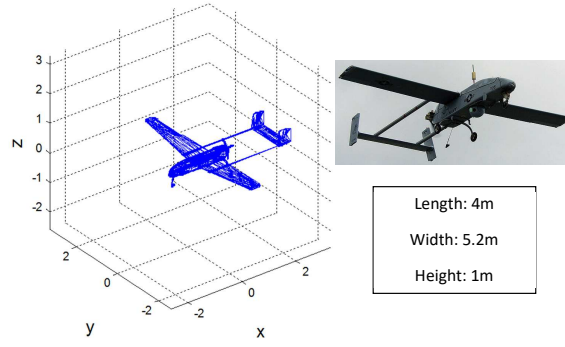
Figure 6.7: AAI RQ-2 Pioneer: 3D CAD model and main dimensions.

Table 6.4: Main scenario parameters

Paramterer	Mazda 6 SPORT	DRONE AAI RQ-2
$PIRE_{IoO}$	20.606 kW	
$S_{IN_{MIN}}$	-145.4458 dBm	
Elevation angles	$\theta_{inc} = 89.47°$	$\theta_{inc} = 89.52°$
	$\theta_{obs} = 89.7°$	$\theta_{obs} = 90.4°$
L	28.671 Km	
h_{IoO}	658 + 232 m	
h_{Target}	626 + 0 = 626m	626 + 20 = 646 m
h_{PBR}	465 m	

obtained from the measurement campaigns carried out in this scenario: the estimated trajectories are associated to those road segment within the system coverage.

The coverage area is directly related to target BRCS but the change in the size of the area can be masked by other scenario parameters as for example excess propagation losses that are mainly related to the scenario relief and target height. In order to show this relation, the system coverage for a low-flying drone is obtained, Figure 6.9. The estimated system area considerably increases respect to the ground target-based one, although the lower BRCS selected to characterize the target.

Table 6.5: Estimated BRCS for the IDEPAR main scenario.

BRCS	Mazda 6 SPORT			Dron AAI RQ2		
(dBsm)	Max.	Min.	Average	Max.	Min.	Average
Global	33.3294	8.6524	23.9683	65.5541	-2.5458	44.9344
$\beta = 55°$	20.8323	-31.8791	10.6118	13.2404	-30.1251	3.1052
$\beta = 70°$	27.2172	-20.5856	13.7543	37.7961	-21.4957	12.9672
$\beta = 90°$	24.5365	-24.9609	12.9469	38.6338	-22.3837	14.2790
$\beta = 105°$	27.0228	-18.605	12.9589	17.5844	-27.6268	5.8866
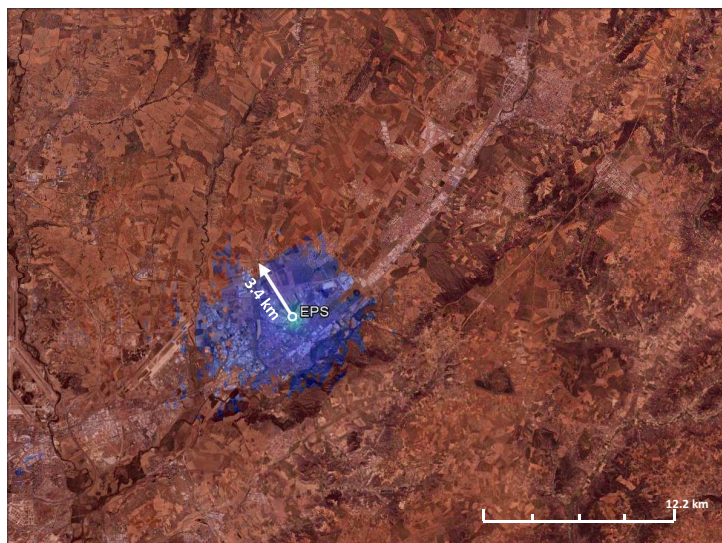
Figure 6.8: Estimated system coverage for a target modelled by a Mazda 6 SPORT car at the main IDEPAR scenario
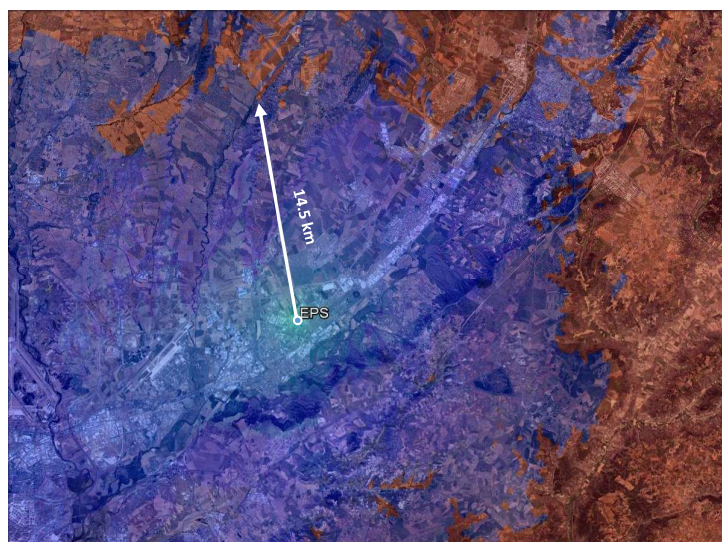
Figure 6.9: Estimated system coverage for a target modelled by an AAI RQ-2 Pioneer drone at the main IDEPAR scenario

6.4   Rural scenario based on CEAR facility location

The Radioelectric Trials and Analysis Centre, *Centro de Ensayos y Análisis Radioeléctrico* (CEAR) is a Spanish Ministry of Defense protected area for testing and analysing radar, communications systems, RF antennas and sensors , IFF (Identification Friend or Foe) systems, warfare systems, receiver and transmitter devices, etc. It is located in Guadalajara in a countryside environment, Figure 6.10.

An alternative scenario sited in CEAR facilities is also analysed in this section, showing

Figure 6.10: CEAR centered scenario top view.

the negative effects that an emplacement with complex relief could gives rise. In Tables 6.6 and 6.7 the scenario locations coordinates and a summary of scenario main parameters are presented, respectively.

Table 6.6: Transmitter and passive receiver location coordinates at the CEAR scenario

Transmitter	Latitude	Longitude	Altitude
Torrespaña illuminator	$40°25'16.64''N$	$3°39'51.39''W$	658 m
Passive receiver	$40°36'41.27''N$	$3°06'51.46''W$	946 m

Table 6.7: CEAR scenario parameters

Paramterer	Mazda 6 SPORT	DRONE AAI RQ-2
$PIRE_{IoO}$	20.606 KW	
$S_{IN_{MIN}}$	-145.4458 dBm	
Elevation angles	$\theta_{inc} = 90.01°$	$\theta_{inc} = 87.78°$
	$\theta_{obs} = 90.03°$	$\theta_{obs} = 88.55°$
L	51.2 Km	
h_{IoO}	658 + 232 m	
h_{Target}	900 + 0 = 900m	900 + 20 = 920 m
h_{PBR}	958 m	

In Figure 6.11 estimated coverage for a representative car is depicted, as in previous scenario the minimum average BRCS was selected, Table 6.8. Results show a small circular area centred on the passive receiver, around 1 Km of radius, modulated by the complex relief giving rise to a very irregular shape.

Table 6.8: Estimated BRCS for the scenario centered on CEAR facilities.

BRCS	Mazda 6 SPORT			Dron AAI RQ2		
(dBsm)	Max.	Min.	Average	Max.	Min.	Average
Global	28.5074	9.2757	23.2747	39.8356	-3.8136	15.7183
$\beta = 55°$	25.4644	-16.441	12.9029	16.3828	-30.6623	3.0835
$\beta = 70°$	22.3684	-18.6675	10.7284	18.9076	-33.2463	5.1882
$\beta = 90°$	23.140	-9.3822	11.2612	18.4268	-355542	5.0041
$\beta = 105°$	22.3843	-14.6620	11.0325	17.9957	-32.9340	5.6443
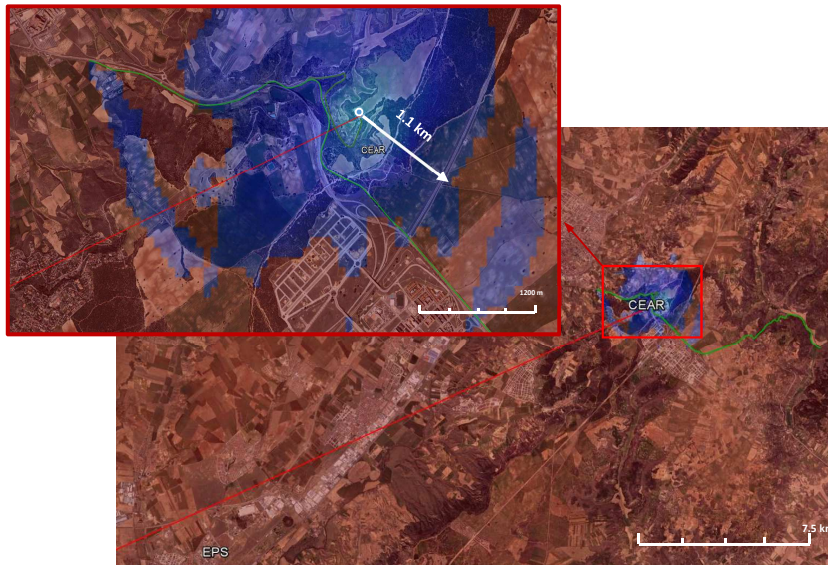
Figure 6.11: Estimated system coverage for a target modelled by a Mazda 6 SPORT car at the CEAR scenario

As in the main scenario, the higher coverage obtained when a drone, flying a low altitude, is depicted in Figure 6.12. A very irregular coverage area is shown, due to the complex relief the area of interest presents.

The very restrictive coverage region, its irregular shape, in combination with the roads emplacements, makes this scenario a very challenging one for the ground target monitoring purposes IDEPAR is focused on.

6.5   EO-SAR based passive radar scenario

Keeping in mind the purpose of improving the versatility capacities of the passive radar system, satellite IoOs were considered due to the high availability expected from this kind of system and their almost total invulnerability against both, natural disasters and physical attacks. EO-SAR satellites were considered in a first approach. Compared to
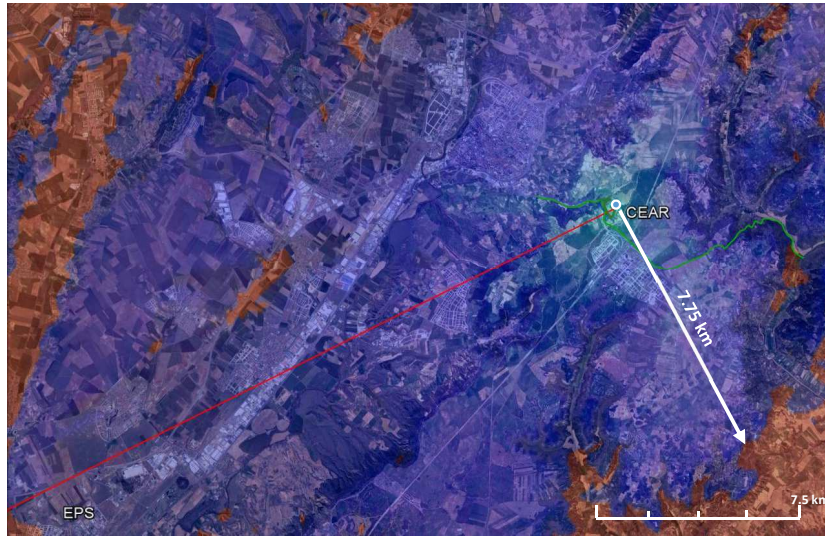
Figure 6.12: Estimated system coverage for a target modelled by AAI RQ-2 Pioneer drone at the CEAR scenario

other satellite systems, they are characterized by the use of radar signals, lower orbits and higher transmitted power. The PAZ system was selected to be analysed. It was developed by the Spanish National Earth Observation Program, PNOTS and it is a X-band SAR instrument mounted on a TerraSAR-X-like platform. An analysis of a scenario based on the use of this sensor is presented taking into consideration system coverage and bistatic geometry. The passive radar receiver was again located on the roof to the Superior Polytechnic School already used in the main IDEPAR scenario.

An analysis of the BRCS for the selected car, Mazda 6 SPORT, was carried out. Two incidence elevation angles were selected, taking into consideration the receiver location and the IoO orbit characteristics 15° and 65°. In Figure 6.13 the variation of the incidence azimuth angle is depicted for both cases.

For each selected incidence elevation angle, an average BRCS value was obtained using only the first estimation methodology due to the special characteristics the use of a space-borne illuminator gives rise: very large baseline, split coverage areas, etc. In Figure 6.14 and 6.15 2D estimated BRCS maps are depicted, in addition BRCS averaged value along the incidence azimuth direction is shown for $\theta_{inc} = 15°$ and $65°$ respectively. In Table 6.9 the BRCS values obtained are summarized, considering a set of incidence elevation angle $\theta_{inc} = [15°, 25°, 35°, 45°, 55°, 65°]$.

Due to the great distance between the IoO and the Passive Radar Receiver, PRRX, $L > 2(R_T R_R)$, the coverage area is split into two regions centered on the illuminator and the PRRX, respectively. The area of interest must be located inside this last oval, so the PRRX and the area under surveillance are in the same coverage region. The coverage area, imposed by the available power at the PBR antenna, was calculated assuming an incidence angle for the IoO that can varies in $[15°, 65°]$ and associated Equivalent Isotropic

(a) $\theta_{inc} = 15°$ (b) $\theta_{inc} = 65°$
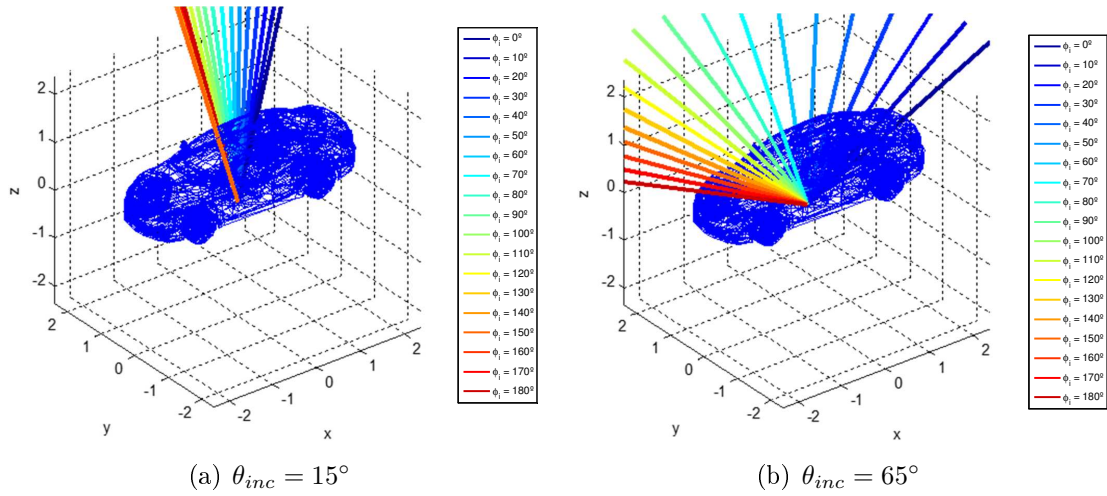
Figure 6.13: Study of the spatial and time variation of the system geometry parameters.

(a) BRCS estimated 2D map   (b) Averaged BRCS along incidence az-
                                           imuth dimension
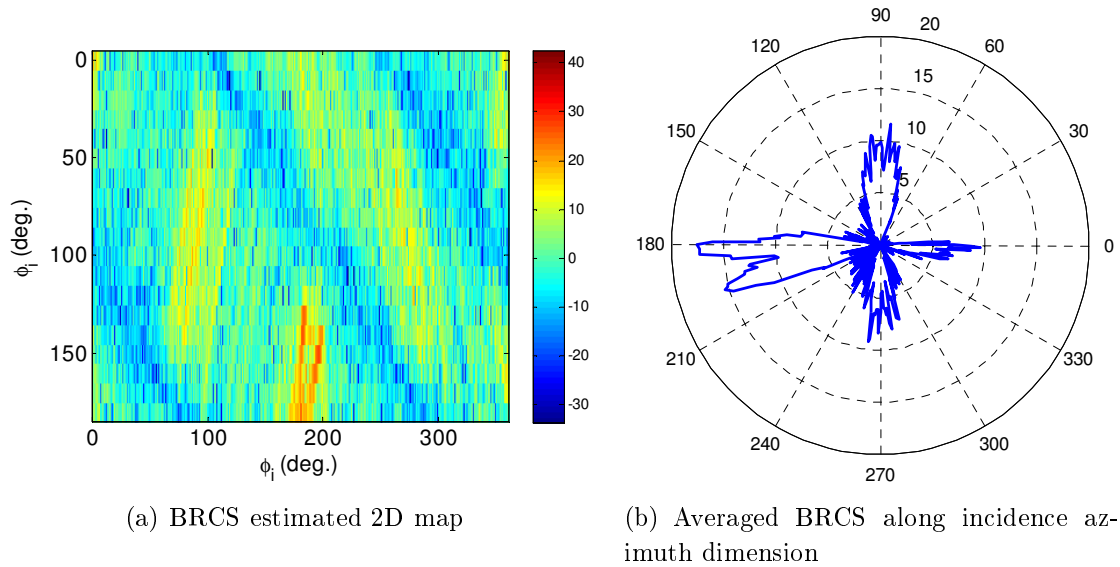
Figure 6.14: Study of the estimated BRCS for $\theta_{inc} = 15°$.

Radiated Power (EIRP) that goes from 65.4 dBm for $\alpha = 15°$, to 63.4 dBm for $\alpha = 65°$, and it is presented in Figure 6.16.

For satellite platforms characterized for non geosynchronous orbits, the IoO location cannot be considered as a constant in the system geometry: there will be a displacement between the IoO and the passive receiver. The main geometry parameters (R_T, R_R and β) can be estimated for each detected target as functions of time in order to check its effect onto passive radar capabilities.

Due to its similarities, TerraSAR-X platform dynamic was used to modulate the PAZ one, that it is not yet deployed. Its instantaneous position can be determined using the Simplified General Perturbation model (SGP4) and then a bistatic system geometry analysis could be carried out throughout the coverage area (Figure 6.17), assuming that

(a) BRCS estimated 2D map

(b) Averaged BRCS along incidence az-imuth dimension
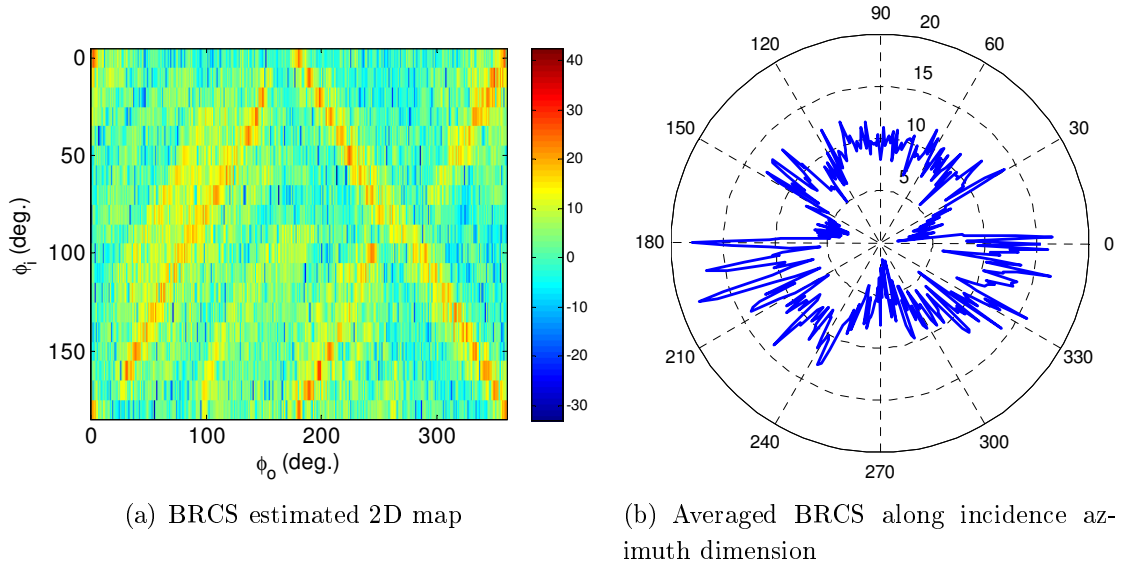
Figure 6.15: Study of the estimated BRCS for $\theta_{inc} = 65°$.

Table 6.9: Obtained BRCS values for car target assuming space-borne scenario.

	$\theta_{inc} = 15°$	$\theta_{inc} = 25°$	$\theta_{inc} = 35°$	$\theta_{inc} = 45°$	$\theta_{inc} = 55°$	$\theta_{inc} = 65°$
Max.	17.504	21.751	18.944	15.749	15.873	18.224
Min.	-4.173	-2.842	-1.454	-2.023	-0.984	1.619
Average	6.19	7.345	7.986	8.764	8.388	9.969

a non-moving ground target was located at the center of each cell of a grid that covers all the area: for each grid location or cell, the evolution of the system geometry parameters are obtained along 1.5 seconds.

The PR receiver was located at the center of the area of interest. The satellite movement can be associated with the following system parameter:

1. The bistatic angle is now time-dependent. In Figure 6.13(a) the total variation of the bistatic angle during the whole acquisition time is represented. The maximum bistatic angle variations is equal to 1.17°.

2. Because of the satellite movement, the bistatic time delay and the associated bistatic range are also a function of time. This makes the estimated target location a time-dependent variable. In Figure 6.18(b), the total variation of the bistatic range during the whole acquisition time is represented. In this case, variations of 50 m are calculated.

In Figure 6.19, the virtual trajectory of a stationary target located at the upper right corner cell of Figure 6.13(b) is depicted. During the acquisition time, an average speed of 38 m/s and a total variation of the bistatic range of around 55 m were estimated.
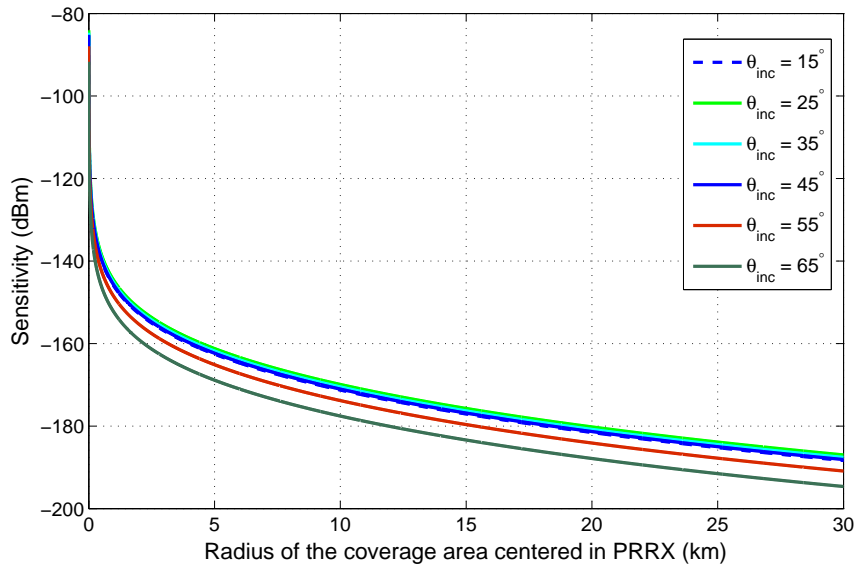
Figure 6.16: Coverage area of PAZ as the IoO depending on the sensitivity of the system and the incidence angle of the satellite's illumination beam.
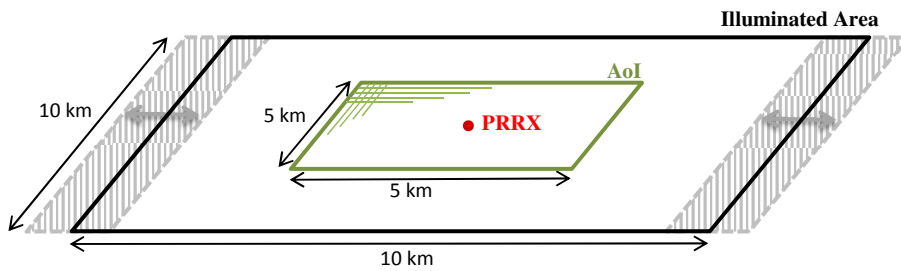
Figure 6.17: Case study geometry analysis scheme.

(a) Bistatic angle variation

(b) Bistatic range variation
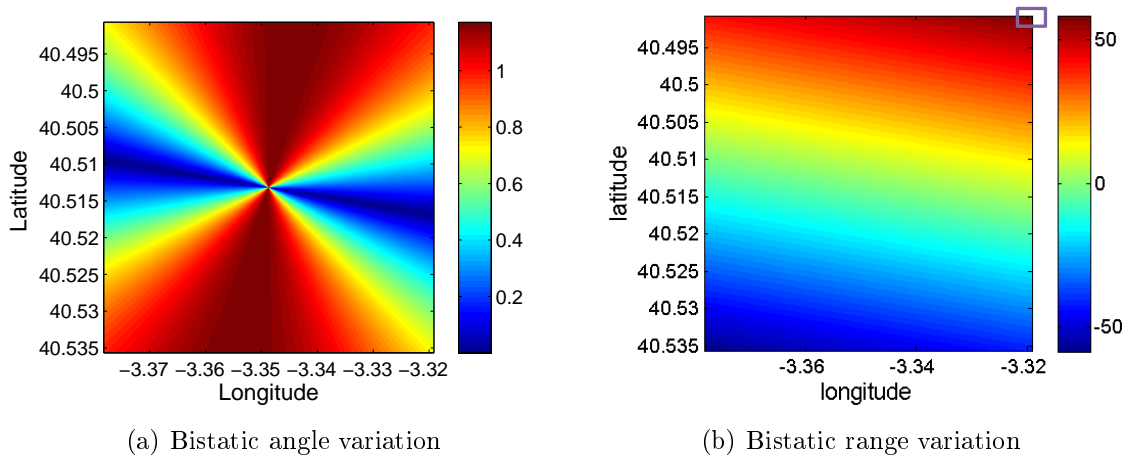
Figure 6.18: Study of the spatial and time variation of the system geometry parameters.
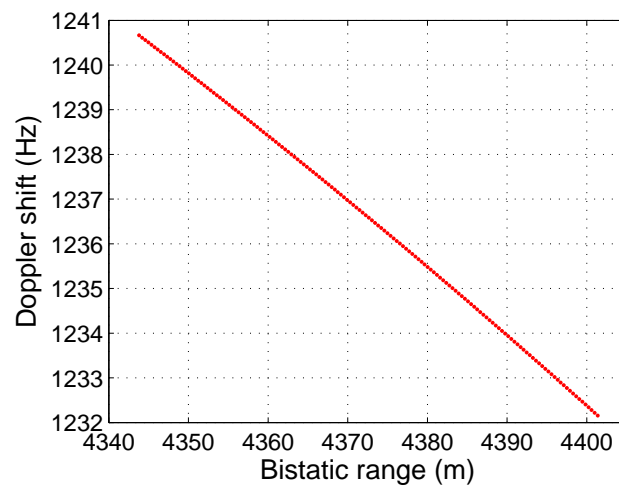
Figure 6.19: Virtual displacement for a fixed point inside the area of interest.

Chapter 7

Zero Doppler Interference Reduction Strategies

7.1   Introduction

In section 4 a study of the state of the art in adaptive filtering strategies for ZDR in passive radar applications was presented. In the available literature, most of the solutions are based on LMS and ECA approaches. The advantajes and drawbacks of the proposed strategies were also described in section 4. Main drawbacks of these algorithms were: convergence time, stability, robustness and computation cost. In general the parameters used for the performance analysis are Steady-State misadjustmen(SSM), convergence time, and sometimes main lobe SNR measured using CAF output.

In this PhD thesis, a different approach is presented and applied, which considers two aspects:

- The impact of the filtering stage on the global detection and tracking performance of the system. This approach allows to take advantage of, for example, the relation between consecutive CPIs.

- The associated computational cost, especially in the study cases of most interest, related to the processing of high bandwidth signals.

In the study presented in section 4, filtering approaches were applied to FM, DRM, Chinese Digital Television and WiFi signals. In this PhD Thesis, multichannel DVB-T signals acquired by the IDEPAR demonstrator were used. The main features of the defined problem were the following:

- As a first approach for increasing range resolution, the demonstrator was designed for the acquisition of three consecutive channels, with a bandwidth of 24 MHz, and guard intervals between channels. For integration times of 250ms and 500ms, the number of samples per CPI was equal to 6 and 12 millions of complex samples, respectively

- Filtering solutions based on batches processing were avoided in order to maintain a Doppler resolution only dependent on the integration time.

- Filter parameters selection criteria were analysed in terms of detection and tracking performance on the global system.

- Challenging computational cost constraints associated to the high bandwidths required the proposal of alternative approximated solutions compatible to real time operation.

7.2   Proposed methodology

The proposed methodology is based on the definition of two quality parameters which are calculated on the RDS in order to evaluate algorithms disturbance rejection performance:

- Target location SNIR: defined as the ratio between the target location RDS level (estimated from a window centred on the target), and the background level estimated from data contained in a outer window, centred on the target, that excludes the inner window). From the CFAR detector point of view:

  1. The inner window provides the information about the Cell-Under-Test, (CUT), target levels in the CFAR algorithms.

  2. The outer window provides the information about the variable surrounding interference level, used by the CFAR algorithms to adaptively vary the detection threshold to maintain the false alarm probability constant. Different types of CFAR algorithms use different sets of cells to estimate interference level.

- Zero Doppler Interference Rejection ratio, ZDIR: A new window was defined centred on the zero Doppler line of the CAF, and including three windows. The central one was used for estimating the interference level concentrated close to the zero Doppler line, and two outer windows for evaluating the pedestal value around the inner one.

Figure 7.1 shows examples of windows definition for SINR evaluation (the upper one with target, red, and background, blue, subwindows), and the yellow one with the zero Doppler interference area and the surrounding area in green. If both windows are defined centred in the same range cell as the target, the effect of target and ZDI dispersion throughout the CAF can be evaluated.

In the presented results, acquisitions of 20s. were used, and consecutive CPIs of 250ms were processed. In Figure 7.2 the RDS used in the analysis is depicted. Data acquired in the main trial scenario during the measuring campaigns carried out in 2014 were used. In this chapter, for saving space and without loss of generality, all results are presented using a RDS, but all the conclusions can be extended to any of the database acquisitions. In Figure 7.2 the considered RDS is presented without applying any pre-processing stage.
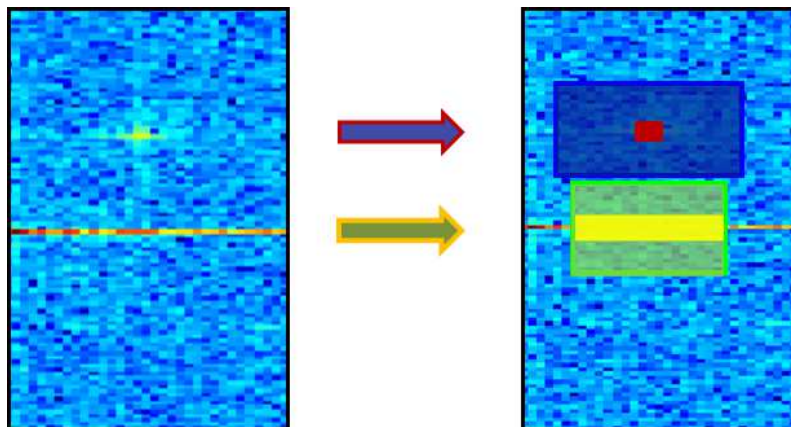
Figure 7.1: RDS regions used in the algorithm performance analysis: target area in red, target background in blue for the evaluation of SNIR; yellow one with the zero Doppler interference and its surrounding area coloured in green for ZDIR evaluation.

The information related to the RDS points under study is also presented: 10 points composed of 7 potential targets and additional 3 ones used as a control set without an associated possible target (only for ZDI analysis purposes). All the main high level peaks in the RDS are considered, with high or low Doppler shifts of both signs, and with high or low associated range bin. In Table 7.1 the location of the reference points is summarized.

Table 7.1: Reference points used in the filtering analysis

Reference Points (ID)	Range Bin	Doppler Shift [Hz]
1	32.0	.92
2	138.0	-61.5
3	195.5	92
4	218.5	65
5	514.0	-44
6	616.0	92
7	678.5	92
8 (ZDI)	439.5	134
9 (ZDI)	503.5	142
10 (ZDI)	581.0	142
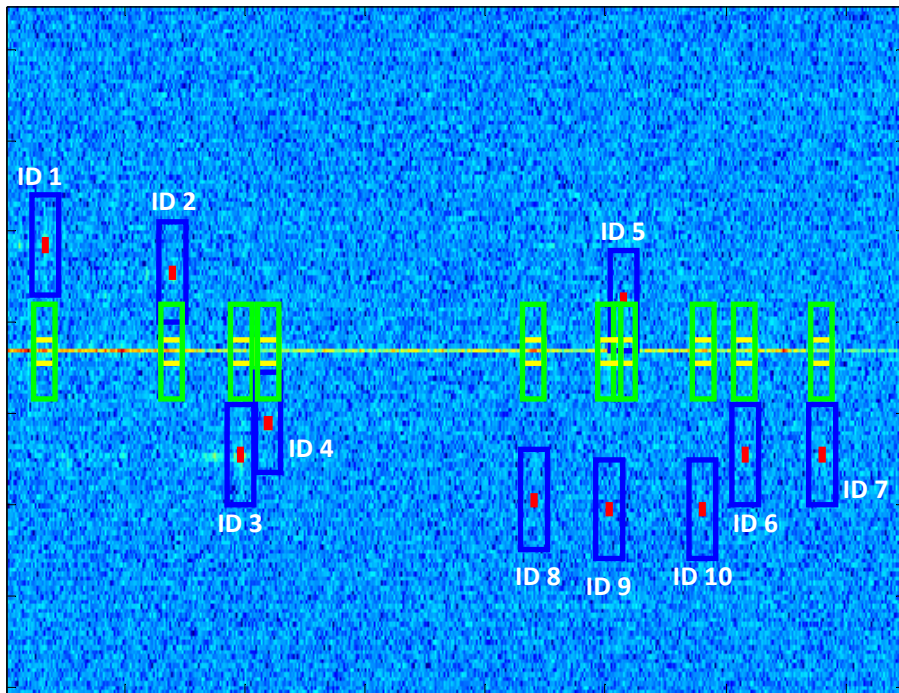
Figure 7.2: RDS and points used in the algorithm analysis

7.3   RLS filtering strategy

In this section a study of the detection parameters evolution of the RLS algorithm with respect to the filter order and the forgetting parameter λ was carried out. The main algorithm fundamentals can be found in section 4.4. The algorithm updating rule is repeated here for convenience:

$$\mathbf{w}(n) = \mathbf{w}(n-1) + \mathbf{k_G}(n)F^*_{WLS}(n) \tag{7.1}$$

In Figure 7.3 the range-Doppler surfaces for two different filters with number of weight coefficients K = [70, 200] are presented (the filter order is K-1). There is a level reduction for lower range locations than equally spreads throughout all Doppler values reducing the CAF level at those locations where targets are expected.

The α parameter controls the algorithm recursive mechanism. In Figure 7.4 the evolution of the SNIR and ZDIR with respect to the forgetting parameter is depicted. RLS algorithm is unable to reach an stable state for λ lower than 0.85, and also for higher values, the filtering is not obtaining the desired results, reducing considerably the SNIR at the targets positions, Figure 7.4.

The algorithm performance for $\lambda = 0.99$ with respect to the filter order is presented in Figure 7.5, where only filters of order lower than 205 have been considered:

- The SNIR shows that the system detection capabilities will be strongly degraded due to the use of the RLS filtering approach: in 7.5(a) this is shown as the difference
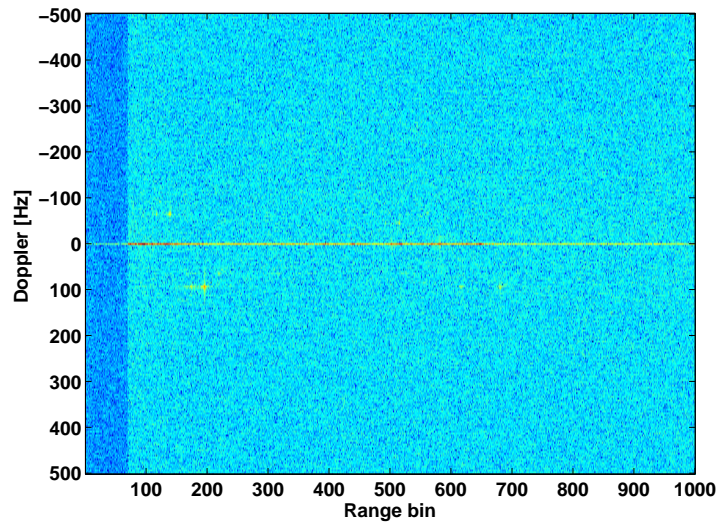
(a) K = 70
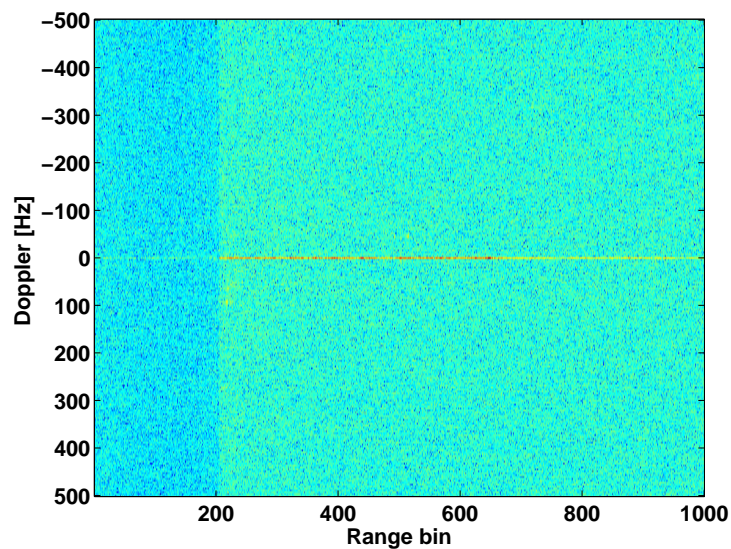
(b) K = 205

Figure 7.3: Range-Doppler surface of CPI 70 filtering with RLS algorithm using different filter orders

between dotted and continuous coloured lines, representing results using raw and filtered signals respectively.

- There is a rejection of the undesired components obtained for those filtered targets, presented in Figure 7.5(b) as a reduction in the ZDIR of each target (continuous coloured lines) respect to the obtained when the raw signals are used (dotted coloured lines).

(a) SNIR

(b) ZDIR
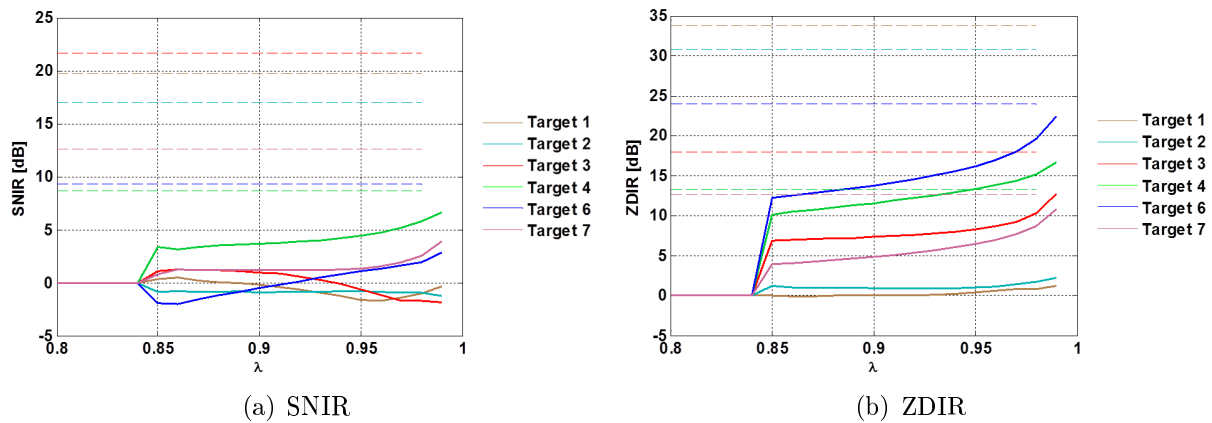
Figure 7.4: Variation of the detection parameters with λ, for the following targets: T1 (Rb = 32), T2 (Rb = 138), T3 (Rb = 198.5), T4 (Rb = 218.5), T6 (Rb = 616) and T7 (Rb = 678).

(a) SNIR

(b) ZDIR
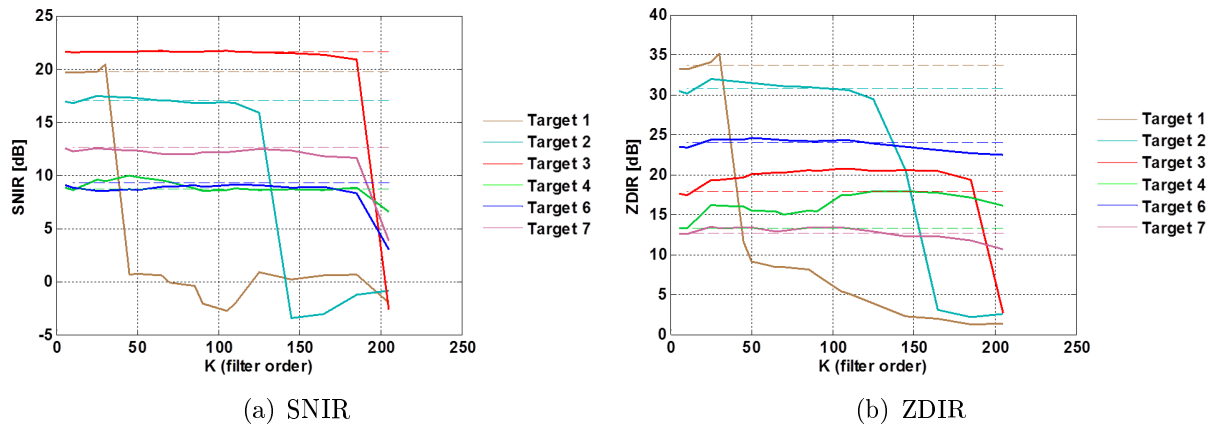
Figure 7.5: RLS filtering detection parameters variation with k (filter order),for the following targets: T1 (Rb = 32), T2 (Rb = 138), T3 (Rb = 198.5), T4 (Rb = 218.5), T6 (Rb = 616) and T7 (Rb = 678).

Taking into consideration the obtained results, the use of this algorithm in the IDEPAR demonstrator is not recommended, due to the loss in target detection capability the SNIR reduction gives rise. In addition, the computational cost increases considerably with the filter order for the CPI length, making this approach the less suitable for the system characteristics.

7.4 LMS based filtering strategies

In this section, the results of the analysis of LMS-based filtering strategies is shown, using the defined parameters to take into consideration their impact on the demonstrator detection capabilities. In Figure 7.6 RDSs obtained after applying the conventional LMS filter for a conventional LMS are depicted, assuming a fixed value of 250 for K, showing the general RDS level variation that the filtering process gives rise for three selected step-size parameters: $\mu = [10^{-5}, 10^{-6}, 10^{-7}]$. This level variation was locally analysed through the estimation of the SNIR parameter at the defined reference points, for $\mu = 10^{-5}$, and results are shown in Figure 7.7.

If the region that spreads from the zero range bin to the K range bin including all Doppler shifts is considered, the filtering not only reduces the RDS level of the zero-Doppler line, but also affects to all Doppler values, being this effect dependent on the RDS position. A border effect located around the $k - th$ range bin and spreads throughout all Doppler values is clearly observed. How this RDS level reduction evolves along the Doppler dimension depends on the algorithm parameters:

- For high μ values, the adaptive algorithm is not able to achieve good filtering results, an associated decrease in the SNIR parameters for the commented K is shown in Figure 7.7(a). But reduce the obtained CAF levels in those points with a range-bin lower than K, generating a reduction in the general RDS region level, Figure 7.6(a). Additionally an abruptly reduction in the SNIR level is detected for all the targets when the filter order is close to their respective range location. This notch is generated by the windowing technique selected to obtain the SNIR parameter itself.

$$y(n) = \mathbf{w}^H(n)\mathbf{S}_{REF,n} \tag{7.2}$$

- As the μ values get lower, the filtering is improved, and the level reduction is more focused on the Zero-Doppler interference region, Figures 7.6(b) and 7.6(c) preserving the target level. This effect is also shown in 7.7(b), where for a higher step-size parameter, $\mu = 5 \cdot 10^{-6}$, the SNIR values improves those obtained using $\mu = 10^{-6}$.

- An undesired effect derived of the step-size reduction is the increase of the convergence time of the adaptive process. Low range bins levels will be progressively disturbed: in Figure 7.6(b) and 7.6(c) the progression of this effect is clearly visible, for example at range bins close to 100. This undesired effect could reduce target information and zero-Dopper interference rejection, Figure 7.6(c).

Derived from convergence time consideration, there is a lower limit for the μ values, but according to the convergence condition (7.3), there is, in addition, an upper limit that depends on the signal energy and the algorithm tap input vector length, determined by

(a) $\mu = 10^{-5}$
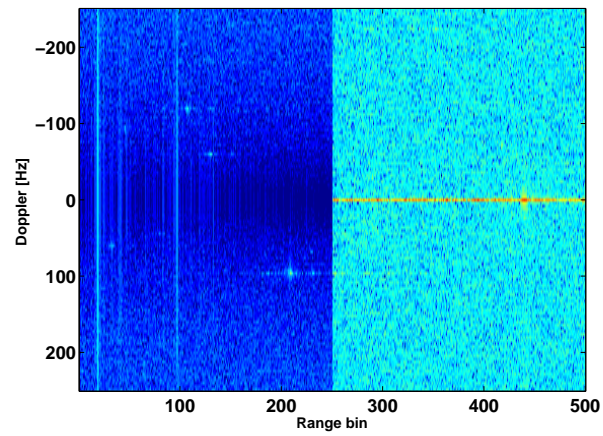
(b) $\mu = 10^{-6}$
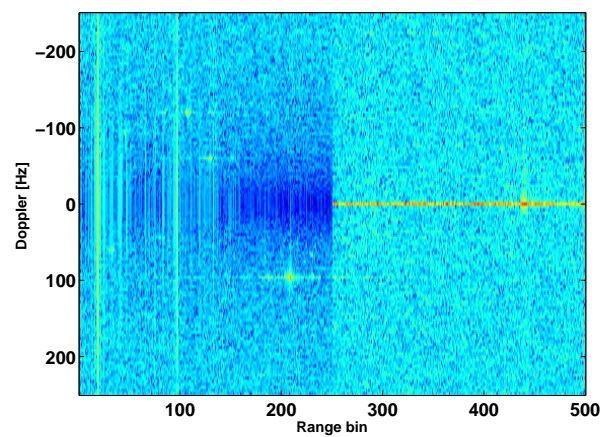
(c) $\mu = 10^{-7}$

Figure 7.6: RDS after filtering with LMS algorithm.

(a) LMS filtering using $\mu = 10^{-5}$

(b) LMS filtering using $\mu = 5 \cdot 10^{-6}$
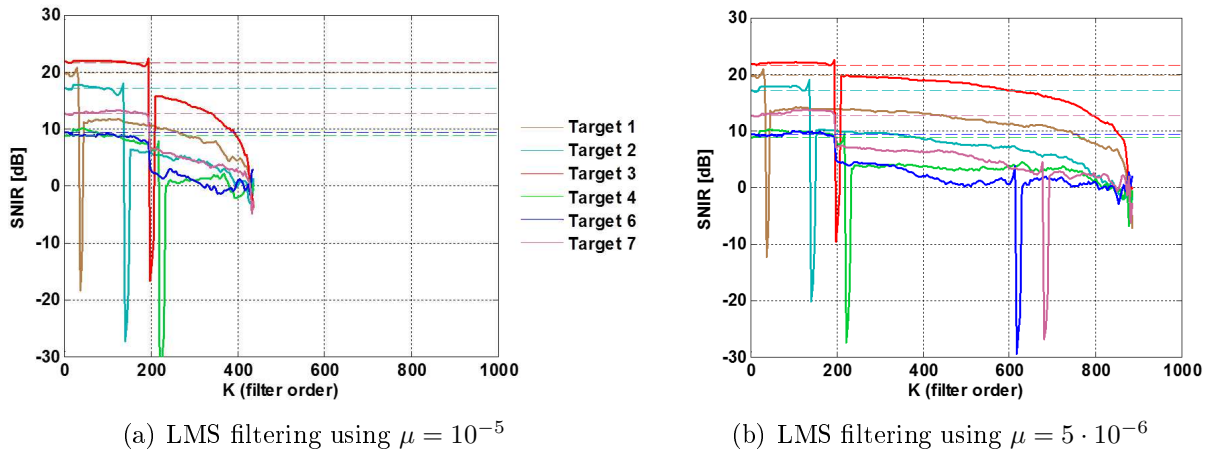
Figure 7.7: Filter order limitation with respect to the step-size parameter μ, for the following targets: T1 (Rb = 32), T2 (Rb = 138), T3 (Rb = 198.5), T4 (Rb = 218.5), T6 (Rb = 616) and T7 (Rb = 678).
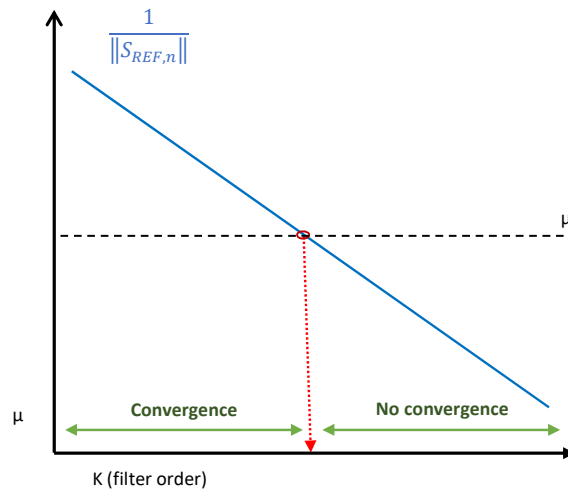
Figure 7.8: Convergence zones for fixed μ parameter according to the filter order k

the filter order.

$$o < \mu < \frac{2}{\sum\limits_{m=0}^{K-1} E|\mathbf{S}_{REF,n}(n-m)|^2} \tag{7.3}$$

In Figure 7.8 the relation between both parameters are depicted, in addition, Figure 7.7 show the changes in this linking effect with respect to the step-size parameter. The effect of this limitation could be observed in two different ways:

1. For a fixed range bin location where the filtering is desired to be applied, there is an associated upper limit for the step-size value and therefore, the distortion related to high convergence time could not be always avoided.

(a) Variation of the SNIR   (b) Variation of the ZDIR
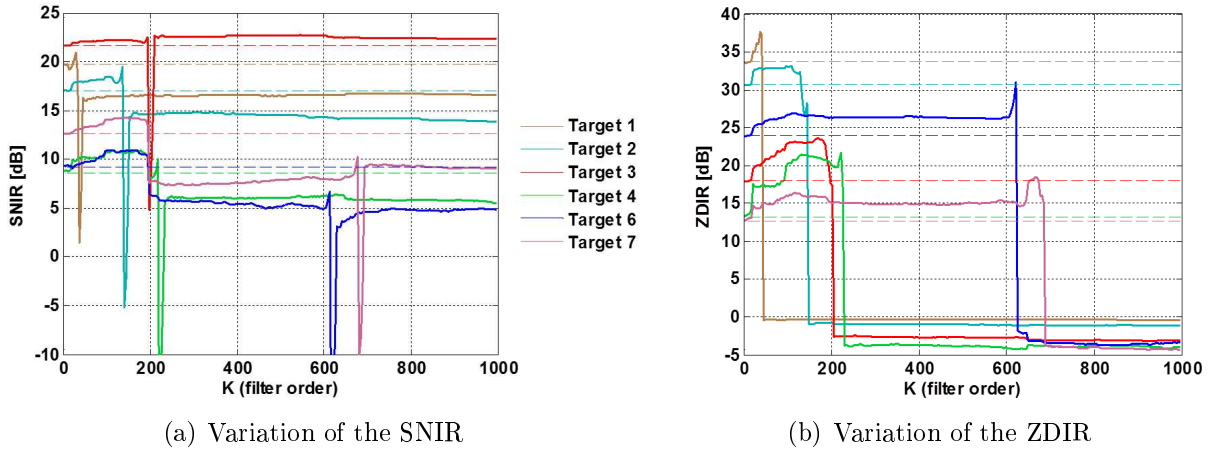
Figure 7.9: Algorithm performance for the following targets: T1 (Rb = 32), T2 (Rb = 138), T3 (Rb = 198.5), T4 (Rb = 218.5), T6 (Rb = 616) and T7 (Rb = 678), using $\mu = 10^{-6}$.

2. For a fixed step-size value, a upper limit for K value may appear, a maximum range bin value that sets where the improvements due to the zero-Doppler interference reduction can be exploited. In Figure 7.7 this effect is depicted, showing how the SNIR is progressively degraded as the filter order increases, until the filtering ceases to work.

For μ values lower than $2 \cdot 10^{-6}$, the filtering can be considered free of this limitation for the range-bins considered in this work. In Figure 7.9 the variation of the SNIR and ZDIR with respect to the filter order are shown for a step-size value that fulfils this criterion but still high enough to avoid the undesired convergence-time effect gets too relevant. A great reduction in the disturbance level is observed for all studied targets locations, Figure 7.9(b) and the SNIR level is slightly reduced. The study of the target 5 is depicted separately in Figure 7.10 due to its location close to the zero-Doppler region. For this target, a great improvement in its detection capability its expected due to the SNRI improvement shown in 7.10(a).

In sections 7.4.1 and 7.4.2 strategies to face the algorithms limitations derived from the steps-size constrains will be proposed.

7.4.1   LMS modification: weights inheritance

Taking advantage of the segmentation applied to the acquisition data, a weights inheritance mechanism has been implemented in order to avoid the undesired effects of the convergence time.

1. A null weight vector is used for the first segment of the data measurement. For this segment, all the convergence time effects commented in section 4.3 should be still considered.

(a) Variation of the SNIR

(b) Variation of the ZDIR
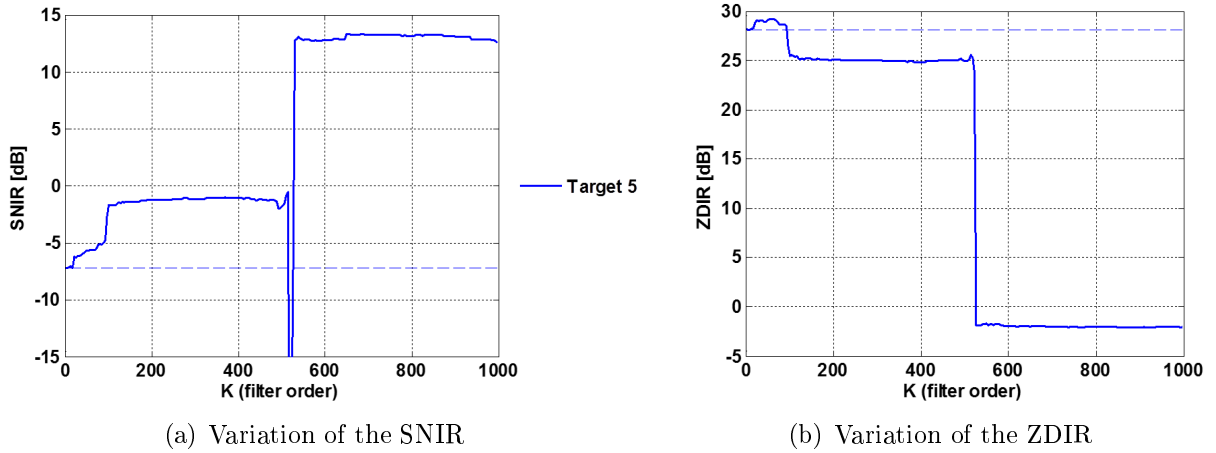
Figure 7.10: Algorithm performance for target 5 (Rb = 514) using $\mu = 10^{-6}$

2. The resulting weights vector obtained at the end of a CPI filtering process is used as the LMS initialisation vector for the next CPI, reducing the time required for the adaptive algorithm convergence. This approach is based on the hypothesis of stationarity of the zero Doppler interference between consecutive CPIs. In the case of study, consecutive CPIs are processed, so this feature can be assumed.

In Figure 7.11, the global RDS level variation show an improved filtering without the distortion drawback aforementioned. From the filtering design point of view, the μ lower limit has been lowered, at the cost of the degradation of the first CPI, that always will be initialized with a null weight vector. In Figure 7.12 a comparison for the same algorithm parameters configuration is depicted showing the improvement the proposed weight inheritance mechanism introduces. When equal μ parameters are used, there is an improvement in the performance only for those targets associated with low range bin locations, where the convergence time effect affects. As the μ gets lowered, this effect spreads for all targets. In Figure 7.13, a comparison for the SNIR variation for targets 2 and 7 are shown: the increase in the SNIR for target 7 its only remarkable for $\mu = 10^{-8}$, but for target 2, with a lower range bin, a noticeable improvement for $\mu = 10^{-7}$ is also shown.

In Table 7.2a comparison between the inclusion or not of the weight memory is summarized.

For target 7, an unexpected behaviour is observed: the measured SNIR reduces abruptly for a filter order associated with a bistatic range not related to it, $R_{bin} = 195$ but with the target 3. In addition this reduction is not associated to the aforementioned SNIR reduction peak derived from the windowing effect, as all the other level steps are. Target 6 SNIR evolution is also related to target 3 position in a similar way. This relation disappears for the lowers μ values, the filtering process is more focused on the zero-Doppler line, which can be explained for a direct relation in the targets echoes, as for example, that target 6 and 7 could be, in fact, ghost echoes produced by multipath.
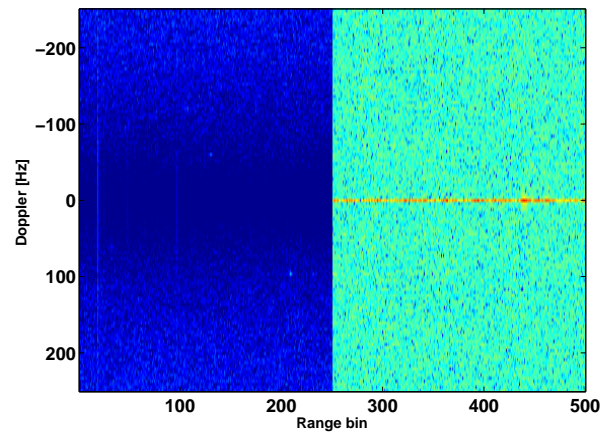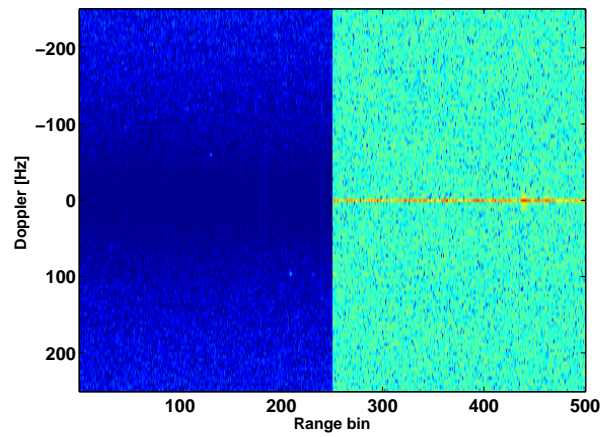
(a) $\mu = 10^{-5}$
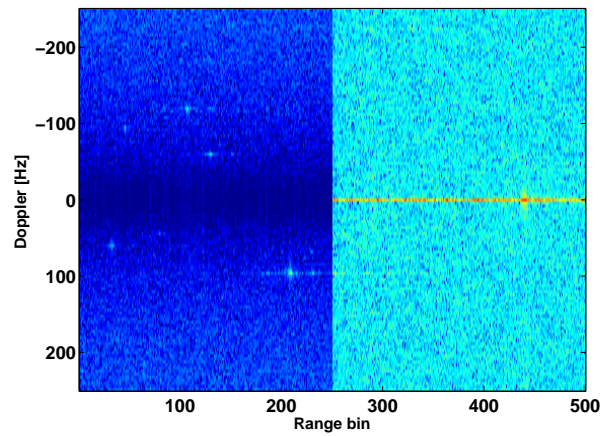
(b) $\mu = 10^{-6}$
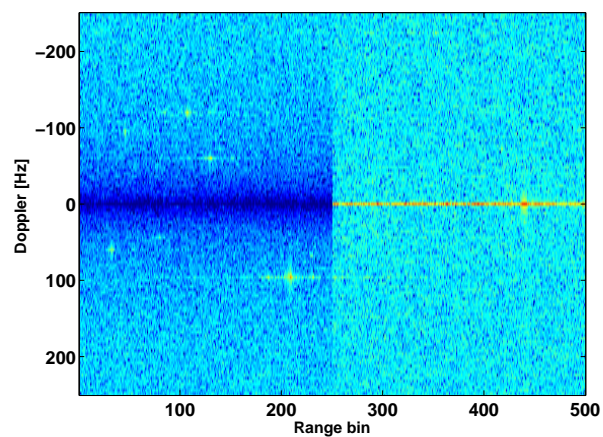
(c) $\mu = 10^{-7}$

Figure 7.11: RDS variation with step-size (μ), applying LMS and weighs inheritance
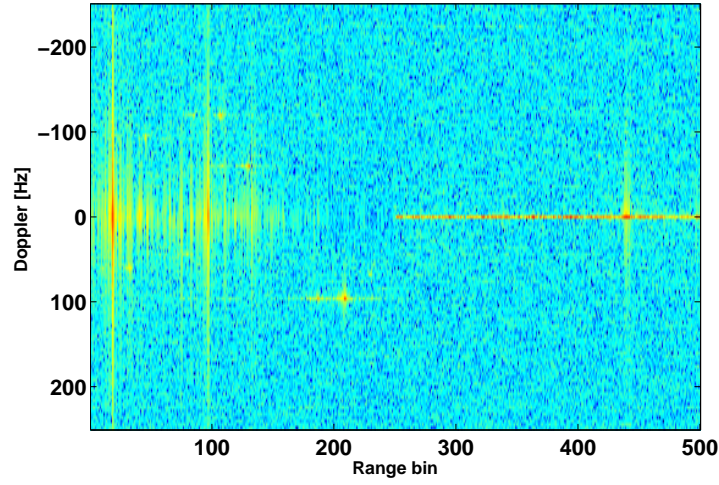
(a) Without applying weights inheritance
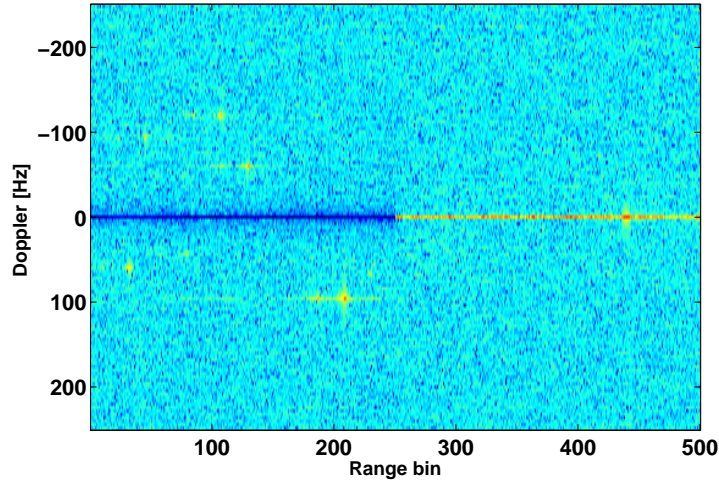
(b) Applying weights inheritance

Figure 7.12: RDS using LMS with and without weight inheritance and $\mu = 10^{-8}$

This relation can be expressed using a simplification of the signal model where the multipath component is affected by a delay and loss factor, τ_{MP} and A_{MP} respectively, equation (7.4). In surveillance channel, (7.5) only one target has been considered, modelled with $A_m, \tau m$ and f_{d_m} and DPI has been suppressed.

$$S_{REF}(n) = s_{IoO}(n) + A_{MP}S_{IoO}(n - \tau_{MP}) + n_{R_{ref}(n)} \tag{7.4}$$

$$S_{SURV}(n) = A_m S_{IoO}(n - \tau_m)e^{j2\pi f_{d_m}n} + n_{R_{surv}}(n) \tag{7.5}$$

Obtaining the CAF for a Doppler equal to the surveillance signal, elements can be grouped in 2 terms, one corresponding to the real target position and the other one around the ghost target, related to τ_{MP}:

Table 7.2: LMS algortihm results for different step-size parameters.

Target	SNRI				ZDIR			
	LMS	WH-LMS			LMS	WH-LMS		
	$\mu = 10^{-6}$	$\mu = 10^{-6}$	$\mu = 10^{-7}$	$\mu = 10^{-8}$	$\mu = 10^{-6}$	$\mu = 10^{-6}$	$\mu = 10^{-7}$	$\mu = 10^{-8}$
1	-3.16	-0.20	0.84	1.38	34.08	36.7	40.85	38.85
2	-2.35	-0.71	0.88	1.99	31.68	34.31	38.60	36.45
3	0.95	0.94	1.13	0.70	20.73	20.01	22.73	22.89
4	-2.56	-2.72	-0.97	2.68	17.07	17.18	20.71	17.44
5	20.35	20.47	23.01	25.16	30.15	30.07	37.74	32.86
6	-4.50	-4.54	-0.35	2.28	27.52	27.00	29.49	28.65
7	-3.32	-3.31	0.25	2.42	16.73	16.01	20.03	17.51
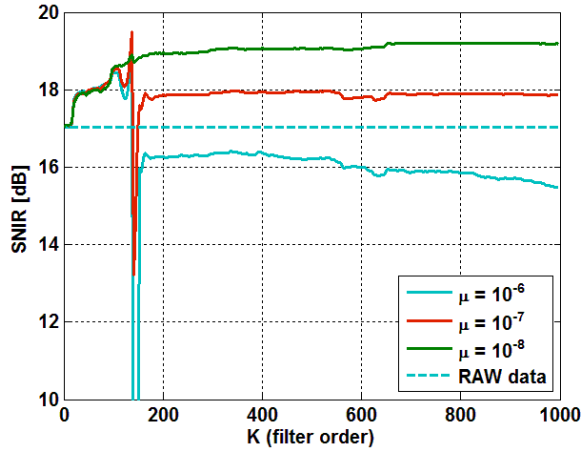
(a) Target 2: range bin 138   (b) Target 7: range bin 678.5
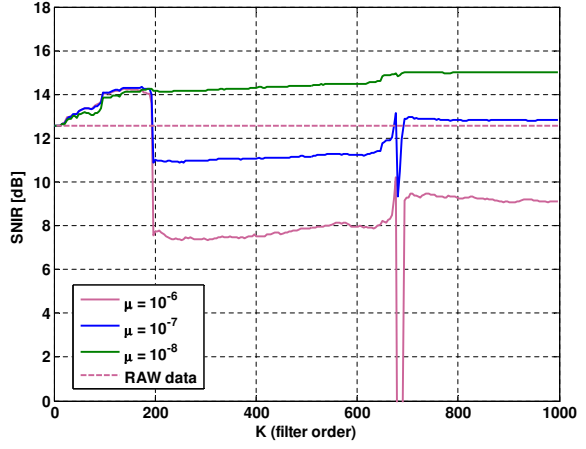
Figure 7.13: SNIR variation using modified algorithm, with filter order parameter for several step-size parameter considering targets 2 and 7.

$$CAF = \sum_{m=0}^{N-1} S_{IoO}^*(n-m)AmS_{IoO}(n-\tau_m) + \sum_{m=0}^{N-1} A_{MP}^* S_{IoO}^*(n-\tau_{MP}-m)AmS_{IoO}(n-\tau_m)$$

(7.6)

If the attenuation of the target due the filtering process (A_{ZDI}) is considered, its effects are presented in both terms:

$$S_{SURV}(i) = A_{ZDI}A_m s_{IoO}(n-\tau_m)e^{j2\pi f_{d_m}n} + n_{R_{surv}}(n)$$

(7.7)

$$CAF_{ZDI} = \sum_{m=0}^{N-1} S_{IoO}^*(n-m)A_{ZDI}Am s_{IoO}(n-\tau_m)+$$

$$\sum_{m=0}^{N-1} A_{MP}^* S_{IoO}^*(n-\tau_{MP}-m)A_{ZDI}AmS_{IoO}(n-\tau_m)$$

(7.8)

So the analysis of the RDS before and after the filtering, could provide information about ghost targets generated by DPI multipath, that could be used for improving system detection capabilities.

7.4.2 NLMS algorithm

The use of a normalization in the weight vector updates, makes bigger the LMS algorithm step-size upper limit. In this work, the NLMS algorithm is combined with the weight inheritance approach. In Tables 7.3 and 7.4 the improvements in the SNIR and ZDIR parameters are presented.

Table 7.3: SNIR improvement using NLMS algorithm for different step-size parameters.

Target	$\mu = 10^{-1}$	$\mu = 10^{-2}$	$\mu = 10^{-3}$	$\mu = 10^{-4}$	$\mu = 10^{-5}$
1	0.15	1.09	1.36	1.17	0.52
2	-0.29	1.42	1.97	1.84	0.95
3	1.17	0.96	0.66	0.67	0.26
4	-2.53	0.54	2.72	2.52	0.91
5	22.10	24.46	24.69	14.23	1.85
6	-2.53	1.76	2.31	2.08	0.48
7	-1.98	2.25	2.37	2.10	0.48

Table 7.4: ZDIR improvement using NLMS algorithm for different step-size parameters.

Target	$\mu = 10^{-1}$	$\mu = 10^{-2}$	$\mu = 10^{-3}$	$\mu = 10^{-4}$	$\mu = 10^{-5}$
1	37.80	41.30	36.83	14.46	3.15
2	35.09	38.85	35.60	19.55	3.35
3	20.80	23.55	20.97	8.63	0.90
4	18.45	20.52	15.61	6.33	-0.24
5	31.99	35.28	28.94	12.63	1.55
6	28.03	30.11	25.68	11.75	1.33
7	18.38	19.66	14.67	1.55	0.28

The SNIR values change slowly with μ parameter, but taking into consideration the evolution of the ZDIR, there is a breaking point (around 10^{-3}) at which the performance quickly gets worse. Values of the SNIR and ZDIR for targets 2 and 5, considering steps sizes values of $\mu = [10^{-1}, 10^{-2}, 10^{-3}, 10^{-5}, 10^{-5}]$ are depicted in Figures 7.14 and 7.15 in order to analysis this effect. Results shown the improvement obtained in SNIR when the μ value is reduced, but also how the ZDIR improvement respect the raw values is decreased too.

For those step-sizes with an associated level reduction in regions with non-zero Doppler frequencies, the SNIR link between target 2 and targets 6 and 7 is still present making reasonable their consideration as ghost targets. In Figure 7.16 it is shown how the target 7 SNIR reduction for the range bin location of the target 3 (198.5) disappears when the step-size parameter gets lower than 10^{-2}.

Through the analysis of target 5, an example of the filtering performance for targets close to zero-Doppler line is presented. For these targets, considerably better SNIR is expected, due to it is directly affected by ZDIR. The ZDIR for this kind of targets shows a small increase, due to the target level rise up the estimated pedestal value considered in the parameter calculation (green coloured window in 7.1).

(a) SNIR   (b) ZDIR
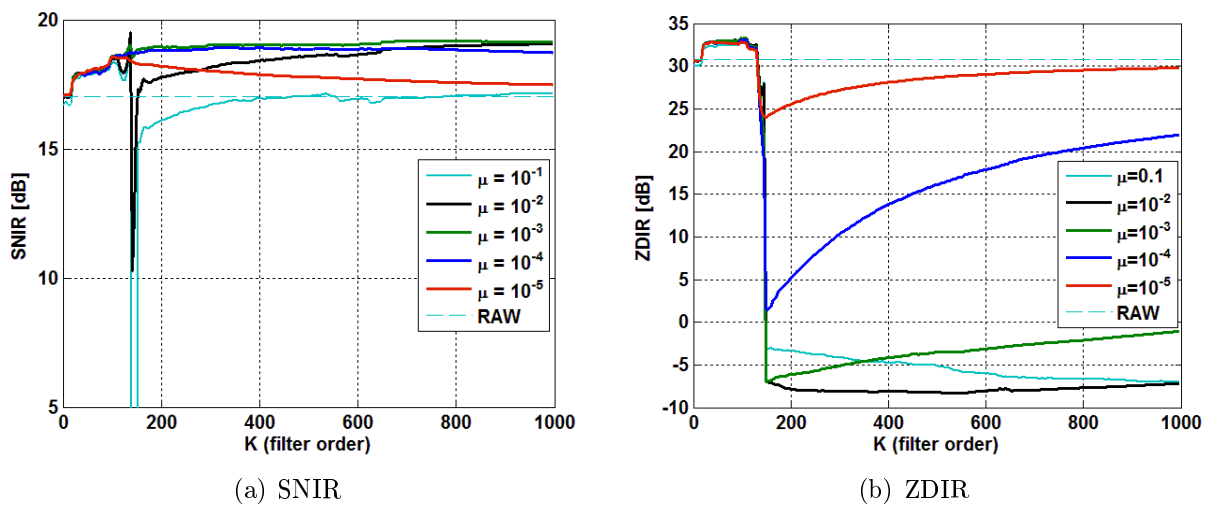
Figure 7.14: NLMS results for target number 2 (Rb = 138) for several step-size parameter.

(a) SNIR   (b) ZDIR
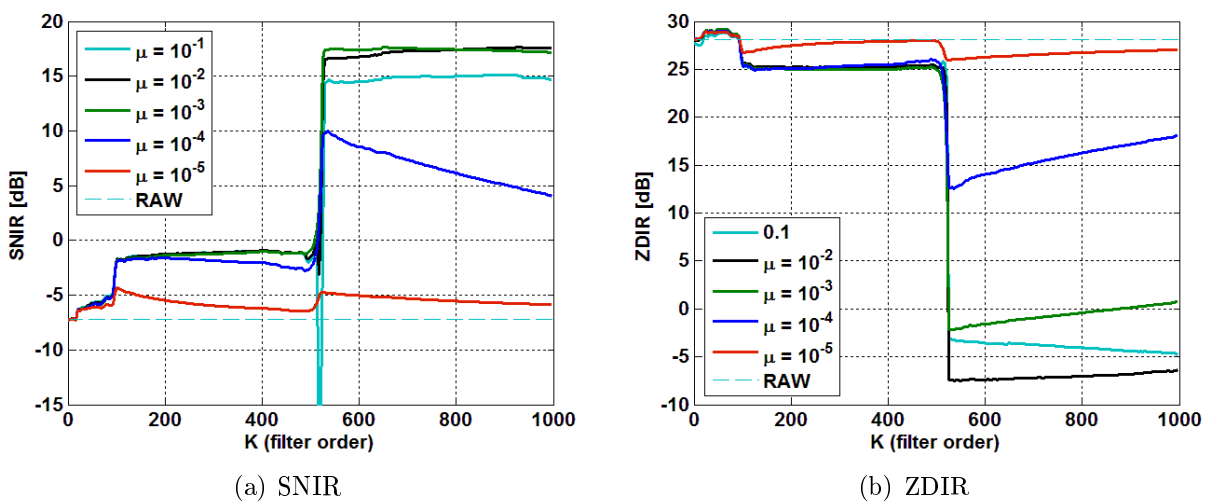
Figure 7.15: NLMS results for target number 5 (Rb = 514) for several step-size parameter.
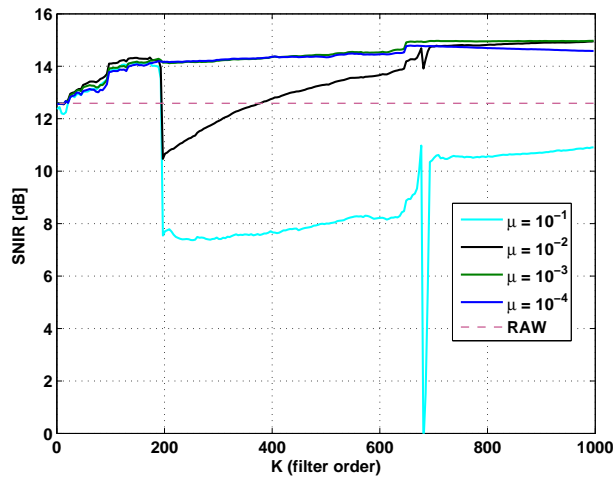
Figure 7.16: Analysis of the target 7 (Rb = 678) SNIR evolution with respect to filter order, showing its relation with the target 3 range bin position (198.5).
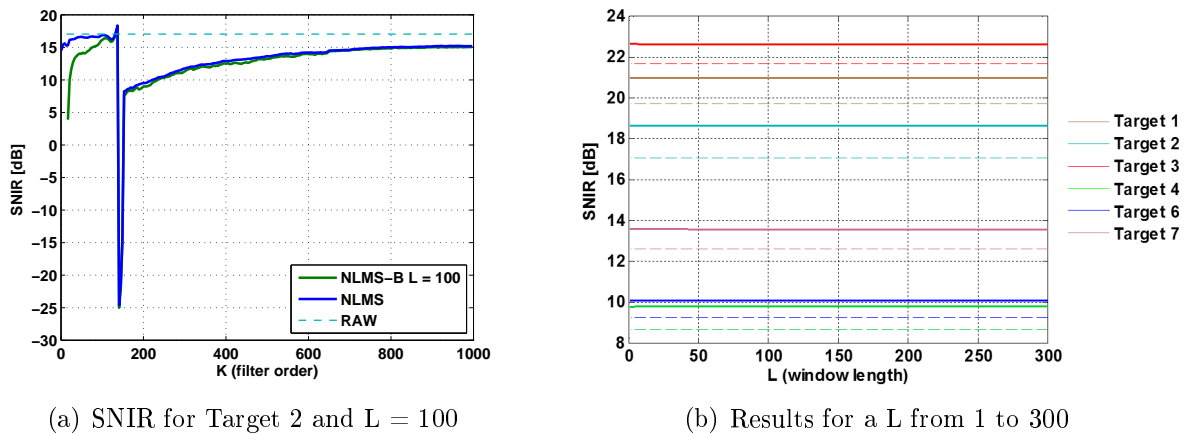
(a) SNIR for Target 2 and L = 100

(b) Results for a L from 1 to 300

Figure 7.17: Results for a WI-NLMS for a fixed and variable batch length.

A batches estimation process of the instant filter error can be implemented in order to improve the gradient estimation. A memory vector with length 'L' was used to obtain a temporal mean of the instant variation. In Figure 7.17(a) the effect to of using a buffer vector with length equal to 100 for target 2 is depicted. No significant improvement with respect to the conventional NLMS algorithm has been detected for the processed acquired data. The evolution of the performance parameters with respect to the length of the estimation vector has been carried out in Figure 7.17(b) and it was not detected any evolution in the algorithm performance.

The conventional NLMS approach in addition to weight inheritance,WI-NLMS , could be considered the most profitable of the stochastic gradient algorithms studied in this work.

7.5   ECA-based strategy: LS-Matrix

In section 4.5.1 it was shown how the computational cost of ECA-based algorithms increases with the filter order and mainly with the length of the input signal vector. In IDEPAR, three DVB-T channels were acquired, with a total bandwidth of 24 MHz. Integration times of 250 ms and 500ms were considered, and, for the selected scenario, K=900 was required, so the associated computational cost could be estimated as 2 GFLOP approximately. As an alternative to ECA-B and ECA-Sliding, a LS-Matrix based approach is proposed, that can be applied to any type of signal, in contrast to ECA-by-Carrier.

Returning to the least square basic principles 4.2.1, in witch the ECA algorithm is based, the value of the weight vector can be expressed in (7.9).

$$\hat{\mathbf{w}} = \mathbf{\Phi}^{-1} \mathbf{z_{S_{REF},d}} \tag{7.9}$$

Matrix $\mathbf{\Phi}$ is defined in (7.10), where each matrix element can be expressed as in (7.11):

$$\mathbf{\Phi} = \begin{bmatrix} \phi(0,0) & \phi(1,0) & \dots & \phi(K-1,0) \\ \phi(0,1) & \phi(1,1) & \dots & \phi(K-1,1) \\ \vdots & \vdots & \dots & \vdots \\ \phi(0,K-1) & \phi(1,K-1) & \dots & \phi(K-1,K-1) \end{bmatrix} \tag{7.10}$$

$$\phi(c,m) = \sum_{i=K}^{N} \mathbf{S}_{REF}(i-m)\mathbf{S}_{REF}^*(i-c) \qquad 0 \le (c,m) \le K-1 \tag{7.11}$$

The calculation of the $\mathbf{z_{S_{REF},d}}$ vector does not require a big computational effort, but the calculation of $\mathbf{\Phi}^{-1}$ can demand a critical amount of computational and memory resources.

If the data for time instants $i < m$ is equal to zero, each element of the matrix can be considered as an autocorrelation for different time instants of the reference channel signal, or a linear combination of it.

- For those matrix elements belonging to the diagonal, c = m:

$$\phi(c,m) = \mathbf{R}_{S_{REF}}(0) - \mathbf{R}_{S_{REF}}(0)|_{corm}$$
$$\mathbf{R}_{S_{REF}}(\tau) = \sum_{n=1}^{N-m} \mathbf{S_{REF}}(n+\tau)\mathbf{S_{REF}}^*(n) \tag{7.12}$$

where $\mathbf{R}_{S_{REF}}$ is the autocorrelation of the received signal defined as in expression (7.12), and $\mathbf{R}_{S_{REF}}|_v$ is defined as its last v terms.

- For those matrix elements defined for t > m, with $\tau = c - m$:

$$\phi(c,m) = \mathbf{R}_{S_{REF}}(\tau) - \mathbf{R}_{S_{REF}}(\tau)|_m \tag{7.13}$$

- For those matrix elements defined for c < m, with $\tau = m - c$:

$$\phi(c, m) = \mathbf{R}^*_{S_{REF}}(\tau) - \mathbf{R}^*_{S_{REF}}(\tau)|_c \qquad (7.14)$$

As the calculation of the autocorrelation is a problem very optimized in a computational cost point of view, if the method is expressed in a matrix way, a great reduction in the filtering time could be obtained.

This method, is included as a result although the same conclusions were obtained in a published paper (January 2016) but with a slightly different theoretical starting point: instead of $\mathbf{\Phi}$ and $\mathbf{z}_{\mathbf{S_{REF}}, \mathbf{d}}$, $(\mathbf{X}^H \mathbf{X})^{-1} \mathbf{X}^H \mathbf{S}_{SURV}$ is used, [Colone et al., 2016].

The proposed approach, LSM-ECA, was applied to the three channels DVB-T signal for K=300 and K=500 , taking into account the filter order as the only customizable filter parameter.

In Figure 7.18 the RDS after filtering are depicted for two values for parameter K. The level of the RDS is reduced for those range locations associated with range-bins lower than the filter order but this reduction is only significant for the zero-Doppler row components:

- For the filtered locations, RDS non zero-Doppler values are not significantly modified. There is not level reduction for those locations, so the detection system capabilities for the targets should stay unaffected. In fact, a slight improvement in SNIR is detected, Figure 7.19(a), for most of the potential targets.

- In Figure 7.19(b) ZDIR evolution with K for each target is depicted showing the algorithm disturbance cancellation performance for each of the RDS location under study, showing a defined interference level decrease when the considered filter order comprehend the range bin target location.

- For those targets in which its SNIR is directly affected by zero-Doppler interference components, a great improvement in the system detection capabilities is expected. In Figure 7.20 the analysis parameters evolution for target number 5 is depicted: in 7.20(a) an improvement higher than 20 dB is shown for the SNIR, but a slightly increase in ZDIR is detected in 7.20(b), due to the way the parameter is calculated.

The absence of a generalized reduction at non zero-Doppler shifts, makes the targets 6 and 7 ZDIR values detached from the target 3 one.

In Table 7.5 SNIR and ZDIR results when LSM-ECA technique is applied are summarized. In addition, results when a WI-NLMS approach are also repeated her for comparison purposes.

Taking into consideration theses results, a very similar system detection capabilities are expected for both pre-processing techniques: in terms of processing time, the LSM-ECA approach clearly outperforms the LMS based optcion due to it reaches the desired weights vector in a single step. But when the WI-NLMS approach is used, the selection
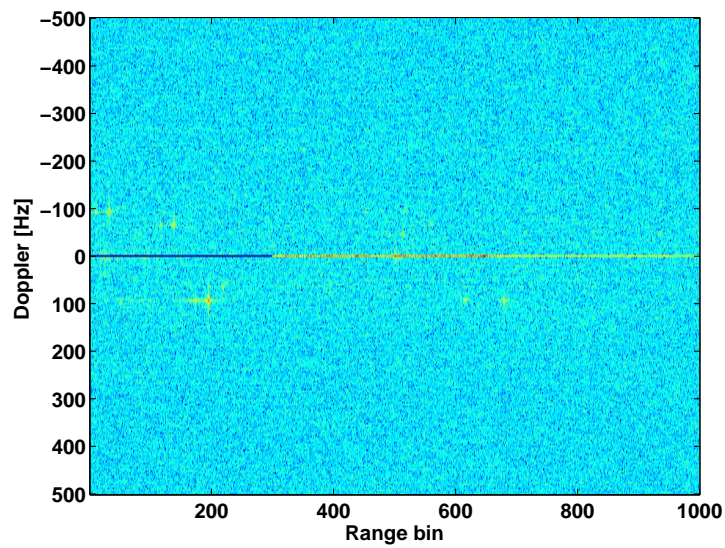
(a) Filter order, k= 300
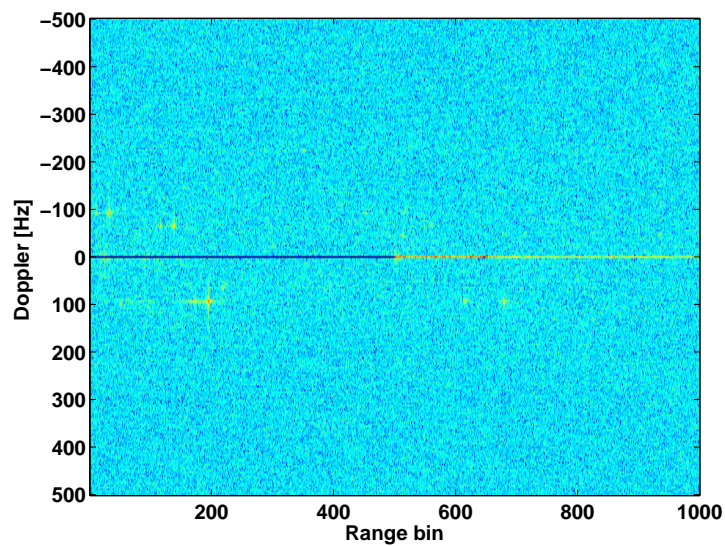
(b) Filter order, k= 500

Figure 7.18: Range-Doppler surface of CPI 70 using ECA algorithm for different filter orders.

of the step-size parameter gives rise to small customization component, that could allow the identification of ghost targets.

(a) SNIR

(b) ZDIR
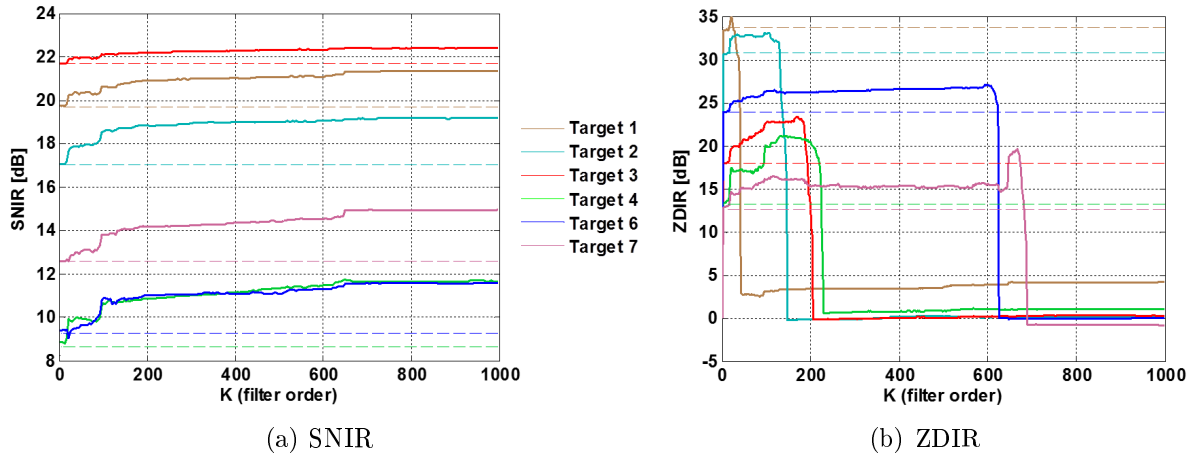
Figure 7.19: Evolution of the LSM-ECA filtering with the parameter K (filter order) for the following targets: T1 (Rb = 32), T2 (Rb = 138), T3 (Rb = 198.5), T4 (Rb = 218.5), T6 (Rb = 616) and T7 (Rb = 678).

(a) SNIR

(b) ZDIR
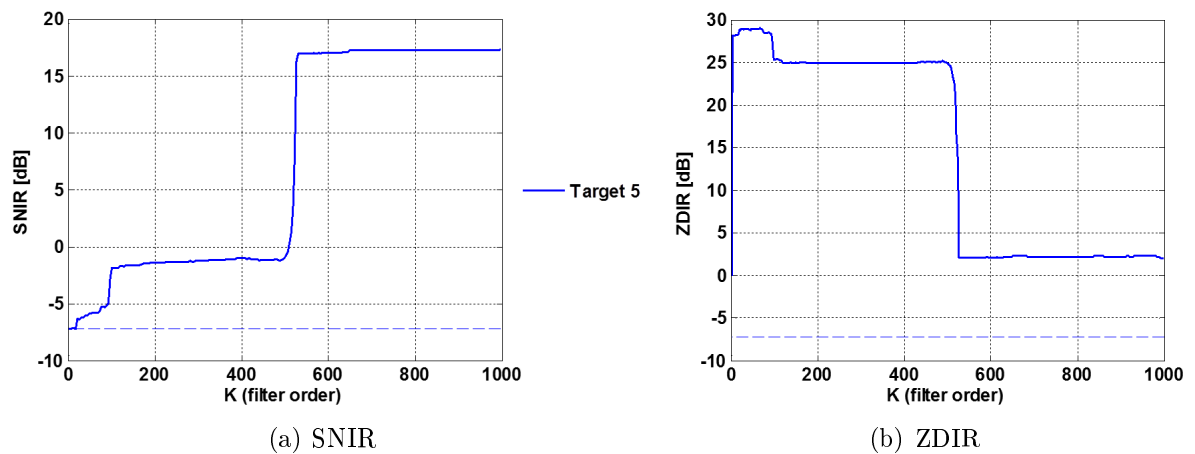
Figure 7.20: Evolution of the LSM-ECA filtering with the parameter K (filter order) for the target number 5, located at Rb = 514.

Table 7.5: SNIR and ZDIR results for LSM-ECA technique in comparison with respect to WI-NLMS ($\mu = 10^{-3}$).

Target	SNIR		ZDIR		
	LSM-ECA	**WI-NLMS** $(\mu = 10^{-2})$	**RAW**	**LSM-ECA**	**WI-NLMS** $(\mu = 10^{-2})$
1	1.3283	1.3571	33.7315	30.117	36.8229
2	1.9087	1.9714	30.7634	30.7974	35.5966
3	0.6611	0.6633	17.9640	17.8994	20.9726
4	2.5996	2.7164	13.2445	12.3691	15.6072
5	24.4011	24.6910	28.1229	25.9268	28.9377
6	2.3081	2.3132	23.9461	23.9945	25.6810
7	2.3525	2.3714	12.6268	13.3987	14.6737

Chapter 8

Validation of the IDEPAR demonstrator

In this chapter, detection and tracking capabilities of the IDEPAR system are verified, using the real data acquired by the demonstrator in a ground scenario. The IDEPAR system was located at the roof of the Superior Polytechnic School of the University of Alcalá. A more detailed analysis of the selected scenario can be found in section 6.3.

The superimposition of the whole set of CPI detections can be analysed in order to highlight the trajectories of the detected targets. An example of detector outputs for an acquisition of 20 s. composed of 80 CPIs is presented in Figure 8.1. The regions where the targets are expected to be detected and their related roads are also shown.

The data used in this work belong to a database acquired during 2015. Several co-operative targets provided with GPS receivers were used for verification purposes. In this chapter, and without loss of generality, two measurements were considered, *data1* and *data2*, that consist of 30-second data acquisitions, with 120 CPIs obtained using an integration time and a PRI of 250 ms. The measurements considered in this work were obtained focussing on the control of the cooperative targets along Meco road, considering low traffic level time intervals.

8.1   System detection capabilities analysis

The system detection capabilities can be evaluated through the analysis of the P_D and P_{FA}. In this section, a study of the detection performance of the IDEPAR demonstrator is carried out, considering two of the zero-Doppler interference cancellation techniques presented in section 7: LSM-ECA and WI-NLMS solutions.

For each considered pre-processing stage, P_D and P_{FA} parameters were estimated. Ground-truths at the output of the detector are required for accurate estimations, but due to the complex nature of the electromagnetic backpropagation process, targets dynamics and radar system, the real ground-truth is not available. Using confirmed tracker
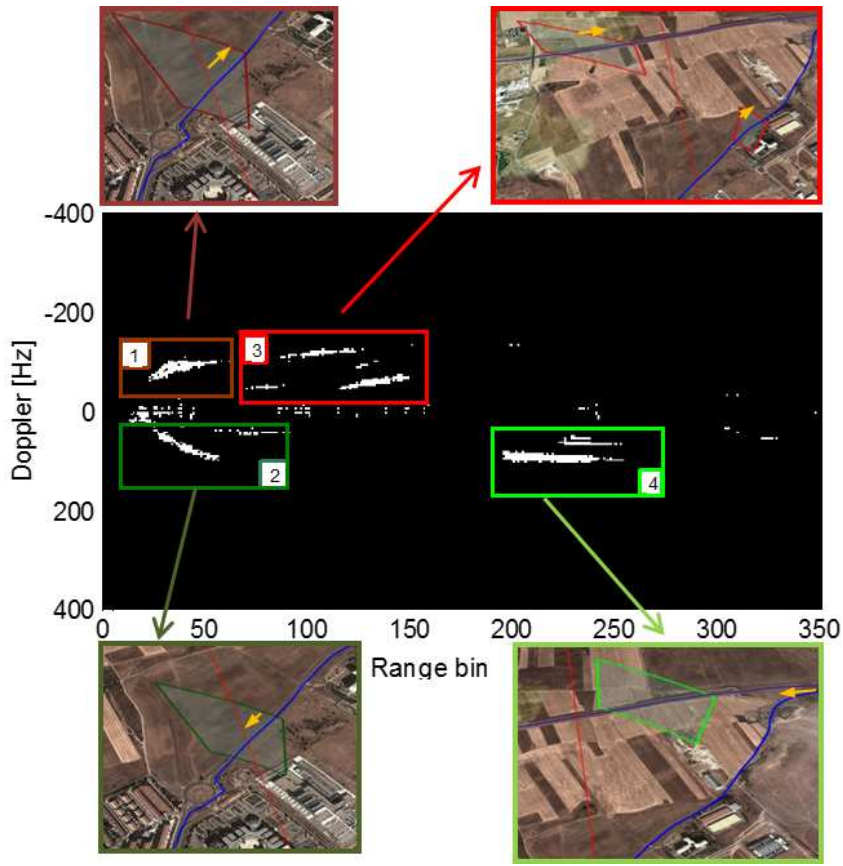
Figure 8.1: An example of IDEPAR demonstrator measurement: different detection regions in the area of interest

tracks, a ground truth was generated for each CFAR detector. Tracker tracks were previously confirmed using GPS data (cooperative vehicles) and visual information about non-cooperative targets present in Meco road during the acquisitions. The following methodologies were applied for Pfa and Pd estimations [Jarabo-Amores et al., 2016]:

- P_{FA} estimation: target contributions in the RDM were removed. In each CPI, the set of pixel detections associated with a single target must be grouped, to estimate the centroid that will be applied to the tracker. If the plot is assigned to a track, all pixel detections related to the centroid will be removed from the RDM for P_{FA} estimation purposes. As each CFAR detector generates different groups of pixel detections for a single target, they were combined using a logic OR operation for generating the common ground-truth.

- P_D estimation: the complexity of P_D estimation was higher than for P_{FA} due to the errors associated with the pixel detections grouping technique. Because of that, P_D was estimated at plot level, using confirmed tracker outputs.

Detection results for each measurement were analysed separately, when four CA-CFAR

detectors (RANGE, DOPPLER, AND and 2D-Window), were applied. These detectors were briefly introduced in section 5.2.3.2. The selection of the number of reference and guard cells at each side of the CUT for every detector were selected considering ground target and scenario characteristics, Table 8.1.

Table 8.1: Cell configuration for the selected CA-CFAR detectors.

Cells	RANGE	DOPPLER	2D-WINDOWS
Reference	32	4	(32/4)
Guard	6	3	(6/3)
N_{CELL}	64	8	1064

8.1.1 *data1* detection results

In this acquisition, several cars were running along the roads withing the area of interest. One of them was a cooperative one, carrying a GPS receiver. The P_{FA} results for *data1* measurement are summarized in Table 8.2, showing the variation of the results with the different detectors and with the different filtering strategies:

- First, detection performance without any pre-processing stage was analyzed, as a reference case. In Figure 8.2, the RDS obtained for the CPI 79 is depicted, showing in the zoomed regions two targets considered in detection parameters estimation.
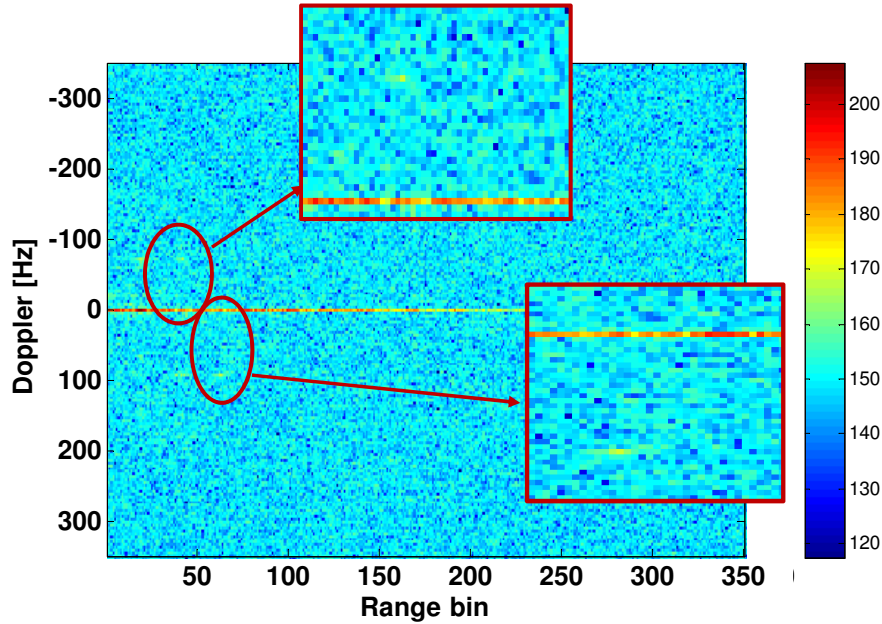
Figure 8.2: RDS of CPI 79, without applying any pre-processing technique. Zoomed regions show details of two of the considered targets for P_D and P_{FA} estimations.

Table 8.2: P_{FA} results for *data1*.

Filtering Technique	RANGE	DOPPLER	AND	2D-WINDOW
Without Filtering	$3.7939 \cdot 10^{-5}$	$2.1200 \cdot 10^{-3}$	$2.615 \cdot 10^{-5}$	$7.2060 \cdot 10^{-4}$
WI-NLMS ($\mu = 0.05$)	$1.7551 \cdot 10^{-5}$	$1.7464 \cdot 10^{-5}$	$6.1995 \cdot 10^{-6}$	$3.2220 \cdot 10^{-5}$
WI-NLMS ($\mu = 0.01$)	$1.8468 \cdot 10^{-5}$	$2.8510 \cdot 10^{-5}$	$7.3780 \cdot 10^{-6}$	$4.5537 \cdot 10^{-5}$
WI-NLMS ($\mu = 0.0075$)	$2.3959 \cdot 10^{-5}$	$3.0649 \cdot 10^{-5}$	$8.4261 \cdot 10^{-6}$	$5.0078 \cdot 10^{-5}$
WI-NLMS ($\mu = 0.005$)	$5.5235 \cdot 10^{-5}$	$3.2657 \cdot 10^{-5}$	$9.3866 \cdot 10^{-6}$	$5.6103 \cdot 10^{-5}$
WI-NLMS ($\mu = 0.0025$)	$2.6806 \cdot 10^{-5}$	$4.0865 \cdot 10^{-5}$	$1.0303 \cdot 10^{-5}$	$6.6145 \cdot 10^{-5}$
WI-NLMS ($\mu = 0.001$)	$3.1260 \cdot 10^{-5}$	$6.1647 \cdot 10^{-5}$	$1.3796 \cdot 10^{-5}$	$7.9678 \cdot 10^{-5}$
WI-NLMS ($\mu = 0.0005$)	$4.3397 \cdot 10^{-5}$	$1.0731 \cdot 10^{-4}$	$1.7201 \cdot 10^{-5}$	$1.1038 \cdot 10^{-4}$
LSM-ECA	$3.0867 \cdot 10^{-5}$	$3.5975 \cdot 10^{-5}$	$7.6403 \cdot 10^{-6}$	$1.0182 \cdot 10^{-4}$

As the stationary clutter contributions is mainly located along the zero-Doppler line, and taking into consideration how the CA-CFAR reference cells are configured for each detector, the worst result is expected for DOPPLER CA-CFAR detector, which reference cells extend along the Doppler dimension, and can include the zero Doppler line and/or other components of stationary clutter that spread along the Doppler dimension. On the other hand, AND detector is expected to present the best P_{FA} results, because only declares a target if the RANGE and DOPPLER CFARs declare it. In addition, the presence of these disturbances, makes the desired objective of $P_{FA} = 10^{-6}$ unreachable when that RDS region is considered, being an evidence about the non-Gaussian statistics of the interference in this region.

- The disturbance reduction obtained with the LSM-ECA technique improves the P_{FA} mainly on the detectors most affected by the clutter along the zero Doppler line, being this improvement of several orders of magnitude for the DOPPLER one. In Figure 8.3 the RDS is depicted. Those false alarms associated with clutter components spreading along Doppler dimension, won't be affected by the ECA filtering as it is shown in Figure 8.4.
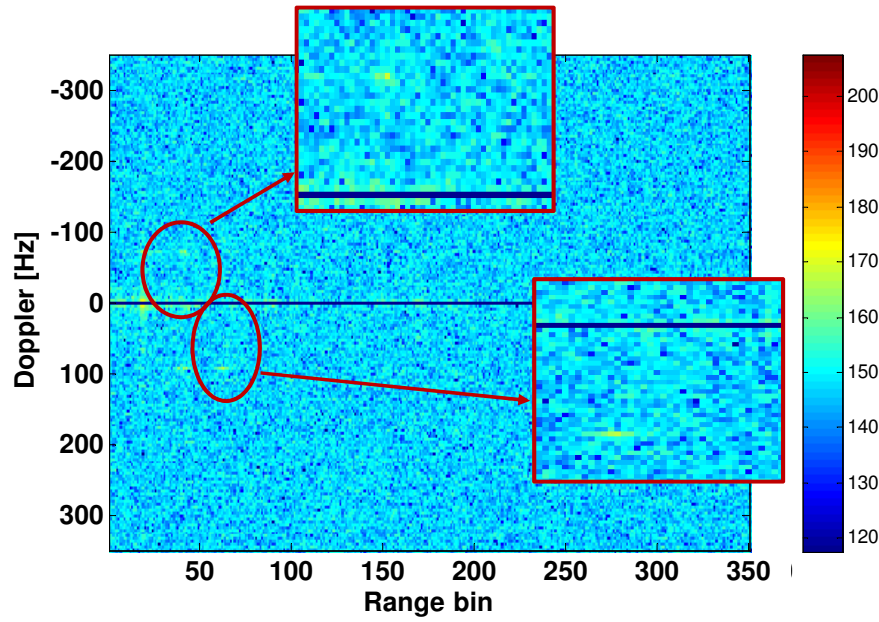
Figure 8.3: RDS of CPI 79 applying a LSM-ECA technique. Zoomed regions show details of the two of the considered targets for the P_D and P_{FA} parameters estimation.

- The disturbance cancellation of the WI-NLMS depends on the step-size parameter and on the Doppler position of the sought target as was commented in section 7.4. In this study, a set of representative values were selected, $\mu = [0.05, 0.01, 0.0075, 0.005, 0.0025, 0.001, 0.0005]$. In Figure 8.5 two examples of RDSs obtained with this approach are shown.

  In Table 8.2 s low degradation of the P_{FA} is observed as the μ parameter is reduced, until a breaking point is reached, after which the P_{FA} performance drops more abruptly. These results are completely coherent with those obtained from the analysis of the ZDIR parameter in chapter 7, making clear the relation between the detection performance parameter, P_{FA}, and the filtering analysis one, ZDIR. In addition, and considering the filtering effect over low Doppler disturbances, as the step-size parameter gets lower, the results are similar to those obtained with the LSM-ECA, as is observed in Figure 8.6: for higher μ the disturbance is completely removed, but as mu decreases, the disturbance rejection was reduced.

The P_D results for *data1* are summarized in Table 8.3. This parameter mainly depends on several factors:

1. The target Signal to Interference Ratio (SIR).

2. The statistical nature of the RDS data. In conjunction with the target SIR, the theoretical minimum P_D can be estimated using the detection curves.
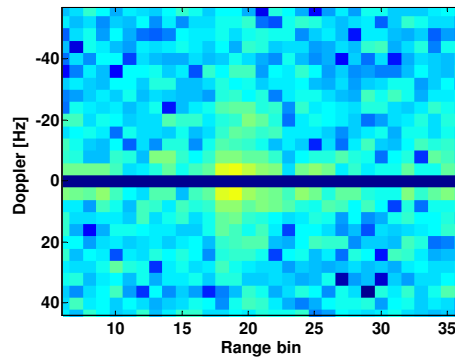
Figure 8.4: RDS of CPI 79: disturbance detailed applying a LSM-ECA technique.

3. The additional SIR required to compensate the estimation error of the interference power surrounding the CUT. This error is directly related to the total number of reference cells (N_{CELL}), and is called CFAR-losses.

4. The presence of interfering targets could introduce an additional reduction in the detection capability, due to they increase the surrounding area interference power and the estimated detection threshold. Similarly, strong clutter or other zero-Doppler disturbances gives rise to a similar performance degradation.

The worst results were obtained with the DOPPLER detector. This is due to its low N_{CELL} that increases the required target SIR, and the fact that this is the detector most affected by the ZDI. Its performance defines the upper limit for the P_D obtained using the AND detector. The best results were obtained when the 2D-Window detector was used. But this detector is associated with the worst results in terms of P_{FA}, discouraging its use in radar systems.

The different filtering techniques also require additional considerations: the filtering modify the statistical properties in the area around the zero Doppler line, giving rise to a detection performance reduction because the applied CFARs assume independent and identical distributed Gaussian interference (exponential intensity).

- Considering the results obtained in the SNIR parameter study in section 7.5 LSM-ECA filtering gives rise to an increase in the target SNR between 1 and 2 dBs. In addition, as its disturbance reduction is centred on a very thinner region of the RDS maps, the P_D capabilities reduction associated with the changes in the data statistical properties was limited. Results show that this filtering approach improves the detection capability a 14% approximately, with respect to the case where no ZDI techniques are applied.

- Considering simultaneously the SIR improvement, and the size of the region over which the disturbance cancellation is focused, the WI-NLMS detection capabilities are directly related to the steps-size parameter. For a higher μ, the region affected by
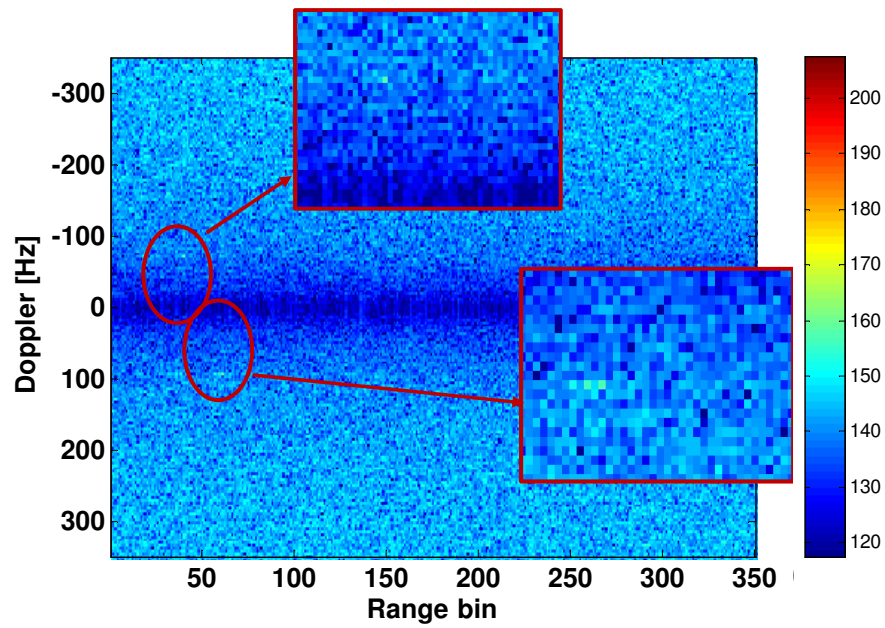
(a) $\mu = 0.05$
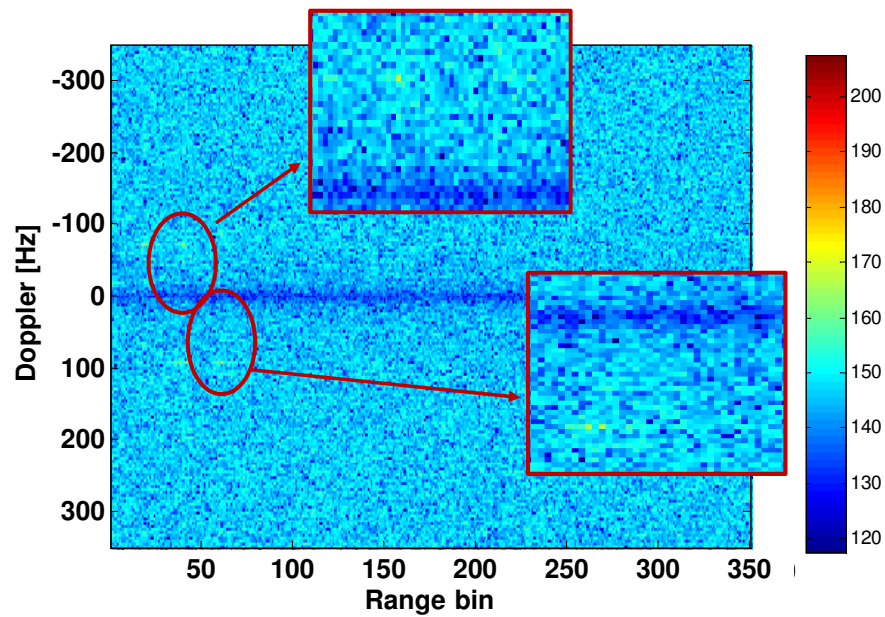
(b) $\mu = 0.005$

Figure 8.5: RDS of CPI 79 applying a WI-NLMS technique. Zoomed regions show details of the two of the considered targets for the P_D and P_{FA} parameters estimation.

the changes in the data statistical nature is wider, reducing the P_D, being similar to the case where no ZDI techniques are applied. When smaller μ parameters were selected, this region was reduced and the detection probability increased. In addition, a low improvement on targets SIR are expected. The obtained results are completely coherent with this conclusions, validating in this case, the SNIR

(a) $\mu = 0.05$ (b) $\mu = 0.005$ (c) $\mu = 0.001$
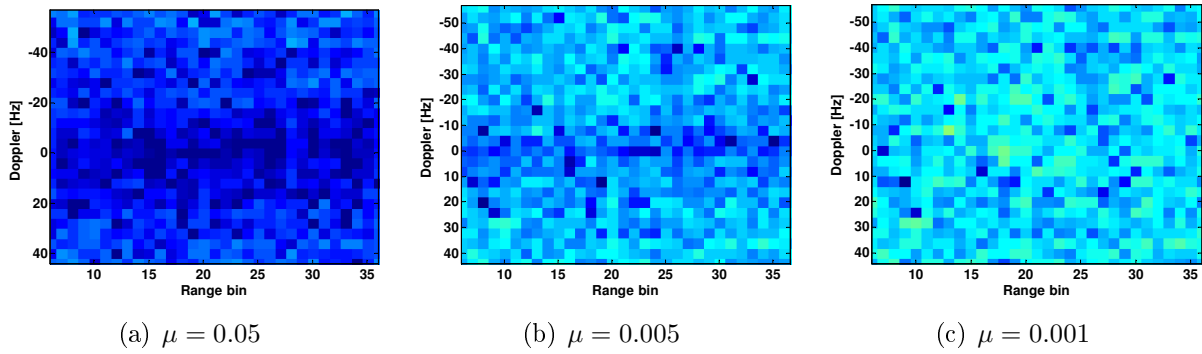
Figure 8.6: RDS of the CPI 79: disturbance detailed applying a WI-NLMS technique for different step-size parameter values.

parameter as an indicator of the P_D performance.

From a system performance point of view, solutions based on LSM-ECA and WI-NLMS ($\mu = 0.001$), give rise to very similar detection capabilities results. LSM-ECA solutions present the lower computational cost, but WI-NLMS based solution allow certain level of customization that can be exploited for achieving trade-off solutions for different scenarios through the adjustment of the step-size parameter.

8.1.2 *data2* detection results

In this acquisition, two controlled cars were running along the roads withing the area of interest, one of them is a cooperative one with a GPS device, but in this measurement, the controlled target trajectories are not coincident in time.

In Figure 8.5, the RDS for the different filtering techniques are depicted. In addition, for each RDS, zoomed regions showing one of the targets considered for detection estimation are also shown.

A study analogous to that presented in section 8.1.1 was carried out: the results of P_{FA} and P_D are summarized in Tables 8.4 and 8.5, respectively. The analysis of the estimated detection performance parameters shows the same global trends that were observed for the *data1* measurement. The most relevant features are the following:

- The obtained P_{FA} was, in general, slightly better than the obtained with the other measurement. In addition, the improvement in terms of false alarm probability obtained using WI-NLMS was also higher, reaching for one of the selected step-size parameters, $\mu = 0.05$, a result close to the desired value, 10^{-6}. On the other hand, when a low μ is selected, the aforementioned degradation in the NLMS-based techniques is more pronounced.

- The obtained results show a reduction in the P_D for all the selected strategies: if no ZDI rejection technique is applied, a detection probability around 15% was obtained,

Table 8.3: P_D results for *data1*.

Filtering Technique	RANGE (%)	DOPPLER (%)	AND (%)	2D-WINDOW (%)
Without Filtering	59.24	42.04	37.58	71.97
WI-NLMS ($\mu = 0.05$)	61.75	42.68	41.40	69.43
WI-NLMS ($\mu = 0.01$)	65.61	52.23	48.41	77.71
WI-NLMS ($\mu = 0.0075$)	66.88	51.59	49.04	80.89
WI-NLMS ($\mu = 0.005$)	69.43	52.87	49.04	81.53
WI-NLMS ($\mu = 0.0025$)	68.79	54.14	50.32	81.53
WI-NLMS ($\mu = 0.001$)	70.06	56.05	53.50	83.44
WI-NLMS ($\mu = 0.0005$)	70.70	56.05	52.87	84.08
LSM-ECA	73.25	55.41	53.50	84.08

very far from the desired 80%. Applying disturbance cancellation techniques, a great improvement was obtained for RANGE detector with respect to the previous case (without ZDI rejection stages), but the estimated P_D of 50% is quite far from the desired value and it is a really undesirable result, because it means that system uncertainty is total.

- To explain the low Pd values obtained, the following fact must be considered:

  - Low target SIR: the analysed targets present lower signal power (up to 2 dBs less than in *data1*).

  - Interfering targets are observed in the region where the controlled trajectories are located.

(a) Without applying any filtering

(b) LSM-ECA

(c) WI-NLMS with $\mu = 0.05$

(d) WI-NLMS with $\mu = 0.005$
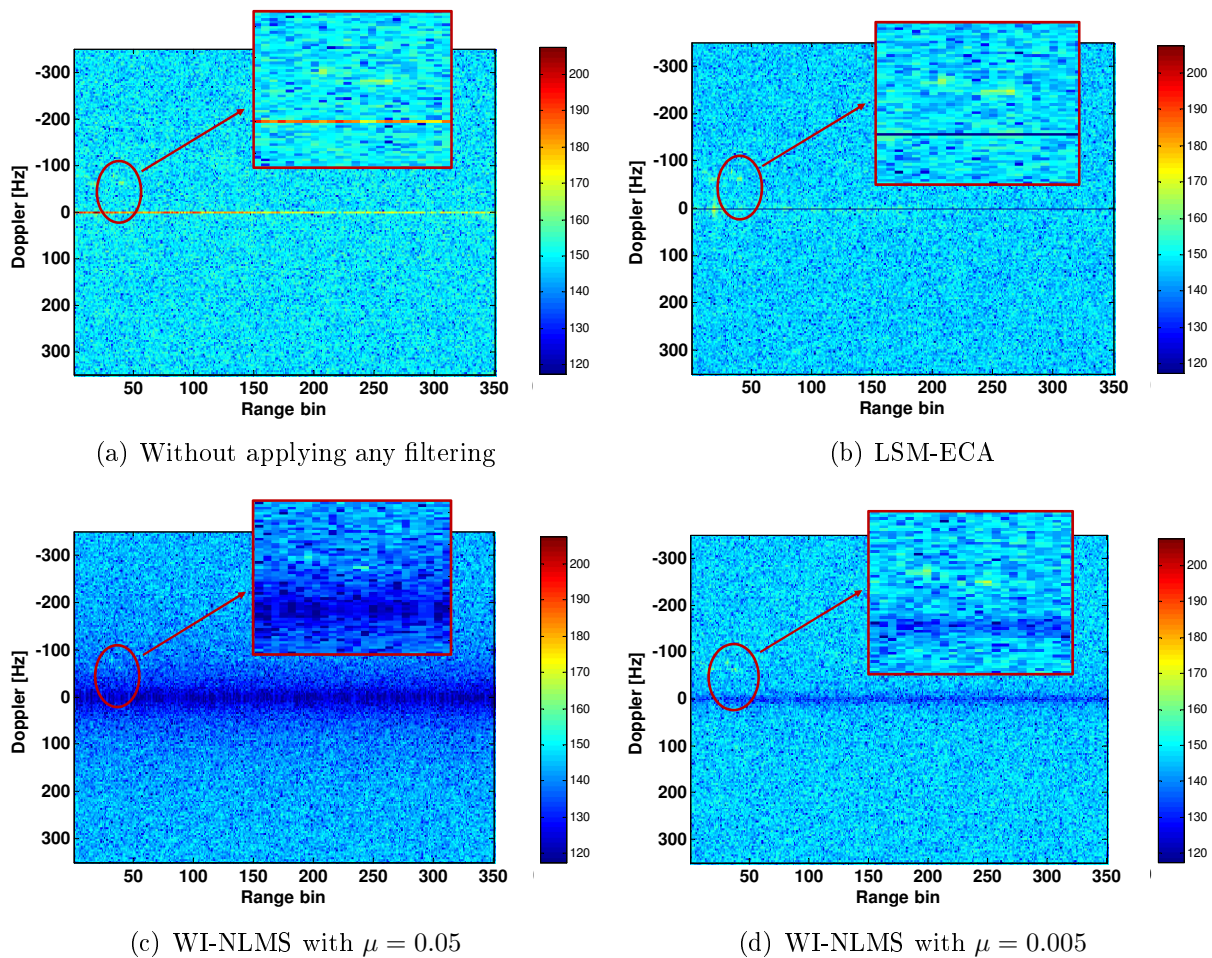
Figure 8.7: RDS of the CPI 55 applying different disturbance cancellation techniques. Zoomed regions show details of one of the considered targets for the P_D and P_{FA} parameters estimation.

Table 8.4: P_{FA} results for *data2*.

Filtering Technique	RANGE	DOPPLER	AND	2D-WINDOW
Without Filtering	$2.96 \cdot 10^{-5}$	$2.0100 \cdot 10^{-3}$	$2.3488 \cdot 10^{-5}$	$6.8356 \cdot 10^{-4}$
WI-NLMS ($\mu = 0.05$)	$8.688 \cdot 10^{-6}$	$3.5800 \cdot 10^{-6}$	$2.0519 \cdot 10^{-6}$	$1.3621 \cdot 10^{-5}$
WI-NLMS ($\mu = 0.01$)	$1.6809 \cdot 10^{-5}$	$5.9812 \cdot 10^{-6}$	$2.6632 \cdot 10^{-6}$	$2.1043 \cdot 10^{-5}$
WI-NLMS ($\mu = 0.0075$)	$1.8686 \cdot 10^{-5}$	$7.3346 \cdot 10^{-6}$	$3.1871 \cdot 10^{-6}$	$2.5104 \cdot 10^{-5}$
WI-NLMS ($\mu = 0.005$)	$2.0781 \cdot 10^{-5}$	$8.775 \cdot 10^{-6}$	$3.8419 \cdot 10^{-6}$	$3.0823 \cdot 10^{-5}$
WI-NLMS ($\mu = 0.0025$)	$2.6413 \cdot 10^{-5}$	$1.4888 \cdot 10^{-5}$	$5.4136 \cdot 10^{-6}$	$4.0821 \cdot 10^{-5}$
WI-NLMS ($\mu = 0.001$)	$3.5669 \cdot 10^{-5}$	$4.2087 \cdot 10^{-5}$	$8.5134 \cdot 10^{-6}$	$5.9856 \cdot 10^{-5}$
WI-NLMS ($\mu = 0.0005$)	$5.2041 \cdot 10^{-5}$	$9.5656 \cdot 10^{-5}$	$1.4058 \cdot 10^{-5}$	$9.1247 \cdot 10^{-5}$
LSM-ECA	$3.2089 \cdot 10^{-5}$	$1.6329 \cdot 10^{-5}$	$5.9812 \cdot 10^{-6}$	$9.1728 \cdot 10^{-5}$

Table 8.5: P_D results for *data2*.

Filtering Technique	RANGE (%)	DOPPLER (%)	AND (%)	2D-WINDOW (%)
Without Filtering	31.09	14.29	10.92	60.50
WI-NLMS ($\mu = 0.05$)	41.18	13.45	12.61	59.66
WI-NLMS ($\mu = 0.01$)	50.42	25.21	24.37	74.79
WI-NLMS ($\mu = 0.0075$)	51.26	30.25	26.89	74.79
WI-NLMS ($\mu = 0.005$)	52.94	36.13	30.25	75.63
WI-NLMS ($\mu = 0.0025$)	58.82	38.66	33.61	81.51
WI-NLMS ($\mu = 0.001$)	53.78	41.18	33.61	82.35
WI-NLMS ($\mu = 0.0005$)	54.62	41.18	32.77	81.51
LSM-ECA	47.06	36.97	27.73	75.63

8.2 GPS-based results validation

In this section, a comparison of the tracker output with the data provided by the controlled car's GPS was carried out in order to validate the global system performance capabilities.

AS pre-processing stages, two solutions were selected, considering the P_D and P_{FA} studies presented in the previous section:

1. A LSM-ECA approach, with a selected K that enables the filtering of the whole range under study (K > 500).

2. A WI-NLMS approach with $\mu = 0.0025$ and K > 500.

The detection stage was implemented using a range-based approach CA-CFAR technique as a trade off between the solutions with best results on P_{FA} and those with good results on P_D.

8.2.1 Tracker results analysis for *data1*

In Figure 8.8 the trajectory of the cooperative car acquired during *data1* is shown over a real map of the AoI, using the information provided by the GPS. The trajectory is related with a car moving along Meco road.
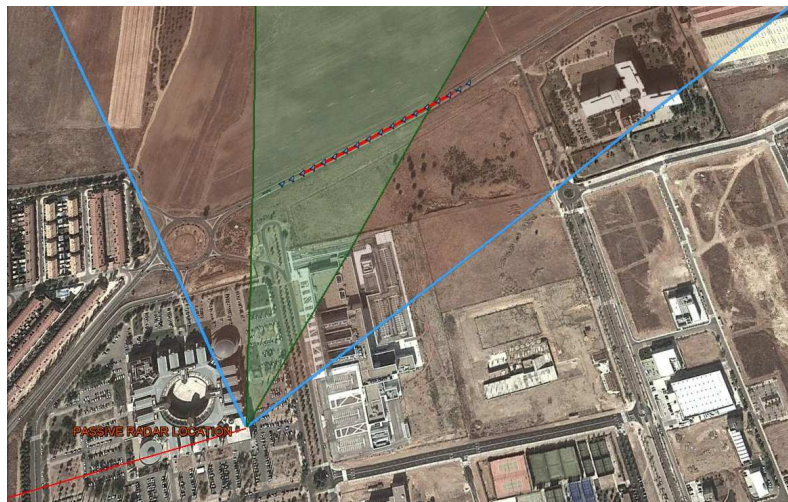
Figure 8.8: Real map trajectory using the GPS track of *data1*

First, the results obtained with a LSM-ECA pre-processing technique are depicted in Figure 8.9. The superimposition of the whole set of detections for the measurement is depicted in Figure 8.9(a), showing that several proto-trajectories were observed at different ranges and velocities, not only the associated with the cooperative target. In Figure 8.9(b) the obtained set of tracks are shown.

In order to validate the system performance, in Figure 8.9(c), the superposition of the detection plot, and the real trajectory provided by the target GPS are compared. Results
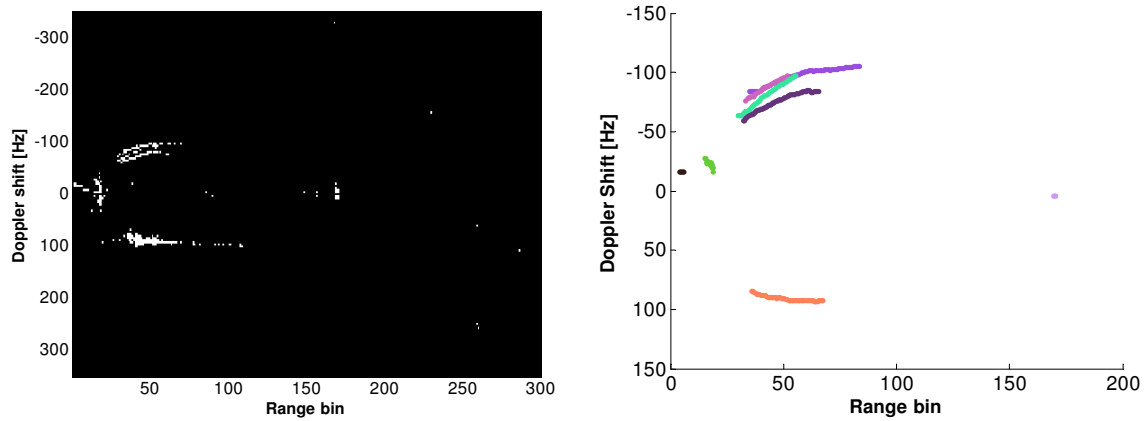
(a) 30 seconds cumulative detection results

(b) Tracks obtained at the output of the Kalman filter
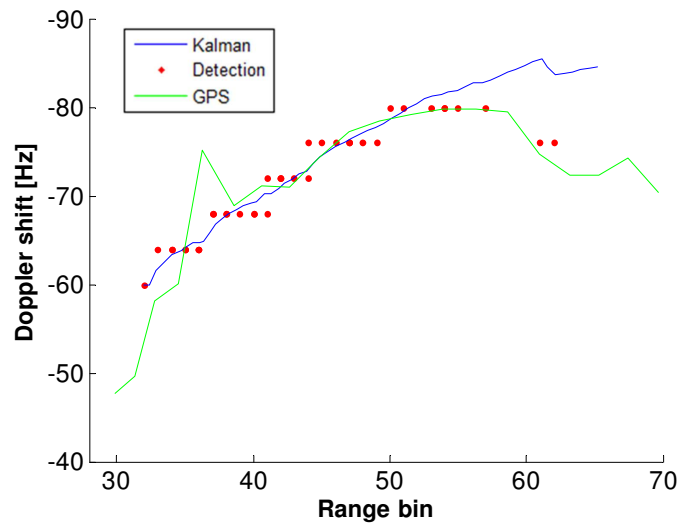
(c) Comparison between controlled track GPS data

Figure 8.9: Detection and tracking stage results, for the *data1* with a LSM-ECA technique.

show how the tracker generates a continuous trajectory, correctly approximating the real manoeuvre of the target.The detections are almost superimposed to the points provided by the GPS, except at the end of the trajectory where the target enters a region shadowed by one big building close to the Polytechnic School.

Results obtained considering a WI-NLMS are shown in Figure 8.10.

Considering the detection point of view, small amount of differences are observed with respect to the LSM-ECA approach, Figure 8.10(a), but these variations are enough to change the tracks provided by the Kalman filtering stage. In Figure 8.10(b), one of the outgoing tracks (associated with negative Doppler) was missed and other was clearly cut. On the other hand, the track associated with the GPS data was still correctly generated, without appreciating any significant variation when the both tracks are compared in Figure 8.10(c).

(a) 30 seconds cumulative detection results

(b) Tracks obtained at the output of the Kalman filter

(c) Comparison between controlled track GPS data
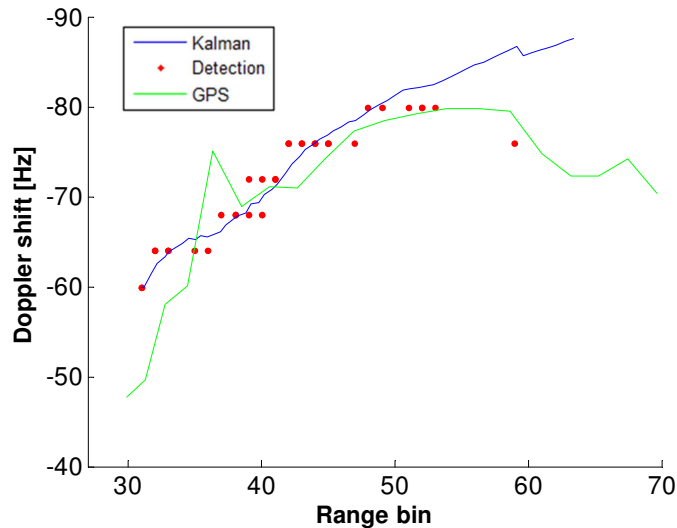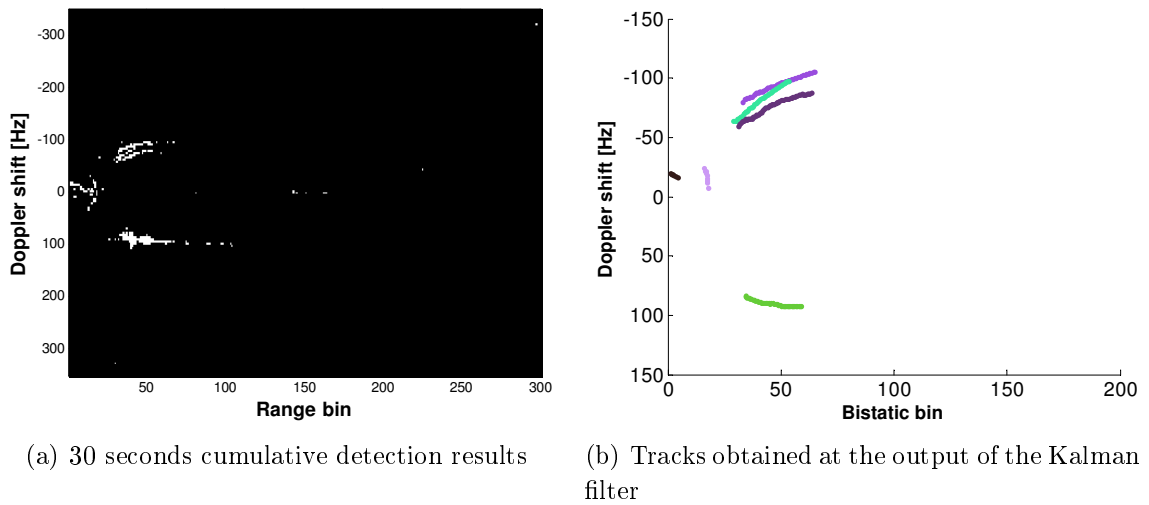
Figure 8.10: Detection and tracking stage results, for *data1* measurement with a WI-NLMS technique.

8.2.2 Tracker results analysis for *data2*

In Figure 8.11 the trajectory of the cooperative car acquired during *data2* is shown. The controlled trajectory is also associated with Meco road and is very similar to the obtained in *data1*.

In Figure 8.12, results obtained with a LSM-ECA are depicted. As the P_D obtained in this measurement is lower than the obtained with *data1*, less track definition is obtained when the whole set of detections are superimposed (Figure 8.12(a)). The tracking stage is able to compensate part of this performance degradation: it is able to obtain a set of well composed tracks (Figure 8.12(b)).

As in the previous measurement, the tracker stage output shows a continuous and well
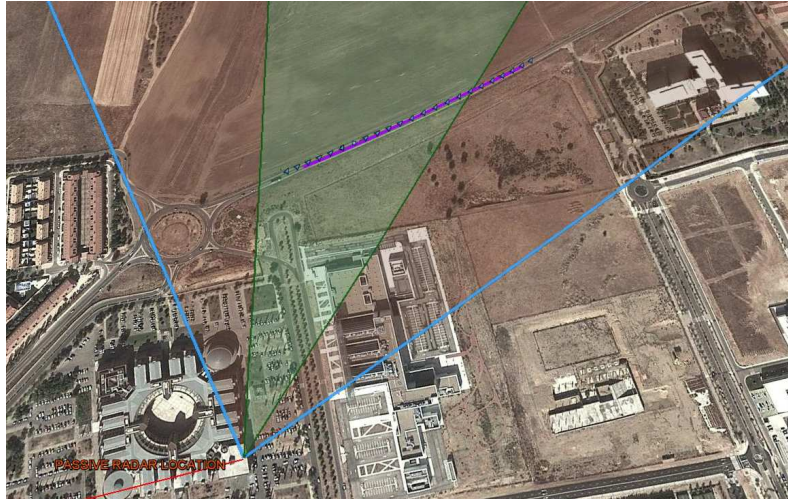
Figure 8.11: Real map trajectory using the obtained GPS track of *data2* in the AoI

estimated track for the cooperative car with few tracking errors (Figure 8.12(c)).

Conversely, when WI-NLMS was applied, a great reduction in the tracking performance was observed, giving rise to several tracks losses, Figure 8.13(b), in spite of the fact that for the controlled tracks, the obtained P_D is higher than the achieved with LSM-ECA. But, again, the tracker is able to achieve a very remarkable result for the track associated whit the cooperative target (Figure 8.13(c)).

Considering the results of the GPS cooperative track analysis, IDEPAR system is able to obtain very accurate trajectory estimations, that can be considered precise enough for ground control monitoring applications.
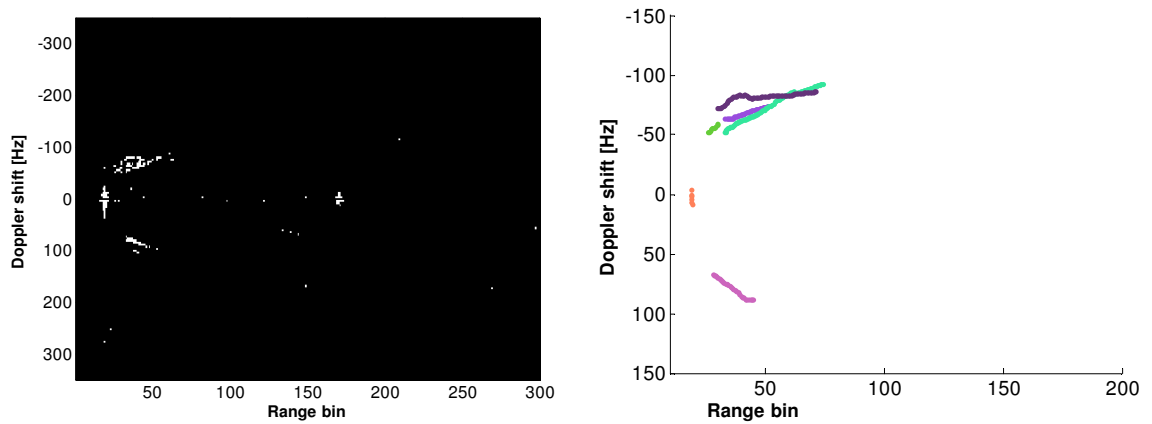
(a) 30 seconds cumulative detection results

(b) Tracks obtained at the output of the Kalman filter
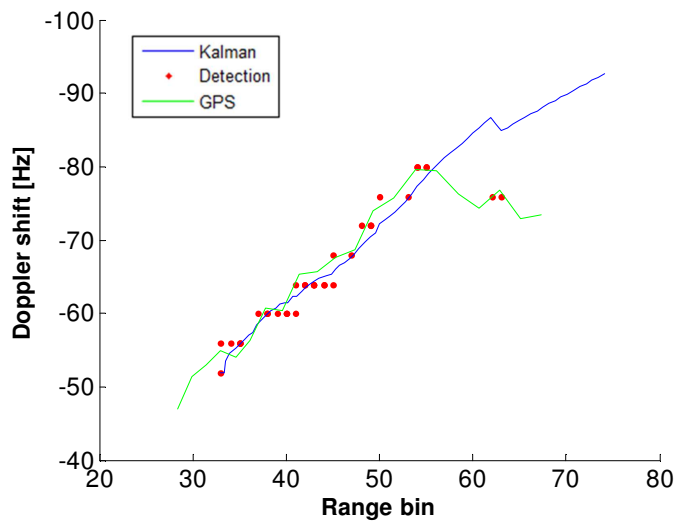
(c) Comparison between controlled track GPS data

Figure 8.12: Detection and tracking stage results, for the *data2* with a LSM-ECA technique.

(a) 30 seconds cumulative detection results

(b) Tracks obtained at the output of the Kalman filter
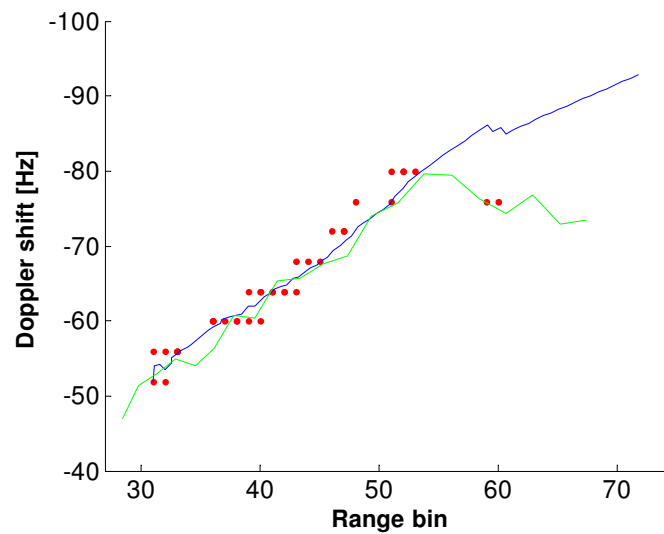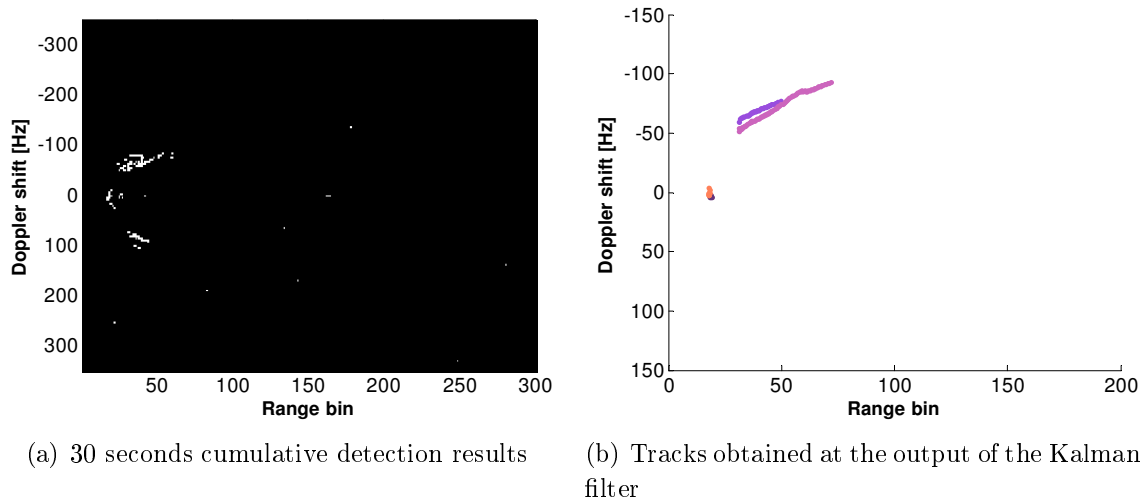
(c) Comparison between controlled track GPS data

Figure 8.13: Detection and tracking stage results, for the acquired *data2* measurement, pre-processed with a WI-NLMS technique.

Chapter 9

Systems robusteness improvements and updates

9.1   Introduction

In section 2 the dependency of the system with the electromagnetic spectrum available on the passive receiver surrounding area, was presented as one of the main drawbacks of this kind of radar systems, due to the lack of control over IoOs allocation. A COTS-based approach is proposed in order to improve the system robustness against changes in the electromagnetic spectrum. The target discrimination capabilities of a passive radar system are completely related to the range and angular resolutions. Range resolution can be increased acquiring higher instantaneous bandwidths, objective closely related to the dependency on available IoOs previously commented, but angular resolution is defined by the radar antenna system. An analysis of antenna system elements in order to improve system angular discrimination was carried out.

9.2   System robustness against IoO channel allocation

The switch-over from analogue to digital TV broadcasting was scheduled by the end of 2012 in Europe. The digital compression systems used by the DVB-T signals, frees up a large frequency band, that will be available for other commercial broadcasters. The Radio Spectrum Policy Programme (RSPP) mandated the opening up of the 800 MHz band to non television purposes: the higher channels of the DVB-T band were reallocated at lower frequencies, in order to allow LTE 800MHz band transmissions. In Spain this spectrum reassignment was carried out on the mid-term of 2015.

Table 9.1: DVB-T channel distribution in three Spanish regions: Madrid, Barcelona and Valencia

Channel	Madrid	Barcelona	Valencia	Channel	Madrid	Barcelona	Valencia
22	X		X	44		X	
23		X	X	45			
26	X	X		46			X
27		X		47		X	
28			X	48		X	
29		X		49	X		
31		X		50	X		
33	X	X	X	54			
34		X		55	X		
39	X			57			X
40			X	58	X		X
41	X	X		59	X		
43			X				

9.2.1 Problem formulation

System IDEPAR was designed for working with up to 3 consecutive channels, at the higher DVB-T frequency band. As it is shown in Table 9.1, there is not enough consecutive channels in the DVB-T spectrum to fulfill the resolution requirements achieved with the original spectrum allocation, the frequency at witch most of the channels can be acquired was considerably reduced, and the spectrum allocation changes from one region to another.

In order to overcome the high channel dispersion, and to provide the system with robustness against the local channel distribution, a solution based in digital DVB-T channel mixers is proposed taking into consideration that the less modifications on the receiver chain are desired, and the limitation in instantaneous bandwidth defined by the Ettus boards.

Twin A/D T.0X processors from Televes were selected due to its channel converter capabilities: the mixer changes the frequency at witch a DVB-T channel is centred. The DVB-T channel is then moved from its original frequency location to a new one. Each processors is able to displace up to two different signal segments simultaneously using the two modules which is composed of, Figure 9.2.

Then, the selection of the IoO channels that will be used in the PBR will be configurable, detaching the acquisition and processing chain design from the local DVB-T distribution. In addition, system improves its robustness against future changes in the commercial spectrum allocations scheduled by Spanish government for the next years.

In Figure 9.1 an example of the basic scheme of the use of these components is presented, assuming that three channels are processed. The main drawbacks of this working scheme are the frequency offset that these components gives rise, and the target Doppler dispersion.

The frequency offset is generated by the use of local oscillators, not only for each Twin A/D T.0X processor, but for each module that the hardware is composed by. In
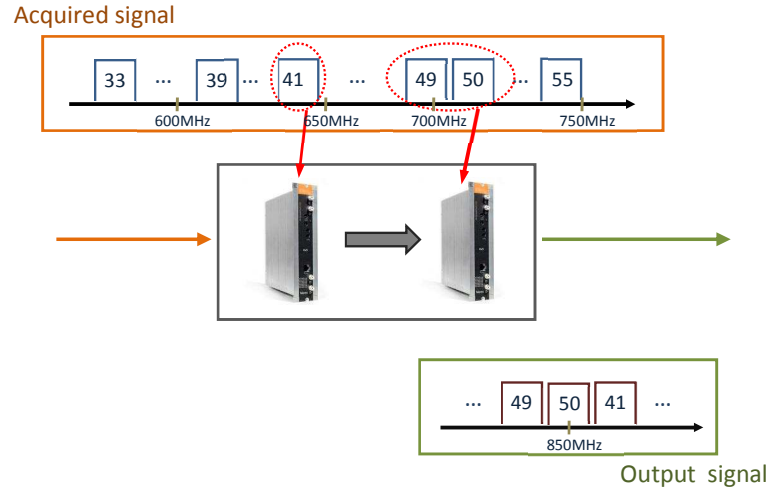
Figure 9.1: Proposed working scheme for the DVB-T channels mixers in IDEPAR system
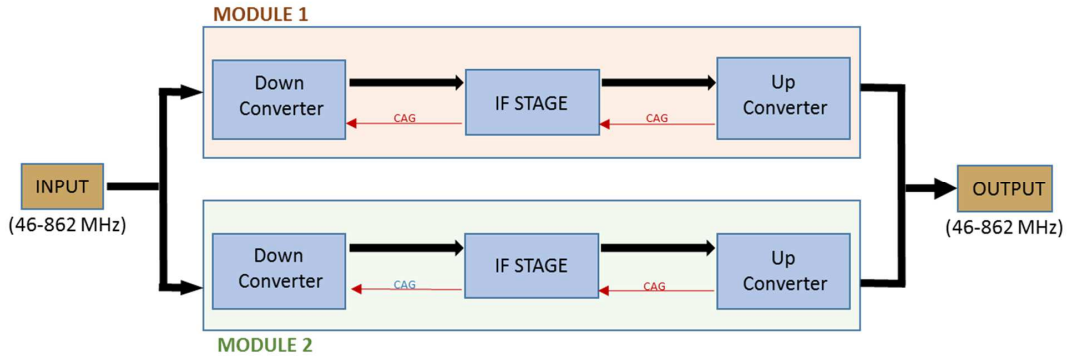
Figure 9.2: Twin A/D T.0X processors block diagram.

Figure 9.3 a detailed block diagram of an individual module is depicted, showing the two frequency conversions carried out during the signal displacement that give rise to the frequency mismatches. In expression (9.1), the real central frequency of the reference and surveillance signals at the output of the mixer is presented, when only one DVB-T channel is considered:

$$fc_{surv} = f_c \pm \Delta fc_{surv}$$
$$fc_{ref} = f_c \pm \Delta fc_{ref} \tag{9.1}$$

where f_c is the central frequency of the output configured channel, and $\Delta f_{c_{ref}}$ and $\Delta f_{c_{surv}}$ are the offsets that different modules introduce at the reference and surveillance signals respectively. These offsets give rise to an error in the coherent processing carried out by the CAF: if the offset is constant, this error consist in a displacement of the zero-Doppler line to a new position that can be located out of the scope considered during CAF generation. Additional zero-Doppler row replicas could appears at linear combinations of the surveillance and reference processed signals offsets.

This displacement, for the studied components, goes from a few hundreds of Hz up to
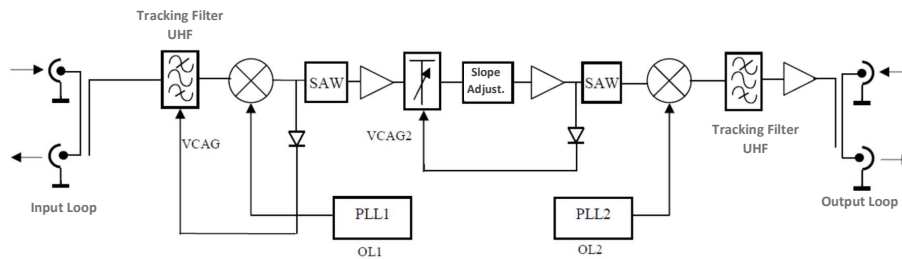
Figure 9.3: Detailed working scheme for an individual processor's module.

several tens of kHz and it is not constant: it changes every time the module is switched on, and varies with time during its operation. In Figure 9.4 the estimated offset brought in by a mixer is depicted, using segments of 5 seconds (20 offset samples) with a time separation of 10 minutes. This experiment resemble the offset behaviour expected in a measurement campaign, with signal acquisition composed of several CPIs of a small duration (blocks), with a bigger time separation between them. Differences of several tens of Hz between blocks, and of near 10 Hz within a block, can be observed, variations that are bigger than system Doppler resolutions,(4 Hz for tint = 250ms).
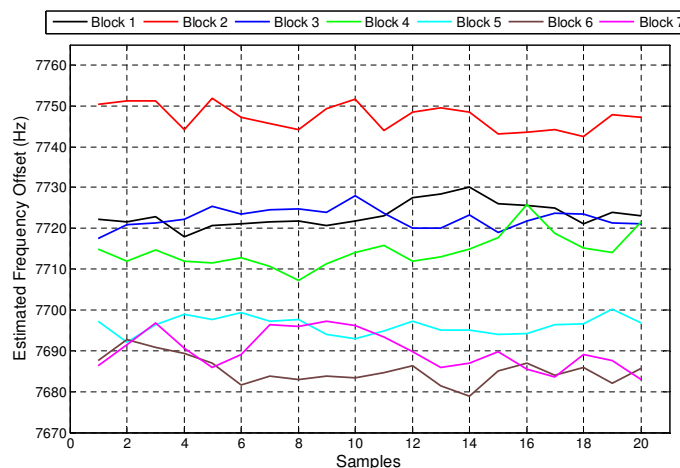
Figure 9.4: Temporal variation of an example estimated offset

9.2.2   Frequency offset compensation

To face this RDS distortion, a new pre-processing stage must be included in the PBR system. In this stage, an estimation of frequency offsets of acquired signals should be obtained and then compensated. As the offset are not associated to the acquisition channel, but to the DVB-T channels, this signal processing must be carried out on the filtered DVB-T signals, in ordert o apply this technique to each channel individually. In addition, this compensation process must be afforded each acquisition time, due to the aforementioned offset time variation. The main steps of the proposed compensation technique are

(a) Reference channel
(b) Surveillance channel
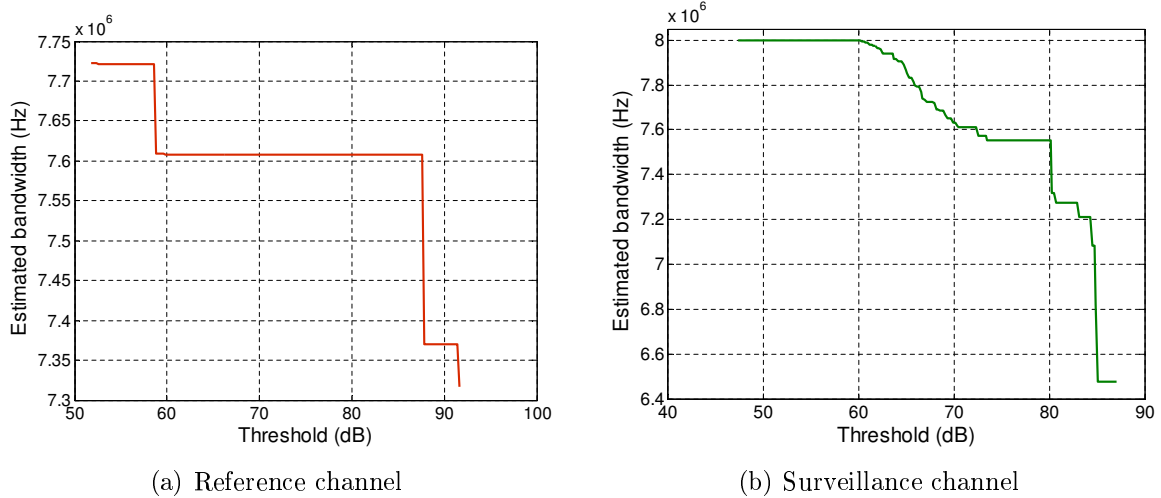
Figure 9.5: Estimated bandwidth respect to the spectrum threshold.

the following:

- Rough offset calculation at the acquisition channels. In this stage, the main offset component of reference and surveillance channels will be estimated. The algorithm takes advantage of the well known shape of a DVB-T channel spectrum: each channel is composed of 7.607 MHz of data information, and two adjacent guard bands in order to complete the 8 MHz of bandwidth. For a sliding spectrum level, an estimated channel bandwidth is obtained from the interval between the first and the last frequency that surpass the threshold. The associated central frequency is stored as the power level is reduced step by step, until the estimated bandwidth gets higher than a pre-fixed value near the theoretical one. Averaging the central frequencies obtained from those bandwidths close to 7.607 MHz, an estimated channels offset can be compensated. In Figure 9.5 an example of the relation of the estimated channel bandwidth with the spectrum level threshold is depicted for surveillance and reference channels.

  In order to improve the accuracy of this estimation step, two strategies could be used: obtaining the estimated offset mean value along a set of consecutive CPI, and/or improve the DVB-T channel spectrum shape through multi-CPI cumulative spectrum instead single-CPI one. The misadjustment derived of the inter-CPI offset differences could be compensated in the second stage of the algorithm, that only works at CPI level.

- Surveillance channel frequency displacement. In Figure 9.6 , RDSs obtained before and after applying gross compensation stage are depicted for a DVB-T signal displaced from channel 41 (634 MHz) to channel 68 (850 MHz). The zero Doppler interference is still displaced several Doppler cells away the central position and a blurring effect over that line, its adjacent ones, and over the targets, can be ob-

(a) Before offset compensation   (b) After gross offset compensation
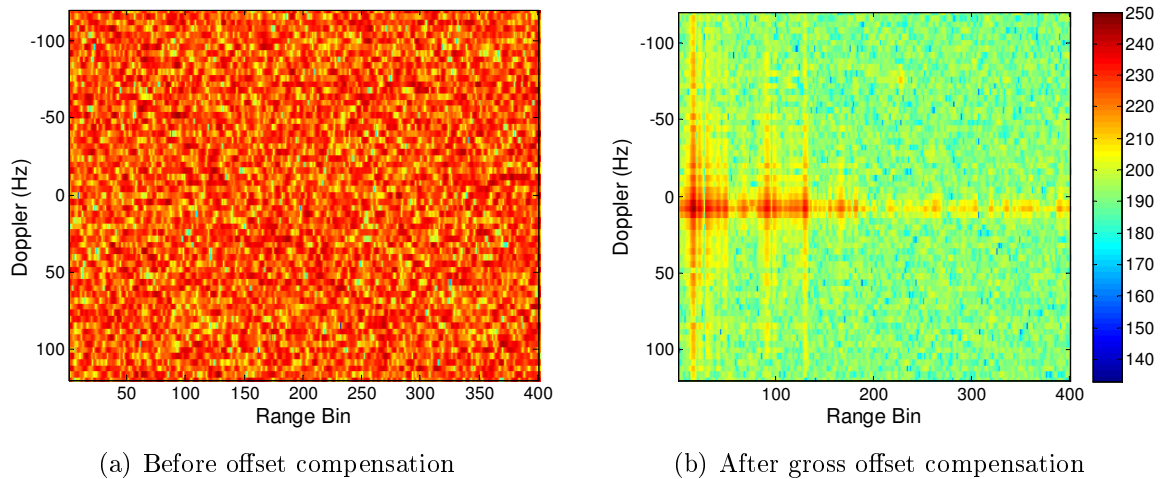
Figure 9.6: Results of gross offset compensation over the RDS.

served. These effects give rise due to the estimation error and the variation of the hardware offset within the acquisition time.

A frequency displacement will be applied to surveillance channels in order to couple, at each CPI, its central frequency to the reference one. In a first step, an estimation of the Zero-Doppler line misadjustment is carried out: the value of the Doppler row in the RDS that presents the higher level could be used for RDS compensation through displacing the surveillance channel the same value but with opposite sign. The system Doppler resolution will be the maximum accuracy achievable in this step: in the example, signals length of 250 ms are used, so frequency steps of 4 Hz are expected. In order to break through this accuracy limitation, a multi-resolution recursive algorithm could be used:

1. A set of equispaced frequencies are selected around the Doppler displacement estimated in previous step. For each frequency, a shifted copy of the surveillance channel and its associated RDS are obtained.

2. Through the analysis of the column associated with the higher zero Doppler disturbance, searching the lower power dispersion, the frequency under consideration for the next iteration will be selected.

3. The algorithm is restarted reducing the gap between the elements of the frequency vector. A trade off between accuracy and computational cost must be achieved through the selection of frequency step-size at each iteration level, and the number of iterations itself.

In Figure 9.7, RDSs obtained before and after applying fine compensation steps are shown. The improvement in the zero-Doppler disturbance location at a central row is observable. In addition, the blurry effect was significantly reduced.

(a) After first stage   (b) After second stage
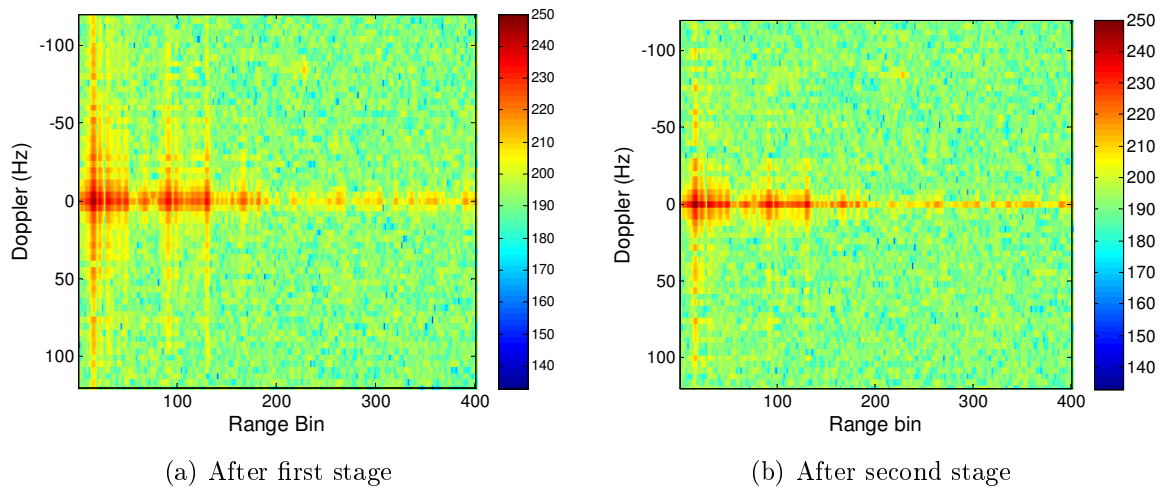
Figure 9.7: Fine offset compensation results.

When the offset is compensated, the second commented drawback could give rise, the dispersion of the Doppler information of the target. The Doppler shift information associated to each target is related to the signal working frequency. If displaced channels are used in the coherent processing, there is as associated Doppler-shift for each of the original pre-mixers signals. The differences between those values are related to the separation between the transmitted selected individual DVB-T channels. The study of this effect will be faced in MASTERSAT project, which can be considered as IDEPAR follow-on project.

9.3 Antenna subsystem study for improving angular discrimination

In section 5.2.1, the antenna DAT HD75 BOSS was presented as the chosen one for the IDEPAR demonstrator because to its high gain and front-to-back ratio, FB. For passive radar systems, a great receiver gain is required due to a low echo signal level is expected. In addition, a high FB ratio helps the system to isolate reference and surveillance channels from interferences, and also for reducing the DPI through the use of the radiating pattern on the surveillance antenna as a kind of spatial filtering in combination with the selection of a favourable geometry, if possible. In Table 9.2 its main characteristic are summarized, and in Figure 9.8 the 3D radiation pattern and the estimated gain are also depicted, assuming a working frequency of 750MHz, taking into consideration the IoO spectrum re-allocation commented in section 9.2.

Table 9.2: DAT HD75 BOSS main characteristics

Frequency	Beamwidth		FB Ratio	Gain
	Azimuth (θ)	Elevation (ϕ)		
750 MHz	24.06°	23.5°	30.26 dB	17.31

(a) Antenna gain

(b) 3D radiation pattern
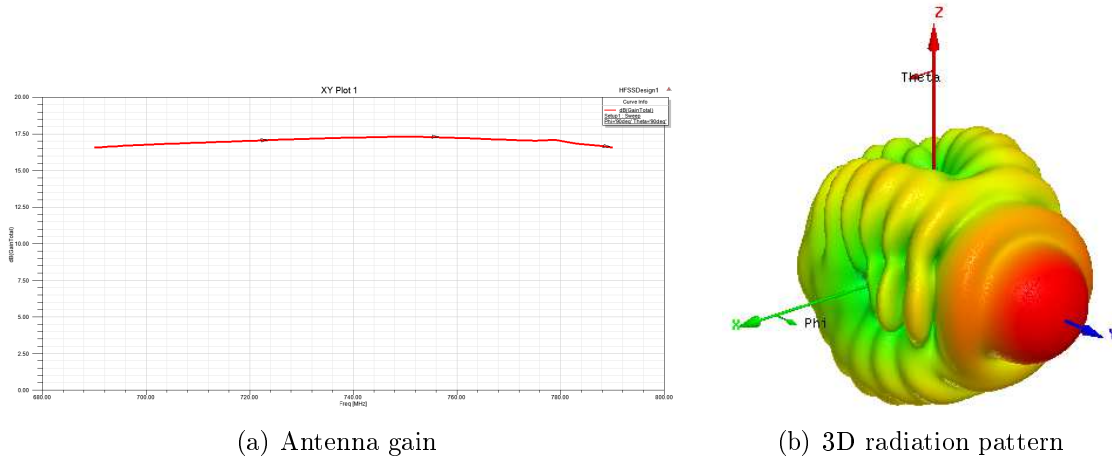
Figure 9.8: Additional DAT HD75 BOSS working parameters.

9.3.1 Problem formulation

The use of a single radiating element for the acquisition system do not allow any angular discrimination at detector level: the targets are associated to the steering direction the antenna is configured. The more accurate target position estimation is provided for tracking stage through the use of additional data as Doppler profiles for the region of interest. But due to the complexity of the bistatic geometry, the georreferenced coordinates estimation of the detected targets is a very complex problem, especially in systems with low angular resolution.

An improvement in the angular resolution of the system can be achieved through the use of array antenna and digital beamforming: taking into consideration the array geometry and its number of elements, the coherent combination of the acquired signal of each of the array sensors give rise to customizable radiation patterns, different from the single one. Then, thinner beamwidths and electronically configurable pointing direction are the key elements beamforming tools provide for improving target angular discrimination.

The characteristics of the single radiating element due to its influence over the overall beamforming technique performance are the following:

- Antenna gain and beamwidth: The single element radiation pattern must be as smooth as possible in the angular interval where beamforming techniques will be designed for varying the antenna array pointing direction. If this is not the case, undesired effects, such as blind pointing directions or high sidelobes can affect beamforming techniques performance.

| (a) | (b) HFSS model |
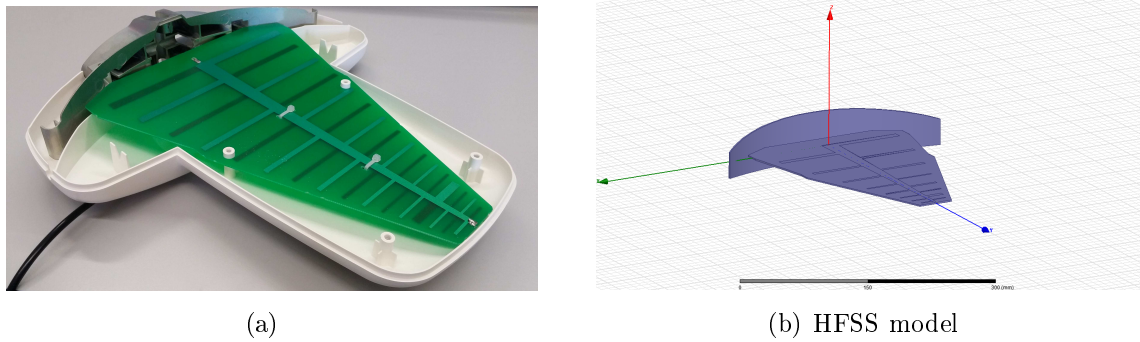
Figure 9.9: TELEVES 4G-NOVA antenna [TELEVES 4G-NOVA, 2016]

- Physical size: in order to avoid the grating lobe effect, the array inter-element spacing in general must be $d \leq \frac{\lambda}{2}$. So the physical antenna dimensions must fulfil this constrain. On the other hand, the coupling effect among array elements is a function of the physical inter-element spacing.

The conclusion of study of the feasibility of the DAT-HD75 antenna, taking into consideration these factors, showed that this antenna was not well suited to be used as an element of an array designed for digital beamforming techniques application: its physical dimension , $width = 560mm$ does not fulfil the grating lobes constrain, $d = 1.2879\lambda$ at the lower frequency of the DVB-T band. In addition, it presents a high directivity and an irregular main lobe shape.

9.3.2   New antenna selection

In order to select a better option for the array sensor, the 4G-NOVA antenna was also analysed. This antenna model is a log-periodic one based on microstrip technology, and covered with a radome that increase its physical dimensions but that can be easily removed 9.9. The minimum array inter-element distance achievable at the lower DVB-T frequency band when this antenna is used, $d = 0.6196\lambda$, considering the plastic cover, still generates grating lobes, but as the array pointing direction must be configured within the single radiation element main lobe limits, these undesired secondary lobes do not affect to the system. If the radome is removed, the grating lobes will be completely avoided for the lower frequency band. In Table 9.3 the antenna main parameters are summarized assuming it works at 750 MHz, that is approximately in the centred of the DVB-T considered frequency band.

Table 9.3: 4G-NOVA main characteristics

Frequency	Beamwidth		FB Ratio	Gain
	Azimuth (θ)	Elevation (ϕ)		
750 MHz	59.94°	92.4°	19.49 dB	8.3

The antenna radiation patter is not so directive as the DAT antenna one, but the main-lobe shape is very regular and presents a smooth gradient, both facts are improvements in terms of the array point of view. The loses in terms of directivity will be compensated in the beamforming process. The 4G-NOVA's elevation pattern is also very regular. 3D-radiation pattern and its main cuts obtained after the HFSS simulations are depicted in Figure 9.10.

(a) 3D radiation pattern

(b) 2D Azimuth radiation pattern

(c) 2D Elevation radiation pattern
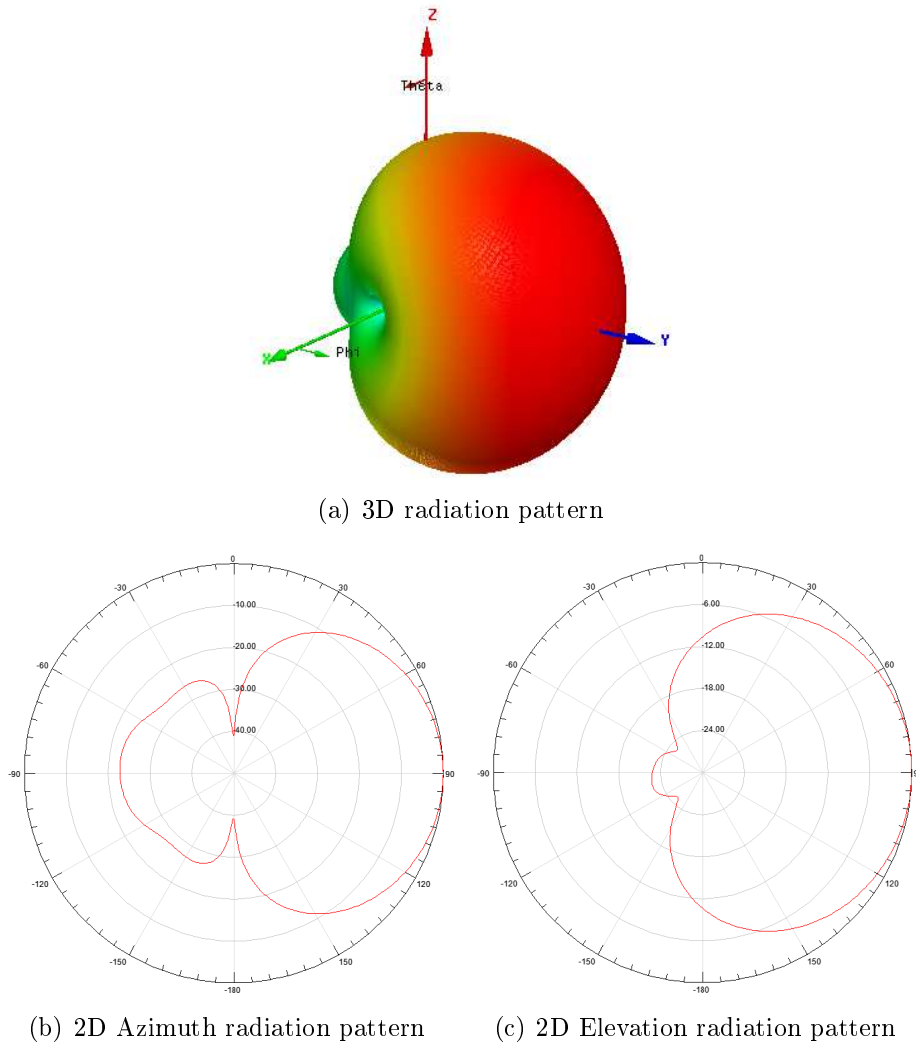
Figure 9.10: 4G-NOVA antenna radiation pattern obtained with HFSS software

9.3.2.1 Anechoic chamber real measurements

In order to obtain more precise antenna analysis, due to its promising array-oriented characteristics, the antenna was characterized through measurements in the High Technology and Homologation Centre, *Centro de Alta Tecnología y Homologación*, (CATE-CHOM) [CATECHOM, 2016], assuming a working frequency of 760 MHz.

Figure 9.11: CATECHON anechoic chamber.

CATECHOM is a Centre Supporting Investigation in the University of Alcalá. Its objective is to support the activities of investigation and technological development in relation with telecommunications, electronics and information technologies, for the university community and for other public and/or private institutions as well.

The CATECHOM has an infrastructure, an instrumentation, and a high qualified staff, for the achievement of tests in different fields: EMC, climate, vacuum, electrical security and antennas, and also to calibrate electrical and electronic equipments. The introduced Quality Management System located in the standard terms of the UNE-EN ISO/IEC 17025:2005, is applied to all the sections of the Centre. The anechoic chamber and the basic antenna measurement scheme are presented in Figures 9.11 and 9.12, respectively.

Suitable absorbent material and probe antenna are required for the specified considered scenario. The measurement system bandwidth must be able to afford multiple consecutive DVB-T channels and their broadcasting frequency band:

- The microwave absorber is EHP-8PCL (ETS-LINDGREN) except in the areas where specular reflection is expected. In those areas EHP-12PCL (ETS-LINDGREN) has been used. Their main characteristics are summarized in 9.13, showing the suitability of both absorbers.

- For the frequency band of interest, an AT4002A antenna (Amplifier Research) is available, Figure 9.14(a). The gain of the antenna is depicted in 9.14(b), as a function of the frequency.

The anechoic chamber is provided with a roll-over-azimuth positioning system (an spherical measurement system) as depicted in Figure 9.15, where the main accuracy parameters of the positioning stage are summarized. So, 3D radiation patterns can be measured.
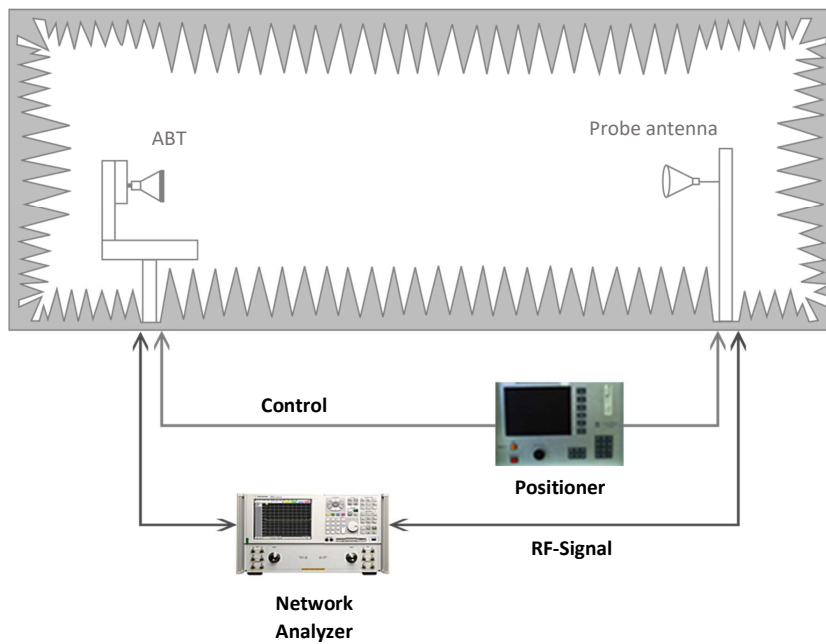
Figure 9.12: Antenna measurement system basic scheme.
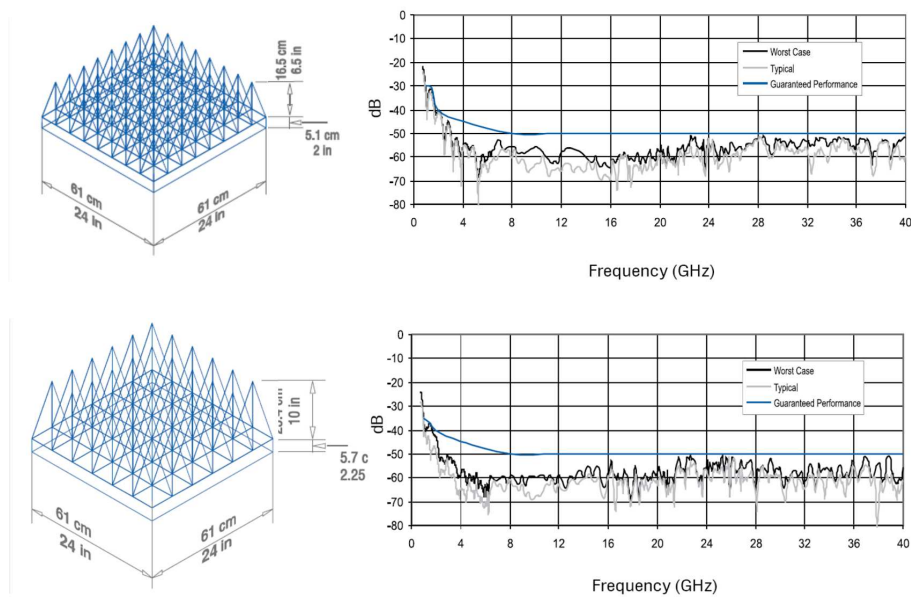
Figure 9.13: Anechoic chamber absorber: EHP-8PCL (top) and EHP-8PCL (bottom) [ETS-LINDGREN, 2016].

Due to the dimensions of the chamber, measurements will be performed in near field conditions and should be converted to far field. The CATECHOM antenna measurement system includes the software application EXPAND for performing this transformation [Harrington, 1961, Hansen, 1988]. This software has been developed by the Madrid Polytechnic University (UPM) and has been validated using the transformation routine

(a) AT4002A antenna
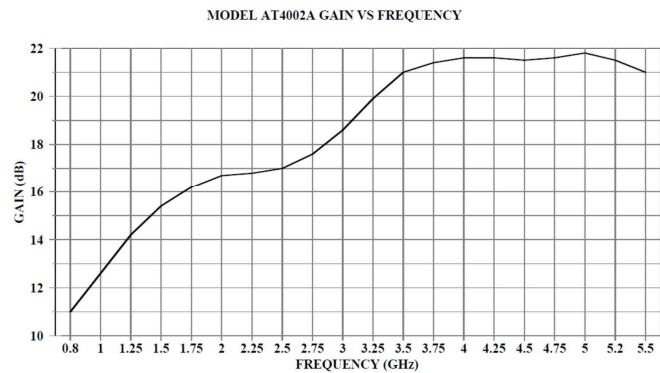
(b) AT4002A antenna gain

Figure 9.14: Anechoic chamber probe antenna:AT4002A (*Amplifier Research*).
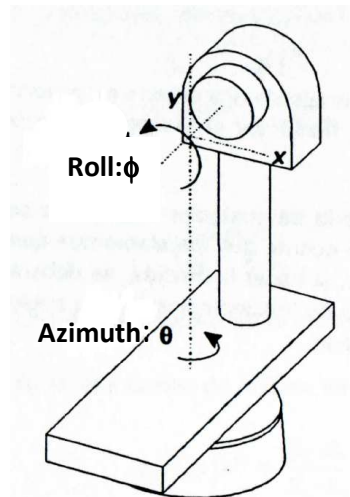
Rotary Joint	Roll and Azimuth Accuracies	Maximun Antenna Weight	
		Azimuth	Roll
To 40Ghz	0.03°	500 Kg	40 Kg for a 15 cm arm

Figure 9.15: Anechoic chamber roll-over-azimuth positioner: Divimek PHV-200 (roll), Divimek PHV-300 (azimuth).

SNIFTD or ASY-EXPAND (the ASYSOFT Spherical Near-Field to Far Field Transformation routine developed by Antenna System Solutions [SNIFTD, 2016]. This software is used by the UPM laboratory of antenna test and compliance, which has been certificated by ENAC (*Entidad Nacional de Acreditación*, National Entity for Accreditation) under the norm UNE-EN ISO/IEC 17025: 2005.

The 4G-NOVA antenna performance was measured in CATECHOM chamber. In Figure 9.16(a) is depicted how the antenna is located at the chamber positioner. Results obtained for azimuth and elevation radiation patterns show a measured antenna behaviour very similar to the predicted by the simulations:

- Azimuth plane, Figure 9.16(b): small differences can be observed mainly at the
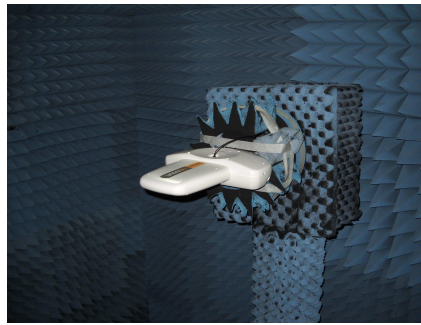
(a) 2D Azimuth radiation pattern
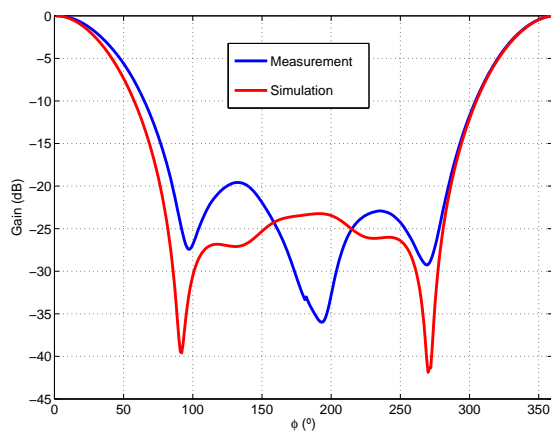
(b) 2D Azimuth radiation pattern
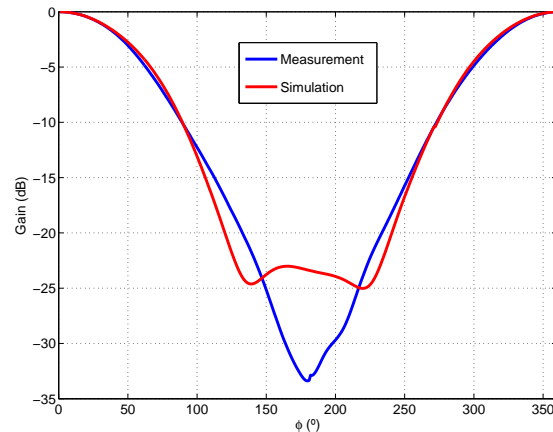
(c) 2D Elevation radiation pattern

Figure 9.16: Comparison between simulated radiation pattern and anechoic chamber measurement.

backside of the radiation pattern. In addition a variation in the shape of the main-lobe is detected too, reducing its symmetry.

- Elevation plane, Figure 9.16(c): the mainlobe matches almost perfectly with the obtained through HFSS simulation, and the variation in the backside of the pattern are not relevant.

So, the measurements prove that the conclusions reached through the analysis of the HFSS simulations are completely valid.

9.3.2.2 First beamforming results

In this section, a fist approach to beamforming performance analysis for IDEPAR demonstrator using 4G-NOVA antenna is carried out, taking into consideration the proposed single radiating element characteristics, the DVB-T illuminator signal parameters and also the scenario. A General Data Independent Response Design (GDIRD) technique was selected to be used in this work, due to its capacity to design a customized radiation pattern, allowing the selection of several steering directions and/or the position of nulls
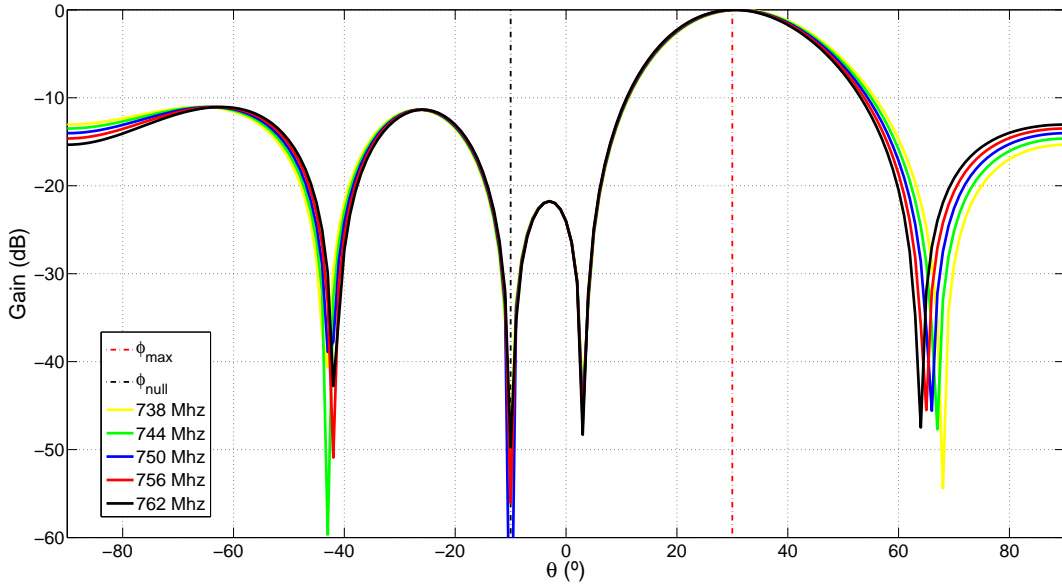
Figure 9.17: Beamformer radiation patter for different working frequencies: $\phi_{max} = 30°$ and $\phi_{null} = -10°$

if the interference direction of arrival is known [Veen and Buckley, 1988]. Before applying narrowband beamforming, the narrowband assumption constrains [Krim and Viberg, 1996] must be verified, equation (9.2):

$$E_{arr} \ll \frac{f_c}{B} \qquad (9.2)$$

where E_{arr} is the array aperture expressed as the array physical size measured in wavelengths, f_c is the working frequency and B is the signal bandwidth. This expression can be re-formulated in terms of the number of elements of the array (N), and the physical separation between them (d), equation (9.3):

$$TBP = \frac{B \cdot (N-1) \cdot d}{c} \ll 1 \qquad (9.3)$$

Assuming $B = 24MHz$, a DVB-T signal composed of 3 consecutive channels, $f_c = 478MHz$ as the lower limit in the DVB-T frequency band, and an array conformed by 5 elements, $TBP = 0.125$, a value very close to the limit of the assumption. Taking into consideration that this value depends on the signal central frequency, in Figure 9.17, the beamformer radiation pattern for different frequencies are compared, selecting $\phi = 30°$ as the maximum radiation pattern direction and setting a null at $\phi = -10°$. The variation between the considered frequencies at the radiation pattern point of interest are really small, so the behaviour of the bearformer performance can be considered almost constant within the used frequency band.

The beamformer gain using the 4G-NOVA antenna as single radiating element, obtained trough the HFSS simulation, is depicted in Figure 9.18. The improvement respect
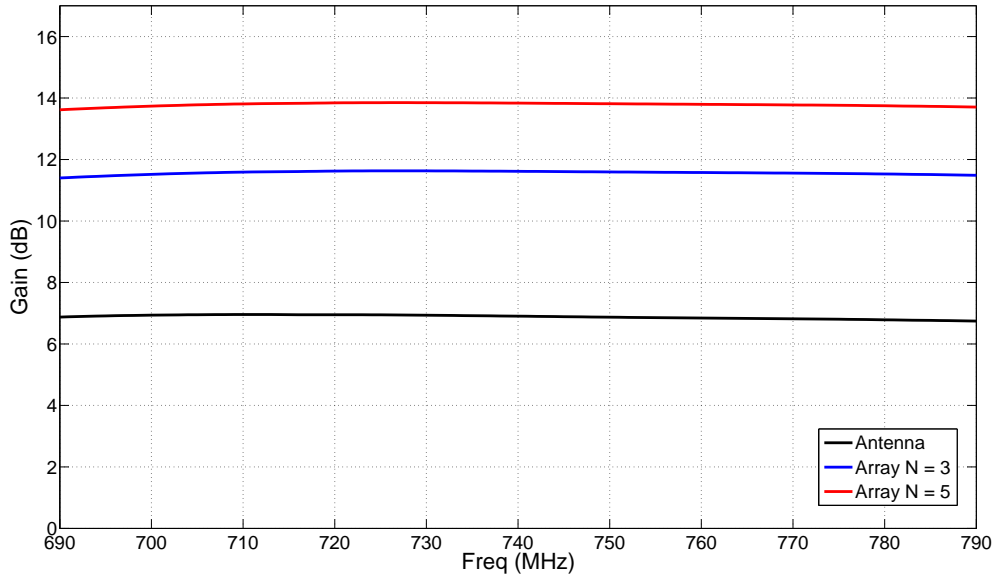
Figure 9.18: Antenna and beamformer output gain in the considered frequency range considering an array composed of 3 and 5 elements.

to the single antenna performance is around 5 dB when using 3 array elements, and around 7dB when the number of elements was increased to 5, compensating the lower gain the antenna has.

The use of the array in a PBR define a scenario with an unknown number of sought targets within the area of interest defined by the coverage constrains the system impose. In addition, the direction of the surrounding IoOs (desired one and the interference ones) must be considered. For each of the conformed beams, a set of nulls can selected or reduce the DPI or other known interference sources.

In order to improve the angular target discrimination, the simultaneous beam conformation at different steering directions were proposed: if the azimuthal resolution is enough, the detection output for all beams can be used to develop 3D detection stages, or a data fusion can be carried out to gives rise to an individual detection output.

In Figure 9.19, a superposed beamformer outputs using this scheme are depicted, using a simulated DBV-T signal composed of 3 consecutive channels: 5 beams are generated at $\phi = [-40°, -20°, 0°, 20°, 40°]$, obtaining radiation patterns with a mainbeam of $\pm 20°$, that is an improvement of a 33% respect to the single antenna. For the beams designed to $\phi_{max} = \pm 20°$ a pointing error of 2° is observed, doubling this error, 4°, for the pointing angles of $\phi_{max} = \pm 40°$. These two beams are pointing outside the main beam of the single radiating element, presenting the highest sidelobes, the $SLL_{\phi_{max}=\pm 40°} \approx -8dB$ but for the central pointing angles is $SLL_{\phi_{max}=[\pm 20°,0°]} \approx -11.5dB$, and the shape of their main lobes is less symmetrical, these differences can be observed in Figures 9.20(a) sand 9.20(b). Using an array composed of more elements these undesired effect will be mitigated: the pointing error will be reduced and in addition, a thinner mainlobe can be obtained. The
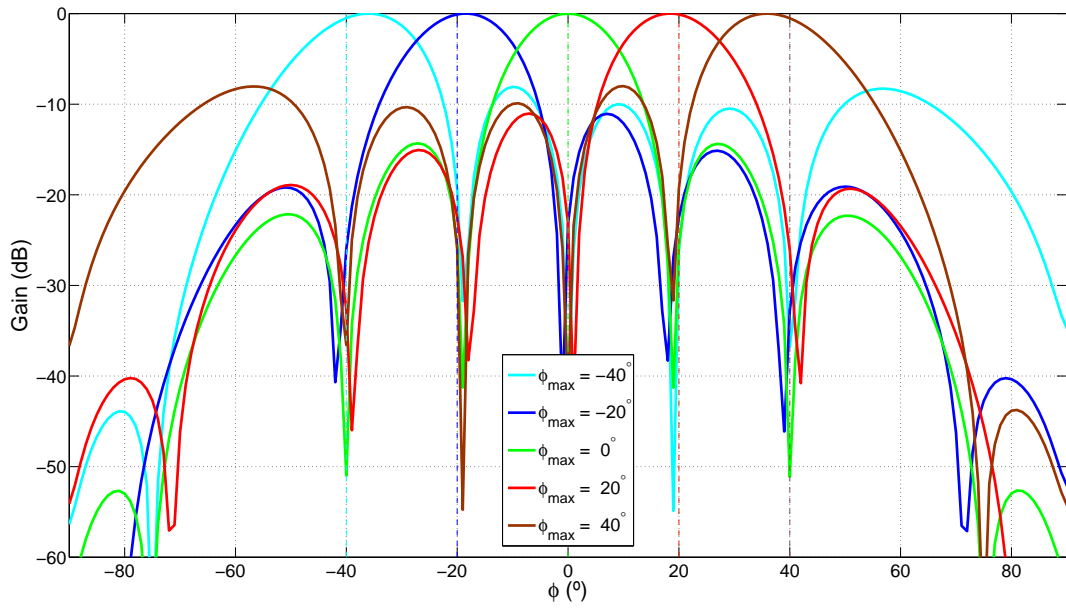
Figure 9.19: 5 simultaneous beams conformed pointing to $\phi_{max} = [-40°, -20°, 0°, 20°, 40°]$

(a) $\phi_{max} = 40°$

(b) $\phi_{max} = 20°$
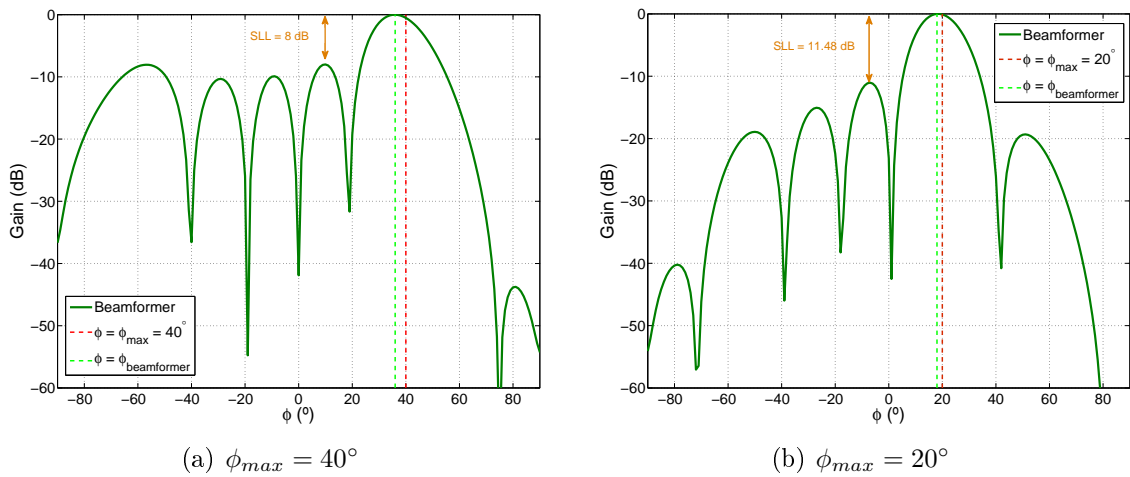
Figure 9.20: Beamformer mainbeam shape variation and SLL increments for two different pointing direction.

maximum number of elements of the array in this work is N = 5, imposed by the number of receiver chains available.

The main advantage is the total control over the radiation patter the proposed method gives rise allowing the customization of the antenna system performance in order to adapt it to the particular radar scenario.

Chapter 10

Conclusions

This PhD. Thesis is the result of an intense research activity in passive radar sensors, an emerging technology that is acquiring high relevance. The origin of this Thesis was the APIS project, and from the beginning to the end of this work, the interest on these sensors has experienced a great impulse, with the activities of numerous international research groups and different calls in European Defence Agency, FP7 and H2020 European programs. Thanks to the funding provided by the Spanish Ministry of Economy and Competitiveness under the IDEPAR project, this Thesis was proposed with two main objectives:

- **Scientific objective**: To study passive radars capabilities and propose solutions for improving their performance taking into consideration different aspects:

  - These systems are highly dependent on the scenario (geometry, relief, available IoOs, targets of interest, etc). Many of the studies presented in the literature dealt with aerial applications. As APIS proved the feasibility of commercial airplanes detection and tracking in landing and taking off manoeuvres, this Thesis focused on terrestrial targets and started the study of drons detection. In this line, space based IoOs were analyzed as alternatives/complements of terrestrial ones. The geometries of these scenarios are quite different from passive systems based on terrestrial IoOs. The long distances between the IoO and the receiver and the area of interest, and the movement of the IoO platform were analysed in detail.

  - Bistatic radar cross section of the targets of interest at UHF frequencies for geometries associated to passive radars based on terrestrial IoOs, and at X band, for geometries associated to passive radars based on satellite IoOs.

  - Analysis of multichannel DVB-T signals as opportunity ones, and the impact of the dispersion of DVB-T channels, their different allocations in different areas of a same country, and the changes associated to the Digital Dividend and future changes scheduled for 2020.

143

   – Preprocessing techniques for rejecting DPI and clutter in the surveillance chan-
   nel, and adjust the reference signal. These stages are critical because their
   direct impact of system detection performance and computational cost.

- **Technological objective**: Design and development of a portable technological
  demonstrator for the acquisition of real data and the validation of the proposed
  processing solutions.

The acquisition system design and hardware selection in order to fulfil detection ca-
pabilities requirements, the analysis of the available radar scenarios to estimate system
performance, and the selection and implementation of the required signal pre-processing
stages to reduce Zero-Doppler disturbance as one of the most relevant passive radar
drawbacks, are the main system elements under study in this PhD Thesis. In addi-
tion, IDEPAR improvements in terms of antenna subsystem, and of robustness against
IoO spectrum allocation are also considered.

As an added value, a feasibility study of satellite IoOs based passive radars was pre-
sented as a first answer to the problem of guaranteeing IoOs availability in remote scenarios
where DVB-T signals are not present.

Contributions and conclusions derived from this PhD Thesis are presented in the
following sections. In addition, future research lines will be described.

10.1   Regarding scenario analysis methodology

The use of non-controlled IoOs not designed for radar detection purposes, and the bi-
estatic/multistatic nature of the target radar echo, complicate the design and analysis of
passive radar systems:

- Available IoOs location with respect to the area of interest, their waveform charac-
  teristics, the radiated power and the radiation pattern of the transmitting antenna,
  are usually not the most favourable for the passive radar system design.

- Passive radar emplacement must be selected among those available, and, again, are
  usually not the most favorable for the passive radar system design.

- In radar literature, bistatic RCS studies of targets are significantly less extended that
  monostatic ones. On the other side, most of the available bistatic and monostatic
  RCS studies focus on typical radar frequencies, that are higher than the UHF ones
  exploited by the selected IoOs (DVB-T).

- Passive radar systems have been validated in aerial scenarios, being necessary the
  study of their capabilities in terrestrial ones for the detection of ground targets.
  The different cases of study that can be defined (rural, semi-urban, urban, farm,
  etc) complicate the definition of system parameters and the proposal of solutions to
  fulfill the desired requirements.

- Geometries for passive radars exploiting terrestrial and satellite IoOs are quite different. Specific studies were carried out for both cases.

The scenario analysis is the key element for the system design in order to fulfill desired performance requirements. As a result, the coverage area will be estimated as the area were the most challenging target among those defined as interest ones, can be detected with specified probabilities of detection and false alarm, and, if required, under specific weather conditions. The main contributions and conclusions associated to the PhD Thesis are the following:

10.1.1 Bistatic radar cross section studies at UHF frequencies.

The POFACETS software was used to estimate bistatic RCS values of the defined targets of interest. Two methodologies were proposed:

1. A first approach is based in an estimation of a BRCS using all angular combinations, giving a global information of the target despite off its position.

2. A second approach was proposed for considering the specific radar scenario geometry in the BRCS study. For each type of desired target, the most probable or most interesting trajectories were defined and the associated elevation and bistatic angles calculated. For each selected elevation and bistatic angles, the target was rotated in the azimuth plane and the average BRCS was estimated. This method was described and applied in [Bárcena-Humanes et al., 2015]. Values estimated from the second approach are usually lower than those obtained from the first one. This result is mainly due to the high contributions if the forward propagation in the first approach.

10.1.2 System coverage estimation

As a first approach, the coverage area was estimated assuming free space propagation in the IoO-target and target-PR paths. This solution is widely extended in the bibliography and was used in [Jarabo-Amores et al., 2016]. A more precise methodology was developed using complex propagation models for both paths. The WinProp electromagnetic simulator was used in [Gómez-del Hoyo et al., 2016, Gómez-del Hoyo et al., 2016]. Results showed that the first approach, based on free space losses was really optimistic, being necessary a more accurate simulation of the propagation losses. In this PhD Thesis, a more detailed study was performed considering target altitude. This study was motivated by the problem of detecting small targets flying at low altitudes. Drons are challenging targets that are demanding great efforts for improving radar sensors in order to make possible their detection and tracking.

10.1.3   Selected scenarios

The main IDEPAR validation scenario was analyzed. This semi-urban scenario was located in the roof of the Superior Polythecnic Scholl of the University of Alcalá with a highway and a road. The first one was far from the reviever and was characterized by a low traffic and a high average speed, while the road was closer and characterized by a higher traffic and a lower average speed. In order to shown the effects of a complex relief and an adverse IoO allocation, the analysis of the scenario centered on CEAR facilities was carried out, showing the great reduction of the system coverage for ground targets. Both scenarios were also studied considering a low-flying drone. Results showed that the higher altitude of the drone with respect to the previously considered cars provided a higher coverage in spite of the significantly lower radar cross section of the drone.

10.2   Regarding Space-borne illuminators feasibility for passive radars

The case study of scenarios based on satellite IoOs was considered as a natural evolution of IDEPAR. A detailed study was carried out in order to analyze the feasibility of a passive radar exploiting an Earth Observation SAR sensor [Bárcena-Humanes et al., 2015] as the PAZ satellite. The main conclusions are the following:

- The transmitted signal is characterized by periodic ambiguity peaks that limit the coverage area and the target dynamics, but the limits imposed by the signal AF are beyond the limits imposed by these other factors, so the ambiguity peaks have no practical effect on system performance.

- A study of potential bistatic geometries was carried out in order to determine the time availability and the instrumented spatial coverage. The orbital parameters, the acquisition modes and the operation schedule impose critical limitations to the IoO availability.

- Different study cases were defined to analyze the impact of OI orbit. The virtual displacement of a target was modelled and practical values calculated.

- Incident power density and required sensitivity. The available power at the PR antenna was estimated as a function of the target-to-PR distance, proving the feasibility of PAZ (coverages of 15 km are achievable with affordable system sensitivities).

- PBR based on PAZ can provide speed and trajectory of moving target to improve the information extraction from the acquired SAR images in the operational phase. Or being used as a low-cost easily deployable and configurable calibration tool in the commissioning phase of the SAR sensor, or in posterior maintenance processes.

10.3   Regarding IDEPAR demonstrator

The IDEPAR demonstrator was developed in the University of Alcalá, to be used as a design and testing platform for the analysis and improvement of PBRs components (software and hardware selection). The main task considered along development process were:

- IDEPAR is a DVB-T based passive bistatic radar, designed to work in the higher part of the DTV broadcasting band, using up to three consecutive channels to obtain improved resolution capabilities.

- COTS philosophy was considered for the acquisition chain components and processing hardware selection: commercial antennae subsystem and standard RF front-end components and SDR acquisition boards. The versatility and modularity these components provide improve the system added value for research purposes.

- Off-line digital processing scheme or pre and post processing stages, in order to allow a easy integration of algorithms and their validation using real data acquired under controlled conditions.

In this PhD work, the basic signal processing architecture for PBR, which will be the selected one for be implemented in the demonstrator, was presented. The semi-urban scenario used along developing and evaluation system stages is considered for results validation: cooperative targets and other non-cooperative ones controlled by visual inspection are used, and ground-truths at the output of the detector are generated for improving the detection performance estimation. Results show that the detection of low speed cars in presence of big buildings is feasible, although signal processing techniques need to be modified to fulfil the desired detection requirements ($P_{FA} = 10^{-6}$ and $P_D = 80\%$).

10.4   Regarding Zero-Doppler Interference suppression techniques

A deep study of different adaptive filtering strategies for disturbance cancellation was carried out. LMS, RLS and ECA solutions were analyzed from a theoretical point of view, and in the context of passive radar applications. Most of the previous research was focused on convergence properties, clutter attenuation and disturbance to main peak ratio reduction in the CAF. Studies were applied to FM, DVB-T, WiFi and DRM signals.

The analysis of the selected algorithms was carried out from the point of view of global system performance, considering detection and tracking capabilities, and computational cost. For the characterization of the algorithm in terms of detection and tracking capabilities, two analysis parameters were defined:

- Signal to Noise and Interference Ratio (SNIR), related to system sensitivity for specified system performance parameters (P_{FA} and P_D).

- Zero Doppler Interference Rejection (ZDIR), that quantifies the rejection/reduction of interference components located close to the zero Doppler line in the RDS.

A design methodology based on the analysis of the evolution of these parameters as a function of the different adaptive approaches design parameters was proposed. The main conclusions extracted from the study of the considered LMS approaches and the proposed solutions are summarized:

- **LMS filters** LMS algorithms family introduces a level reduction along the Doppler dimension, but this reduction decreases as the Doppler shift increases. How fast this reduction decreases depends on specific filter implementation and step-size parameter configuration. The LMS study proved that there was a upper limit of the step-size value, μ. As a result, the possibility of avoiding the distortions related to high convergence times is not guaranteed. On the other hand, for a fixed step-size value, a range limitation may appear, observed as a SNIR degradation as the filter order increases. For solving these problems, the following solutions were analysed:

    - The use of a normalization in the weight vector updating rule increases the LMS algorithm step-size upper limit, NLMS algorithms.

    - Weights inheritance: a weights inheritance mechanism was implemented to avoid the undesired effects of the convergence time. Based on the hypothesis of stationarity of the zero Doppler interference, the weights vector obtained at the end of a CPI was used for initializing the adaptive process of the next CPI.

- **RLS filters**

    The RLS algorithm reduces the RDS level throughout all the Doppler dimension in a more homogeneous way, independently of filter parameters (K and forgetting factor). Furthermore, the algorithm is unable to achieve an acceptable filtering performance for the selected set of parameters.

- **ECA filters** Least Square Matrix based ECA, that takes advantage of LS-fundamentals to reduce its computational cost, only reduces zero Doppler shift positions on the RDS, achieving a great rejection of the undesired interferences without a reduction on the target detection capabilities, but introducing a little improvement. This very specific setting prevents the system to completely remove interferences that are spread around several non zero Doppler rows, clutter with an small associated Doppler.

Attending to detection point of view, Weights Inheritance NLMS algorithm and the ECA-based one obtained very similar results, being those obtained by the first approach slightly better for both parameters SNIR and ZDIR.

LSM-ECA algorithm is clearly the most time efficient of the analyzed processing tool, but the WI-NLMS presents a certain degree of customization that could help during system design and validation stages. As a side effect of the level reduction along non-zero Doppler frequencies, multipath ghost target can be identified through the analysis of the commented RDS parameters evolution of each target with respect to filter order.

10.5 Regarding the DVB-T channels allocation problem

One of the main passive radar drawbacks is the near complete lack of control over the illuminator and the need of adjust the acquisition stages to the available signals and their electromagnetic spectrum allocation: for example, changes in government commercial broadcasting signals regulations could require system hardware readjustment. Along this PhD work, one major change in the DVB-T channel spectrum distribution happened, and as a result, the working central frequency and the number of consecutive channels available have been reduced. In order to face this problem, a low cost solution is proposed based in commercial broadcast mixers that allow the channel displacement before the RF front-end, partially detaching acquisition chain design and the local channel allocation.

Derived from the general purpose nature of the selected hardware, an offset compensation stage must be included due to the imbalance between mixers local oscillators. The central frequency offset changes between each DVB-T channel displaced, any time the hardware is switched off and also has a small temporal migration. This frequency uncoupling between reference and surveillance channel gives rise to a great error in the coherent processing.

A compensation stage is proposed based in the a-priori knowledge about the signal spectrum shape, through a two steps strategy:

- A rough offset estimation applied to both system acquisition channels. The compensation of this offset improves RDS generation, but a Doppler error and a blurring effect are still present due to the characteristics of the offset.

- A fine compensation, where the surveillance channel working frequency is displaced to the reference one, through an iterative approximation.

After this stage, the zero-Doppler line errors were reduced to a level lower than system resolution, and also the blurring was mitigated, making possible the target parameter estimation.

10.6   Future research lines

IDEPAR demonstrator development and validation has encouraged all the RS3Lab group activities in passive radar research field. Future works, many of them are being developed nowadays, and have given rise to three new PhD Thesis that are in progress, can be classified as follows:

1. Study and optimization of PBR main signal processing stages.

2. Signal processing improvements associated to the development of array antennas and the application of beamforming techniques.

3. Demonstrator update for satellite IoOs exploitation: new antenna subsystem, changes in the acquisition chain in order be able to acquire DVB-S signals at working frequencies higher than 10 GHz, etc.

4. New signal processing techniques for high bandwidth/sparse signals.

5. Design of customized low cost patch antennas as single radaiting elements for antenna array performance improvement

6. Multistatic systems development and analysis: data fusion techniques for detection, tracking, and robustness improvement.

7. Computing platforms for reducing the gap towards real time implementation. The computation on GPU devices using available Global Purpose GPU (GPGPU) utilities, as for example CUDA, should be a priority task to be faced. On the other hand, signal processing capabilities of new acquisition boards with high performance integrated FPGAs will be explored.

10.6.1   Study and optimization of PBR main signal processing stages

Using the current IDEPAR system version as development platform, and taking advantage of the availability of real data, and the presented results on ZDI rejection techniques, improved detection and tracking solutions are being developed.

Regarding the detection stage, there are several research tasks in progress:

1. A complete statistical analysis of the RDS data is expected to be useful to improve the system performance. This analysis must include the effects of the different disturbance cancellation techniques, and other pre-processing stages.

2. Other detectors but CA-CFAR must be considered: different CFAR approaches as Greatest Of CFAR (GO-CFAR), Smallest Of CFAR (SO-CFAR) or Variability Index CFAR (VI-CFAR). Alternative solutions based on intelligent agents could be used.

Other detection techniques as Moving Target Indicator (MTI) or Moving Target Detector (MTD) could be analysed as potential detection stages improvement.

10.6.2 Array antennas development and beamforming techniques application

In this PhD Thesis, a preliminary study of commercial antennas based arrays for improving IDEPAR angular coverage and resolution was carried out. The possibility of generating multiple and simultaneous beams, will impulse the improvement of ZDI rejection techniques, and the development of 3D detection and tracking solutions.

Due to beamforming techniques constrains imposed to the single radiating element, the selection of a commercial antenna is a complicated task. In this PhD Thesis, the TELEVES 4G-NOVA antenna was considered, but in order to fulfil all the specified requirements, a wideband patch antenna is being afforded, taking into consideration the exploitation of DVB-T signals in the selected scenarios.

Digital beamforming tools will be tested over real data acquired in different scenarios in order to improve system detection an tracking capabilities and to validate the results obtained in this PhD Thesis using simulated signals. Another important related research line is that related to the implementation of Direction of Arrival (DoA) estimation techniques, which are expected to improve tracking capabilities and will allow the study of solutions for authomatic IoO selection.

10.6.3 New signal processing techniques for high bandwidth/sparse signals

High bandwidths are desired for increasing range resolution. The variability and channel dispersion of DVB-T channels generate a critical challenge to guarantee the performance of a PBR in any emplacement.

In this PhD Thesis, a low cost solution based on commercial mixers was proposed and calibration techniques were developed for allowing the use of those devices.

A more promising, but more expensive, solution is the acquisition of wideband signals. Due to the nature of DVB-T signal, different channels and frequency gaps will be acquired in this bigger bandwidth. Available channels and gaps will depend on the local DVB-T channel allocation. This sparse nature of the acquired signal will require the design and analysis of specific signal processing stages for disturbance cancellation, detection and tracking.

Both solutions are expected to suffer target Doppler dispersion that must be studied for minimize its impact on system capabilities.

Glosary

ADC: Analog-to-Digital Converter

AoI: Area of Interest

BNLMS: Block based Least Mean Square

CA-CFAR: Cell Averaging CFAR

CAF: Cross Ambiguity Function

CATECHOM: *Centro de Alta Tecnología y Homologación*, High Technology and Homologation Centre

CEAR: Centro de Ensayos y Análisis Radioeléctrico

CFAR: Constant False Alarm Rate

CUDA: Computed Unified Devide Architecture

CUT: Cell Under Test

DFT: Discrete Fourier Transform

DOA: Direction of Arrival

DRM: Digital Radio Mondiale

DSGN: Digital Satellite News Gathering

DVB-S: Digital Video Broadcasting- Satellite

DVB-T: Digital Video Broadcasting- Terrestrial

ECA: Extensive CAncellation

ECA-B: Extensive CAncellation Batches

ECA-Sliding: Extensive CAncellation Sliding

ECA-C: ECA-by-Carrier

EMC:	ElectroMagnetic Compatibility
ENAC:	*Entidad Nacional de Acreditación*, National Entity for Acreditation
FB:	Front-to-Back ratio
GDIRD:	General Data Independent Response Design
GO-CFAR:	Greatest OF CFAR
GPU:	Graphics Processor Unit
IFF:	Identification Friend or Foe
IoO:	Illuminator of Opportunity
ISV:	Instantaneous Squared Value
LO-CFAR:	Least OF CFAR
LMS:	Least Mean Square
LNA:	Low Noise Amplifier
LS:	Least Square
LSM-ECA:	Least Square Matrix based ECA
MPEG:	Moving Picture Experts Group
MSE:	Mean Squared Error
MTI:	Moving Target Indicator
MTD:	Moving Target Detector
NLMS:	Normalized Least Mean Squared
OFDM:	Orthogonal Frequency Division Multiplexing
PBR:	Passive Biestatic Radar
QPSK:	Quadrature Phase-Shift Keying
RCS:	Radar Cross Section
RDLMS:	Range-Doppler NLMS
RDM:	Range-Doppler Map
RDS:	Range-Doppler Surface

RLS: Recursive Least Square

SDR: Software Designed Radio

SIR: Signal to Interference Ratio

SLL: SideLobe Level

SFN: Single Frequency Network

SOF: Start Of Frame

SSE: Sum of squares error

SSM: Steady State Misadjustement

TBP: Time-Bandwidth Product

TPS: Transmission Parameter Signalling

UPM: *Universidad Politécnica de Madrid*, Madrid Polytechnic University

VI-CFAR: Variability Index CFAR

VSLMS: Variable Step-size Least Mean Square

WI-NLMS: Weight Inheritance Normalized Least Mean Square

WLS: Weight Least Squares

WiFi: Wireless Fidelity, Wireless Internet

Bibliography

Bibliography

[IEE, 2008] (2008). *IEEE Standar Radar Definitions*. IEEE aerospace and Electronics Sistem Society Sponsored by the Radar System Panel.

[300-744, 1999] 300-744, E. (1999). *Digital Video Broadcasting (DVB): Framing structure, channel coding and modulation for digital terrestrial television (DVB-T))*. European Telecommunication Standars Institute.

[302-307, 2009] 302-307, E. (2009). *Second generation framing structure, channel coding and modulation systems for Broadcasting, Interactive Services, News Gathering and other broadband satellite aplplications (DVB-S2)*. European Telecommunication Standars Institute.

[Al-Ashwal et al., 2011] Al-Ashwal et al. (2011). Statistical analysis of simultaneous monostatic and bistatic sea clutter at low grazing angles. *Electronics Letters*, 47(10):621–622.

[Al-Ashwal et al., 2014a] Al-Ashwal, W., Griffiths, H., and Woodbridge, K. (2014a). Analysis of bistatic sea clutter. Part II: Amplitude statistics. *IEEE Transactions on Aerospace and Electronic Systems*, 50(2):1293–1303.

[Al-Ashwal et al., 2014b] Al-Ashwal, W., Woodbridge, K., and Griffiths, H. (2014b). Analysis of bistatic sea clutter. Part I: Average reflectivity. *IEEE Transactions on Aerospace and Electronic Systems*, 50(2):1283–1292.

[Baker, 2014] Baker, C. (2014). Short course: Passive Radar sensors: theory and application. In *European Mircrowave Week*.

[Baker et al., 2005] Baker, C., Griffiths, H., and Papoutsis, I. (2005). Passive coherent location radar systems. Part 2: waveform properties. *Radar, Sonar and Navigation, IEE Proceedings*, 152(3):160–168.

[Bar-Shalom et al., 1989] Bar-Shalom, Y., Chang, K., and Shertukde, H. (1989). Performance evaluation of a cascaded logic for track formation in clutter. In *Systems, Man and Cybernetics, 1989. Conference Proceedings., IEEE International Conference on*, pages 13–17 vol.1.

[Barcena-Humanes et al., 2014] Barcena-Humanes, J., Martin-de Nicolas, J., Solis-Carpintero, C., Jarabo-Amores, M., Rosa-Zurera, M., and Mata-Moya, D. (2014). DVB-T ambiguity peaks reduction in passive radar applications based on signal reconstruction. In *European Radar Conference (EuRAD), 2014 11th*, pages 597–600.

[Basavarajappa, 2012] Basavarajappa, V. (2012). *Design of a wideband conformal array antenna system with beamforming and null steering, for application in a DVB-T based passive radar*. PhD thesis, TU Delft, Delft University of Technology.

[Bernaschi et al., 2012] Bernaschi, M., Di Lallo, A., Farina, A., Fulcoli, R., Gallo, E., and Timmoneri, L. (2012). Use of a graphics processing unit for passive radar signal and data processing. *Aerospace and Electronic Systems Magazine, IEEE*, 27(10):52–59.

[Bolvardi et al., 2015] Bolvardi, H., Derakhtian, M., and Sheikhi, A. (2015). Reduced complexity generalised likelihood ratio detector for digital video broadcasting terrestrial-based passive radar. *Radar, Sonar Navigation, IET*, 9(8):1021–1029.

[Bárcena-Humanes et al., 2015] Bárcena-Humanes, J.-L., Gómez-Hoyo, P.-J., Jarabo-Amores, M.-P., Mata-Moya, D., and Del-Rey-Maestre, N. (2015). Feasibility study of eo sars as opportunity illuminators in passive radars: Paz-based case study. *Sensors*, 15(11):29079.

[Cantini et al., 2009] Cantini, C., Rosa, E. L., Re, A. L., and Lallo, A. D. (2009). Passive coherent locator signal processor on ibm cell broadband engine (cell be). In *2009 IEEE Radar Conference*, pages 1–6.

[Cao et al., 2010] Cao, T.-T., Palmer, J., and Berry, P. (2010). False alarm control of CFAR algorithms with experimental bistatic radar data. In *Radar Conference, 2010 IEEE*, pages 156–161.

[Capria et al., 2015] Capria, A., Petri, D., Moscardini, C., Conti, M., Forti, A. C., Massini, R., Cerretelli, M., Ledda, S., Tesi, V., Mese, E. D., Gentili, G. B., Berizzi, F., Martorella, M., Soleti, R., Martini, T., and Manco, A. (2015). Software-defined multi-band array passive radar (smarp) demonstrator: A test and evaluation perspective. In *OCEANS 2015 - Genova*, pages 1–6.

[Cardinali et al., 2007] Cardinali, R., Colone, F., Ferretti, C., and Lombardo, P. (2007). Comparison of clutter and multipath cancellation techniques for passive radar. In *Radar Conference, 2007 IEEE*, pages 469–474.

[CATECHOM, 2016] CATECHOM (2016). High technology and homologation center of the university of alcalá. http://www2.uah.es/catechom/index.php?lang=en, accessed 15 September 2016.

[Cherniakov et al., 2010] Cherniakov, M., Gashinova, M., and V.Sizov (2004-2010). Forward scattering Micro-Sensors for Intruder Detection & Classification. In *Final report of DTC EMRS*.

[Cherniakov et al., 2008] Cherniakov, M., Saini, R., Zuo, M., and Plakidis, E. (2008). Experiences gained during the development of a Passive BSAR with GNSS Trensmitters of Opportunity. *International Journal of Navigation and Observation*.

[Colone et al., 2013a] Colone, F., Bongioanni, C., and Lombardo, P. (2013a). Multifrequency integration in fm radio-based passive bistatic radar. part i: Target detection. *IEEE Aerospace and Electronic Systems Magazine*, 28(4):28–39.

[Colone et al., 2013b] Colone, F., Bongioanni, C., and Lombardo, P. (2013b). Multifrequency integration in fm radio-based passive bistatic radar. part ii: Direction of arrival estimation. *IEEE Aerospace and Electronic Systems Magazine*, 28(4):40–47.

[Colone et al., 2006] Colone, F., Cardinali, R., and Lombardo, P. (2006). Cancellation of clutter and multipath in passive radar using a sequential approach. In *Radar, 2006 IEEE Conference on*, pages 7 pp.–.

[Colone et al., 2012a] Colone, F., Falcone, P., Bongioanni, C., and Lombardo, P. (2012a). Wifi-based passive bistatic radar: Data processing schemes and experimental results. *IEEE Transactions on Aerospace and Electronic Systems*, 48(2):1061–1079.

[Colone et al., 2012b] Colone, F., Falcone, P., Bongioanni, C., and Lombardo, P. (2012b). Wifi-based passive bistatic radar: Data processing schemes and experimental results. *IEEE Transactions on Aerospace and Electronic Systems*, 48(2):1061–1079.

[Colone et al., 2014] Colone, F., Langellotti, D., and Lombardo, P. (2014). Dvb-t signal ambiguity function control for passive radars. *IEEE Transactions on Aerospace and Electronic Systems*, 50(1):329–347.

[Colone et al., 2009a] Colone, F., O'Hagan, D. W., Lombardo, P., and Baker, C. J. (2009a). A multistage processing algorithm for disturbance removal and target detection in passive bistatic radar. *IEEE Transactions on Aerospace and Electronic Systems*, 45(2):698–722.

[Colone et al., 2009b] Colone, F., O'Hagan, D. W., Lombardo, P., and Baker, C. J. (2009b). A multistage processing algorithm for disturbance removal and target detection in passive bistatic radar. *IEEE Transactions on Aerospace and Electronic Systems*, 45(2):698–722.

[Colone et al., 2016] Colone, F., Palmarini, C., Martelli, T., and Tilli, E. (2016). Sliding extensive cancellation algorithm for disturbance removal in passive radar. *IEEE Transactions on Aerospace and Electronic Systems*, 52(3):1309–1326.

[Conti et al., 2012] Conti, M., Berizzi, F., Martorella, M., Mese, E., Petri, D., and Capria, A. (2012). High range resolution multichannel dvb-t passive radar. *Aerospace and Electronic Systems Magazine, IEEE*, 27(10):37–42.

[Conti et al., 2011] Conti, M., Petri, D., Capria, A., Berizzi, F., and Martorella, M. (2011). High resolution and artifact cancellation in wideband DVB-T passive radar. *3rd FHR Focus Days on PCL, Wachtberg-Werthhoven*.

[Cristallini et al., 2010] Cristallini, D., Caruso, M., Falcone, P., Langellotti, D., Bongioanni, C., Colone, F., Scafè, S., and Lombardo, P. (2010). Space-based passive radar enabled by the new generation of geostationary broadcast satellites. In *Aerospace Conference, 2010 IEEE*, pages 1–11.

[del Hoyo et al., 2015] del Hoyo, P. G., Barcena-Humanes, J. L., Mata-Moya, D., Juara-Casero, D., and de Lucas, V. J. (2015). Passive radars as low environmental impact solutions for smart cities traffic monitoring. In *EUROCON 2015 - International Conference on Computer as a Tool (EUROCON), IEEE*, pages 1–6.

[del Rey-Maestre et al., 2015] del Rey-Maestre, N., Jarabo-Amores, M. P., Mata-Moya, D., del Hoyo, P. G., and Barcena-Humanes, J. L. (2015). Statistical analysis of uhf bistatic radar clutter in coastal scenarios. In *Radar Conference (EuRAD), 2015 European*, pages 253–256.

[Diniz, 2008] Diniz, P. (2008). *Adaptive Fltering: Algorithms and Practical Implementation*, volume 1. Springer.

[Edrich and Schroeder, 2013] Edrich, M. and Schroeder, A. (2013). Multiband multistatic passive radar system for airspace surveillance: A step towards mature pcl implementations. In *2013 International Conference on Radar*, pages 218–223.

[Edrich et al., 2014] Edrich, M., Schroeder, A., and Meyer, F. (2014). Design and performance evaluation of a mature FM/DAB/DVB-T multi-illuminator passive radar system. *Radar, Sonar Navigation, IET*, 8(2):114–122.

[ETS-LINDGREN, 2016] ETS-LINDGREN (2016). , microwave absorbers. http://www.etslindgren. com, accessed 15 September 2016.

[Falcone et al., 2012] Falcone, P., Colone, F., and Lombardo, P. (2012). Potentialities and challenges of wifi-based passive radar. *IEEE Aerospace and Electronic Systems Magazine*, 27(11):15–26.

[Falcone et al., 2014] Falcone, P., Colone, F., Macera, A., and Lombardo, P. (2014). Two-dimensional location of moving targets within local areas using wifi-based multistatic passive radar. *IET Radar, Sonar Navigation*, 8(2):123–131.

162

[Freedman and Levanon, 1994] Freedman, A. and Levanon, N. (1994). Properties of the periodic ambiguity function. *IEEE Transactions on Aerospace and Electronic Systems*, 30(3):938–941.

[Fulcoli et al., 2015] Fulcoli, R., Sedehi, M., Telli, E., and Timmoneri, L. (2015). AULOS, A Passive Covert Radar System. In *Microwave Yournal*.

[Gandhi and Kassam, 1988] Gandhi, P. and Kassam, S. (1988). Analysis of CFAR processors in homogeneous background. *Aerospace and Electronic Systems, IEEE Transactions on*, 24(4):427–445.

[Glende et al., 2007] Glende, M., Heckenbach, J., Kuschel, H., Müller, S., Schell, J., and Schumacher, C. (2007). Experimental passive radar systems using digital illuminators (dab/dvb-t). In *Proceedings of the International Radar Symposium (IRS)*, page 17.

[Gómez-del Hoyo et al., 2016] Gómez-del Hoyo, P., Bárcena Humanes, J.-L., Rey-Maestre, N., Jarabo-Amores, M.-P., and Mata-Moya, D. (2016). Cobertura de radares pasivos basados en la tdt para la detección de vehículos terrestres. *XXXI Simposium Nacional de la Unión Científica Internacional de Radio*.

[Gómez-del Hoyo et al., 2016] Gómez-del Hoyo, P., Bárcena-Humanes, J. L., del Rey-Maestre, N., Jarabo-Amores, M. P., and Mata-Moya, D. (2016). Ultra-high frequency Passive Radar coverage for cars detection in Semi-Urban scenarios. *18th International Conference on Signal and Information Processing (ICSIP2016)*, page 5.

[Griffiths and Baker, 2005a] Griffiths, H. and Baker, C. (2005a). Measurement and analysis of ambiguity functions of passive radar transmissions. In *Radar Conference, 2005 IEEE International*, pages 321–325.

[Griffiths and Baker, 2005b] Griffiths, H. and Baker, C. (2005b). Passive coherent location radar systems. part 1: performance prediction. *Radar, Sonar and Navigation, IEE Proceedings -*, 152(3):153–159.

[Guillemin and Kalman, 1971] Guillemin, E. A. and Kalman, R. (1971). *Aspects of network and system theory*. Holt, Rinehart and Winston.

[Hansen, 1988] Hansen, J. E. (1988). *Spherical near-field antenna measurements*, volume 26. Iet.

[Harrington, 1961] Harrington, R. F. (1961). *Time-harmonic electromagnetic fields*. McGraw-Hill.

[Haykin, 2008] Haykin, S. S. (2008). *Adaptive Filter Theory*, volume 1. Prentice Hall.

[Howland et al., 2005] Howland, P. E., Makisimiut, D., and Reitsma, G. (2005). FM radio based bistatic radar. In *IEE Proceedings on Radar, Sonar and Navigation*, volume 152, pages 107–115.

[Hsia, 1983] Hsia, T. (1983). Convergence analysis of LMS and NLMS adaptive algorithms. In *Acoustics, Speech, and Signal Processing, IEEE International Conference on ICASSP '83.*, volume 8, pages 667–670.

[Jarabo-Amores et al., 2016] Jarabo-Amores, M., Bárcena-Humanes, J., Gómez-del Hoyo, P., Rey-Maestre, N., Juara-Casero, D., Gaitán-Cabañas, F., and Mata-Moya, D. (2016). IDEPAR: a multichannel digital video broadcasting-terrestrial passive radar technological demonstrator in terrestrial radar scenarios. *IET Radar, Sonar and Navigation.*

[Jenn, 2016] Jenn, D. C. (2016). Dr. David C. Jenn's Personal Page. Retrieved March 10, 2014, from http://faculty.nps.edu/jenn/.

[Jie et al., 2013] Jie, S., Teng, L., and You, H. (2013). Adaptive cancellation of direct wave interference based on a new variable-step-size nlms algorithm. In *Radar Conference 2013, IET International*, pages 1–4.

[Jishy et al., 2010] Jishy, K., Lehmann, F., Moruzzis, M., Gosselin, F., and Salut, G. (2010). Tracking maneuvering target with particle filter techniques on passive radar using fm and dvbt broadcasting signals. In *Radar Conference, 2010 IEEE*, pages 642–646.

[Knott, 2011] Knott, P. (2011). Antenna array design for a passive radar demonstrator system. *3rd FHR Focus Days on PCL, Wachtberg-Werthhoven.*

[Knott et al., 2011] Knott, P., Nowicki, T., and Kuschel, H. (2011). Design of a disc-cone antenna for passive radar in the dvb-t frequency range. In *2011 German Microwave Conference*, pages 1–4.

[Krim and Viberg, 1996] Krim, H. and Viberg, M. (1996). Two decades of array signal processing research: the parametric approach. *IEEE Signal Processing Magazine*, 13(4):67–94.

[Kuschel et al., 2008] Kuschel, H., Heckenbach, J., Muller, S., and Appel, R. (2008). On the potentials of passive, multistatic, low frequency radars to counter stealth and detect low flying targets. In *Radar Conference, 2008. RADAR '08. IEEE*, pages 1–6.

[Lallo et al., 2012] Lallo, A. D., Tilli, E., Timmoneri, L., Battisti, T., and Campana, A. (2012). Design, analysis and implementation of a passive integrated mobile system for detection and identification of air targets. In *2012 13th International Radar Symposium*, pages 32–36.

164

[Levanon and Monzeson, 2004] Levanon, N. and Monzeson, E. (2004). *Radar signal.* Wiley Interscience.

[Li and Jilkov, 2003] Li, X. and Jilkov, V. (2003). Survey of maneuvering target tracking. Part I. dynamic models. *Aerospace and Electronic Systems, IEEE Transactions on,* 39(4):1333–1364.

[Maio et al., 2008] Maio, A. D., Foglia, G., Pasquino, N., and Vadursi, M. (2008). Measurement and analysis of clutter signal for GSM/DCS-based Passive Radar. *IEEE Radar Conference,* pages 1–6.

[Maio et al., 2010] Maio, A. D., Foglia, G., Pasquino, N., and Vadursi, M. (2010). Measurement and comparative analysis of clutter for GSM and UMTS passive radars. *IET Radar, Sonar and Navigation,* 4(3):421–423.

[Malanowski and Kulpa, 2008] Malanowski, M. and Kulpa, K. (2008). Digital beamforming for passive coherent location radar. In *Radar Conference, 2008. RADAR '08. IEEE,* pages 1–6.

[Malanowski and Kulpa, 2012] Malanowski, M. and Kulpa, K. (2012). Two methods for target localization in multistatic passive radar. *Aerospace and Electronic Systems, IEEE Transactions on,* 48(1):572–580.

[Malanowski et al., 2011] Malanowski, M., Kulpa, K., Bączyk, M., Maślikowski, ., and Janas, E. (2011). Passivecoherentlocation dbv-t demonstrator at warsaw university of technology. *3rd FHR Focus Days on PCL, Wachtberg-Werthhoven.*

[Malanowski et al., 2008] Malanowski, M., Kulpa, K., and Misjurewicz, J. (2008). PaRaDe - Passive Radar Demostrator family development at Warsaw University of Technology. *Microwaves, Radar and Remote Sensing Symposium,* pages 75–78.

[Mancinelli, 2010] Mancinelli, R. (2010). AULOS, italian passive coherent location (PCL). In *Virtuelle Instrumente in der Praxis VIP.*

[Masjedi et al., 2011] Masjedi, M., Modarres-Hashemi, M., and Sadri, S. (2011). Direct path and multipath cancellation in passive radars using subband variable step-size lms algorithm. In *2011 19th Iranian Conference on Electrical Engineering,* pages 1–5.

[Meller, 2012] Meller, M. (2012). Cheap cancellation of strong echoes for digital passive and noise radars. *IEEE Transactions on Signal Processing,* 60(5):2654–2659.

[Moscardini et al., 2015] Moscardini, C., Petri, D., Capria, A., Conti, M., Martorella, M., and Berizzi, F. (2015). Batches algorithm for passive radar: a theoretical analysis. *IEEE Transactions on Aerospace and Electronic Systems,* 51(2):1475–1487.

[Neyman and Pearson, 1933] Neyman, J. and Pearson, E. (1933). On the problem of the most efficient test of statistical hypotheses. *Philosophical Transactions of the Royal Society of London*, A 231(9):289–337.

[O Hagan et al., 2014] O Hagan, D., Schroder, M., Basavarajappa, V., Knott, P., Kuschel, H., and Simeoni, M. (2014). Wideband antenna array for Digital Video Broadcast terrestrial-based passive bistatic radar applications. *Radar, Sonar Navigation, IET*, 8(2):106–113.

[Olivadese et al., 2013] Olivadese, D., Giusti, E., Petri, D., Martorella, M., Capria, A., and Berizzi, F. (2013). Passive isar with dvb-t signals. *IEEE Transactions on Geoscience and Remote Sensing*, 51(8):4508–4517.

[Palmarini et al., 2015] Palmarini, C., Martelli, T., Colone, F., and Lombardo, P. (2015). Disturbance removal in passive radar via sliding extensive cancellation algorithm (ecas). In *2015 IEEE Radar Conference*, pages 162–167.

[Pastina et al., 2015] Pastina, D., Colone, F., Martelli, T., and Falcone, P. (2015). Parasitic exploitation of wi-fi signals for indoor radar surveillance. *IEEE Transactions on Vehicular Technology*, 64(4):1401–1415.

[Petri et al., 2011] Petri, D., Capria, A., Conti, M., Berizzi, F., Martorella, M., and Mese, E. D. (2011). High range resolution multichannel dvb-t passive radar: Aerial target detection. pages 129–132.

[Rihaczek, 1971] Rihaczek, A. W. (1971). Radar waveform selection - A simplified approach. *Aerospace and Electronic Systems, IEEE Transactions on*, AES-7(6):1078–1086.

[Ruck et al., 2009] Ruck, D., Rogers, S., Kabrisky, M., and Oxley, M. (2009). A new approach for DVB-T cross-ambiguity function evaluation. *EuRAD 2009: European Radar Conference*, (37–49).

[Saini and Cherniakov, 2002] Saini, R. and Cherniakov, M. (2002). Investigation of Digital TV signal for Radar application. *EUPISCO-2002: XI European Signal Processing Conference, Toulouse*, pages 15–18.

[Saini et al., 2003] Saini, R., Cherniakov, M., and Lenive, V. (2003). Direct path interference suppression in bistatic system: DTV based radar. In *Radar Conference, 2003. Proceedings of the International*, pages 309–314.

[Saini and M.Cherniakov, 2005] Saini, R. and M.Cherniakov (2005). DTV signal ambiguity function analysis for radar applications. In *IEE Proceedings on Radar, Sonar and Navigation*, volume 152, pages 133–142.

[Schroder, 2011] Schroder, A. (2011). Second-generation mobile multiband passive radar demonstrator. *3rd FHR Focus Days on PCL, Wachtberg-Werthhoven.*

[Schroeder and Edrich, 2014] Schroeder, A. and Edrich, M. (2014). Passive radar sensor cluster operation. In *2014 15th International Radar Symposium (IRS)*, pages 1–4.

[Schroeder et al., 2012a] Schroeder, A., Edrich, M., and Winkler, V. (2012a). Multi-illuminator passive radar performance evaluation. In *2012 13th International Radar Symposium*, pages 61–64.

[Schroeder et al., 2012b] Schroeder, A., Edrich, M., and Winkler, V. (2012b). Multiband pcr systems in multistatic configurations for enhanced air and ground surveillance. In *Sensors & Electronics Technology Panel Workshop SET-177 Athens.*

[Schroeder et al., 2013] Schroeder, A., Edrich, M., and Winkler, V. (2013). Stationary cassidian fm passive radar demonstrator for 24/7 operation and sensor cluster measurements. In *2013 14th International Radar Symposium (IRS)*, volume 1, pages 161–166.

[Schwark and Cristallini, 2016] Schwark, C. and Cristallini, D. (2016). Advanced multi-path clutter cancellation in ofdm-based passive radar systems. In *2016 IEEE Radar Conference (RadarConf)*, pages 1–4.

[SELEX Sistemi Integrati Passive Radar, 2015] SELEX Sistemi Integrati Passive Radar (2015). From http://www.ni.com/video/2786/en/, accessed 11 November 2015.

[Sizov et al., 2007] Sizov, V., Cherniakov, M., and Antoniou, M. (2007). Forward scattering radar power budget analysis for ground targets. *IET Radar, Sonar Navigation*, 1(6):437–446.

[Skolnik, 2008] Skolnik, M. (2008). *Radar Handbook. Third Edition.* Mc-Graw Hill.

[SNIFTD, 2016] SNIFTD (2016). Software package for spherical near-field far-field transformations with full probe correction. https://www.ticra.com/sites/default/files/Product_sheets/SNIFT.pdf, accessed 24 November 2016.

[Stwart, 1973] Stwart, G. W. (1973). *Introduction to Matrix Computations*, volume 1. Academic Press.

[Szumski et al., 2009] Szumski, K., Malanowski, M., Kulpa, J., Porczyk, W., and Kulpa, K. (2009). Real-time software implementation of Passive Radar. In *Radar Conference, 2009. EuRAD 2009. European*, pages 33–36.

[TELEVES 4G-NOVA, 2016] TELEVES 4G-NOVA (2016). From https://www.televes.com/en/catalogo/producto/4gnova-antenna, accessed 10 October 2016.

[TELEVES DAT HD BOSS 75, 2015] TELEVES DAT HD BOSS 75 (2015). From http://www.televes.com, accessed 11 November 2015.

[Veen and Buckley, 1988] Veen, B. D. V. and Buckley, K. M. (1988). Beamforming: a versatile approach to spatial filtering. *IEEE ASSP Magazine*, 5(2):4–24.

[Villano et al., 2013] Villano, M., Colone, F., and Lombardo, P. (2013). Antenna array for passive radar: Configuration design and adaptive approaches to disturbance cancellation. *International Journal of Antennas and Propagation*, 2013.

[Weiss and Mitra, 1979] Weiss, A. and Mitra, D. (1979). Digital adaptive filters: Conditions for convergence, rates of convergence, effects of noise and errors arising from the implementation. *Information Theory, IEEE Transactions on*, 25(6):637–652.

[Widrow and Hoff, 1960] Widrow, B. and Hoff, M. (1960). Adaptive switching circuits. *IRE WESCON Conv.*, pages 96–104.

[Widrow and Stearns, 1985] Widrow, B. and Stearns, S. D. (1985). *Adaptive Signal Processing*, volume 1. Prentice Hall.

[Willis, 2005] Willis, N. J. (2005). *Bistatic Radar*. SciTech Publishing Inc.

[Willis and Griffiths, 2007] Willis, N. J. and Griffiths, H. D. (2007). *Advances in Bistatic Radar*. SciTech Publishing Inc.

[Wu et al., 2012a] Wu, D., Shen, L., Xie, J., and Wang, Y. (2012a). Improved LMS algorithm and its application in direct path and multipath cancellation for passive radar. In *Communication Technology (ICCT), 2012 IEEE 14th International Conference on*, pages 1301–1305.

[Wu et al., 2012b] Wu, D., Shen, L., Xie, J., and Wang, Y. (2012b). Improved lms algorithm and its application in direct path and multipath cancellation for passive radar. In *Communication Technology (ICCT), 2012 IEEE 14th International Conference on*, pages 1301–1305.

[Xiaode et al., 2014] Xiaode, L., Jichuan, L., Kuan, L., Daojing, L., and Yi, Z. (2014). Range-doppler nlms (rdnlms) algorithm for cancellation of strong moving targets in passive coherent location (pcl) radar. In *2014 International Radar Conference*, pages 1–5.

[Zhai and Wu, 2015] Zhai, Y. and Wu, J. (2015). A clutter cancellation method in passive radar based on music time delay estimation. In *Computer and Communications (ICCC), 2015 IEEE International Conference on*, pages 347–351.

[Zhao et al., 2013] Zhao, Y. D., Zhao, Y. K., Lu, X. D., and Xiang, M. S. (2013). Block nlms cancellation algorithm and its real-time implementation for passive radar. In *Radar Conference 2013, IET International.*

[Zhao et al., 2012] Zhao, Z., Wan, X., Shao, Q., Gong, Z., and Cheng, F. (2012). Multipath clutter rejection for digital radio mondiale-based hf passive bistatic radar with ofdm waveform. *IET Radar, Sonar Navigation,* 6(9):867–872.

Contributions

Published contributions organized in descending chronological order.

International Journals

- N. Del-Rey-Maestre, M.P. Jarabo-Amores, D. Mata-Moya, **J.L. Bárcena-Humanes**, P. Gómez-del-Hoyo. " Statistical analysis of UHF passive ground clutter". Transactions on Aerospace and Electronic System. Under revision.

- N. Del-Rey-Maestre, D. Mata-Moya, M.P. Jarabo-Amores, P. Gómez-del-Hoyo, **J.L. Bárcena-Humanes**. "Artificial Intelligence Techniques for Small Boats Detection in Radar Clutter. Real Data Validation". Engineering Application of Artificial Intelligence. Under revision.

- M.P. Jarabo-Amores, **J.L. Bárcena-Humanes**, P. Gómez-del-Hoyo, N. Del-Rey-Maestre, Diego Juara-Casero, Fco-Javier Gaitán-Cabañas, D. Mata-Moya. " IDE-PAR: A multichannel DVB-T passive radar technological demonstrator in terrestrial radar scenarios". IET Radar, Sonar & Navigation, 2016. JCR impact factor: Q3 (Telecommunications-SCIE). Available in : http://digital-library.theiet.org/content/journals/10 rsn.2016.0087

- **J.L. Bárcena-Humanes**, P. Gómez-del-Hoyo, M.P. Jarabo-Amores, D. Mata-Moya, N. Del-Rey-Maestre. "Feasibility Study of EO SARs as Opportunity Illuminators in Passive Radars: PAZ-Based Case Study". Sensors 2015. JCR impact factor: Q1 (Instruments & Instrumentation). Available in : http://www.mdpi.com/1424-8220/15/11/29079

- Jaime Martín de Nicolás, Mª Pilar Jarabo Amores, David de la Mata Moya, Nerea del Rey Maestre, **José Luis Bárcena Humanes**. "Statistical Analysis of SAR Sea Clutter for Classification Purposes". Remote Sensing 2014. JCR impact: Q1 (Remote Sensing)Available in : http://www.mdpi.com/2072-4292/6/10/9379

International Conferences

- Pedro Gómez del Hoyo, **José Luis Bárcena Humanes**, Nerea del Rey Maestre, Mª Pilar Jarabo Amores y David Mata Moya."Ultra-high frequency Passive Radar coverage for cars detection in Semi-Urban scenarios". 18th International Conference on Signal and Information Processing (ICSIP2016),2016.

- Pedro Gómez del Hoyo, **José Luis Bárcena Humanes**, David Mata Moya, Diego Juara Casero and Verónica Jiménez de Lucas. "Passive Radars as Low Environmental Impact Solutions for Smart Cities Traffic Monitoring". 16th International Conference on Computer as Tool (Eurocon2015),2015.

- Jaime Martín de Nicolás Presa, Mª Pilar Jarabo Amores, Nerea del Rey Maestre, Pedro Gómez del Hoyo and **José Luis Bárcena Humanes**. "Robustness of a Generalized Gamma CFAR Ship Detector Applied to TerraSAR-X and Sentinel-1 Images". 16th International Conference on Computer as Tool (Eurocon15)2015.

- Nerea del Rey Maestre, Mª Pilar Jarabo Amores, David Mata Moya, Pedro Gómez del Hoyo and **José Luis Bárcena Humanes**. "Statistical analysis of UHF bistatic radar clutter in coastal scenarios".12th European Radar Conference (EuRAD 2015), 2015.

- Jaime Martín de Nicolás Presa, Mª Pilar Jarabo Amores, Nerea del Rey Maestre, David Mata Moya and **José Luis Bárcena Humanes**."A Non-Parametric CFAR Detector based on Sea clutter statistical modeling".IEEE International Conference on Image Processing 2015 (ICIP 2015),2015.

- **José Luis Bárcena Humanes**, Nerea del Rey Maestre, Mª Pilar Jarabo Amores, David Mata Moya and Pedro Gómez del Hoyo. "Passive radar imaging capabilities using space-borne commercial illuminators in surveillance applications". Signal Processing Symposium 2015 (SPSympo2015), 2015.

- David Mata Moya, Mª Pilar Jarabo Amores, Nerea del Rey Maestre, Jaime Martín de Nicolás Presa and **José Luis Bárcena Humanes**. "An Adaptive Threshold technique for the LR detector in K-clutter". IEEE International Instrumentation and Measurement Technology Conference (I2MTC), 2015.

- **José Luis Bárcena Humanes**, Jaime Martín de Nicolás Presa, Carla Solís Carpintero, Mª Pilar Jarabo Amores, Manuel Rosa Zurera, David Mata Moya. "DVB-T Ambiguity Peak Reduction in Passive Radar Applications Based on Signal Reconstruction". 11th European Radar Conference (EuRAD 2014), 2014

- Jaime Martín de Nicolás Presa, David de la Mata Moya, Mª Pilar Jarabo Amores, Nerea del Rey Maestre, **José Luis Bárcena Humanes**. "Neural Network Based

Solutions for Ship Detection in SAR Images". International Conference on Digital Signal Processing (DSP 2013), 2013.

- Nerea del Rey Maestre, David de la Mata Moya, Mª Pilar Jarabo Amores, Jaime Martín de Nicolás Presa, **José Luis Bárcena Humanes**. "Incoherent Detection of Targets with Unknown Doppler Shift in Spiky K-distributed Clutter". International Conference on Digital Signal Processing (DSP 2013), 2013.

- **José Luis Bárcena Humanes**, David de la Mata Moya, Mª Pilar Jarabo Amores, Nerea del Rey Maestre y Jaime Martín de Nicolás. "Sea Clutter Neural Network Classifier: Feature Selection and MLP Design". International Work Conference on Artificial Neural Networks (IWANN13), 2013.

- David de la Mata Moya, Mª Pilar Jarabo Amores, Nerea del Rey Maestre, **José Luis Bárcena Humanes** y Jaime Martín de Nicolás. "SONN and MLP Based Solutions for Detecting Fluctuating Targets with Unknown Doppler Shift in Gaussian Interference". International Work Conference on Artificial Neural Networks (IWANN13), 2013.

- Nerea del Rey Maestre, David de la Mata Moya, Mª Pilar Jarabo Amores, Jaime Martín de Nicolás Presa, **José Luis Bárcena Humanes**. "Doppler Processors as Suboptimum Approaches for Detecting Targets with Unknown Doppler Shift". Computational Intelligence, Communication Systems and Networks (CICSyN2013), 2013.

- **José Luis Bárcena Humanes**, David de la Mata Moya, Mª Pilar Jarabo Amores, Nerea del Rey Maestre, Jaime Martín de Nicolás Presa. "Analysis of NNs Detectors for Targets with Unknown Correlation in Gaussian Interference". Computational Intelligence, Communication Systems and Networks (CICSYN2013), 2013

- Jaime Martín de Nicolás Presa, David de la Mata Moya, Mª Pilar Jarabo Amores, Nerea del Rey Maestre, **José Luis Bárcena Humanes**. "Segmentation Techniques for Land Mask Estimation in SAR Imagery". Computational Intelligence, Communication Systems and Networks (CICSYN2013), 2013

- J. Alvarez, J. Gaitán, F. Berizzi, A. Capria, M. Conti, E. Giusti, M. Martorella, C. Moscardini, D. Olivadese, D. Petri, **J. L. Bárcena**, D. De La Mata, P. Jarabo, M. Rosa, A. Podda, A. Sulis, C. Benedek, T. Szirányi, G. Georgiou, A. Papanastasiou, C. Topping. "Array Passive ISAR adaptive processing (APIS) project: an overview" .ET187 Specialist Meeting on Passive Radar, PCL (4th focus days on PCL),2013

- Jaime Martín de Nicolás Presa, **José Luis Bárcena Humanes**, Ángel Palma Vázquez, David de la Mata Moya, Mª Pilar Jarabo Amores. "Supervised Landmask Estimation using Contextual Information in SAR Data". IEEE Intelligent Vehicles Symposium, 2012

- Jaime Martín de Nicolás Presa, David de la Mata Moya, Mª Pilar Jarabo Amores, **José Luis Bárcena Humanes**, Ángel Palma Vázquez. "High-Order Neural Network-Based Ship Detection Algorithms Applied to SAR Imagery". European Conference on Synthetic Aperture Radar (EUSAR2012), 2012 .

National Journals and Conferences

- Pedro Gómez del Hoyo, **José Luis Bárcena Humanes**, Nerea del Rey Maestre, Mª Pilar Jarabo Amores y David Mata Moya. "Cobertura de Radares Pasivos Basados en la TDT, para la Detección de Vehículos Terrestres".XXXI Simposium Nacional de la Unión Científica Internacional de Radio, URSI 2016, 2016

- Mª Pilar Jarabo Amores, María José González Bonilla, David de la Mata Moya, Jaime Martín de Nicolás, Nerea del Rey Maestre, **José Luis Bárcena Humanes** y Víctor Manuel Peláez Sánchez. "Explotación científica de productos PAZ en tareas de vigilancia y monitorización costera." Revista de Teledetección. Editorial: Asociación Española de Teledetección.2014

- Mª Pilar Jarabo Amores, Manuel Rosa Zurera, David Mata Moya, **José Luis Bárcena Humanes**, Nerea del Rey Maestre, Javier Álvarez Álvarez, Fco. Javier Gaitán Cabañas. "Radares pasivos en aplicaciones de seguridad y defensa. El sistema APIS". Congreso Nacional de I+D en Defensa y Seguridad (DESEi+d 2013), 2013.

- David Mata Moya, Mª Pilar Jarabo Amores, Nerea del Rey Maestre, **José Luis Bárcena Humanes**, José Miguel Fernández Fructuoso. "Detectores radar neuronales en aplicaciones de vigilancia costera". Congreso Nacional de I+D en Defensa y Seguridad (DESEi+d 2013), 2013.

- Mª Pilar Jarabo Amores, Manuel Rosa Zurera, David de la Mata Moya, **José Luis Bárcena Humanes**, Nerea del Rey Maestre, Javier Álvarez y Javier Gaitán."APIS, radar pasivo en el JIP-CET." Boletín de Información Tecnológica en Defensa.